STUDY OF EFFECTIVE METHODS OF CHARACTERISATION OF MAGNETOSTRICTION AND ITS FUNDAMENTAL EFFECT ON TRANSFORMER CORE NOISE

PhD thesis

Shervin Tabrizi

A thesis submitted to the Cardiff University in candidature for the degree of Doctor of Philosophy

December 2013

Wolfson Centre for Magnetics
Cardiff School of Engineering
Cardiff University
Wales, United Kingdom

Abstract

Magnetostriction of core laminations is one of the main sources of transformer acoustic noise. The magnetostriction of grain oriented silicon steel is extremely sensitive to applied compressive stress. A measurement system using piezoelectric accelerometers has been designed and built. This was optimized for magnetostriction measurements under stress within the range of 10 MPa to -10 MPa on large as-cut sheets. This system was used for characterization of wide range of grain-oriented grades.

Laboratories around the world are using many different methods of measurement of the magnetostrictive properties of electrical steel. In response to this level of interest, an international round robin exercise on magnetostriction measurement has been carried out and eight different magnetostriction-measuring systems have been compared. Results show a reasonable correlation between the different methods.

In this study the influence of factors such as the domain refinement process, curvature, and geometry on the magnetostriction of 3% grain oriented silicon steel were investigated. The study shows that both laser scribing and mechanical scribing have a similar effect on the sample's domain structure and would cause an increase in magnetostriction. A proposed domain model was used successfully to estimate the effect of scribing on magnetostriction.

Correlation between magnetostriction of 3% grain oriented silicon steel with transformer vibration was investigated. It was shown that increasing the clamping pressure to 4Nm can decrease the out of plane vibration in the joint regions due to the increase of friction and reduction of air gap which reduces the air gap flux and consequently the Maxwell forces. Also it has been shown that the primary source for the differences between the vibration of the cores under the same magnetic excitation and clamping pressure in the measured cores is due to the differences in the magnetostriction characteristics of the grades of electrical steels. Correlations between the magnetostriction harmonics and the vibration of the cores have been determined.

ACKNOWLEDGMENTS

My first and sincere appreciation goes to Dr. Philip Anderson, my senior supervisor for all I have learned from him and for his continuous help and support in all stages of this thesis. I would also like to thank him for being an open person to ideas, and for encouraging and helping me to shape my interest and ideas.

I would like to express my deep gratitude and respect to Prof. Anthony Moses whose advices and insight was invaluable to me. For all I learned from him, He always challenged me in alternative views and his insight knowledge improved this work significantly.

I am very thankful to Dr. Hugh Stanbury for his guidance and encouragement from the beginning to end of my PhD studies, especially regarding round robin exercise. His supervision and professional expertise improved my work and knowledge significantly. I am also very grateful to Dr. Jeremy Hall and Dr.Yevgen Melikov for their support, guidance and helpful suggestions. And also thanks to my colleague Mr Teeraphon Phophongviwat.

I gratefully acknowledge the funding sources that made my Ph.D. work possible. I was funded by ABB AB, AK Steel Crop., Alstom Grid, Brush Transformers Ltd, CG Holdings Belgium N.V., Cogent Power Ltd, Koleltor Etra Energetski transformatorji d.o.o., Kncar Distribution and Special Transformers Inc., Legnano Teknoelectric Company S.p.A., Nuova Eletrofer S.p.A., SGB Starkstorm Gerätebay Gmbh, and ThyssenKrupp Electrical Steel GmbH.

I would like to thank my family, especially my mother and father for always believing in me, for their continuous love and their supports in my decisions. Without whom I could not have made it here. And most of all for my loving, supportive, encouraging, and patient wife Khoosheh, whose faithful support during the final stages of this Ph.D., is so appreciated. Thank you.

List of Symbols

v	Velocity
λ	Magnetostriction
Φ	Misorientation Angle
σ	Applied Stress
ω	Angular Frequency
Φ_z	Inter laminar Flux
μ	Permeability
A	Acceleration
B	Magnetic induction
CGO	Conventional Grain Oriented
DR	Domain Refined
E	Young's Modulus
E_λ	Magnetoelastic Energy
E_K	Magnetocrystalline Anisotropy Energy
E_m	Magnetostatic Energy
f	Frequency
H	Magnetic field

HGO	High Permeability Grain Oriented
J	Magnetic Polarization
LDV	Laser Doppler Vibrometer
L_{va}	A-weighted Magnetostriction Velocity
M	Magnetisation
N_D	Demagnetising Factor
P_s	Specific Power Loss
RD	Rolling Direction
x	Susceptibility
X	Displacement
α, β	Direction cosines

1. Chapter 1: Introduction and objectives

1.1. Introduction:

In recent years there has been growing interest in quiet transformers. The noise emitted by a transformer could interfere with comfortable life of the residents leaving near substations. Moreover, increased urbanization is requiring people to live in higher local concentration and as a result electric power has to be located close to these centers. Therefore, there is a high demand to minimize the noise generated by transformers. The generated noise can be reduced in three different ways, reducing the transmission of the noise, placing barriers between the source and the residents or reducing noise at the source.

1.2. Parameters affecting noise:

1.2.1. Transmission:

The noise is transmitted into the atmosphere from the tank through the insulation oil [1]. This generated noise may be reduced by mounting a close-fitting sound insulation panel on the side of a transformer tank,[1] or by insertion of a barrier built from oil resistant rubber or some form of gas filled medium[2] An overall noise reduction of 14 dB(A) can be obtained using sound insulation panel on a 650 MVA transformer [1].

1.2.2. Sound barrier:

Outside the transformer, noise may be controlled by using sound barrier panels on the transformer outside which could effectively attenuate sound waves generated from the transformer. An effective sound barrier should shield the receiver against the predominant portion of the sound energy produced from the

source and directed toward the reception point[3] .Using a barrier could reduce the transformer noise by 10 ~ 20dB(A)[4].

The noise shell theory is an acoustical theory of closed-spaced enclosure proposed by Jackson [5] , is based on the assumption that the sound medium is elastic and there is no mechanical coupling between the source of the noise and the attenuating plate, Moreover, it is assumed that the sound waves are normal to the plate [6].

The easiest type of sound barrier is a brick wall that is used for surrounding the transformer on all side. This can be improved in several ways. Covering the walls with a sound absorbing material i.e. glass wool increases the noise reduction. Also a separate layer of sound absorbing material with a small distance inside the wall would deliver additional improvements. For achieving more reduction in sound level the Box-in method shall be used, which is achieved by the addition of a roof to provide total enclosure [7].

1.2.3. Sound source:

The emitted noise by transformers can be categorized into the following:

- Winding noise
- Accessory devices such as fans and pumps
- Core noise, e.g. magnetic core vibration, core construction and design

The primary and most importance source of transformer noise is the core noise [8, 9].

1.2.3.1.Winding noise:

Winding noise, known as load noise or current noise, primarily comes from the winding. This type of noise is caused by Lorentz forces resulting from the magnetic stray field of the load current in one current carrying winding and the total electric currents in the conductors of the other winding [8]. These forces result in vibrations in the winding and cause acoustic noise with twice the line frequency [10, 11]. The frequency of the winding noise is twice the power frequency as it is caused by the electromagnetic force [12].

1.2.3.2.Fans and pump noise

The other source of the noise in transformers is from cooling-fans or oil pump noise, as no transformer is truly an ideal transformer, each will incur a certain amount of energy loss, which is mostly transformed into heat. As a result the insulating medium inside the transformer (usually oil) is used in order to remove the heat from the winding and transformer core.

Also over the years the emitted noise increases as a result of the gradual wear processes of elements of power appliances at the substations, mostly the cooling systems of the transformer units [13].

1.2.3.3.Magnetic core vibration:

Core vibrations are produced by the combined effects of magnetostriction [14] and magnetic forces[8]. Magnetostriction and magnetic forces (also known as Maxwell forces) are both a function of magnetization. Affects of these parameters on core vibration are explained separately in order to understand their affects on core noise.

- **Magnetostriction:**

The atomic moment interactions giving rise to ferromagnetism and magnetic anisotropy also produce forces between atoms that tend to strain the lattice anisotropically [15]. This phenomenon is known as magnetostriction and can be divided into linear magnetostriction, volume magnetostriction and form effect.

Joule [16] first discovered in 1842 the fact that the ferromagnetic material changes the length when magnetised by using an iron bar. He also examined the effects of external stresses on the magnetostriction of iron and showed that, under tension-applied stress, the magnetostriction value reduces for all field strengths.

Linear magnetostriction exists below saturation and could be either positive or negative. Positive magnetostriction is used to define an increase in length with increasing field and negative magnetostriction defines a decrease in length. Also every magnetostrictive effect has a related opposite effect. The longitudinal magnetostriction, which is also known as the Joule effect, has its reverse effect, known as the Villari effect [17], which is the change of magnetization, formed by an external stress.

The magnetostriction is independent of the sign of the flux, this results in magnetostriction having a fundamental frequency of twice that of the excitation signal with harmonics at integer multiples of this. Due to the response characteristic of the human ear, the effect of the magnetostriction harmonics becomes more important[18].

Volume magnetostriction occurs if a ferromagnetic material (e.g. silicon steel) is magnetized larger than their technical saturation, the magnetostriction observed is principally a volume change and the strain would be equal in all directions [19].

Ferromagnetic materials would still have a magnetostriction effect due to the fact that their demagnetizing energy is dependent on strain, even if the lattice deformations created by both the exchange and anisotropy energies be zero [20].

- **Maxwell forces:**

A second source of core vibration is Maxwell forces. These can be divided into attractive or repulsive forces.

I. **Repulsive forces:** these occur among adjacent layers of magnetised areas e.g. limbs or yokes [21]. This type of force is negligible due to its weak intensity.
II. **Attractive forces:** This type of force primarily occurs at joint corners due to the interlaminar forces resulting from the induction arising in air-gap regions. The induction in the joint area is strongly dependent on step number, which is explained in more details in Chapter10.

1.3. Objectives:

The main aims of this investigation are to

1. Study the effect of magnetostriction on the transformer core vibration and acoustic noise.
2. In order to achieve objective 1, it is required to develop a new magnetostriction measurement system.
3. Investigate the influence of the domain refinement process, residual curvature (coil set), and geometry on peak-to-peak magnetostriction of 3% silicon steel.

4. Organize and evaluate the finding of a round robin magnetostriction measurement comparison within leading world laboratories.
5. Find a correlation between magnetostriction and transformer core noise.

References for Chapter 1

1. Kanoi, M., et al., *TRANSFORMER NOISE REDUCTION WITH NEW SOUND INSULATION PANEL.* IEEE transactions on power apparatus and systems, 1983. **PAS-102**(N 9): p. 2817-2825.
2. Saha, P., *POWER TRANSFORMER NOISE - GENERATION, PROOPAGATION AND CONTROL - A REVIEW.* American Society of Mechanical Engineers (Paper), 1981.
3. Kurze, U.J., *NOISE REDUCTION BY BARRIERS.* Journal of the Acoustical Society of America, 1974. **55**(3): p. 504-518.
4. Ver, I.L., G.S. Anderson, and C.G. Gordon. *BARRIER-ENCLOSURE; AN EFFECTIVE WAY TO CONTROL THE NOISE EMISSION OF POWER TRANSFORMERS*. 1981.
5. Jackson, R.S., Jump, L and Lawrence, J.D, *The reduction of transformer noise by attached panels*, in *I.E.E Conference , Acoustic Noise and Its Control*1967.
6. Ellingson, E.F., *TRANSFORMER NOISE ABATEMENT USING TUNED SOUND ENCLOSURE PANELS.* Proceedings of the Technical Programme - INTERNEPCON: International Electronic Packaging and Production Conferences: p. 184-191.
7. Yang, Y. and X. Zhang, *Study on noise reduce for equipment at UHVDC converter station.* Gaodianya Jishu/High Voltage Engineering, 2006. **32**(9): p. 149-152.
8. Weiser, B., H. Pfützner, and J. Anger, *Relevance of magnetostriction and forces for the generation of audible noise of transformer cores.* IEEE Transactions on Magnetics, 2000. **36**(5 II): p. 3759-3777.
9. Moses, A.J., et al. *Contribution of magnetostriction to transformer noise*. 2010.
10. Rausch, M., et al., *Combination of finite and boundary element methods in investigation and prediction of load-controlled noise of power transformers.* Journal of Sound and Vibration, 2002. **250**(2): p. 323-338.
11. Pengfei, S., et al., *Electromagnetic Vibration Analysis of the Winding of a New HVDC Converter Transformer.* Power Delivery, IEEE Transactions on, 2012. **27**(1): p. 123-130.
12. Harlow, J.H., *Electric power transformer engineering*. 2nd ed. Electrical engineering handbook series. 2007, Boca Raton, Fla. ; London: CRC Press/Taylor & Francis.
13. Borucki, S., T. Boczar, and A. Cichoń, *Technical possibilities of reducing the sound pressure level emitted into the environment by a power transformer.* Archives of Acoustics, 2011. **36**(1): p. 49-56.
14. Moses, A.J., *MEASUREMENT OF MAGNETOSTRICTION AND VIBRATION WITH REGARD TO TRANSFORMER NOISE.* IEEE Transactions on Magnetics, 1974. **MAG-10**(2): p. 154-156.
15. Shilling, J.W. and G.L. Houze Jr, *MAGNETIC PROPERTIES AND DOMAIN STRUCTURE IN GRAIN-ORIENTED 3% Si-Fe.* IEEE Transactions on Magnetics, 1974. **MAG-10**(2): p. 195-223.
16. Joule, J.P., *On a new class of magnetic forces* Ann.Electr.Magn.Chem, 1842. **8**: p. 219-224.
17. Villari , E., *Change of magnetization by tension and by electric current.* Ann. Phys. Chem, 1865. **126**: p. 87–122.

18. Mapps, D.J. and C.E. White. *LONGITUDINAL AND TRANSVERSE MAGNETOSTRICTION HARMONICS IN (110) (001) SILICON-IRON*. 1984.
19. Lee, E.W., *Magnetostriction and magnetomechanical effects.* Reports on Progress in Physics, 1955. **18**(1): p. 184-229.
20. Stauss, H.E., *Form effect in linear magnetostriction.* Journal of Applied Physics, 1959. **30**(5): p. 698-701.
21. Lackey, J.G. and S. Palmer, *Transformer core vibrations.* IEEE Power Eng Soc, Winter Meeting Report, 1977.

Chapter 2: Electromagnetism

This Chapter delivers the basic theories of magnetism, ferromagnetic material and magnetisation processes as well as a discussion of magnetisation characteristics and microstructures of electrical steel sheets.

2.1. Basic terms in magnetism

One of the most essential ideas in magnetism is the concept of magnetic field (*H*) and is generated whenever an electric charge is in motion. This can be produced due to an electrical current in a wire or the orbital motions and spins of electrons in permanent magnet [1]. According to Ampere's law, when a magnetic field is generated, the mediums response to the generated field is called magnetic induction (*B*). The relationship between magnetic field (Amperes per meter) and magnetic induction (Tesla) is defined by a property of a medium called permeability (μ) and expressed as follow:

$$B = \mu H \tag{2.1}$$

Free space is considered as a medium and has a permeability value of $4\pi\times10^{-7}$ H.m^{-1} and is given the symbol μ_0.

In other mediums, especially ferromagnetic and ferromagnetic materials, magnetic induction (*B*) is not a linear function of (*H*) anymore and can be expressed relative to free space:

$$B = \mu_0 \mu_r H \tag{2.2}$$

Where μ_r is the dimensionless relative permeability of the material and is a function of the flux density.

2.2. Ferromagnetism

The magnetic behaviour of materials can be classified using magnetic parameters. Ferromagnetism is used to classify materials with positive susceptibility greater than 1, susceptibility is defined as the ratio of magnetization by magnetic field. This means that these materials are not exhibiting spontaneous net magnetisation in the absence of the external magnetic field.

The ferromagnetism phenomena can be explained by considering that every electron in an atom has an electronic magnetic moment, associated with two components: an orbital motion, and a spin magnetic moment due to electron spin [1].

Weiss suggested that in ferromagnetic materials it is preferable for spin moments to spontaneously align so that their magnetic moments are parallel in order to be in a stable low energy situation [2].The spontaneous magnetisation progressively weaker as temperature increases to Curie temperature, below the curie temperature the material is ferromagnetically ordered [3].

2.3. Energies of a Ferromagnetic

2.3.1. Magnetocrystalline anisotropy energy

Silicon steel has body-centered cubic lattice. This crystal structure does not have a close-packed plane but {0 1 1} is the most densely packed plane and easy axes align parallel to it on [100] directions. Figure 2-1 shows the easy axes directions of a body centered cubic crystal [4]. The [110] and [111] are respectfully

the medium and hard directions, and magnetisation in these directions needs higher magnetic field than in [100] direction.

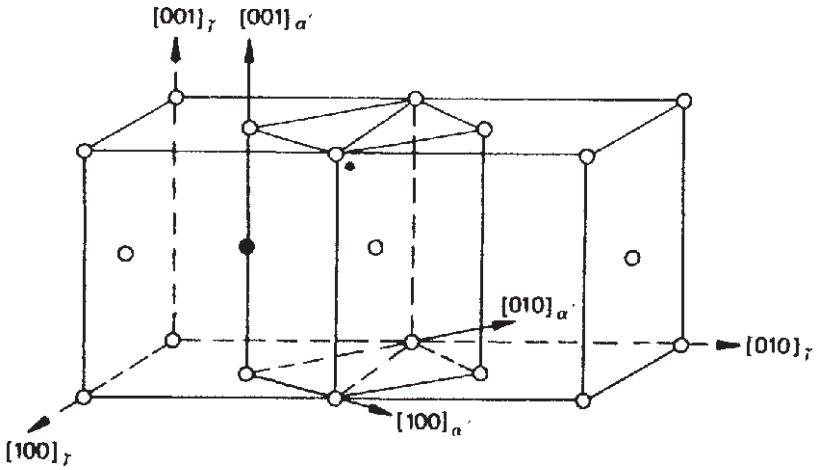

Figure 2- 1: Schematic of the bcc structure easy axes [100] directions [4]

The energy of a ferromagnetic material is dependence on the direction of the magnetization relative to the structural axes of that material, which is described by the anisotropy energy. The Magnetocrystalline anisotropy energy of such a structure results from spin-orbit interaction and may be expressed as follows

$$E_K = K_0 + K_1(\alpha_1^2\alpha_2^2 + \alpha_2^2\alpha_3^2 + \alpha_1^2\alpha_3^2) + K_2(\alpha_1^2\alpha_2^2\alpha_3^2) + \cdots \quad (2.3)$$

Where K_0, K_1 and K_2 are anisotropy constants α_1, α_2 and α_3 are the direction cosines of magnetisation with respect to the [100] directions. The higher order terms are generally neglected. The K_0 is independent of angle and is also neglected [5].

2.3.2. Magnetostatic Energy

If a bulk ferromagnetic material contains only a single domain, which is saturated along the [001] axis, then the discontinuous ends of the sample would act as free magnetic poles and would generate a large internal magnetic field. Figure 2-2, shows a sheet of ferromagnetic material containing only one domain and is

saturated along the ‘y’ direction. This generated field would cause an increase in the potential energy compared with demagnetized state. This would generate a field in the sample that is known as the demagnetizing field to minimize the potential energy [6].

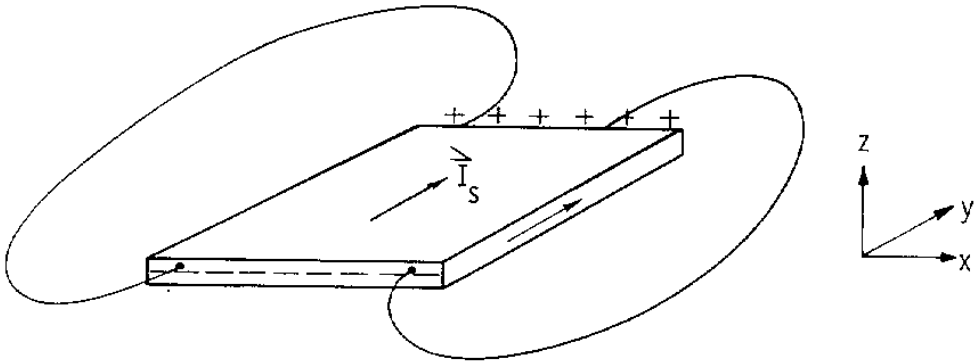

Figure 2- 2: ferromagnetic sheet containing only a single domain, saturated along ‘y’ direction [6]

The Magnetostatic field is the energy of a sample in its own field that can be expressed as

$$E_m = \frac{1}{2} N_D M^2 \tag{2.4}$$

Where E_m is the Magnetostatic energy (J/m^3)

N_D is the demagnetizing factor

M is the magnetisation of the sample (A/m).

The demagnetizing factor N_D is dependent of the shape and would be zero for an infinitively long thin sample along their long axis whilst it would be very large for a strip of ferromagnetic material perpendicular to the plane [7].

Subdividing the material into more domains magnetized in the opposite directions may reduce both demagnetizing field and the Magnetostatic energy as shown in Figure 2-3.

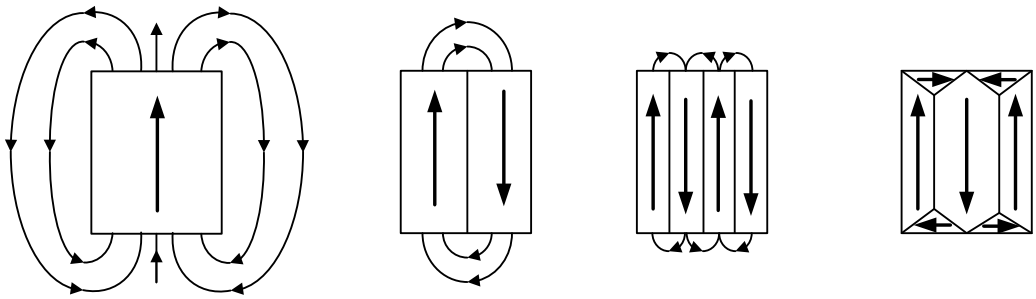

Figure 2- 3: Ferromagnetic single crystal sheets demagnetized by formation of domain structures [5]

Subdividing and increasing the number of domains in the grain may reduce the Magnetostatic energy further. However on the other hand, the number of domains is limited by another factor, domain wall energy, which is discussed in the following section.

2.3.3. Domain Wall Energy

The interface between regions in which the spontaneous magnetisation has antiparallel direction is called a domain wall. The magnetisation direction has to change direction from one easy direction axes to another at the domain wall interfaces[8]. Figure 2-4 shows schematic drawing of an 180^{o} domain wall with y direction along *'y'* axis.

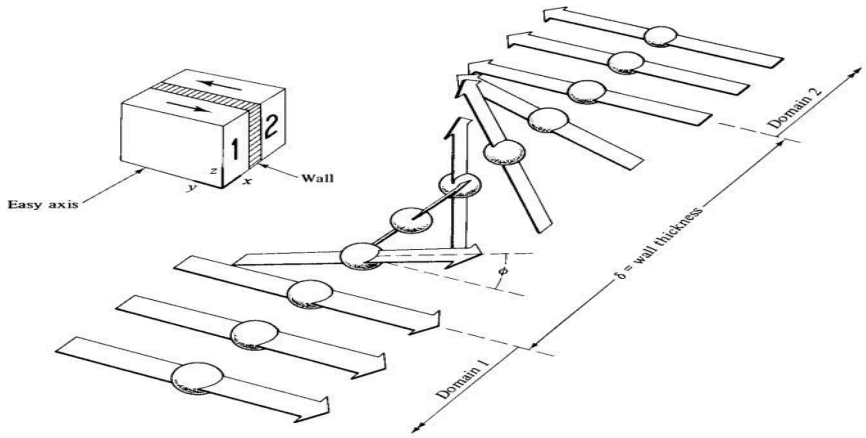

Figure 2- 4: Schematic drawing of 180^0 domain wall structure[5]

The overall domain wall energy is the sum of the anisotropy and exchange energies. The wall would have large exchange energy when adjacent moments are aligned antiparallel and the exchange energy is at its lowest when neighbouring spins are parallel, as a result the atoms change spin direction gradually over N (infinite ideally) atoms with an angle ϕ between them [5].

On the other hand the crystal anisotropy energy is minimum while the magnetic moments are aligned in easy directions, so it tries to make the wall as narrow as possible in order to reduce the number of spins pointing in non-easy direction.

Consequently, the domain wall has a non-zero width and a definite structure that was first examined by F.Bloch in 1932 and therefore is called Bloch wall [5].

2.3.4. Magnetoelastic Energy and Spontaneous Magnetostriction

The atomic moment interaction, also produce forces between atoms that tends to strain the lattice anisotropically [6]. A magnetic body is deformed due to

the magnetic interaction; this deformation is explained by an asymmetric tensor of elastic distortion. This effect may be observed if a sample containing a single crystal is heated above its Cure temperature and then cooled, The Curie Temperature is the temperature at which point all ferromagnets become paramagnetic at this temperature the permeability of a ferromagnets drops suddenly and both coercivity and remanence become zero [1]. When the sample is cooled below the Curie temperature, it tries to restore the previous crystal structure and as a result it applies a spontaneous strain to the lattice, which is called spontaneous magnetostriction.

The spontaneous magnetostriction can be separated into two parts. The first term is an isotropic volume changes only dependent upon the magnitude of the spontaneous magnetization and the second part is a change of the shape of the lattice almost without any volume change [9].

The spontaneous magnetostriction along the direction of the domain magnetisation is equal to the saturation magnetostriction 'λs' and will cause Magnetoelastic energy 'E_λ', this can be calculated for an isotropic material using following equation:

$$E_\lambda = -\frac{3}{2}\,\lambda_s \sigma sin^2\theta \tag{2.5}$$

Where 'θ' is the angle between the direction of magnetisation and direction of the applied stress 'σ'.

The resultant magnetostrictive interaction for cubic crystals such as silicon iron, may be calculated by using the following equation that is widely known as the Becker-Döring equation [10].

$$\lambda = \frac{3}{2}\lambda_{100}\left(\alpha_1^2\beta_1^2 + \alpha_2^2\beta_2^2 + \alpha_3^2\beta_3^2 - \frac{1}{3}\right) + 3\lambda_{111}(\alpha_1\alpha_2\beta_1\beta_2 + \alpha_2\alpha_3\beta_2\beta_3 + \alpha_1\alpha_3\beta_1\beta_3) \quad (2.6)$$

Where α_1, α_2 and α_3 are the direction cosines of the magnetisation direction and β_1, β_2 and β_3 are the direction cosines of the strain-measurement direction with respect to the cube edges. λ_{100} and λ_{111} are the saturation magnetostriction constants in the [100] and [111] directions respectively.

2.4. Ferromagnetic Domain Structure

Weiss has suggested that the due to an interaction field between the atomic moments inside a ferromagnetic material that causes alignment of magnetic moments. As discussed previously a single domain would have large Magnetostatic energy, breaking large domains into smaller localized regions can minimize this energy by providing a better flux closure and eliminating the flux leakage. So the existence of domains is a result of energy minimization [11]. Figure 2-5 shows a schematic drawing of a single domain with high Magnetostatic energy due to the free pole effects at the edge of the domain, this energy can be reduced, the domain configuration shown on the right would give complete flux closure, and closure flux domains are formed at the end in order to lead the flux.

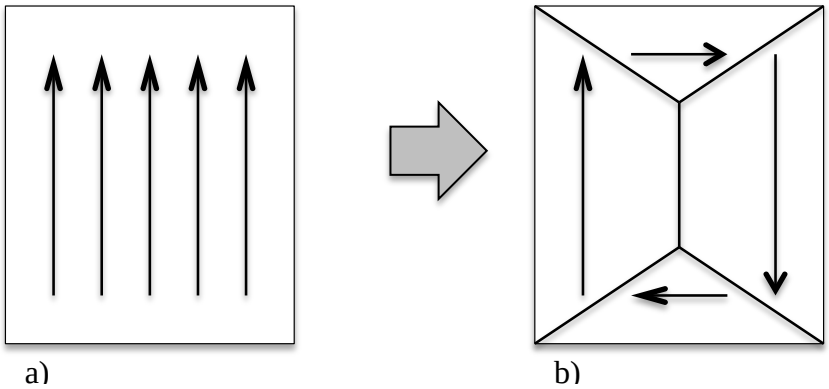

Figure 2- 5: Domain pattern in Ferromagnetic materials. a) Single domain. b) Fully closed structure

The closure domains have a magnetization parallel to the crystal surface. The existence of the closure domains would lead to an increase in the Magnetoelastic energy due to the increased strain in the crystal. As a result in order to minimize the Magnetoelastic energy, the domains continue to subdivide, reaching smaller closure domains and consequently smaller magnetoelastic energy. The subdivision will continues until the sum of the magnetoelastic and domain wall energies becomes a minimum [5].

The domain patterns of cubic crystal structure materials, such as silicon iron, tend to be more complicated due to the existence of different easy directions, also it is now possible for the flux to follow a closed path within the specimen so that no surface or interior poles are formed, and consequently the magnetostatic energy is reduced to zero. However, triangular domains are formed at the ends and, since they are paths by which the flux can close on itself, they are called closure domains [5].

In such a structure [100] and [010] closure domain would strain under magnetization due to the positive λ_{100} and the Magnetoelastic energy stored in them

is relative to their volume. Decreasing the width of the main domains can decrease the total closure-domain volume.

Ideally the structure results in domains being continuous across the grain boundaries. However, the variation in the angle of yaw from a {100} plane (shown in Figure 2-6, would result in free magnetic poles at the grain boundaries with an associated demagnetizing field. Due to the large anisotropy in the transverse domains of the cube on edge structures such domains as presented in Fig 2-5 cannot occur. As a result the resulting increase in Magnetostatic energy can be minimized by the appearance of oppositely magnetised ‘dagger’ domains as shown in Figure 2-6. These domains are commonly referred to as lancet or spike domains, and run through the thickness of the strip by transverse [010] or [001] domains that are oppositely magnetized and as a result the flux is closed and hence Magnetostatic energy minimized [12].

A similar domain structure may be seen at the grain boundaries in the rolling direction of the grain due to the free poles present at the surface of the strip, as the angle increase beyond 4^{o} the lozenge pattern “dragger structures” start to form along the [111] directions necessitated by the need to share the transverse closure structure [12, 13].

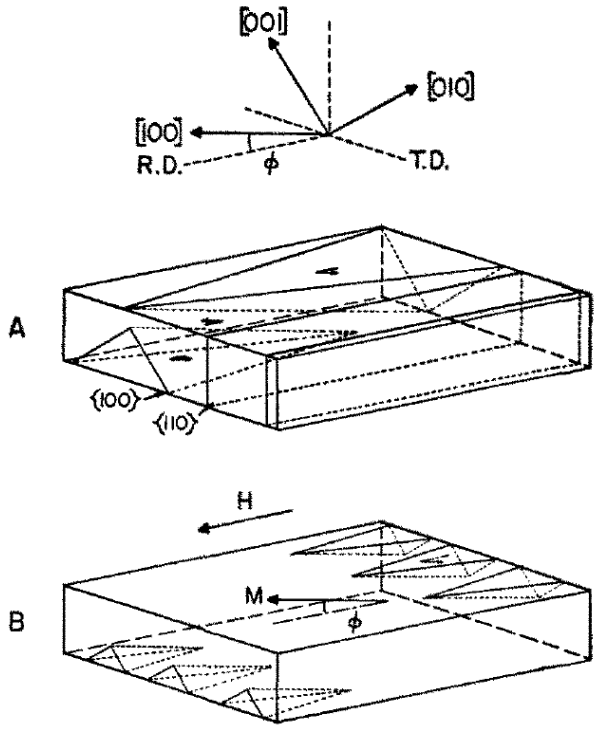

Figure 2- 6: proposed model by Paxton and Nilan for dagger domains. a) The grain in demagnetizing state b) filed applied in the [100] direction [12]

Figure 2-7 shows different domain structure and the effect of domain boundaries on the domain structure of cubic crystal materials. More complicated flux compensation domains are being formed with increasing the nominal magnetic charge (magnetic poles). As it discussed previously (2.3.2) the additional energy due to the formation of the extra domains can be reduced by reducing the basic domain width.

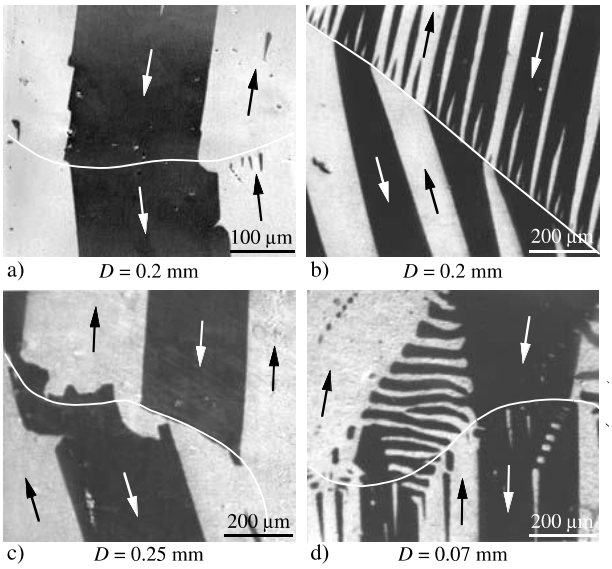

Figure 2- 7: a) perfect domain continuousness. b) Dagger domains c) closure domains by interior transverse domains d) quasi-closure-domains [14]

2.5. The Effect of Applied Field

An external magnetic field applied to ferromagnetic material results in a change in the minimum energy condition; hence the domain walls move in such a way to create Magnetostatic energy to counter-balance the energy from the slowly increasing field, i.e. the demagnetizing field balances the applied field, so the net magnetization is zero. This movement accrues by the 180^{o} and 90^{o} domain wall movement.

If the magnetic moments in the domains rotated out of the easy axes of magnetisation into the direction of applied field, would result in increase in Magnetocrystalline anisotropy energy, this would need higher applied field in order to rotate the magnetic moments to the magnetisation direction [15].

The ideal magnetisation curve for ferromagnetic material is shown in Figure 2-8, in order to process the domain wall movement regarding to

magnetizing field. Magnetic flux density can be presented as a function of magnetisation (M) and magnetic field (H) as follows:

$$B = \mu_0(H + M) \tag{2.7}$$

Where B is in Tesla, H and M are in amperes per meter and $\mu_0 = 4\pi\times10-7$ is permeability of free space [16].

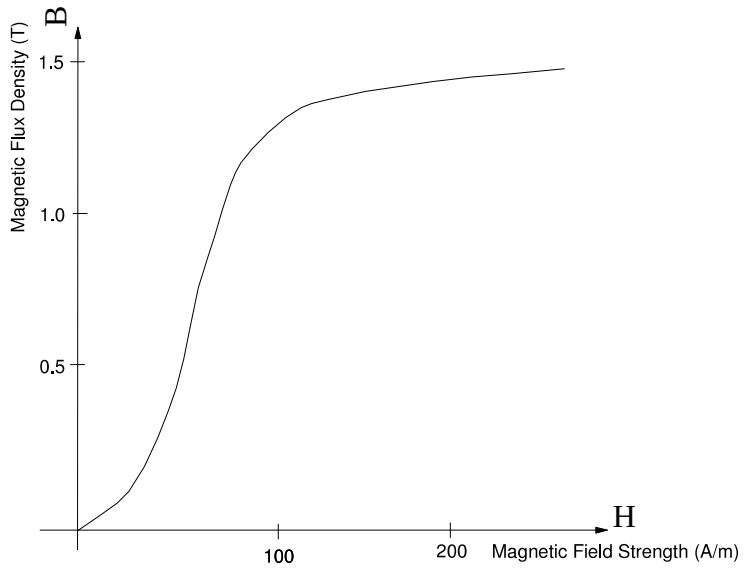

Figure 2- 8: Ideal magnetization curve of a ferromagnetic material [13]

Moreover, the magnetic polarization (J) would be zero in free space as a result the magnetic flux density in ferromagnetic materials such as silicon iron can be written as

$$J = \mu_0 M$$
$$x = \frac{M}{H}$$
$$B = \mu_0 \mu_r H \tag{2.8}$$

Where μ_r is the dimensionless relative permeability of the material, x is susceptibility. From Figure 2-8 can be seen that the domain wall motion is reversible whereas, in materials such as silicon steel due to the domain wall pining

this would be irreversible, i.e. the magnetisation would not return to zero if the field is reduced to zero from saturation and there would be some remanence. This is as a result of sites including impurities and dislocations that pin the moving domain wall till the magnetic field is increased sufficiently to overcome it. This opposed field required to reduce the net magnetisation to zero is called the coercive force H_c. The existence of these pinning sites is causing local differences in Magnetoelastic, wall and Magnetostatic energies in material. Figure 2-9, shows the Hysteretic Magnetisation Characteristic for grain oriented silicon steel and the changes of domain structure during magnetisation.

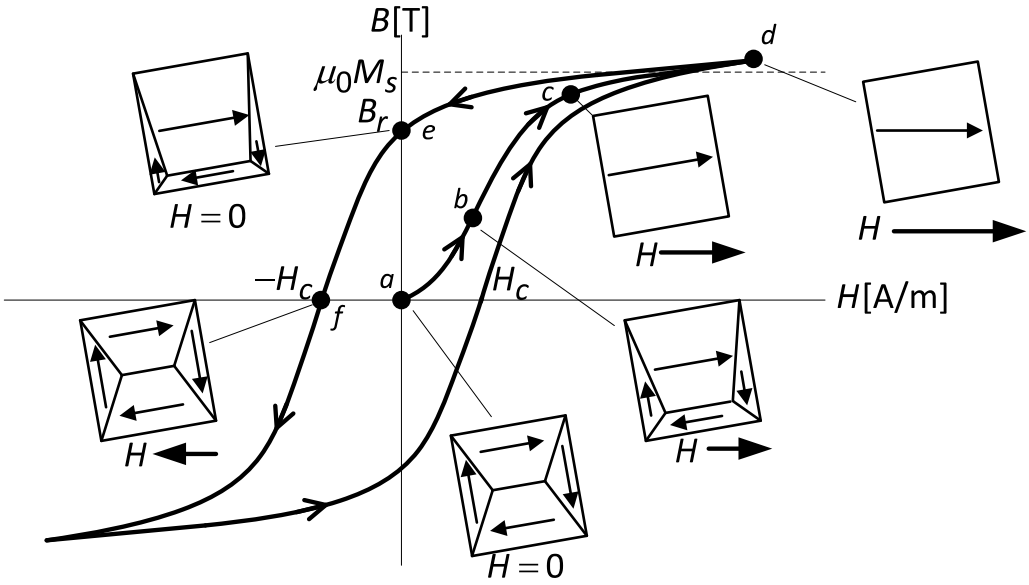

Figure 2- 9: Hysteretic Magnetisation Characteristic for grain oriented silicon steel and the changes in domain structures during the magnetisation process

2.6. Magnetostriction under Applied Field

Magnetic domains of silicon iron are strained in the direction of spontaneous magnetisation as explained previously. As a result any rearrangement of the domain structure may cause a change in the net strain of the material. This could be caused by the application of an external energy such as applied field. The effect appears by applying an external field along the axis of grain, which contains closure domains with 90^{o} walls, this would cause the domains in the direction of the field to rotate to the direction of the applied field and grow. A schematic drawing if the effect is shown in Figure 2-10.

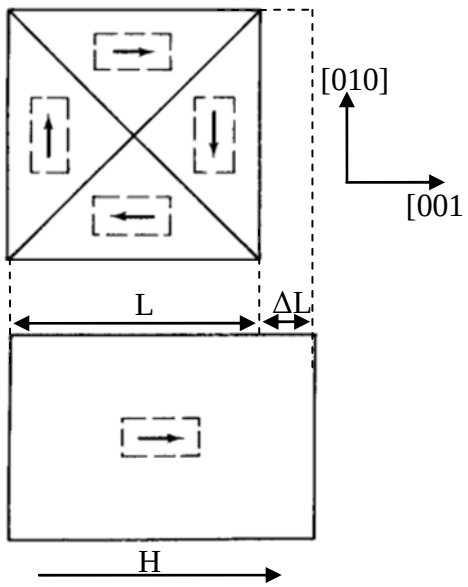

Figure 2- 10: Schematic drawing of a single domain magnetisation, magnetised in the easy direction [5]

The change in the magnetostrictive strain, $\Delta\lambda$, can be calculated using Becker Döring equation, by subtracting the final stage, which is the stage where all the domains are being converted to [001] domains, from the first stage.

$$\lambda = \frac{3}{2}\lambda_{100}\left(\alpha_1^2\beta_1^2 + \alpha_2^2\beta_2^2 + \alpha_3^2\beta_3^2 - \frac{1}{3}\right) + 3\lambda_{111}(\alpha_1\alpha_2\beta_1\beta_2 + \alpha_2\alpha_3\beta_2\beta_3 + \alpha_1\alpha_3\beta_1\beta_3) \quad (2.9)$$

Where λ_{100} and λ_{111} are the saturation magnetostriction constants in the [100] and [111] directions respectively, α_1, α_2 and α_3 are the direction cosines of the magnetisation direction and β_1, β_2 and β_3 are the direction cosines of the strain measurement direction with respect to the cube edge [10].

When samples are magnetised in their rolling direction, they have 180° domain wall movement mechanism where only the $[00\bar{1}]$ rotates into [001] as a result $\Delta\lambda$ can be calculated by subtracting the final stage by the starting stage. In the starting point (the $[00\bar{1}]$) $\alpha_1=\alpha_2=0$ and α_3 is equal 1, whereas in the final stage the $\alpha_3 = -1$. The values of β stay constant in both stages. As a result the overall Δλ would be zero.

$$\Delta\lambda = \lambda_{final} - \lambda_{initial} = \frac{3}{2}\lambda_{100}\left((-1)^2\beta_3^2 - \frac{1}{3}\right) - \frac{3}{2}\left((1)^2\beta_3^2 - \frac{1}{3}\right) = 0 \quad (2.10)$$

On the other hand, when samples are magnetised transverse to their easy direction ([010] domain) 90° domain wall motion would accrue, in this case the $\alpha_2 = \alpha_3 = 0$ and α_1 is equal 1 and in the final stage (all domains are rotated to the magnetising direction) $\alpha_1 = \alpha_2 = 0$ and α_3 is equal 1. Thus $\Delta\lambda$ can be calculated as follows:

$$\Delta\lambda = \lambda_{final} - \lambda_{initial} = \frac{3}{2}\lambda_{100}\left((1)^2\beta_3^2 - \frac{1}{3}\right) - \frac{3}{2}\lambda_{100}\left((1)^2\beta_1^2 - \frac{1}{3}\right)$$

$$= \frac{3}{2}\lambda_{100}(\beta_3^2 - \beta_1^2) \quad (2.11)$$

Then $\beta_1=1$ and $\beta_3=0$ for a perfectly oriented, Goss textured. Therefore the change in the magnetostriction is given by:

$$\Delta\lambda = \frac{3}{2}\lambda_{100} \tag{2.12}$$

So it can be said that 90° domain wall motion is the primary reason of magnetostriction in the Goss textured materials. Consequently in order to minimize the magnetostriction of a material, the volume of supplementary [010] [100] closure structure must be minimized.

References for Chapter 2

1. Jiles, D., *Introduction to magnetism and magnetic materials*. 2nd ed. 1998, London: Chapman & Hall. xxvii, 536 p.
2. Weiss, P., *The variation of ferromagnetism with temperature.* Comptes Rendus Hebdomadaires Des Seances De L Academie Des Sciences, 1906. **143**: p. 1136-1139.
3. Beckley, P., *Electrical steels : a handbook for producers and users*. 2000, Newport, Wales: European Electrical Steels. Various pagings.
4. Honeycombe, R.W.K., *Steels : microstructure & properties*. Metallurgy and materials science series. 1980: Edward Arnold.
5. Cullity, B.D., *Introduction to magnetic materials*. Addison-Wesley series in metallurgy and materials. 1972, Reading, Mass. ; London: Addison-Wesley. xix,p. 666-667.
6. Shilling, J.W. and G.L. Houze Jr, *MAGNETIC PROPERTIES AND DOMAIN STRUCTURE IN GRAIN-ORIENTED 3% Si-Fe.* IEEE Transactions on Magnetics, 1974. **MAG-10**(2): p. 195-223.
7. Chikazumi, S.o., *Physics of magnetism*. 1978, Huntington, N.Y: Krieger. xii,554p.
8. Brown Jr, W.F. and A.E. Labonte, *Structure and energy of one-dimensional domain walls in ferromagnetic thin films.* Journal of Applied Physics, 1965. **36**(4): p. 1380-1386.
9. Sato, H., *Magnetostriction and elastic properties of ferromagnetic substances at high magnetic fields.* Journal of Applied Physics, 1958. **29**(3): p. 456-458.
10. Becker, R., *Ferromagnetismus*. 1939, Berlin: Julius Springer.
11. Landau, L.D., *On the theory of the dispersion of magnetic permeability of ferromagnetic bodies.* physik Z, 1935. **8**: p. 145-169.
12. Paxton, W.S. and T.G. Nilan, *Domain configurations and crystallographic orientation in grain-oriented silicon steel.* Journal of Applied Physics, 1955. **26**(8): p. 994-1000.
13. Anderson, P., *A Novel Method of Measurement and Characterisation of Magnetostriction in Electrical Steels*, 2001 Cardiff of Wales
14. Hubert, A. and R. Schäfer, *Magnetic domains : the analysis of magnetic microstructures*. 1998, Berlin ; New York: Springer. xxiii, 696 p.
15. Williams, H.J. and W. Shockley, *A simple domain structure in an iron crystal showing a direct correlation with the magnetization.* Physical Review, 1949. **75**(1): p. 178-183.
16. Jiles, D.C. and D.L. Atherton, *Theory of ferromagnetic hysteresis (invited).* Journal of Applied Physics, 1984. **55**(6): p. 2115-2120.

Chapter 3: Domain structure under applied stress

It has been known that the magnetic properties of ferromagnetic materials such as permeability, magnetostriction, power loss, etc. are sensitive to mechanical stress .The ferromagnetic domain pattern of a crystal, which is an indicator of its magnetic properties, changes with changes of strain of the crystal due to the applied stress and as long as the applied stress is within the elastic range of the material the original pattern returned after unloading the applied stress [1].

When an external stress is applied to material it would change the Magnetoelastic energy to the free energy of a crystal, the Magnetoelastic energy introduced for a cubic structure such as silicon steel can be calculated from [2]:

$$E = -\frac{3}{2}\lambda_{100}\sigma\left(\alpha_1^2\beta_1^2 + \alpha_2^2\beta_2^2 + \alpha_3^2\beta_3^2 - \frac{1}{3}\right) \\ -3\lambda_{111}\sigma(\alpha_1\alpha_2\beta_1\beta_2 + \alpha_2\alpha_3\beta_2\beta_3 + \alpha_1\alpha_3\beta_1\beta_3) \quad (3.1)$$

This Chapter presents the detailed changes in domain pattern of grain-oriented silicon-iron under applied stress.

3.1. Domain structure under in plane applied stress

3.1.1. Tensile Stress in the Rolling Direction

A tensile stress applied parallel to the rolling direction of grain oriented silicon steel has little effect on a well-oriented grain as most of the domains are aligned in the [001] direction, as $\alpha_2 = \alpha_3 = 0$ and $\alpha_1 = 1$ also $\beta_2 = \beta_3 = 0$ and $\beta_1 = 1$, hence the Magnetoelastic energy is reduced ($-\lambda_{100}\sigma$). Whereas, supplementary domains (the [010] or [100] domains) attached to the main domain will be refined the domain wall spacing decreases [3]. As a result domains along the rolling

direction grow as the expense of the transverse domains as they are energetically favourable. The decrease in wall spacing reaches it optimum and after a certain value domains will start narrowing in order to reduce the demagnetizing field [4].

3.1.2. Longitudinal Compressive Stress

The effect of in plane compressive stress applied in the rolling direction can also be calculated from Magnetoelastic energy. In this case the $\alpha_2 = \alpha_3 = 0$ and $\alpha_1 = 1$ also $\beta_1 = \beta_3 = 0$ and $\beta_2 = 1$ so the Magnetostatic energy reduces to ($E = \lambda_{100}\frac{\sigma}{2}$). The positive sign of the equation indicates that the [010] and [100] directions are energetically favourable. Therefore the domain pattern reorganizes in order to reduce the overall energy by increasing the volume of supplementary, these type of domains was first observed by Dijkstra and Martius [1] .Two distinct patterns were within the elastic range of the material; these were named Stress Pattern I and Stress Pattern II. Stress Pattern I is the simplest of the two structures and appears first when the domain is under compressive stress, a schematic drawing of the Stress Pattern I is shown in Figure 3.1.

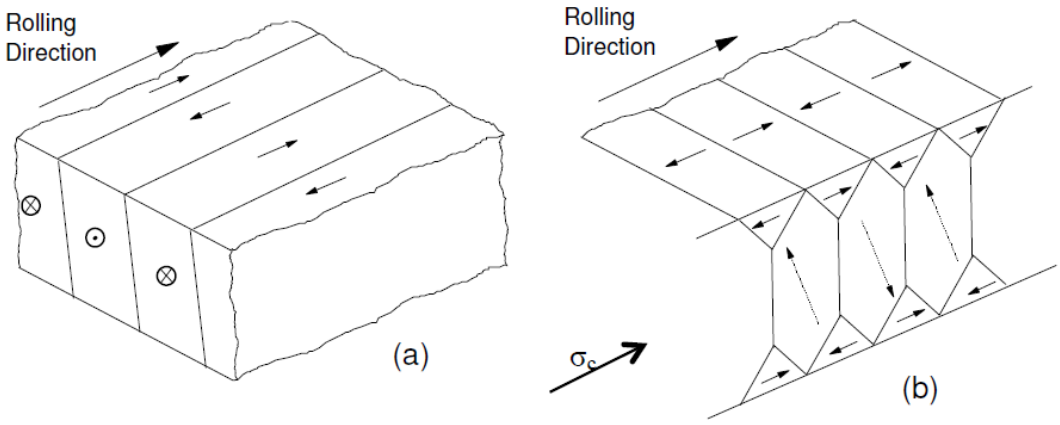

Figure 3- 1: Effect of compressive stress along rolling direction a) unstressed b) Stress Pattern I

The main domains under Stress Pattern I consist of [100] domains with small triangular [001]-closure domains. By increasing the compressive stress the Magnetoelastic energy increases, which causes the expansion of the [100] main domains by decreasing the volume of the closure [001] domains. Consequently with increasing compressive stress the bulk domain wall spacing increases in order to reduce the Magnetoelastic energy. In Stress Pattern I, the main domains wall energy and the closure domain spacing increases with an increase in the applied stress [5].

Under higher compressive stresses, Stress Pattern II forms, this has a more complex pattern. The transition between Stress Pattern I and Stress Pattern II was first suggested by Corner and Mason [5]. It was suggested that the main domain in Stress Pattern II is still in the same [100] direction but the domain walls change from 90^{o} to the [010] direction. Figure 3.2 shows graphic drawing of the Stress Pattern II.

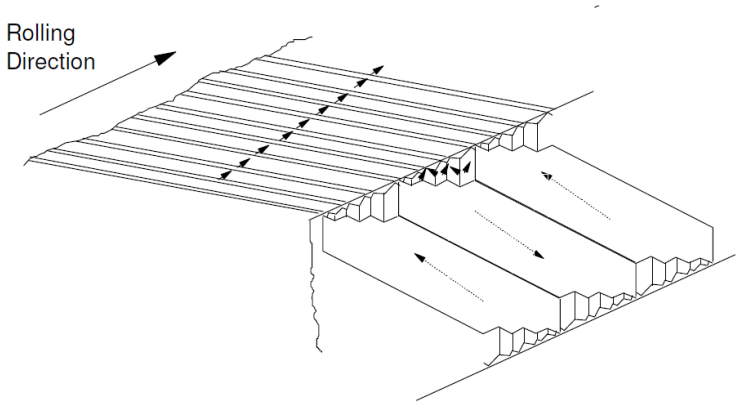

Figure 3- 2: Stress Pattern II for a typical grain oriented silicon steel [6]

Moreover, it was proposed by Corner and Mason that in Stress Pattern II, the domain wall energy reduces with increasing compressive stress. The closure domain structure in Stress Pattern II can be spotted on the surface of a material as

typical zigzag patterns. This transition usually happens at a compressive stress of 2 to 3 MPa [6].

3.1.3. Applied stress in the transverse direction

It was observed by Dijkstra that the domain pattern formed under tensile stress applied in the transverse direction is identical with the one formed under compressive stress along the rolling direction as shown in Figure 3-3. The main [001] domains switch to [100] or [010] directions which have an angle of 45° with the [110] direction, because due to the high energy needed domains cannot rotate. Therefore in order to minimize the energy they align along other easy directions in crystal.

Moreover, Banks and Rawlinson proposed that transverse stress has the same effect on the grain oriented silicon steel as longitudinal compressive stresses of half the magnitude[7]. Also compressive stress applied in the normal direction to the surface will have an identical effect as a tensile stress applied in the rolling direction and vice versa.

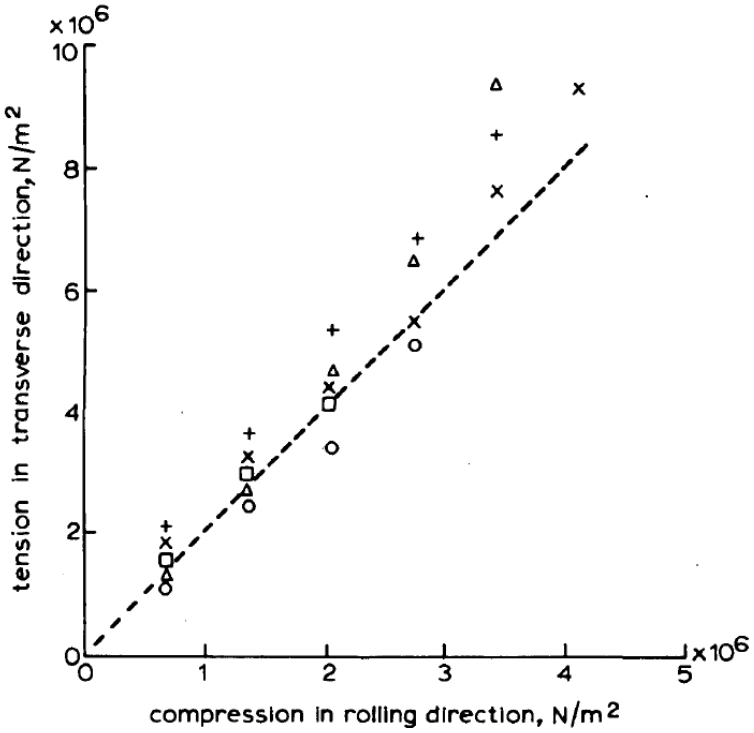

Figure 3- 3: Tensile "stress in the transverse direction against compression in rolling direction. It shows that both produce the same effect [8]

3.2. The effect of a magnetic field on domain structure under applies stress

The stress affects the Magnetoelastic energy of the domains, which results in domain reorientation. Applying an external magnetic field causes domain wall movement so that the volume of the domains closest to the field direction increases. Figure 3-4 shows a schematic drawing of the effect of applied field and stress on a domain structure of Grain Oriented silicon steel. In this section the effect of external magnetic field on the magnetic domain structures under applied stress is considered.

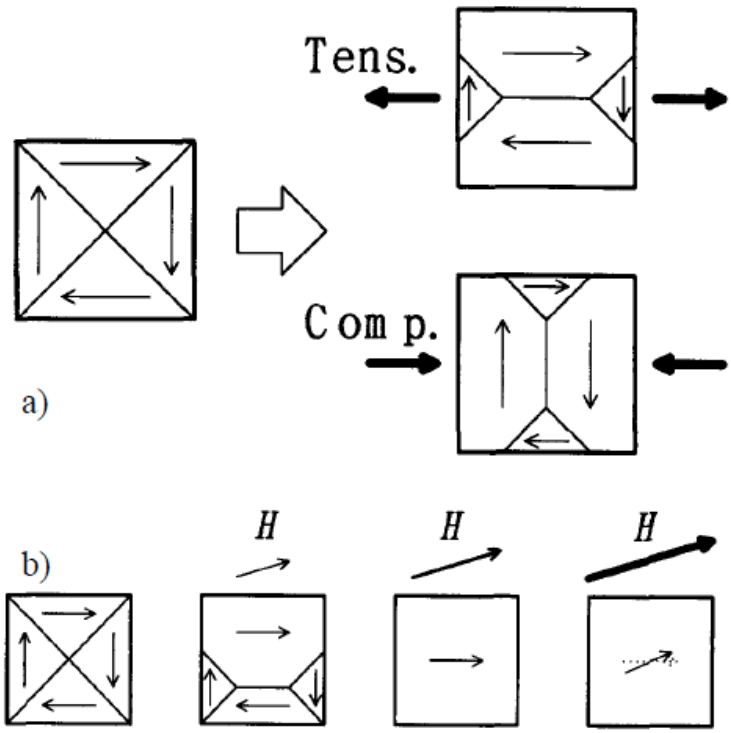

Figure 3- 4: a) Effect of applied stress on domain structure b) Domain reorientation by external magnetic field

3.2.1. Domain structure under longitudinal Tensile Stress

Due to the reduction of the supplementary transverse domains under applied longitude tensile stress, the overall miss-orientation is improved and hence the similar Stress Pattern can be found to that in an ideal unstressed condition Figure 3-5 shows the effect of applied tensile stress on domain wall spacing. At high fields i.e. above 1 Tesla, the magnetisation can have different effects, once the previously removed supplementary domains due to the applied stress reappears in order to reduces the Magnetostatic energy [4].

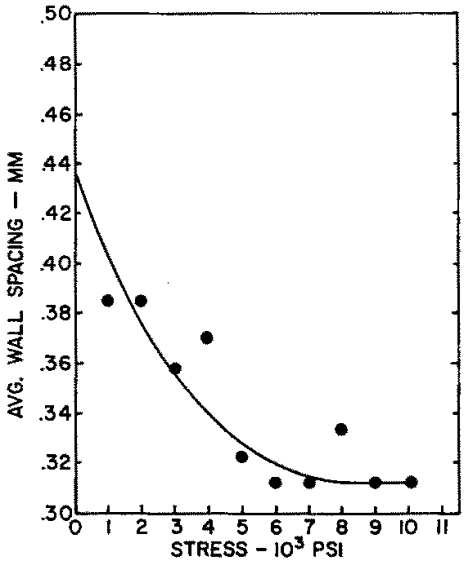

Figure 3- 5: Effect of longitude tensile stress on domain wall spacing of grain oriented silicon steel [9]

By increasing the magnetic field the domain wall movement and hence Magnetostatic energy increases until the Magnetostatic energy and Magnetoelastic energy can be reduced by the re-appearance of supplementary domains. This would cause the permeability of a material to decrease under tension[9].

3.2.2. Domain structure under longitudinal compressive Stress

Increasing compressive stress along the rolling direction generates characteristic stress patterns I and II that makes the [100] domain energetically favourable due to decreasing Magnetoelastic energy. Applying a magnetic field and compressive stress in the [001] direction causes 90^{o} domain wall movement and as a result makes it harder for [100] domain to switch to the [001] direction[5]. Figure 3-6 shows the effect of compressive stress on the B-H loops of grain oriented silicon steel.

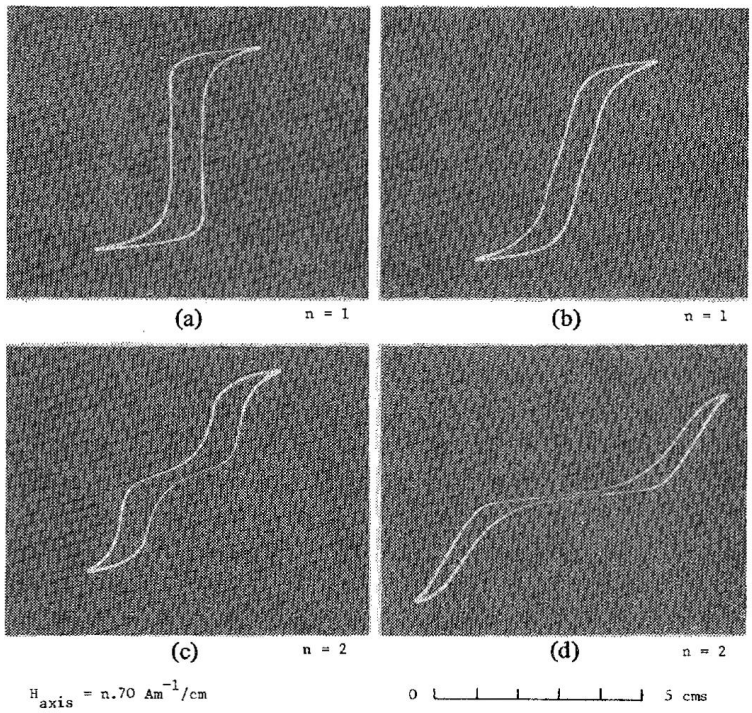

Figure 3- 6: effect of applied stress on the magnetic properties of Goss textured silicon steel. (1.5T 50Hz) a) Zero stress b) Tension 20MPa c) Compression 10MPa d) compression 40 MPa [10]

3.3. Effect of stress on magnetostriction of grain oriented silicon steel

The magnetostriction of grain oriented electrical steel is sensitive to applied stress and is often characterized by stress sensitivity curve. A typical magnetostriction curve under stress is shown in Figure 3-7. These changes are due to the changes made to the domain structure under applied stress and in particular 90^{o} domain wall movement.

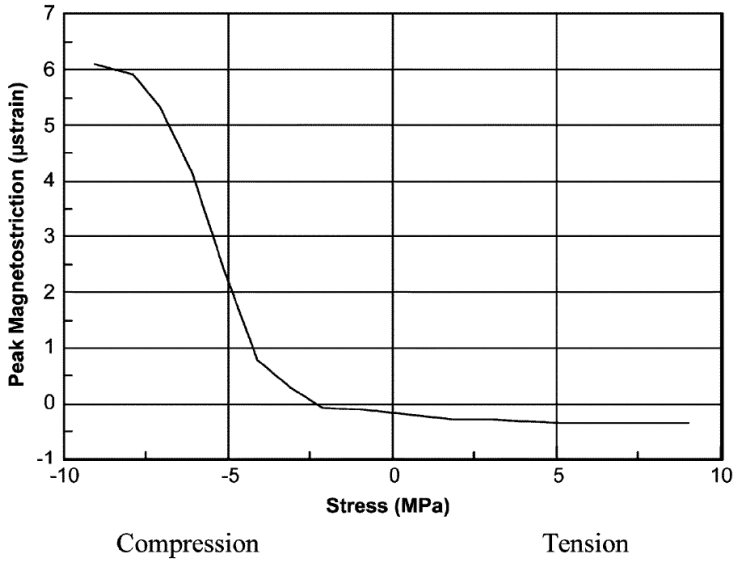

Figure 3- 7: typical magnetostriction vs. stress curve for grain oriented silicon steel in the rolling direction (1.5 T, 50 Hz) [11]

3.3.1. Domain structure under longitudinal tensile stress

As described in section 3.2.1 the transverse supplementary domains, which were previously removed by applied tension, reappear during magnetisation process. The reorganization from longitudinal domains to transverse supplementary domains leads to small negative magnetostriction, which increases with increasing applied tension till all the supplementary structure has been removed as shown in Figure 3-4.

3.3.2. Domain structure under longitudinal compressive Stress

As explained in section 3.1.2 stress patterns occur in grain oriented silicon steel under compressive stress applied along the rolling direction. The Magnetoelastic energy changes during magnetising process due to the removal of the [100] domains in the stressed stage to [001] domains. This conversion is causing the positive magnetostriction in Goss textured silicon steels.

The magnetostriction versus stress characteristic for conventional grain oriented steel is shown in Figure 3-7. In a real material the typical misorientation of the domains from the rolling direction is 7^{o} for conventional grain oriented material, which causes the variation of the Magnetoelastic energy from grain to grain. Also due to the existence of internal stresses in the grain, which would cause the transition to the stress, pattern does not happen simultaneously in all grains.

Simmons and Thompson proposed a model that estimates the effect of applying a magnetic field to the stressed material [8]. The proposed model describes the transition to Stress Pattern I. Figure 3-8 shows a longitudinal section of the grain used for the model, where *'θ'* is the angle between the diagonal of the closure domain and the surface, *'d'* is the average width of the closure domains and *'t'* is the strip thickness.

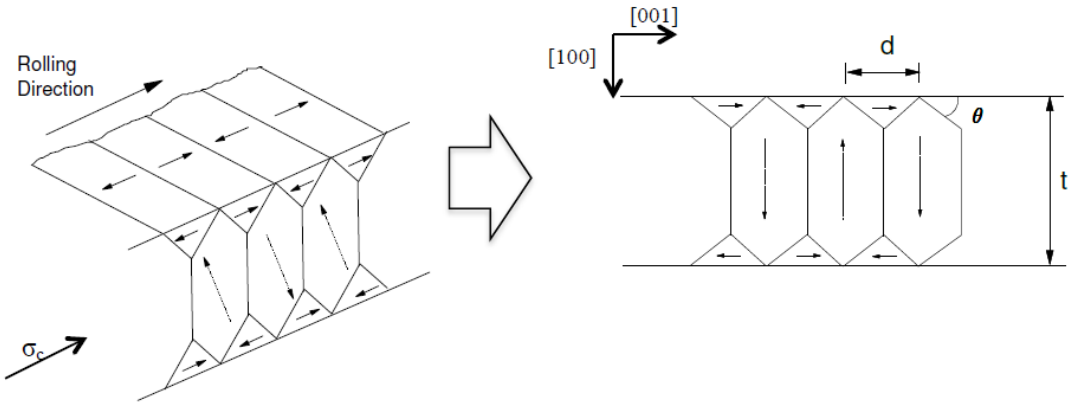

Figure 3- 8: Longitudinal section through a grain exhibiting Stress Pattern I

For simplicity of the model, the following assumptions were made

I. In the stressed condition all the grains have Stress Pattern I

II. The change to Stress Pattern I is immediate in all grains

III. The grains under compression only contains [001] and [100] domains.

IV. The single grain has a misorientation angle from the rolling direction, θ, this value is a representative of the average angle of misorientation for the polycrystalline materials. The other angles such as dip are not included due to the simplicity.

The volume fraction, V_f, of [001] closure domains can be calculated by multiplying V_f into the third dimension e.g. width

$$V_f = 2 \times \frac{d}{2} \times \frac{d}{2} \tan\theta \times \frac{1}{d \times t}$$

$$= \frac{d}{2t} \tan\theta \tag{3.2}$$

The magnetostriction in each domain may be calculated by using the above equation. For the closure domains along the [001] direction the equation may be simplify by putting $\alpha_1=\alpha_2=0$, $\alpha_3=1$, and $\beta_3= Cos\ \phi$. Hence magnetostriction would be

$$\lambda_{closure} = \frac{3}{2}\ \lambda_{100}(cos^2\phi - \frac{1}{3}) \tag{3.3}$$

And respectfully for the bulk domains along the [100] direction it may be calculated by putting $\alpha_1=1$, $\alpha_2=\alpha_3=0$, and $\beta_3=sin\ \phi$

$$\lambda_{bulk} = \frac{3}{2}\ \lambda_{100}(sin^2\phi - \frac{1}{3}) \tag{3.4}$$

By summing the magnetostriction of these, the initial magnetostrictive strain may be calculated; as it was assumed that the domain structure is completely Stressed Pattern I.

$$\lambda = \frac{3}{2}\lambda_{100}\left(cos^2\phi - \frac{1}{3}\right)V_f + \frac{3}{2}\lambda_{100}\left(sin^2\phi - \frac{1}{3}\right)(1 - V_f)$$

Then by subtracting V_f from equation (3.2) into the equation

this can be further simplified into,

$$\lambda = \frac{3d}{2t}\lambda_{100}(tan\phi \times \cos(2\phi)) + \frac{3}{2}\lambda_{100}\left(sin^2\phi - \frac{1}{3}\right) \quad (3.5)$$

It is assumed that each grain is compromised of only one [001] domain aligned in the magnetisation direction when the sample is magnetically saturated at magnetic flux density of B_s, then the volume fraction of [001] domains at a magnetic flux density of B may be calculated as

$$V_f' = \frac{B}{B_s}\cos\phi \quad (3.6)$$

So by subtracting this value the final magnetostrictive strain can be written as

$$\lambda = \frac{3}{2}\lambda_{100}\left(cos^2\phi - \frac{1}{3}\right)V_f' + \frac{3}{2}\lambda_{100}\left(sin^2\phi - \frac{1}{3}\right)(1 - V_f')$$

Then subtracting V'_f from equation (3.6) into the equation

this can be further simplified into,

$$\lambda = \frac{3B}{2B_s}cos\,\phi\,\lambda_{100}\left(cos^2\phi - \frac{1}{3}\right) + \frac{3}{2}\lambda_{100}\left(sin^2\phi - \frac{1}{3}\right) \quad (3.7)$$

The magnetostriction of a sample under applied field can be calculated as

$$\lambda_{measured} = \lambda_{final} - \lambda_{initial}$$

$$= \left[\frac{3B}{2B_s} cos\,\phi\,\lambda_{100}\left(cos^2\phi - \frac{1}{3}\right) + \frac{3}{2}\lambda_{100}\left(sin^2\phi - \frac{1}{3}\right)\right] - \left[\frac{3d}{2t}\lambda_{100}(tan\phi \times \cos(2\phi)) + \frac{3}{2}\lambda_{100}\left(sin^2\phi - \frac{1}{3}\right)\right]$$

Then,

$$\lambda_{measured} = \frac{3}{2}\lambda_{100}\cos 2\phi \ \left(\frac{B}{B_s}\cos\phi - \frac{d}{2t}\tan\phi\right) \quad (3.8)$$

This equation (3.8) can be used to estimate the saturation magnetostriction based on misorientation, change in the closure domains, and magnetic flux density. However the use of this equation is limited, as the values for *d*, and ϕ must be found by experimental domain observations for each stress.

3.4. Effect of stress on loss of grain oriented silicon steel

The power loss values of grain oriented silicon steel changes under stress due to the change in the domain structure. As it was mentioned in section 3.1.1 the application of a tensile stress along the rolling direction would cause the [001] domains grow as the expense of the transverse domains as they are energetically favourable, therefore improves the net misorientation of the material and improve the loss [12]. Figure 3-9 shows the effect of tension stress applied in the rolling direction at different frequencies.

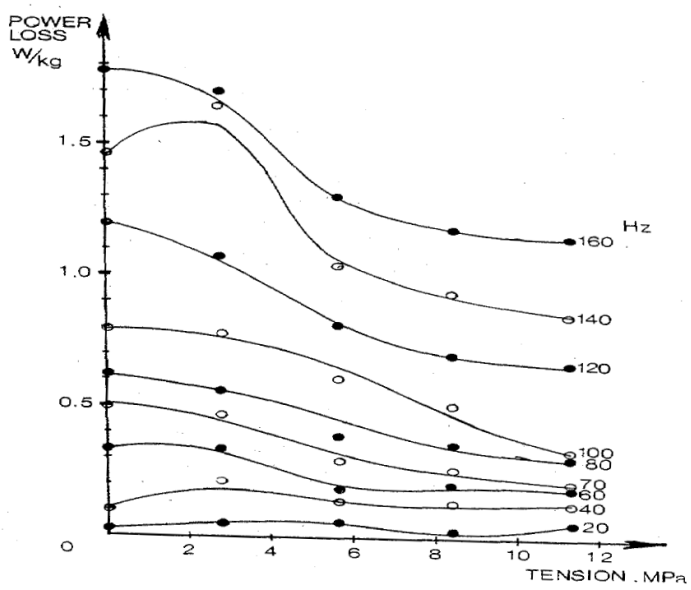

Figure 3- 9: effect of tension stress on power loss of grain oriented silicon iron at different frequencies [13]

On the other hand, as it was pointed out in section 3.1.2 application of compressive stress to the sample would generate Stress Pattern I and II which when magnetised, cause magnetostriction. The effect of compressive stress on the domain structure is shown in Figure 3-1 (b), which would cause an increase in power loss as in order to magnetize the stress structure, considerable domain rotation must occur and the domain walls must move further and faster than in the unstressed state [10]. Moses, A.J., et al. [10] claimed that the constriction of the B-H loop was occurring at a critical compressive stress that is independent of flux density and magnetizing frequency. He also proposed that the critical field (H_{crit}), a magnetic field occur to magnetize the compressive sample, is proportional to the applied compressive stress and can be calculated from

$$H_{crit} = {(3\lambda_{100}\sigma)}/{2M} \tag{3.9}$$

Where *'σ'* is the applied stress and *'M'* is the magnetization

References for Chapter 3

1. Dijkstra, L.J. and U.M. Martius, *Domain pattern in silicon-iron under stress.* Reviews of Modern Physics, 1953. **25**(1): p. 146-150.
2. Becker, R., *Ferromagnetismus*. 1939, Berlin: Julius Springer.
3. Moses, A.J., *Effects of stresses on magnetic properties of silicon-iron laminations.* Journal of Materials Science, 1974. **9**(2): p. 217-222.
4. Shilling, J.W. and G.L. Houze Jr, *MAGNETIC PROPERTIES AND DOMAIN STRUCTURE IN GRAIN-ORIENTED 3% Si-Fe.* IEEE Transactions on Magnetics, 1974. **MAG-10**(2): p. 195-223.
5. Corner, W.D. and J.J. Mason, *The effect of stress on the domain structure of Goss textured silicon-iron.* British Journal of Applied Physics, 1964. **15**(6): p. 709-718.
6. Anderson, P., *A Novel Method of Measurement and Characterisation of Magnetostriction in Electrical Steels*, 2001 Cardiff of Wales
7. Banks, P.J. and Rawlinso.E, *Dynamic Magnetostriction and Mechanical Strain in Oriented 3 Per Cent Silicon-Iron Sheet Subject to Combined Longitudinal and Transverse Stresses.* Proceedings of the Institution of Electrical Engineers-London, 1967. **114**(10): p. 1537-&.
8. Simmons, G.H. and J.E. Thompson, *Magnetic properties of grain- oriented silicon iron- 5.* Proceedings of the Institution of Electrical Engineers, 1971. **118**(9): p. 1302-1306.
9. Houze Jr, G.L., *Effect of longitudinal tensile stress on the static and 60 Hz domain structures of grain-oriented silicon steel.* Journal of Applied Physics, 1969. **40**(3): p. 1090-1091.
10. Moses, A.J., et al., *Influence of compressive stress on magnetic properties of commercial.* Magnetics, IEEE Transactions on, 1980. **16**(2): p. 454-460.
11. Anderson, P.I., A.J. Moses, and H.J. Stanbury, *Assessment of the stress sensitivity of magnetostriction in grain-oriented silicon steel.* IEEE Transactions on Magnetics, 2007. **43**(8): p. 3467-3476.
12. Yamamoto, T. and T. Nozawa, *Effects of tensile stress on total loss of single crystals of 3% silicon-iron.* Journal of Applied Physics, 1970. **41**(7): p. 2981-2984.
13. Overshott, K.J. and G.E. Foot, *EFFECT OF TENSILE STRESS ON THE POWER LOSS OF 3% GRAIN-ORIENTED SILICON-IRON.* IEEE Transactions on Magnetics, 1982. **Mag-18**(6 Nor): p. 1496-1498.

Chapter 4: Methods of magnetostriction measurement

Magnetostriction, as mentioned in Chapter 2 is the change of the volume fraction of magnetic domains, $\Delta l/l$, which can be measured in the dynamic AC or DC magnetisation conditions. Magnetostriction under DC magnetisation is measured as the strain of the material when magnetising from the de-magnetised state to magnetic saturation. Due to the remanence in the material and complications of starting from the de-magnetising state, this type of measurement is difficult to perform.

Since the condition wherein the transformer is used is under AC magnetisation, and the interest is in the noise generated by a transformer then the AC measurement will be used. Below the definition of the principle terms that are used in magnetostriction measurement is given:

i. **Butterfly loop:** Hysteresis loop of the strain measured in the direction of applied field versus magnetic polarization.
ii. **Zero-to-Peak magnetostriction:** Net strain measured in the direction of applied field from zero magnetic polarization.
iii. **Peak-to-Peak magnetostriction:** strain measured in the direction of applied field under alternating magnetisation.

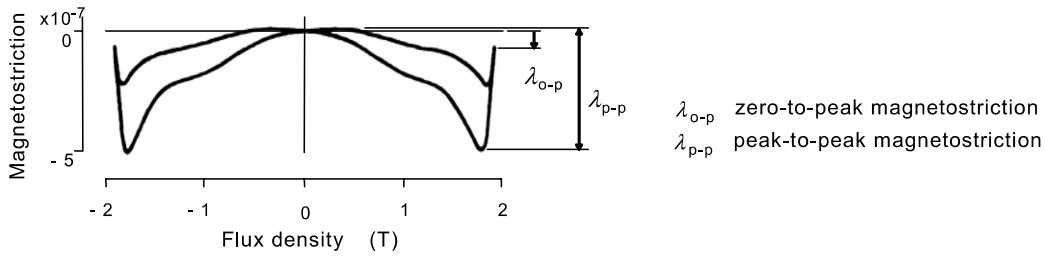

Figure 4- 1: typical magnetostriction butterfly loop of grain oriented silicon steel and the definition of zero-to-peak and peak-to-peak magnetostriction [1].

Figure 4-1 shows an example of the butterfly loop of grain oriented silicon steel with determination of zero-to-peak and peak-to-peak magnetostriction [1]. The value of peak magnetostriction for grain oriented silicon steel in on order of 10^{-6}, hence in order to measure such small displacement an extremely sensitive transducer is needed. The transducer is required to convert one form of energy to another and generate a signal. The measured parameter can be displacement or either the velocity or acceleration, which can be converted to displacement by single or double integration.

4.1. Vibration Measurement methods:

In this section several common methods of measuring vibration are discussed and their possible advantage and disadvantage is given.

4.1.1. Resistance strain gauge

The resistance strain gauge is one of the most broadly used techniques of measuring displacement [2-6]. As a transducer the electrical energy is supplied to the strain gauge and the physical effect modulates this energy. The simplest type is the wire gauge, which consists of a grid or coil winding of fine resistance wire wound on a paper and bonded into cement. The other type is the foil gauge, which consists of an epoxy-ethylene lacquer backing bonded to foil that is printed and etched to the required configuration [7].

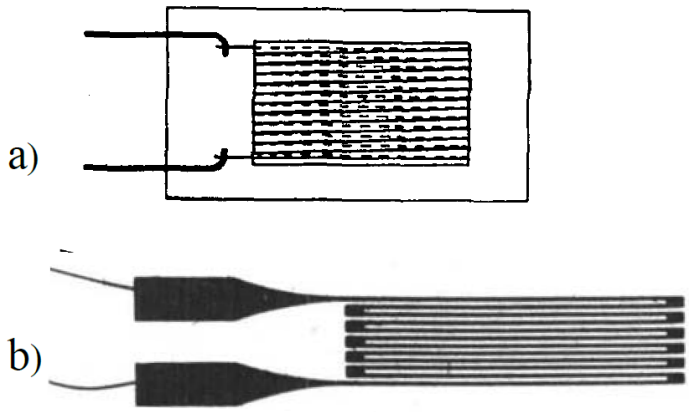

Figure 4- 2: Schematic drawing of the two types of resistance strain gauge a) wire strain gauge b) foil strain gauge

The gauge is fixed to the surface of the specimen therefore any strains in the specimen will be proportionally reproduced in the strain gauge. Due to the strain in the substrate the length of the gauge wire or foil is changed and, since the resistance is proportional to the length and inversely related to the cross sectional area, the resistance will change in proportion with the strain. For normal gauges the relation between the stain and the resistance may be written as:

$$\frac{\Delta R}{R} = K\varepsilon \tag{4.1}$$

Where K is a constant known as a gauge factor,

ε is the strain

The resolution of strain gauges is approximately in the range of 0.1×10^{-6} [5], which is a reasonable sensitivity for magnetostriction measurement of grain oriented silicon steel. Below some of the main advantages and disadvantages of this technique are given:

Advantage: Low cost, localized measurement, and high resolution

Disadvantage: time consuming exercise due to the preparation, very sensitive to the vertical vibrations and bending and also it is difficult to adjust the gauge in the required direction.

4.1.2. Linear variable differential transformers

The linear variable differential transformer (LDVT) is another widely used displacement transducer [8-10]. The LDVT is an electromechanical device, which generates electrical output that is proportional to the mechanical displacement. The device consists of a primarily excitation coil and two secondary coils that are connected in schematic of the technique is shown in Figure 4-3.

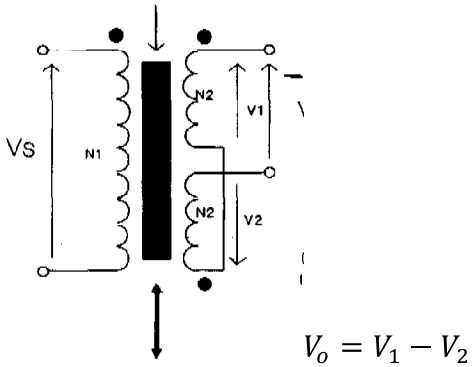

Figure 4- 3: Schematic of linear variable differential transformer [8]

The core is placed inside the coils at the centre. The central emitter coil (V_S) is magnetised with a sinusoidal signal at frequency between 10 to 20 KHz, and is fixed between the two secondary coils. The two secondary coils are identical. Movement of the core would cause a flux leakage in the secondary coils. When the core is moved away from the centre position, a differential voltage appears across the secondary coils and a sinusoidal signal appears on the receiver coils. The displacement can be measured with the use of a phase sensitive detector. If the coil is moved in the opposite direction the sign of the induced sinusoid is changed [9].

Advantage: Friction free measurement, high resolution, excellent linearity, low sensitivity to unwanted vibration

Disadvantage: sensor picks up a stray field during the measurement, difficult zero position adjustment

4.1.3. Capacitive displacement sensors

Capacitive displacement sensors generate an electrical signal as a result of the elastic deformation of a membrane. The common capacitive sensor consists of a set of plates, at least two plates, separated by a distance 'd' by a dielectric (usually air) [11]. One of the plates is attached to the free end of the lamination whilst the other one is fixed. Vibration in the sample produces a change of capacitance, as it will change the surface or the distance between the plates and can be calculated as[12]:

$$C = \varepsilon\left(\frac{A}{d \pm \Delta d}\right) \tag{4.2}$$

$$\frac{C}{C_0} \approx 1 - \frac{\Delta d}{d} \tag{4.3}$$

Where ε is the permittivity of the medium between the plates, A is the surface area and 'd' is the distance between the two plates, schematic of a simple capacitive is shown in Figure 4-4.

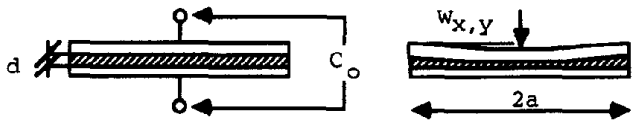

Figure 4- 4: Schematic drawing of a simple capacitor, consist of two plates separated by a dielectric [12].

In order to measure the change of capacitance, the capacitor plates form the tuned circuit of an oscillator. The change of frequency with reference to a fixed frequency oscillator finally generates a voltage signal, which is proportional to the change in length of the specimen [13]. The capacitive displacement sensors have a very high resolution of around 0.1×10^{-8} [14, 15].

Advantage: High resolution, non-contact measurement, low temperature sensitivity, relatively low cost

Disadvantage: shielding needed from stray electric fields, time consuming setting as each time the gap should be set, requires skill to set up the sensor accurately.

4.1.4. Piezoelectric displacement transducer

Another widely reported method of measuring displacement is the piezoelectric displacement transducer [16-18]. This type of transducer consists of a piezoelectric element, usually Barium Titanate, mechanically linked to a stylus such that a displacement of the stylus leads to a charge being developed across the element. A Schematic of a transducer assembly is shown in Figure 4-5.

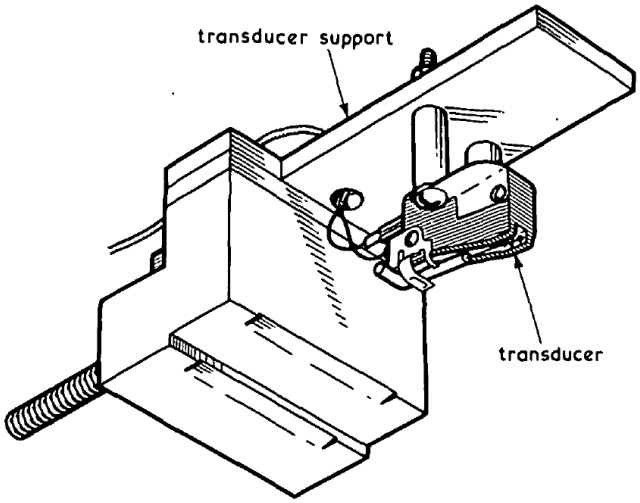

Figure 4- 5: Schematic of a Piezoelectric displacement transducer assembly[16]

For magnetostriction measurement, two transducers are placed on the sample with a known distance, as shown in Figure 4-6, the displacement between two points is obtained by subtracting the differential output of the two transducers. Brownsey and Maples [16] presented that the output of the transducer has a linear correlation to the peak displacement of the stylus for displacements in the range 10^{-9} to 10^{-5}cm with a resolution of 0. 2×10^{-8}. However this type of transducer has a high sensitivity to vibrations in the vertical and transverse directions that can be partially eliminated by using a stereo phonograph cartridge with the outputs connected in series [18].

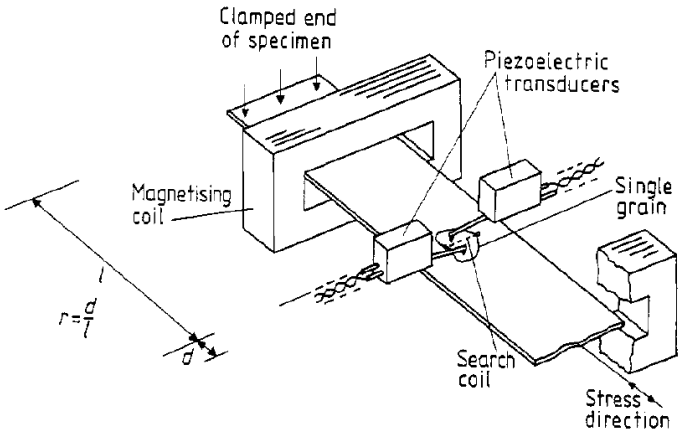

Figure 4- 6: schematic of the magnetostriction measurement system, using piezoelectric transducer technique [17]

Advantage: magnetostriction may be measured between well-defined points, high sensitivity, unaffected by magnetic field, low applied stress to the test specimen

Disadvantage: sensitive to vibration in other directions, direct contact of the sensor with the surface

4.1.5. Piezoelectric accelerometer

The piezoelectric accelerometer is been widely used in the field of industrial vibration measurement, such as magnetostriction measurement [17, 19-21]. The piezoelectric accelerometer consists of a piece of artificially polarized ferroelectric ceramic inserted inside a seismic mass in the housing of the accelerometer. These ceramic layers generate an electric charge when mechanically stressed, which is proportional to the applied force [22]. Cross section of a typical piezoelectric accelerometer is shown in Figure 4-7. The sensors are placed inside aluminium housings that provide shielding against stray electric fields.

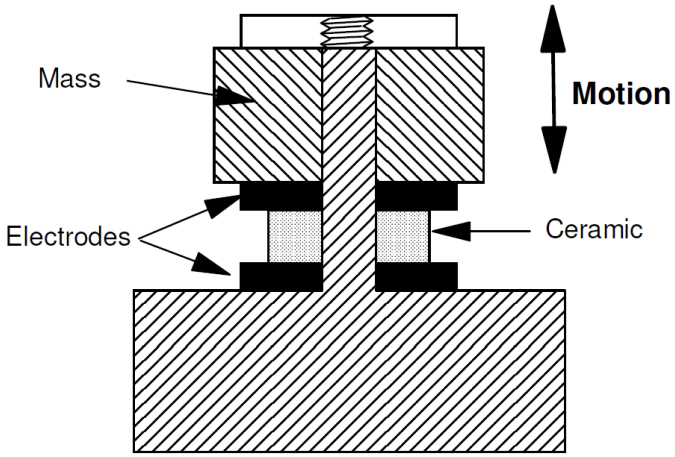

Figure 4- 7:Cross section of a typical piezoelectric accelerometer [23]

An Acceleration output signal is obtained by connecting the accelerometer to a charge amplifier, which converts the charge to voltage, and displacement by double integrating the signal [23]. Typically piezoelectric accelerometers have a resolution of $0.01\times10^{-6.}$ In order to eliminate the surrounding noise, two accelerometers may be used. The first, mounted on the clamp at the second one fixed to a reference point, the relative acceleration is obtained by subtracting the signals [21, 23].

Advantage: High resolution, low cost, low sensitivity to stray magnetic field, little sample preparation, low sensitivity to other directional vibration.

Disadvantage: direct contact with sample, which may affect zero stress measurements

4.1.6. Laser Doppler

The Laser Doppler velocimeter was first presented by Nakata et al [24] as a magnetostriction measurement technique. The velocity of the movement is measured by the Doppler effect of two mirrors mounted on the sample. Figure 4-8

shows the principle of the laser Doppler technique used for magnetostriction measurement by Nakata.

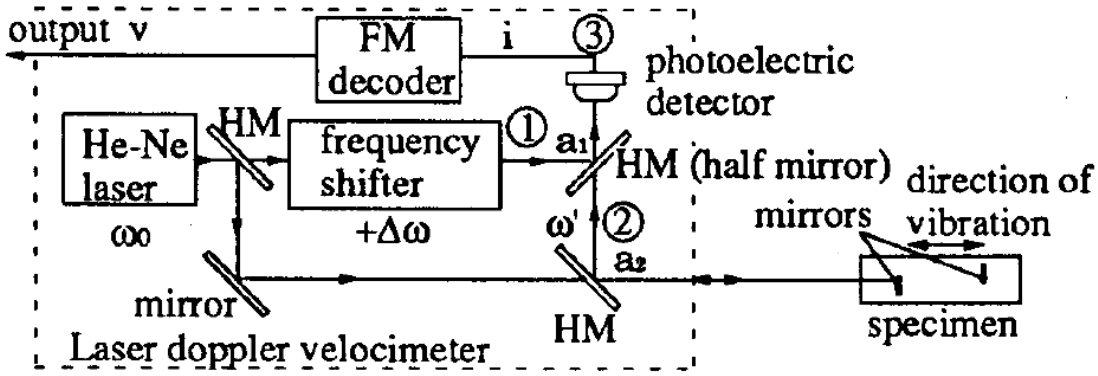

Figure 4- 8: principal of magnetostriction measurement by using the laser Doppler technique [25]

The laser beam is irradiated on the object, the reflected beam is detected by the measurement system, and the measured frequency shift of the wave is described as

$$\Delta f = 2v/\lambda \tag{4.4}$$

Where Δf is the frequency shift, v is the velocity of the object in the direction of the incident light, and λ is the wavelength of the light. In order to measure the velocity, the frequency shift has to be measured at a known wavelength; this can be measured by using laser interferometer. This works on the principle of optical interference, which requires two coherent light beams with different light intensities l_1 and l_2.

The first-order diffracted beam is used as a reference beam and the zero-order beam is focused on the target. The light beam scattered form the object and the frequency shifted reference beam interferes with the other at the surface of the photodiode. The resulting intensity is calculated form:

$$I = K\ (I_1 I_2)^{1/2} \cos(2\pi f_c t + \Phi) \quad (4.5)$$

Where *K* is a constant,

t is time

Φ depends on the optical path length difference between the reference beam and the target beam in time, which, when the object vibrates, is changing according to

$$\Phi = \Phi_0 + 2\pi\Delta f t \quad (4.6)$$

Φ_0 is the phase difference with the object, by substituting Φ in the overall intensity formula:

$$I = K\ (I_1 I_2)^{1/2} \cos(2\pi f_c t + 2\pi\Delta f t + \Phi_0) \quad (4.7)$$

From the formula it can be seen that the movement of the object will result in phase modulation in the signal. If this difference is an integer multiple of the laser wavelength, the overall intensity would be four times a single intensity. Respectively if the two beams have a path length difference of half a wavelength then the overall intensity would be zero [26].

Using two beam heads can eliminate the noise from the surroundings by subtracting measured vibration between the reflectors on the sample and the base [27, 28] and improving the resolution of the system to 0.04×10^{-6}.

Advantage: High three-dimensional resolution, high stability, a wide range of operating frequency and velocity, and are unaffected by magnetic field and temperature.

Disadvantage: Cost, as these systems are very expensive, direct contact of the mirrors with the sample surface, which may affect the zero, stress and also it's a time consuming process.

4.2. Magnetostriction measurement systems:

4.2.1. Test Specimen

The length of the specimen may vary in different measurement techniques from localized measurement [7, 18] to a stack of ten steel sheets (180 mm 40 mm) used by Javorski et al [21] , but according to the IEC/TR 62581 [1] the two widely used sample sizes are:

- Epstein size (305 mm ×30 mm) which needs to be stressed relief annealed in order to remove the cutting stresses [23, 29]. The stress relief annealing may remove the residual stress in the sample as well.
- The other commonly used sample size is 100 mm ×500 mm, which does not require stress relief annealing as the ratio of the effected stress zone to the width of the sample is negligible [6, 24, 30, 31].

Moreover, the test specimen should be cut without forming large burrs or mechanical distortion

4.2.2. Yokes

Several types of yoke may be used for magnetostriction measurement systems such as:

- Horizontal single [23, 29] or double yoke [24, 31]
- Vertical single or double yoke [30]

Each pole face is horizontal in both types of yoke and the sample is placed inside the pole faces. In the case of a single yoke the electromagnetic force may increase out of plane vibrations. In order to eliminate the effect of eddy current and improving the flux distribution two yokes may be used. In this case, a constant gap between the test specimen and the pole faces should be kept for all the measurement, also extra care should be taken to not applying pressure to the test specimen due to the weight of the core [1].

References for Chapter 4

1. Commission, I.E., in *Electrical steel. Methods of measurement of the magnetostriction characteristics by means of single sheet and Epstein test specimens*2010, IEC: geneva. p. 56.
2. Banks, P.J. and Rawlinso.E, *Dynamic Magnetostriction and Mechanical Strain in Oriented 3 Per Cent Silicon-Iron Sheet Subject to Combined Longitudinal and Transverse Stresses.* Proceedings of the Institution of Electrical Engineers-London, 1967. **114**(10): p. 1537-&.
3. Greenough, R.D. and C. Underhill, *Strain-Gauges for Measurement of Magnetostriction in Range 4k to 300k.* Journal of Physics E-Scientific Instruments, 1976. **9**(6): p. 451-454.
4. Moses, A.J., et al., *Influence of compressive stress on magnetic properties of commercial.* Magnetics, IEEE Transactions on, 1980. **16**(2): p. 454-460.
5. Takaki, H. and T. Tsuji, *The measurement of magnetostriction by means of strain gauge.* Journal of the Physical Society of Japan, 1956. **11**(11): p. 1153-1157.
6. Yamasaki, T., S. Yamamoto, and M. Hirao, *Effect of applied stresses on magnetostriction of low carbon steel.* NDT and E International, 1996. **29**(5 SPEC. ISS.): p. 263-268.
7. Jackson, P., *Resistance strain gauges and vibration measurement.* Radio Engineers, Journal of the British Institution of, 1954. **14**(3): p. 106-114.
8. Meydan, T. and G.W. Healey, *Linear variable differential transformer (LVDT): linear displacement transducer utilizing ferromagnetic amorphous metallic glass ribbons.* Sensors and Actuators: A. Physical, 1992. **32**(1-3): p. 582-587.
9. Tariq, H., et al., *The linear variable differential transformer (LVDT) position sensor for gravitational wave interferometer low-frequency controls.* Nuclear Instruments and Methods in Physics Research, Section A: Accelerators, Spectrometers, Detectors and Associated Equipment, 2002. **489**(1-3): p. 570-576.
10. Wu, S.T., S.C. Mo, and B.S. Wu, *An LVDT-based self-actuating displacement transducer.* Sensors and Actuators, A: Physical, 2008. **141**(2): p. 558-564.
11. Birss, R.R., et al., *A capacitive instrument for the measurement of a large range of magnetostriction at low temperatures and high magnetic fields.* Journal of Physics E: Scientific Instruments, 1978. **11**(9): p. 928-934.
12. Puers, R., *Capacitive sensors: When and how to use them.* Sensors and Actuators: A. Physical, 1993. **37-38**(C): p. 93-105.
13. George, W.R., C. Holt, and J.E. Thompson, *Magnetostriction in grain-oriented silicon-iron.* Proceedings of the IEE - Part A: Power Engineering, 1962. **109**(43): p. 101-108.
14. Chae, J., H. Kulah, and K. Najafi, *An in-plane high-sensitivity, low-noise micro-g silicon accelerometer with CMOS readout circuitry.* Journal of Microelectromechanical Systems, 2004. **13**(4): p. 628-635.
15. Krishnan, G. and G.K. Ananthasuresh, *Evaluation and design of displacement-amplifying compliant mechanisms for sensor applications.* Journal of Mechanical Design, Transactions of the ASME, 2008. **130**(10): p. 1023041-1023049.

16. Brownsey, C.M. and G.C. Maples, *Magnetostriction characteristics of 3.1% grain-oriented silicon-iron transformer steel.* Electrical Engineers, Proceedings of the Institution of, 1966. **113**(11): p. 1859-1862.
17. Mapps, D.J. and C.E. White, *Magnetostriction harmonics measurement using a double piezoelectric transducer technique.* Journal of Physics E: Scientific Instruments, 1984. **17**(6): p. 472-476.
18. Simmons, G.H. and J.E. Thompson, *Magnetic properties of grain-oriented silicon iron. Part 1: Use of ceramic displacement transducers for the measurement of magnetostriction.* Electrical Engineers, Proceedings of the Institution of, 1968. **115**(12): p. 1835-1839.
19. Levitin, R.Z., et al., *Magnetostriction measurements under high magnetic fields by a piezoelectric transducer glued on the sample.* Physica B: Physics of Condensed Matter, 1992. **177**(1-4): p. 59-62.
20. Li, Q., *Research and applications of piezoelectric and piezomagnetic acoustoelectric transducer materials.* Yadian Yu Shengguang/Piezoelectrics and Acoustooptics, 1995. **17**(2): p. 43-51.
21. Javorski, M., J. Slavic, and M. Boltezar, *Frequency Characteristics of Magnetostriction in Electrical Steel Related to the Structural Vibrations.* Magnetics, IEEE Transactions on, 2012. **48**(12): p. 4727-4734.
22. Spineanu, A., P. Bénabès, and R. Kielbasa, *A digital piezoelectric accelerometer with sigma-delta servo technique.* Sensors and Actuators, A: Physical, 1997. **60**(1-3): p. 127-133.
23. Anderson, P., *A Novel Method of Measurement and Characterisation of Magnetostriction in Electrical Steels*, 2001 Cardiff of Wales
24. Nakata, T., et al., *Magnetostriction measurements with a laser doppler velocimeter.* IEEE Transactions on Magnetics, 1994. **30**(6 pt 1): p. 4563-4565.
25. Nakase, T., et al., *Measuring system for magnetostriction of silicon steel sheet under AC excitation using optical methods.* IEEE Transactions on Magnetics, 1998. **34**(4 PART 1): p. 2069-2071.
26. *Basic principles of vibrometry*. 14/April/2013]; Available from: http://www.polytec-ltd.co.uk/uk/solutions/vibration-measurement/basic-principles-of-vibrometry/.
27. Mogi, H., et al., *Harmonic analysis of ac magnetostriction measurements under non- sinusoidal excitation.* IEEE Transactions on Magnetics, 1996. **32**(5 PART 2): p. 4911-4913.
28. Bellesis, G.H., et al., *Magnetostriction measurement by interferometry.* Magnetics, IEEE Transactions on, 1993. **29**(6): p. 2989-2991.
29. Klimczyk, P.K., et al., *Influence of Cutting Techniques on Magnetostriction Under Stress of Grain Oriented Electrical Steel.* Magnetics, IEEE Transactions on, 2012. **48**(4): p. 1417-1420.
30. Ban, G. and F. Janosi, *Measuring system and evaluation method of DC and AC magnetostriction behaviour to investigate 3.2%SiFe GO electrical steels.* Journal of Magnetism and Magnetic Materials, 1996. **160**: p. 167-170.
31. Yabumoto, M., et al., *Recent development in grain-oriented electrical steel with low magnetostriction.* Journal of Materials Engineering and Performance, 1997. **6**(6): p. 713-721.

Chapter 5: Measurement systems

5.1. Magnetostriction measurement system:

The new system was adapted from the previous system that was originally designed and built by Anderson. P [1, 2] and improved by Klimczyk. P [3]. The new system has extended the maximum size of the samples from *30mm×305mm* to *100mm×500mm*, which enables as cut samples to be tested. The system will allow digitally controlled magnetisation at frequencies from 20 Hz to 1 KHz under applied stress of ±10 MPa. The design of the new system can be divided into three separate subsystems:

1. Magnetising system
2. Stressing system
3. Magnetostriction measurement

Each stage is explained into more detail below

5.1.1. Magnetising system:

In order to provide a uniform flux density along the length of the sample, the primary (magnetising) enwrapping winding is used. Moreover interior secondary winding (voltage winding) was used in order to measure the average flux density along the sample.

It was calculated that a magnetic field of 500 A/m is required to reach 1.8 Tesla of magnetic flux density over the magnetised length that is defined as the distance between the pole faces of the yoke [4]:

$$B = \mu_r H \tag{5.1}$$

$$H = \frac{NI}{l} \tag{5.2}$$

The number of turns for the primary winding (magnetising) was calculated, using equation (5.1) and (5.2), to be 230, which was wound over the magnetising length. For measuring the flux density, 330 turns of winding was used over the same length. Both the primary and secondary windings were wound around a non-conductive and non-magnetic plastic former. Two laminated yokes wound from grain oriented electrical steel provide flux closure.

A non-conductive, non-magnetic polyethylene terephthalate (PET) is used as a former. Insulation tape is used between the secondary and primary windings to avoid any short circuits between the windings.

Compensation for the effect of air flux was achieved by using a mutual inductor. The primary winding of the mutual was connected in series with the magnetising winding and the secondary winding of the mutual was connected in series opposition to the secondary winding of the test equipment. In order to adjust the mutual inductance, an alternating current was passed through the primary winding in the absence of a test sample until the voltage of secondary circuit was less than 0.1% of the specimen's secondary voltage, therefore, the introduced voltage in the combined secondary winding is only as a result of the flux density in the test sample. The value for the mutual inductance was calculated using:

$$M = \frac{\left(\mu_0 A_{air} N_p N_s\right)}{l} \tag{5.3}$$

Where

M= Mutual inductance (*H*)

μ_0= permeability of free space (H/m)

A_{air}= Cross section area of the air within the former (m^2)

N_P= Number of primarily winding

N_S= Number of primarily winding

l= Solenoid length (m)

Using this equation the value of mutual inductance was calculated to be 2.89×10^{-3}H.

In order to decrease the effect of eddy currents and having more homogeneous flux distribution over the inside of yokes it was decided to use two yokes for loss measurements as the polarity of the generated eddy current due to the normal flux in the pole faces will be cancelled out. On the other hand, for magnetostriction measurements the upper yoke will not be used as it will apply some pressure to sample due to the yoke's weight and may cause some errors.

The distance between the internal edges of the pole faces is taken as the magnetised length and is 435mm with the pole faces being 25mm; this will leave a 7.5 mm overlap at each end to enable clamps to be attached to the strip.

The bottom yoke is placed on an aluminium optical Table and fixed in its place by using 6 plastic supports, Seven PET bars were used inside the pole faces to hold the yoke in its place, these plastic bars were screwed by using brass studding to an optical Table in order to provide complete flat surface as it will explained later is critical for stressing system. The top yoke is placed parallel on top of the bottom yoke, and can be moved up and down. The top yoke is supported

by 4 plastic supports in order to avoid causing any stress to the samples due to the weight of the yoke.

Figure 5-1 illustrates a schematic design of the system. The new system was designed by using the engineering design program Solid Works.

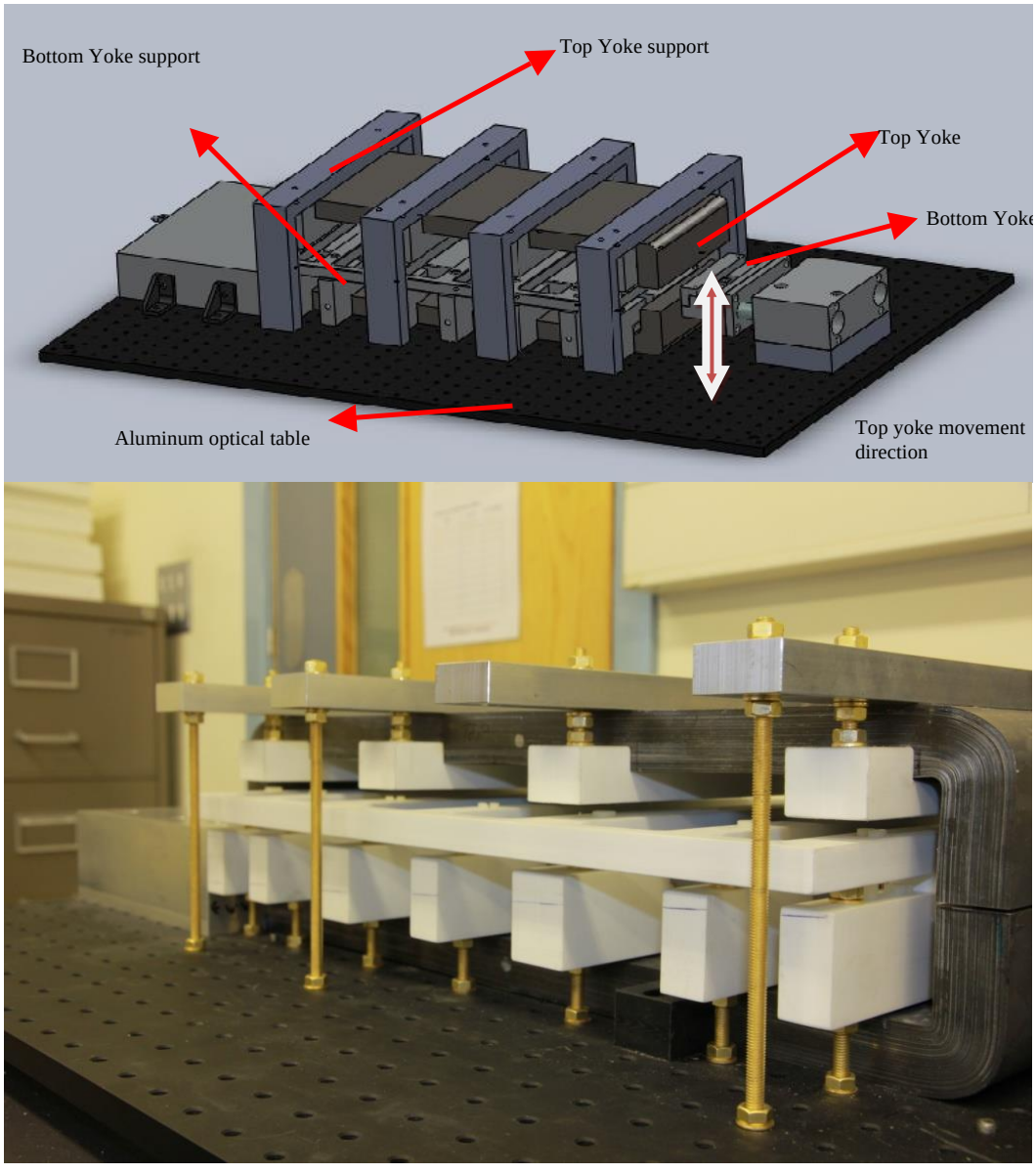

Figure 5- 1: schematic design and picture of the system, the magnetising system

5.1.2. Lab View Virtual Instrument Control System

The magnetization voltage controlled by Lab VIEW program and generated via an output voltage of the acquisition card (DAQ card). The output voltage was then passed through an amplifier and primarily winding. The voltage drop across the shunt resistor (V_{Rsh}) and combined secondary voltage (e) was measured and used for the calculation of magnetic field strength and flux density respectively.

The magnetic field strength (H) is obtained instantaneously in Lab VIEW using equation 5.4:

$$H = \frac{N_1 V_{Rsh}}{l_m R_{sh}} \tag{5.4}$$

Where l_m is the path length. The flux density (B) over the sample length (l) is calculated by mean of digital integration of the secondary voltage signal

$$B = \frac{l\rho_m}{N_2 m}\int e dt \tag{5.5}$$

Where

ρ_m is the density of the samples (kg/m^3)

m is the mass (kg).

The specific power loss (P_s) in a magnetising cycle period (T) is obtained by:

$$P_s = \frac{1}{T\rho_m}\int_0^T H\frac{dB}{dt}d \tag{5.6}$$ [2]

The Lab View program was set to use 20,000 data points per magnetising cycle. Moreover 1,800 points were used in each cycle for the voltage drops in shunt and secondary voltage to avoid quantizing errors (the difference between the analogue value and quantized value).

In order to control the flux density and keep the secondary voltage sinusoidal, feedback control [1, 5] was used to control the flux density and secondary voltage waveforms to be sinusoidal. The form factor error of the secondary induced voltage is set to be within 0.8% range. Respectively B peak error and the total harmonic distortion are set to be 0.5% and 7%. If the criteria are met, the *B* and *H* waveforms will be averaged and saved; if not the magnetising waveform is adjusted by the feedback till it meets the criteria.

Moreover, the average total magnetic power loss per unit mass and frequency, called specific total loss and is measured by using equation below [6]:

$$P = \frac{f}{\delta}\int_0^{1/f} H_{(t)}\frac{dB_{(t)}}{dt}dt \tag{5.7}$$

5.1.3. The stressing system:

The samples should be subjected to a range stresses from -10MPa to +10MPa. In order to achieve this, stress is applied to the sample by an aluminium clamp, which is connected to an integrated guide style pneumatic cylinder with three guides. The maximum pressure supplied by the compressor to the cylinder is 8 bar, in order to be able to apply a required force in both directions (compressive and tension) the cylinder were chosen according to Table 5-1, which shows the

specification of the theoretical force that could be applied by the cylinder. The required force is calculated from equation (5.8) for 0.3mm laminations:

$$F = \delta A \tag{5.8}$$

Table 5- 1: Theoretical Force applied by the cylinder, Theoretical Force (N) =pressure (MPa) x Piston area (mm2)

Bore (mm)	Rod dia. (mm)	Operating direction	Piston area	Operating pressure (MPa)								
				0.2	0.3	0.4	0.5	0.6	0.7	0.8	0.9	1
32	16	Out	804	161	241	322	402	482	563	643	724	804
		In	603	121	181	241	302	362	422	482	543	603

A tension/compression load cell that is placed on a middle guide of a non-rotating cylinder in order to measures the applied stress. The load cell is able to measure forces up to 1KN. The applied stress to sample is calculated using the following formula:

$$\sigma = \frac{V \times \delta \times l}{S \times m} \tag{5.9}$$

Where:

σ = Applied stress (MPa)

V = Load cell output voltage (V)

δ = Sample density (kg/m^3)

l = sample Length (m)

S = Load cell sensitivity (mV/N)

m = Sample mass (kg)

Two solenoid valves were used to control the direction of the applied stress and two electro-pneumatic regulators vary the air pressure and hence the force produced by the cylinder.

The sample was fixed at one end whilst the other was free to vibrate. The fixed end clamp was out of an aluminium block. The top of the clamp was tightened by using two spring loaded threaded rods and wing nuts at either end of the clamp. The free end was clamped to the load cell by using the same method. Figure 5-2 shows the stressing part of the system.

When applying compressive stresses along the length of a sample, it is extremely difficult to prevent the sample from buckling. This is achieved by ensuring that the clamps and pneumatic cylinder are perfectly aligned with the strip [3] .

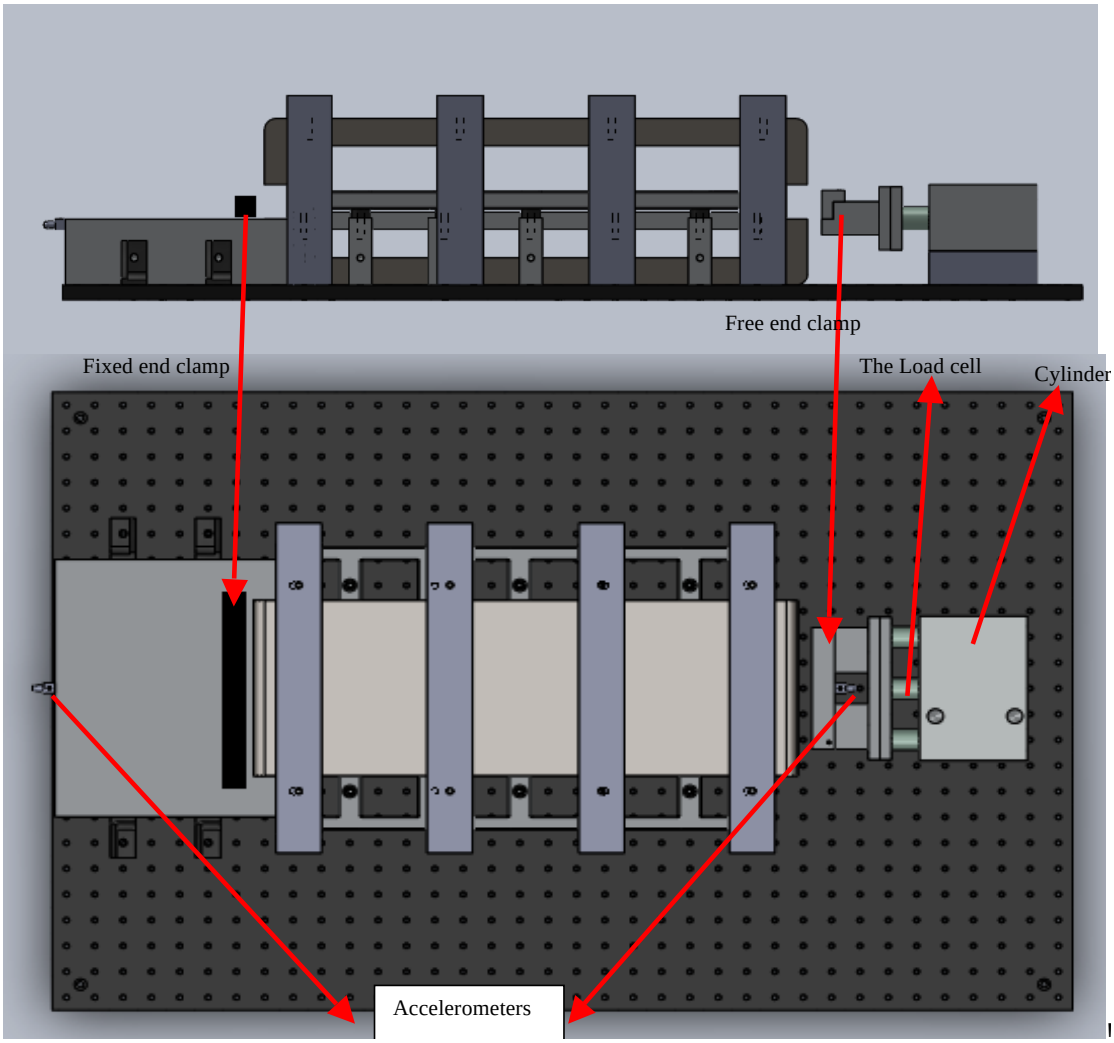

Figure 5- 2: schematic design of the system, magnetostriction measurement and the stressing system

A spacer was machined out of PET plane, six holes were drilled on the spacer to fix it to the CNC machine in order to make sure both two faces of the spacer are perfectly flat and it was not bent during the machining process. A spacer is placed into the windings former together with the strip to make sure that samples would not buckle or move during the measurements. The spacer and the sample should both be placed into the *U* shape sample holder; the width of this sample holder was 101 mm and was placed between the two pole faces. Figure 5-3 shows the *U* shape sample holder and spacer. Also a top frame is placed on top of this *U* shape sample holder to hold the spacer down

Figure 5- 3: U shape sample holder and spacer

The new system is able to measure samples up to 1mm thickness and apply 10MPa tension and compression (for thicker samples such as 0.5 mm thick laminations the pressure would be lower than 10MPa as the cross section area is increased).

5.1.4. Magnetostriction Measurement:

The magnetostriction of samples was measured using single axis piezoelectric accelerometers. The piezoelectric accelerometer was selected over other methods such as strain gauges, capacitance, piezoelectric pick-up and optical methods due to its high sensitivity (~ 500 mV/g) as well as low mass (3.5 gram) and low transverse sensitivity (max 3%) Furthermore, by using the accelerometer method no or less sample preparation is needed and samples can be tested as cut.

In order to choose the most suitable accelerometer for measuring vibration, the peak magnetostriction of the 0.3 mm sample was calculated by double differentiating the displacement using equations below:

$$x = A\sin(\omega t) \tag{5.10}$$

$$\frac{dx}{dt} = A\omega \cos(\omega t) \tag{5.11}$$

$$\frac{d^2x}{dt^2} = -A\omega^2 \sin(\omega t) \tag{5.12}$$

Therefore,

$$a = -\omega^2 x = -(2\pi f)^2 \lambda L \tag{5.13}$$

Where,

a = Acceleration (m/s^2)

x = Displacement (m)

A = Displacement Constant

ω = Angular frequency (Rad/s)

t = Time (s)

f = Magnetostriction fundamental frequency (Hz)

λ = Measured magnetostriction (micro strain)

L = Magnetised length of a strip (m)

The resolution required for the system was 0.01 µm. as a result the peak magnetostriction for the sample with magnetising path of 0.48 m is equal to 0.0048 µm. by putting the values into the equation above the acceleration would be calculated to be 9.1 x 10^{-3} m/s^2 . In order to find the suitable range the acceleration should be converted in "g" (1 g = 9.81 m/s^2). Table 5-2 shows the acceleration expected for saturation magnetostriction under various fundamental frequencies.

Table 5- 2: Acceleration at fundamental magnetostriction frequencies

Magnetisation frequency (Hz)	Magnetostriction fundamental frequency (Hz)	Acceleration (m/s^2)	Acceleration (g)
50	100	9.1	0.9
60	120	13.1	1.3
90	180	29.5	3
120	240	52.4	5.3
140	280	71.3	7.3
150	**300**	**81.9**	**8.3**
160	320	93.1	9.5

The selected accelerometers offered an acceleration range of ±10 g, which covered the requirements; Table 5-3 shows the specification of the selected accelerometers. The frequency range of the accelerometer could reach up to 3 KHz that enabled the accelerometer to measure up to the 30^{th} harmonic (for 50Hz magnetising frequency).

The accelerometers are connected to a power supply/coupler (type 5134) that supply a constant current to the line drive circuits and also amplifies the output signals; in addition the type 5134 power supply/coupler is providing signal filtering and gain up to 100 to the output signal.

The accelerometers were mounted at either end of the strip. One of the accelerometers was mounted onto the free end of the sample and measured vibration where the other one was mounted to the outside edge of the fixed aluminium block as a reference and measured external vibrations.

Table 5- 3: Specification of 8640A10 PiezoBeam accelerometer

Specifications	**Kistler 860A 10 Piezo-Beam Accelerometers**
Acceleration range	± 10 g
Acceleration limit	± 16 g
Sensitivity, ± 10 %	500 mV/g
Frequency Range (± 5 % limit)	0.5Hz to 3 KHz
Resonant Frequency (nom.)	17 KHz
Operating temperature range	-40 to 65 °C
Mass	3.5 g
Transverse sensitivity typ (max 3%)	< 1.5 %

The outputs of the accelerometers were summed since they faced in opposite directions and thus the outputs are in anti-phase. The magnetostriction value was calculated from double integration of the calculated value using the equation below, The integration constant is calculated by setting $\lambda\ (t)$ to be zero at $h=0$:

$$\lambda = \frac{1}{\omega^2} \times \frac{g}{G \times S} \times \frac{1}{L} \times V \times 10^6 \tag{5.14}$$

Where

λ = Pk-to-Pk magnetostriction (µm)

ω = Angular frequency (Rad/s)

g = calibration value equal 9.81 m/s^2

G = Coupler gain (1÷100)

S = Accelerometer sensitivity (V/g)

L = Magnetised length of a strip (m)

V = summed of double integrated Coupler outputs (V)

5.2. List of items

List of items used for constructing the new system is given below

Magnetising system:

- Two yokes. 480mm×170mm×60mm
- Isolation transformer
- Amplifier: crown CE 2000
- Resistor: Tyco BDS4B250R47K
- Wire: primary winding 1mm thick wires and 0.7mm thickness for secondary winding

Stressing system

- Two regulators: SMC IT202-302B
- Two solenoid valves: SMC VT307
- Compact guide cylinder: SMC MGQ-L-50-50
- Load cell: ELPF

Magnetostriction measurement:

- Differential amplifier: AMPO3
- Power supply/coupler: Kistler 8636C10
- Two accelerometer: Kistler 8636C10

Data processing

- PC: RM 300
- Acquisition card: Remote control of PXIe chassis8 channels
- Aluminium plate and a rack case.

5.3. Magnetostriction measurement system assessment

5.3.1. Assess the uniformity of applied stress:

The load cell was tested isolated from the system and also after it was assembled into the system by comparing the result with strain gauges. Results showed a good agreement with the reading data from the strain gauge with R^2 of 0.99. The Figure 5-4 illustrates the results.

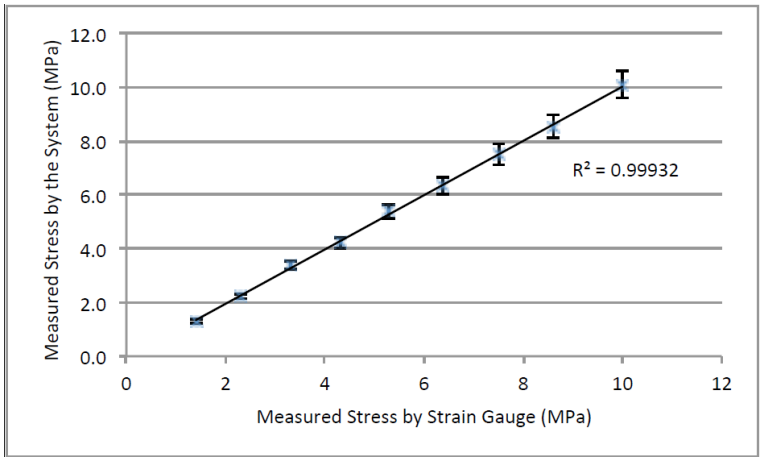

Figure 5- 4: Measured stress by Load cell vs. measured stress by strain gauge shows linear relationship

Moreover, using both pressure sensitive film and strain gauges the stress distribution along the sample was checked. In the first stage, for assessing the

pressure normal to the sample, a pressure sensitive film was placed on the middle, and either side of the sample near the clamp and cylinder, and a compressive pressure up to 12 MPa was applied to the sample.

When pressure was applied on the film, microcapsules in the film burst with respect to the distribution and density of the applied pressure. Consequently their material was released and reacted with the colour developing material. Figure 5-5 shows a schematic view of how pressure sensitive films were placed in the system.

The results show no changes in the colour of the film, so it can be concluded that the pressure normal to the sample is less than 0.01 MPa. The film was tested by applying pressure using tip of a pen too and the colour changes was spotted.

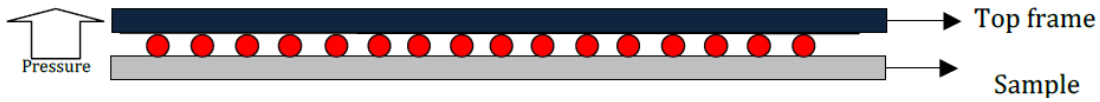

Figure 5- 5: schematic drawing of how the pressure sensitive film is placed, if there is any normal pressure it would causes the microcapsules to breaks.

In the next stage, three strain gauges were used to assess the stress distribution of the system. The results show a good agreement between the strain gauges with maximum of 2.5% error in repeatability. The recorded values as presented in the graph 5-6 the average value from each stage shows less than 1.2% difference from the average value:

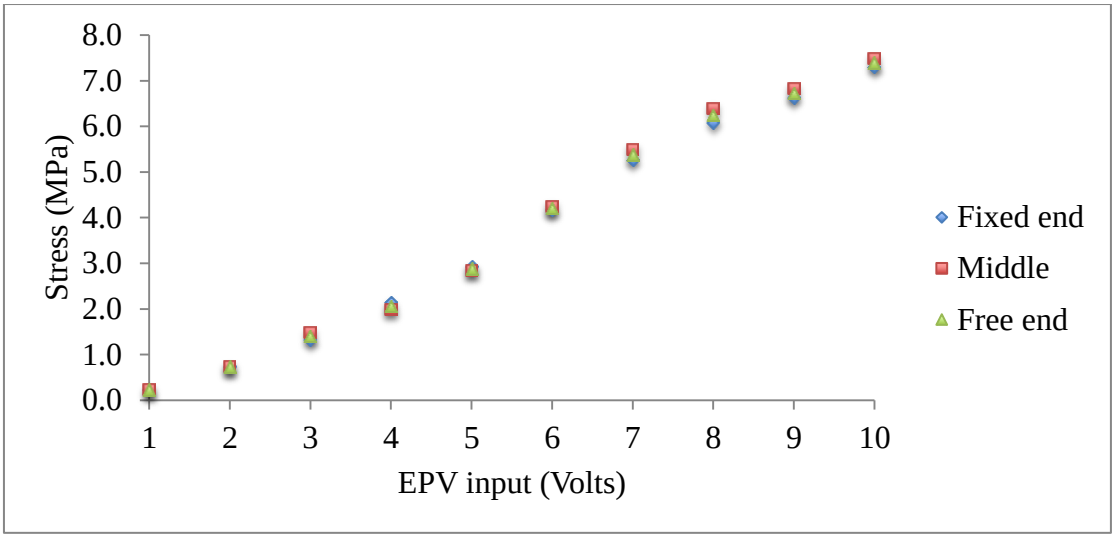

Figure 5- 6: measured stress by three strain gauges along the length of sample vs. applied voltage to the cylinder

5.3.2. Assess the magnetising system:

The applied field was confirmed by using the gauss meter and it has good agreement with the calculated value from the secondary winding. Moreover, the distribution of the field was assessed by comparing the values of the measured value from the system by six-search coils that were wound around the length of the sample. The measured flux density for 1.5 Tesla is presented in Table 5-4. Figure 5-7 shows where the six search coils were placed. Also six strain gauges were attached to the sample, which are shown in the figure.

Table 5- 4: Measured Flux using strain gauge at 1.5T

	Pont 1 (T)	Point 2 (T)	Point 3 (T)	Pont 4 (T)	Point 5 (T)	Point 6 (T)	Ave	B set in the system (T)
Test1	1.50	1.51	1.50	1.54	1.52	1.55	1.52	1.5
Test2	1.56	1.56	1.52	1.49	1.47	1.48	1.51	
Test3	1.54	1.51	1.54	1.54	1.57	1.5	1.53	
Test4	1.53	1.57	1.56	1.48	1.50	1.49	1.52	
Test5	1.55	1.55	1.54	1.51	1.54	1.52	1.53	

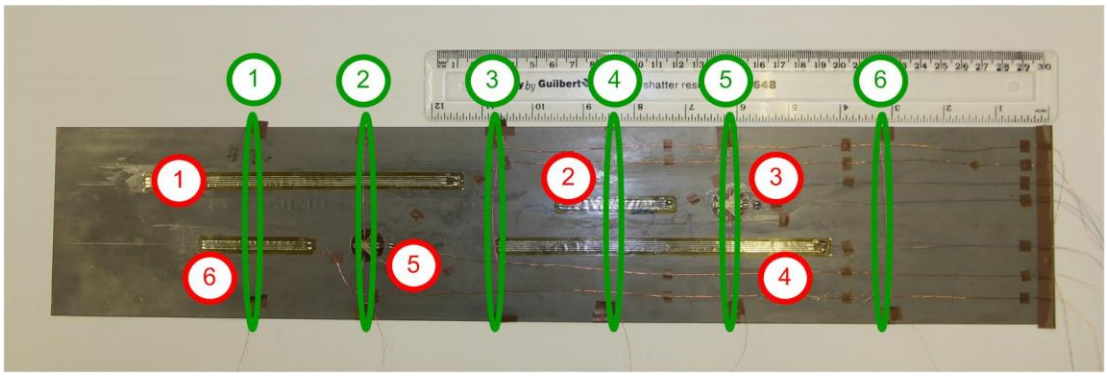

Figure 5- 7: assessed uniformity of field by placing six search coils and comparing by measured value by VI

5.3.3. Access the new system's repeatability:

The System's repeatability was checked before and after annealing. In total 6 Conventional Grain Oriented samples (CGO), 90 mm wide, were selected. Samples were cut by guillotine. Three of these samples were cut in rolling direction and three in the transverse direction. Samples were selected which did not show any burrs, or visual damage. Each sample was tested 3 times; samples were unclamped and taken out of the system completely each time. Figures 5-8 and 5-9 show the repeatability of the system before stress relief annealing; these samples were tested as cut.

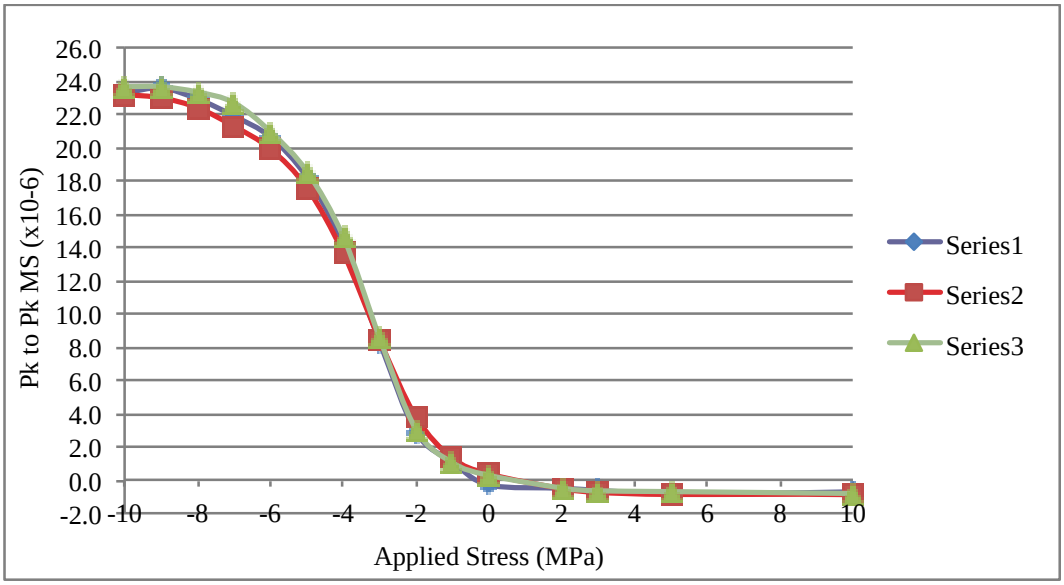

Figure 5- 8: multiple plots of Pk-Pk magnetostriction versus applied stress at 1.7 Tesla, 50Hz, for a single sample of conventional grain oriented sample cutting in rolling direction, before heat treatment

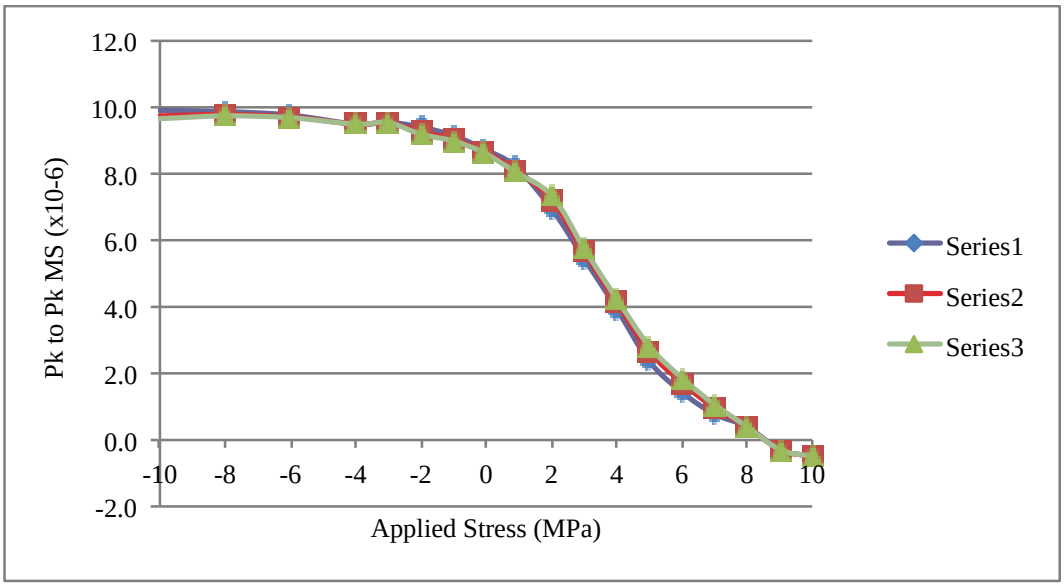

Figure 5- 9: multiple plots of Pk-Pk magnetostriction versus applied stress at 1.3 Tesla, 50Hz, for a single sample of conventional grain oriented sample cutting in transverse direction, before heat treatment

The average standard deviation for the peak-to-peak magnetostriction was calculated from Figure 5-8 and 5-9 as 1.4% and 3.5% respectively. After checking repeatability, samples were stress annealed at 815^{o}C for 1 hour, and the repeatability was checked again. Magnetostriction results were compared before

and after annealing. Graphs below 5-10 and 5-11 illustrate the repeatability after annealing. The test was repeated six times for sample in rolling direction.

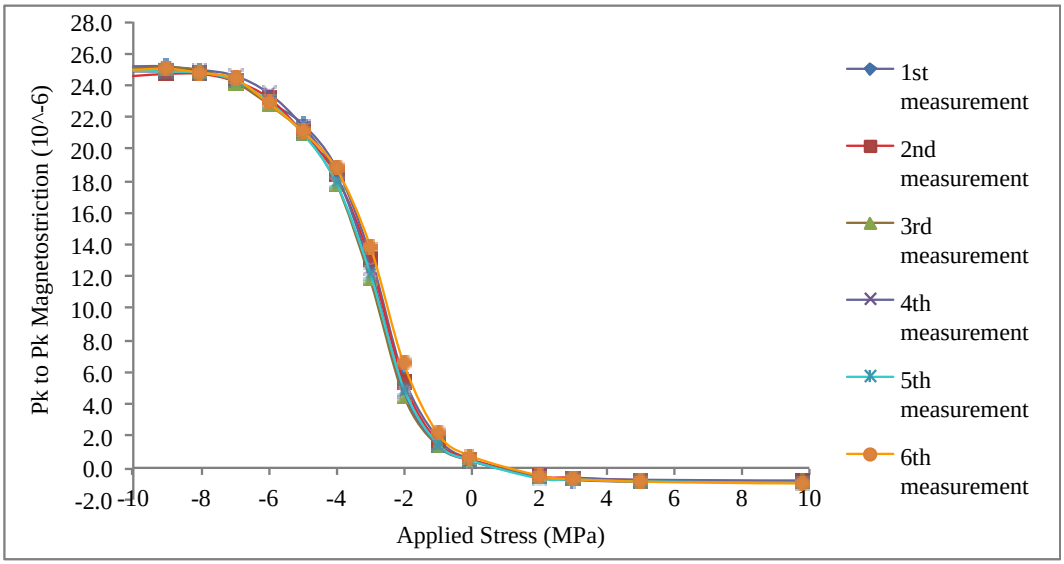

Figure 5- 10: multiple plots of Pk-Pk magnetostriction versus applied stress at 1.7 Tesla, 50Hz, for a single sample of conventional grain oriented sample cutting in rolling direction, stress annealed at 815°C for 1 hour

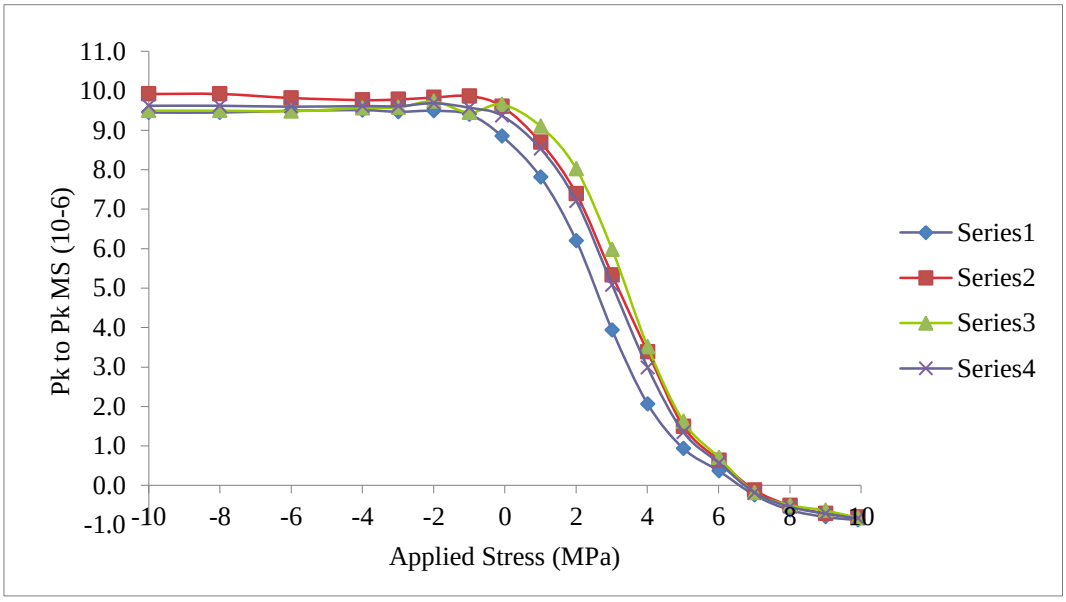

Figure 5- 11: multiple plots of Pk-Pk magnetostriction versus applied stress at 1.3 Tesla, 50Hz, for a single sample of conventional grain oriented sample cutting in transverse direction, stress annealed at 815°C for 1 hour

As can be seen from Figures 5-8 to 11, the system offers excellent repeatability on magnetostriction before and after stress relief annealing. The

average standard deviation for the peak-to-peak magnetostriction was calculated from Figure 5-10 and 11 as 1.2% and 3.7% respectively.

5.3.4. Comparison test with the existing system:

In order to make sure that the new system is measuring magnetostriction correctly, a comparison exercise was carried out with an existing magnetostriction system. Samples were compared in both rolling and transverse direction at a magnetic density of 1.7 T for rolling direction samples and 1.3T for transverse sample.

90 mm wide samples were cut into three Epstein width samples and stress relief annealed at 815^{o}C for 1 hour. Each sample was tested three times on both sides (the sample length was 500mm so it needed to be tested twice each time – reversing the sample between tests) and the average value of their magnetostriction and power loss has been compared with the new system. Figures 5-12 and 5-13 show the results of this comparison for rolling and transverse samples

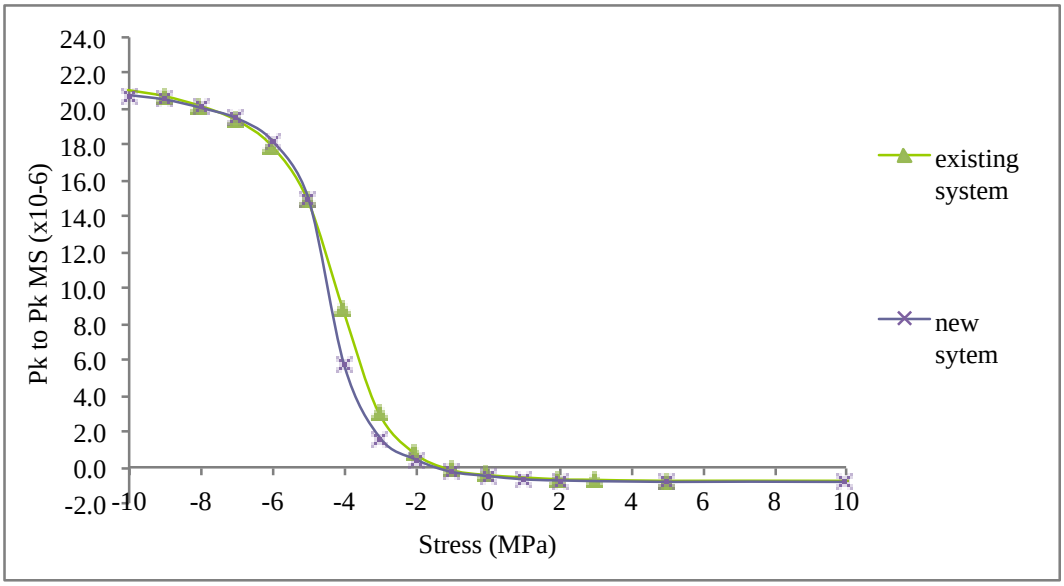

Figure 5- 12: comparison of the peak-to-peak magnetostriction of both systems in rolling direction at 1.7 T, 50Hz

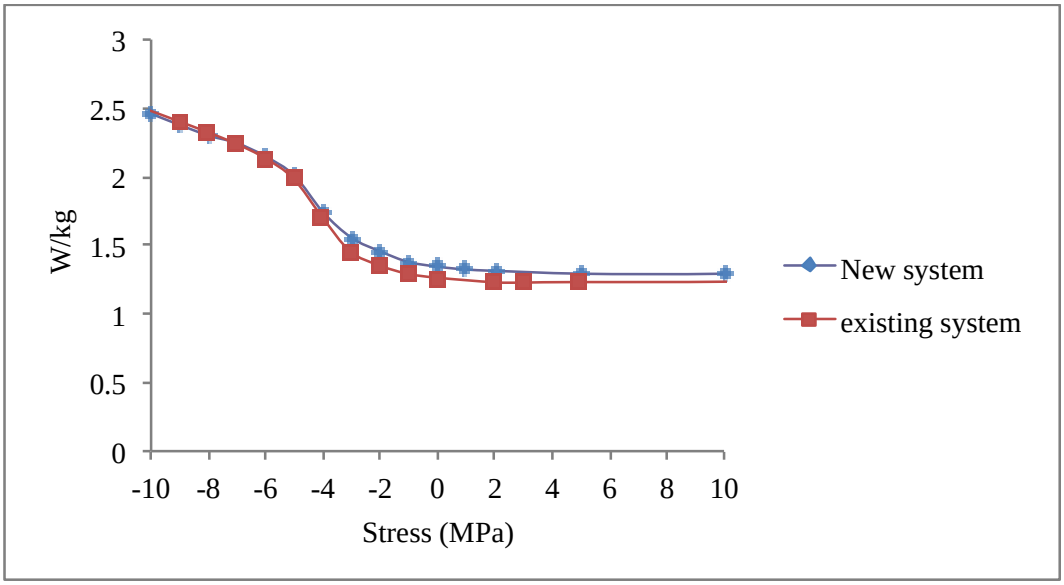

Figure 5- 13: comparison of the power loss of the two system in transverse direction at 1.3 T, 50Hz

Results show a good agreement between both systems, the average difference in peak-to-peak magnetostriction between the systems is in the range of combined uncertainty. Average standard deviation from the mean for the peak-to-peak magnetostriction for the new system and existing system was calculated as 1.3% and 2.7% respectively. The slight difference in the values could be due to various factors such as different magnetising length, number of grains and cut edge. Also the *B-H* loop from both systems was compared, and it was noticed that in the new system the *B-H* loop was less distorted due to the difference in *H* signal due to the smaller number of grains and the cut edge.

5.4. Resonance measurement of the system:

One of the most importance issues in vibration measurement system is the resonance frequency. In the first stages of construction of the system, resonant effects were observed during magnetisation at 50Hz. The issue was overcome by fixing three steel sections below the optical Table in order to increase the weight and rigidity of the system, as these factors influence the resonance frequency. By doing further

investigations it was noticed that the system exhibits resonant effects at a magnetization frequency 150 Hz. The theoretical natural frequency of samples can be calculated by the equation below:

$$f_n = \frac{n}{4l}\left(\frac{\sqrt{E}}{d}\right) \tag{5.15}$$

Where

n= order

l=Length (m)

E=Young's modulus (Pa)

d=Density (kg/m^3)

By putting the values in the formula, the natural frequency of the sample was calculated to be 3.0027 kHz. It can be seen from the calculation that the value of natural frequency of the sample is much higher than the measured value of the system. It is more complex to calculate the theoretical value of natural frequency of the system, as it requires a much more sophisticated model to take into account the shape, mass, springs. Figure 5-14 illustrates the first 10 harmonics of magnetostriction versus magnetising frequency; it shows no effect of resonance frequency.

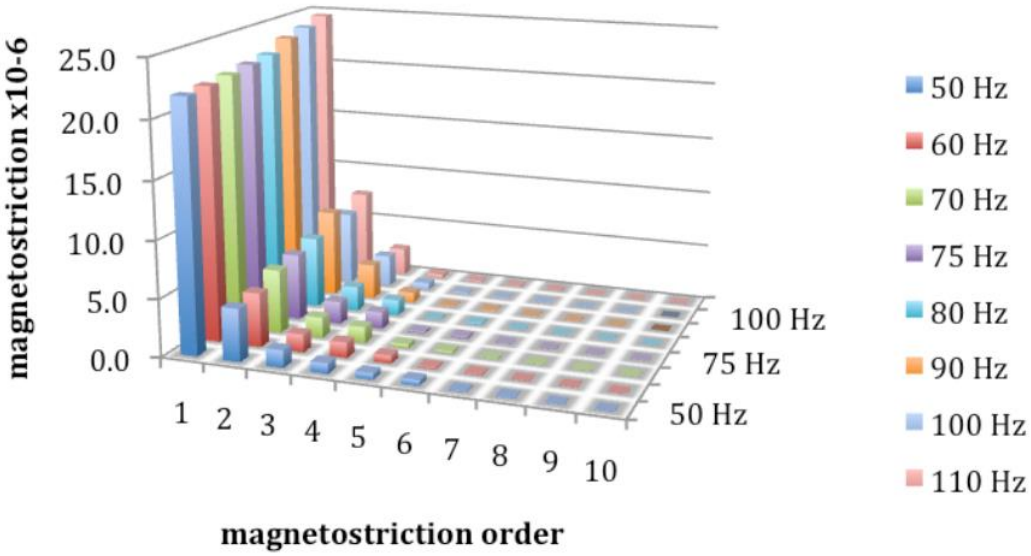

Figure 5- 14: Fundamentals Pk-to-Pk magnetostriction as a function of magnetised frequency

5.5. Uncertainty measurement:

The uncertainty of the magnetostriction measurement system was calculated according to the recommendations given in UKAS M3003[7]. Regarding to the standard UKAS M3003, the standard uncertainty can be divided into two main components, type *A* and *B*. Type *A* uncertainties can be assessed by statistical methods whereas type *B* evaluated by the other means. The calculated quantity *y* is the functional relationship of the input quantities of x_1, $x_2 \ldots x_n$ that can be presented as:

$$y=f(x_1, x_2, \ldots, x_n) \tag{5.16}$$

The standard deviation for the type *A* uncertainty of $u_A(y)$ is calculated from equation 5.17:

$$s = \sqrt{\frac{\sum_{i=1}^{n}(q_i - \bar{q})^2}{n-1}} \tag{5.17}$$

Where q_i is the measured value of *y* and $\bar{q}$ can be defined from

$$\bar{q} = \frac{1}{n}\sum_{i=1}^{n} q_i \tag{5.18}$$

The uncertainty of *u (y)* can be delivered from dividing the calculated standard deviation by square root on *n* as:

$$u(y) = \frac{s}{\sqrt{n}} \tag{5.19}$$

The type *B* uncertainty is measured by standard uncertainties $u\ (x_i)$ of the calculated x_i and can be defined to:

$$u_B^2 = \left(\frac{dx}{dx_1}\right)^2 u^2(x_1) + \left(\frac{dx}{dx_2}\right)^2 u^2(x_2) + \cdots + \left(\frac{dx}{dx_n}\right)^2 u^2(x_n) \tag{5.20}$$

Where (*dx/dy*) is called the sensitivity coefficient and is shown by c_i, moreover, c_i can be delivered from experiment from $\Delta y/\Delta x$.

After evaluating $u_A\ (y)$ and $u_B\ (y)$, the combined standard uncertainty can be determined form:

$$u(y) = \sqrt{\left(u_A^2(y) + u_B^2(y)\right)} \tag{5.21}$$

The calculated value form the above formula is multiplied by the coverage factor k_{95} in order to be calculating the expanded uncertainty. k_{95} gives a confidence level at 95% of the normal distribution [8].

Tables 5-5 illustrate calculated uncertainties of *B*, *H* and μ for the magnetostriction measurement system. The values in the Table were estimated in following order:

- Accuracy of Nie-6535: the accuracy of the voltage was obtained regarding to the National instrument NI 6356/6358. The absolute accuracy for the voltage measurement on the $10V$ range is 2.498 μV. as a result. The relative accuracy can be calculated by dividing the absolute accuracy by the range and multiply by 100.
- Frequency setting: were also taken from NI 6356/6358.
- Sample length: Length of samples is measured using a metal ruler with 0.5 mm resolution.
- Sample mass: The mass of the sample is measured using Avery Berkel FB31 scale. The resolution of the scale is 0.01 g.
- B control and FF: The Lab View program is able to maintain the values for B and FF of the secondary voltage within of 0.02%. However in the program it was set to be 0.8% for the form factor and 0.5% for the *B* value.

The values in the Table 5-6 and 5-7 were estimated as following:

- Load cell drift and calibration and accelerometer calibration were estimated according to the certificate provided by the manufacturer.
- Non-uniformity of stress: As mentioned before in assessing the uniformity of stress it was measured by using six strain gauges along the length of the sample.
- Integration error: The algorithm written in Lab View is able to calculate within ±0.2%.

Table 5- 5: uncertainty budget of the Peak of Magnetic Flux Distribution (J peak), 0.3 mm thick CGO strip, 50Hz, Zero stress

Determination of the uncertainties in Jpeak						
Source of uncertainty	**± %**	**Probability distribution**	**Divisor**	**Ci**	**Ui**	V_i or V_{eff}
Accuracy of Nie-6535	0.250	Normal	2.0000	1	0.12500	∞
Frequency setting	0.010	Rectangular	1.7321	1	0.00577	∞
Sample length measurement	0.500	Normal	2.0000	1	0.25000	∞
Sample mass measurement	0.010	Normal	2.0000	1	0.00500	∞
B control	0.500	Rectangular	1.7321	1	0.28868	∞
FF (form factor) control	0.800	Rectangular	1.7321	2	0.92376	∞
Type A uncertainty (repeatability)	0.050	Rectangular	1.7321	1	0.02887	
Sum of squares					1.01568	
Combined uncertainty					1.00781	
Expanded uncertainty					2.01562	
Declared uncertainty in Jpeak at a confidence level of 95 %					2.0	

Table 5- 6: Determination of the uncertainties in stress in 0.3mm thick CGO strips, 50 Hz

Source of uncertainty	**± %**	**Probability distribution**	**Divisor**	**C_i**	**U_i ± %**	**Vi or V_{eff}**
Load cell calibration	0.25	Normal	2	1	0.125	∞
Load cell drift	0.03	Rectangular	1.7321	1	0.0173	∞
Sample length measurement	0.5	Normal	2	1	0.25	∞
Sample mass measurement	0.01	Normal	2	1	0.005	∞
Non uniformity of stress	0.12	Rectangular	1.7321	1	0.0693	∞
Card calibration	0.25	Normal	2	1	0.125	∞
Type A uncertainty (repeatability)	0.25	Rectangular	1.7321	1	0.1443	
Sum of squares					0.7359	
Combined uncertainty					0.8579	
Expanded uncertainty					1.7157	
Declared uncertainty in Stress at a confidence level of 95 %					1.7	

Table 5- 7: Uncertainty budget of Peak-to-Peak magnetostriction under stress, 0.3mm CG0 sample at 50 Hz

Determination of the uncertainties in magnetostriction under stress 0MPa ≤ σ ≤ 10MPa						
Source of uncertainty	**± %**	**Probability distribution**	**Divisor**	**C_i**	**U_i ± %**	**V_i or V_{eff}**
Accelerometer calibration	0.1	Normal	2	1	0.05	∞
Accuracy of Nie-6535	0.25	Normal	2	1	0.125	∞
Integration error	0.2	Rectangular	1.7321	1	0.11547	∞
Repeatability of measuring magnetostriction	0.4	Normal	2	1	0.2	
Sample length measurement	0.5	Normal	2	1	0.25	∞
Stress setting	1.7	Normal	2	0.02	0.017	
Sum of squares					0.13425	
Combined uncertainty					0.3664	
Expanded uncertainty					0.7328	
Declared uncertainty in Pk-to-Pk magnetostriction at a confidence level of 95 %					0.7	
Determination of the uncertainties in magnetostriction under stress at -5MPa ≤ σ < 0MPa						
Source of uncertainty	**± %**	**Probability distribution**	**Divisor**	**C_i**	**U_i ± %**	**V_i or V_{eff}**
Accelerometer calibration	0.1	Normal	2	1	0.05	∞
Accuracy of Nie-6535	0.25	Normal	2	1	0.125	∞
Integration error	0.2	Rectangular	1.7321	1	0.11547	∞
Repeatability of measuring magnetostriction	2.5	Normal	2	1	1.25	
Sample length measurement	0.5	Normal	2	1	0.25	∞
Stress setting	1.7	Normal	2	0.2	0.17	
Sum of squares					1.68536	
Combined uncertainty					1.29821	
Expanded uncertainty					2.59643	
Declared uncertainty in Pk-to-Pk magnetostriction at a confidence level of 95 %					2.6	

Determination of the uncertainties in magnetostriction under stress at -10MPa ≤ σ < -5MPa						
Source of uncertainty	**± %**	**Probability distribution**	**Divisor**	**C_i**	**U_i ± %**	**V_i or V_{eff}**
Accelerometer calibration	0.1	Normal	2	1	0.05	∞
Accuracy of Nie-6535	0.25	Normal	2	1	0.125	∞
Integration error	0.2	Rectangular	1.7321	1	0.11547	∞
Repeatability of measuring magnetostriction	0.9	Normal	2	1	0.45	
Sample length measurement	0.5	Normal	2	1	0.25	∞
Stress setting	1.7	Normal	2	0.01	0.0085	
Sum of squares					0.29653	
Combined uncertainty					0.54455	
Expanded uncertainty					1.08909	
Declared uncertainty in Pk-to-Pk magnetostriction at a confidence level of 95 %					1.1	

From the Table 5-5 to 5-7 the declared uncertainties for the new magnetostriction system at a confidence level of 95% are as follows:

- J_{peak} = ± 0.6%
- Applied stress = ± 1.7%
- Magnetostriction
    - For 0MPa ≤ σ ≤ 10MPa = ± 0.7%
    - For 5MPa ≤ σ < 0MPa= ± 2.6%
    - For -10MPa ≤ σ < -5MPa= ± 1.1%

An example magnetostriction versus stress curve is presented below in Figure 15 the curve is divided into three different uncertainty sections:

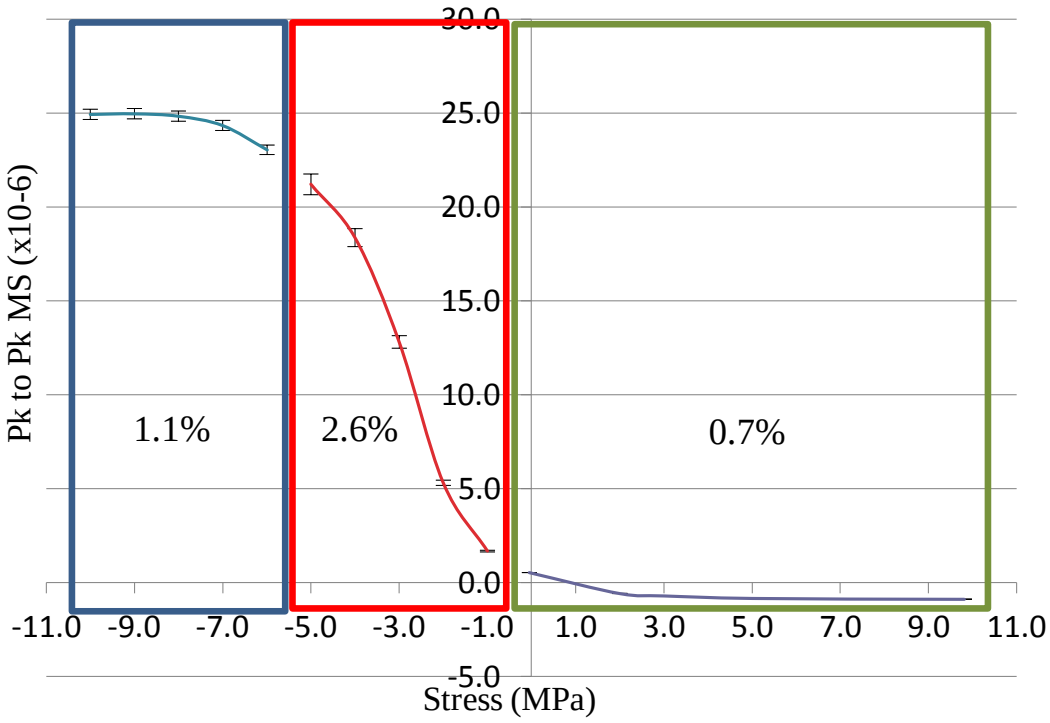

Figure 5- 15: Pk-to-Pk magnetostriction Vs. Stress, 0.3 mm CGO at 1.7 T and 50Hz. The graph shows three areas of uncertainty

5.6. 2D magnetostriction measurement system

Rotational magnetostriction were tested using the system originally developed by Zurek [9] and improved by Somkun et al [10, 11] .The system uses a disc sample with diameter of 80mm and is magnetised using a round yokes that is shown on Figure 5-16 in order to apply homogenous field up to 2 Tesla. Flux density is measured in the middle of the sample using two-search coil. Also the magnetic field components on the sample surface along the RD and TD (h_x and h_y) is measuring the tangential components of the magnetic field close to the sample by orthogonal *h* coils.

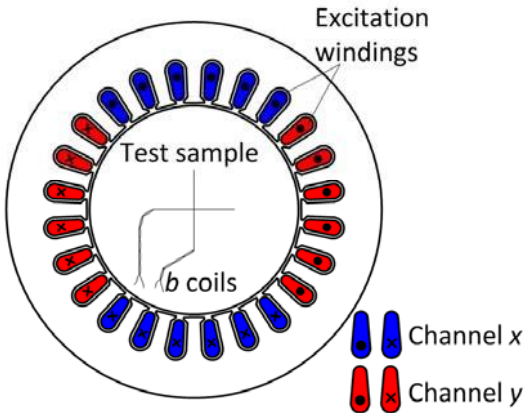

Figure 5- 16: schematic of a round yoke used in the 2D system

Two strain gauges could have been orthogonally placed to measure 2-D magnetostriction measurement. However, the principal axis of the strain in a plane surface may not align with the measurement axis [11] ,as a result in order to measure the 2-D magnetostriction, SGD-6/350-RYT81 rosette strain gauges were used to measure magnetostriction components λ_x , λ_s and the shear magnetostriction. The grid length of each gauge was 6mm long and 2.4 mm wide.

Schematic of the 2-D magnetostriction system is shown in Figure 5-17. The uncertainty of the system was declared to be 12% at confidence level of 95%.

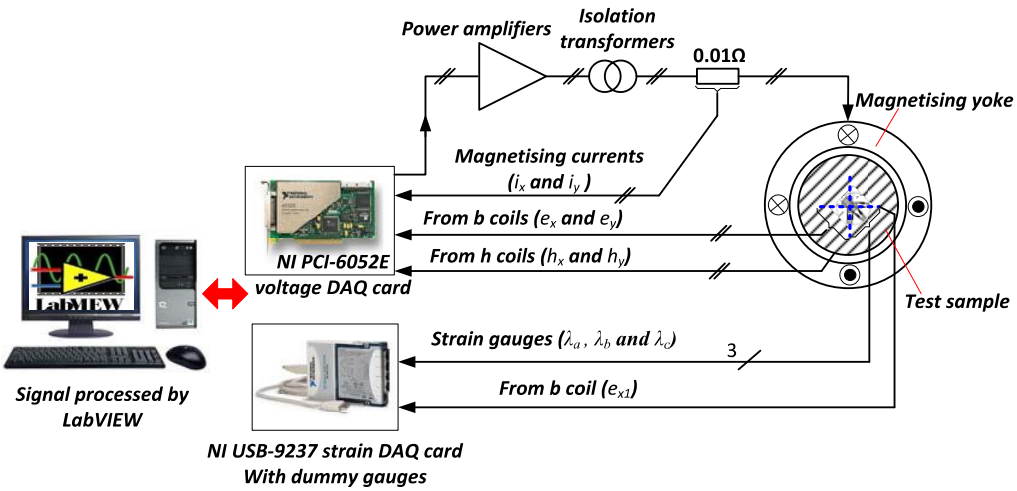

Figure 5- 17: schematic design of the 2-D magnetostriction measurement system [12]

5.7. Experimental technique for core vibration measurement

Analysing the core vibration requires information of vibration components measured in three directions of the core. There are three common methods of measuring core vibrations: strain gauge, piezoelectric vibrometer and laser vibrometer. The strain gauge method could not be used as it was required to measure the vibration in three directions and also strain gauge technique is extremely sensitive to the bending stress. It was reported that the two other methods offer similar accuracy of measurement. However, the piezoelectric vibrometer methods requires direct contact which affects the measurement accuracy and also takes longer time for setting and measuring the core vibration whereas the laser vibrometer provides high three-dimensional resolution with no direct contact and can covers a wide area of the core. Therefore, it was decided to use the laser vibration method for measuring the core vibrations.

The average peak-to peak vibration displacement for conventional core is in order of 0.01 μ m [13, 14] as a result PSV-400 scanning vibrometer is used for measurement of the core vibration and an OFV-303 single point vibrometer was used as a reference to cancel the background vibration noise. Both measurement lasers were of the Helium Neon type with a laser wavelength of 633nm .The technical data for both lasers is given in Table 5-8. Moreover, two mirrors were also used in order to be able to measure the vibration of sides of the cores.

The scanning vibrometer scanned each point three times and the average was saved. Figure 5-18 shows the setting of the measurement. The mirrors were set at an angle of 45^{o}. In the second stage, the position of the laser vibrometers were changed and they were set in the horizontal configuration, so that the scanning

laser vibrometer could measure larger areas on the side of the core with higher resolution.

Table 5- 8: PSV-400 Scanning vibrometer technical data [15, 16]

Technical Data PSV-400 Scanning vibrometer	
Laser type	HeNE (helium–neon)
Wavelength	633 nm
Working distance	With MR lens: 0.04 m…~100 m; with LR lens: 0.35 m…~100 m
Camera	Colour video camera, CCD 1/4", 752x582 pixels, with Auto Focus and 72X Zoom (4X digital, 18X optical)
Scanner	High precision scan unit (scanning range ±20° about X, Y); angular resolution <0.002°, angular stability <0.01°/hr
Scan speed	Up to 30 points/s (typical)
Resolution µm $s^{-1}/\sqrt{Hz}$	0.01-4

Technical Data sensor head OFV-303	
Laser Type	HeNE (helium–neon)
Wavelength	633nm
Cavity length	203nm
Output centre frequency:	40MHz
Focal length mm	Short range (SR) 30
	Mid range (MR) 60
	Long range (QR) 100

The laser beam automatically scanned the drawn area. Moreover, the laser always focused optimally while scanning. All the information was sent to the computer control system where it used the PSV software package to process all the data. The test was set up in an acoustic chamber and no personnel were present in the room during the test.

It should be noted that the laser vibrometer is able to measure the movement in normal direction to the surface. The laser vibrometer measures the

vibration velocity of an object by using the Doppler effect of the laser light. The principles of the laser Doppler are explained in section 4.1.6.

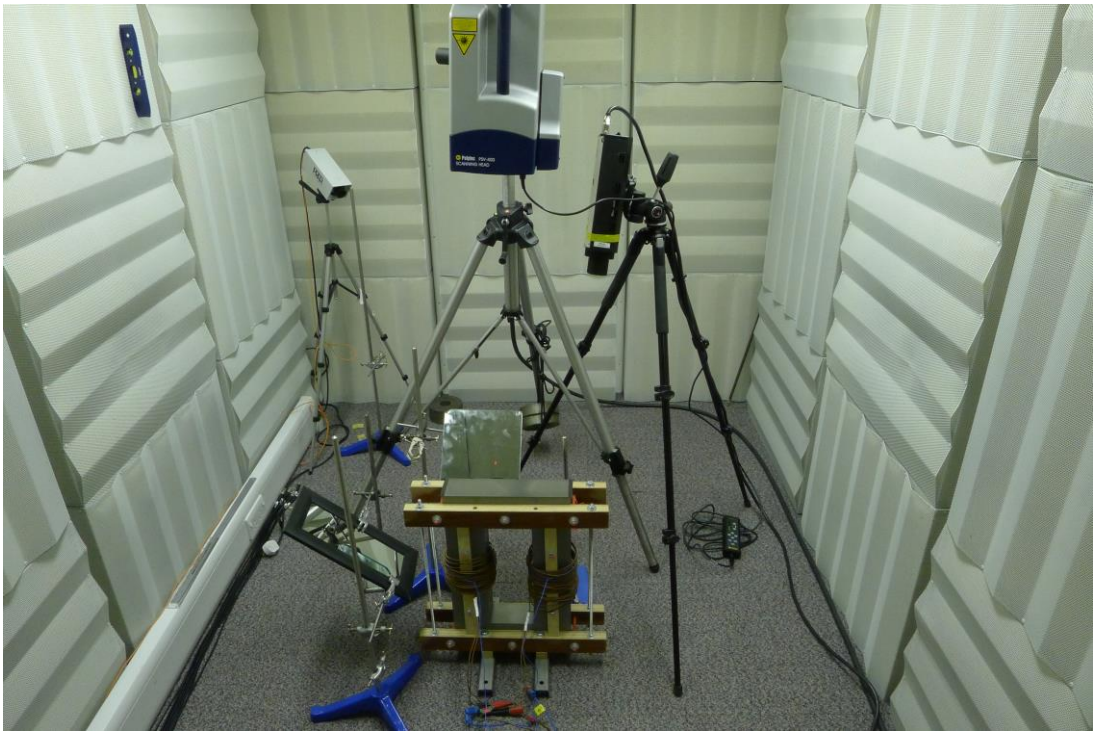

Figure 5- 18: Vibration measurement setting using The PSV-400 scanning vibrometer-single phase transformer

References for Chapter 5

1. Anderson, P.I., A.J. Moses, and H.J. Stanbury, *An automated system for the measurement of magnetostriction in electrical steel sheet under applied stress.* Journal of Magnetism and Magnetic Materials, 2000. **215**: p. 714-716.
2. Anderson, P., *A Novel Method of Measurement and Characterisation of Magnetostriction in Electrical Steels*, 2001 Cardiff of Wales
3. Klimczyk, P., et al., *Challenges in magnetostriction measurements under stress.* Przeglad Elektrotechniczny, 2009. **85**(1): p. 100-102.
4. Commission, I.E., in *Electrical steel. Methods of measurement of the magnetostriction characteristics by means of single sheet and Epstein test specimens*2010, IEC: geneva. p. 56.
5. Zurek, S., et al., *Use of novel adaptive digital feedback for magnetic measurements under controlled magnetizing conditions.* IEEE Transactions on Magnetics, 2005. **41**(11): p. 4242-4249.
6. F, F., *Measurement and characterization of magnetic materials*. 2004: Elsevier Inc.
7. National Measurement Accreditation, S., *The expression of uncertainty and confidence in measurement for calibrations*. 1995: NAMAS.
8. Somkun, S., A.J. Moses, and P.I. Anderson, *Mechanical Resonance in Nonoriented Electrical Steels Induced by Magnetostriction Under PWM Voltage Excitation.* Ieee Transactions on Magnetics, 2008. **44**(11): p. 4062-4065.
9. Zurek, S., *Two ‐dimensional Magnetisation Problems in Electrical Steels*, in *Wolfson center for magnetic* 2005, Cardiff university
10. Somkun, S., A.J. Moses, and P.I. Anderson, *Measurement and Modeling of 2-D Magnetostriction of Nonoriented Electrical Steel.* Ieee Transactions on Magnetics, 2012. **48**(2): p. 711-714.
11. Somkun, S., et al., *Magnetostriction Anisotropy and Rotational Magnetostriction of a Nonoriented Electrical Steel.* Ieee Transactions on Magnetics, 2010. **46**(2): p. 302-305.
12. Somkun, S., *Magnetostriction and Magnetic Anisotropy in Non-oriented Electrical Steels and Stator Core Laminations*, in *Wolfson Centre for Magnetics*2010, Cardiff University.
13. Mizokami, M., M. Yabumoto, and Y. Okazaki, *Vibration analysis of a 3-phase model transformer core.* Electrical Engineering in Japan, 1997. **119**(1): p. 1-8.
14. Weiser, B., et al., *Mechanisms of noise generation of model transformer cores.* Journal of Magnetism and Magnetic Materials, 1996. **160**: p. 207-209.
15. *User Manual Laser Doppler Vibrometer OFV-303/-353*. [cited 2013 15/april];Availablefrom:http://servv89pn0aj.sn.sourcedns.com/~gbpprorg/mil/laserl/Polytec_OFV3001.pdf.
16. *PSV-400 Scanning Vibrometer data sheet*. [cited 2013 15/april]; Available from:http://www.polytecltd.co.uk/fileadmin/user_uploads/Products/Vibrometers/PSV-400/Documents/OM_DS_PSV-400_2011_05_E.pdf.

Chapter 6: Sample selection, preparation and magnetostriction measurement Round Robin:

6.1. Round robin

According to the participating laboratories responses presented in section 6.4.2 (six laboratories in total including Wolfson center), sample size and number were calculated. All samples were cut by guillotine from conventional grain oriented (CGO) material with a thickness of 0.30mm. Samples were stress relief annealed at a temperature of 815^{o}C for 1 hour in an atmosphere of 2% hydrogen and 98% nitrogen in order to remove the cutting stress, which could cause inconsistency in magnetostriction values between different sample sizes as the ratio of the affected area, is different. Samples were all tested at the Wolfson Centre and then transferred in specially designed wooden boxes with a foam interior to avoid any damage to the samples (explained more in Chapter7). Table 6-1 illustrates the number of samples cut in each direction. Each sample was tested three times in each condition.

Table 6- 1: Samples sizes direction

Sample size *mm*	Direction
30 x 305	6 Longitudinal
	6 Transverse
40 x 180	15 Longitudinal
	15Transverce
100 x 610	6 Longitudinal
	6 Transverse
100 x 500	15 Longitudinal
	15 Transverse

Due to sample size differences between the Wolfson-A measurement system (*100mm* × *500mm*), explained in Chapter 5, and some other labs, samples were cut from neighbouring areas. All samples were cut from the same sheet in order to make sure samples of similar magnetostriction characteristics and properties were selected. Figure 6-1 illustrates how the samples were cut in the rolling direction; the transverse samples were cut in a similar manner.

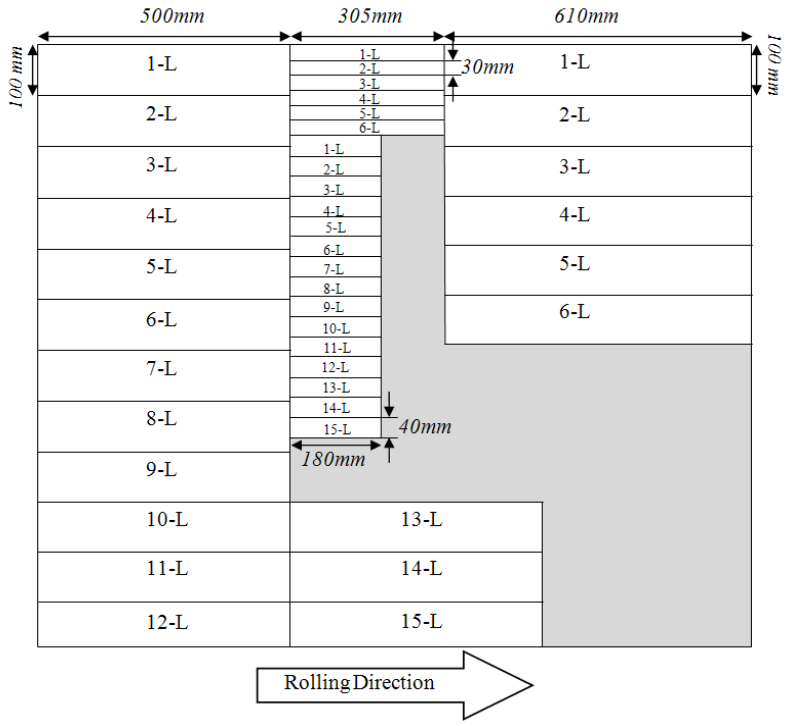

Figure 6- 1: Cutting map of the samples in the rolling direction

6.2. Investigation of Factors Influencing Magnetostriction

6.2.1. Effect of domain refinement process on peak to peak magnetostriction

In this exercise two scribing methods were used. In the first stage magnetostriction and power loss of five 0.3 mm laser-scribed HGO (high permeability grain oriented) materials were measured before and after annealing.

The received samples were scribed at 10 *mm* intervals transverse to the rolling direction of the strips.

All samples were cut to 100 *mm* by 500 *mm* by guillotine from laser-scribed core with a thickness of 0.3*mm*. In total five samples were tested, each sample was tested three times in each stage.

In the second method, a ball-pen [1, 2], mechanical scribing shown in Figure 6-2, with three different loads (6.0 N, 4.9 N and 2.4 N) was used to apply mechanical stress lines spaced at 10*mm* and 5*mm* to the 0.3 *mm* HGO samples. The applied load and line spacing was chosen based on guidance from [3]. All samples were selected from the rolling direction of a 0.3 *mm* HGO sheet and the domain structure of the samples was checked using Bitter technique. Each sample was tested three times and the averaged.

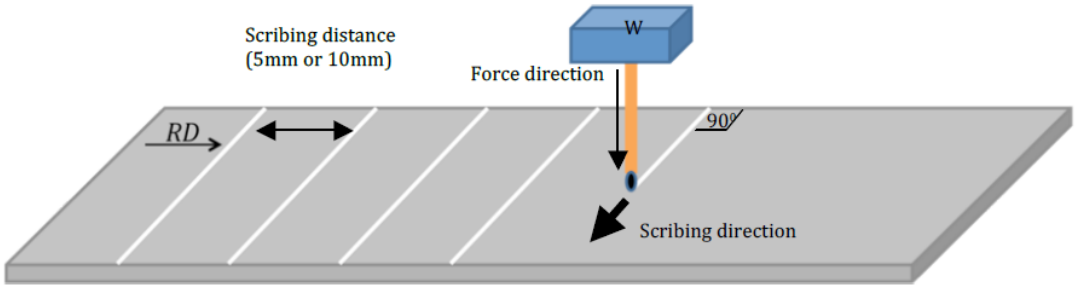

Figure 6- 2: Schematic design on ball-pen unit that used for sample scribing.

Three samples were used for each load. The magnetostriction and power loss was measured after each stage and in the last stage samples were stress relief annealed, and their properties were compared with the starting sample. Figure 6-2 shows a schematic design of how the stress was applied to the samples. The stages are as follows:

Stage 1: HiB (high permeability grain oriented) sample

Stage 2: Scribed at 10mm intervals transverse to the RD

Stage 3: Scribed at 10mm intervals transverse to the RD

Stage 4: Annealed at 810^{oC} for 2 hours

6.2.2. Influence of residual curvature (coil set)

Two set of samples of different coil set, which is known as the natural curvature remaining in coil after it has been unwound, were created regarding to references given by [4, 5] , one with a height of 10 *mm* and one with 5 *mm* ,the height of the curve shown in figure 7-30 . The calculated radius was as shown in Table 6-2. Samples were cut in the rolling direction from a 0.3*mm* thick CGO sheet into 100*mm* by 50*mm* laminations by mechanical guillotine. All the samples were flattened and stress relief annealed.

Table 6- 2: Calculated curvature details

Arc	*Height*	*Radius*
500 mm	*10 mm*	*2246 mm*
500 mm	*5 mm*	*2256 mm*

In the first stage 10 samples were tested at flux densities of 1, 1.5 and 1.7 Tesla. Each sample was tested three times.

In the second stage, five samples were chosen for each curvature. Samples were fixed in pre-designed jigs shown in the Figure 6-3 and stress relief, after cooling the samples were flattened in the magnetostriction measurement system mechanically by the spacer inside the system, and their properties were measured under applied stress.

Figure 6- 3: The design jig for applying different curvature, a set of 10 samples were clamped in a jig and annealed at 810°C for 2hrs.

6.2.3. Influence of strip width

The effect of strip width on magnetostriction was studied in two stages. 100*mm* by 500*mm* Samples were cut by mechanical guillotine in the rolling and transverse directions from a 0.30*mm* CGO sheet and then stress relief annealed.

In the first step, three 100*mm* wide samples cut in the rolling and transverse directions were chosen. At each stage, magnetostriction of the samples was measured and then 10*mm* was cut from the width, then samples were stress relief annealed again. This stage was repeated till samples width gets down to 70*mm*.

In the second stage, samples were cut from 100*mm* into half. The two laminations were annealed and then were put together and tested in order to study the effect of sample size to the width of surface closure domains. Afterward samples were cut into 25*mm* width sheets then put back together and tested. Figure 6-4 shows sample width after each stage.

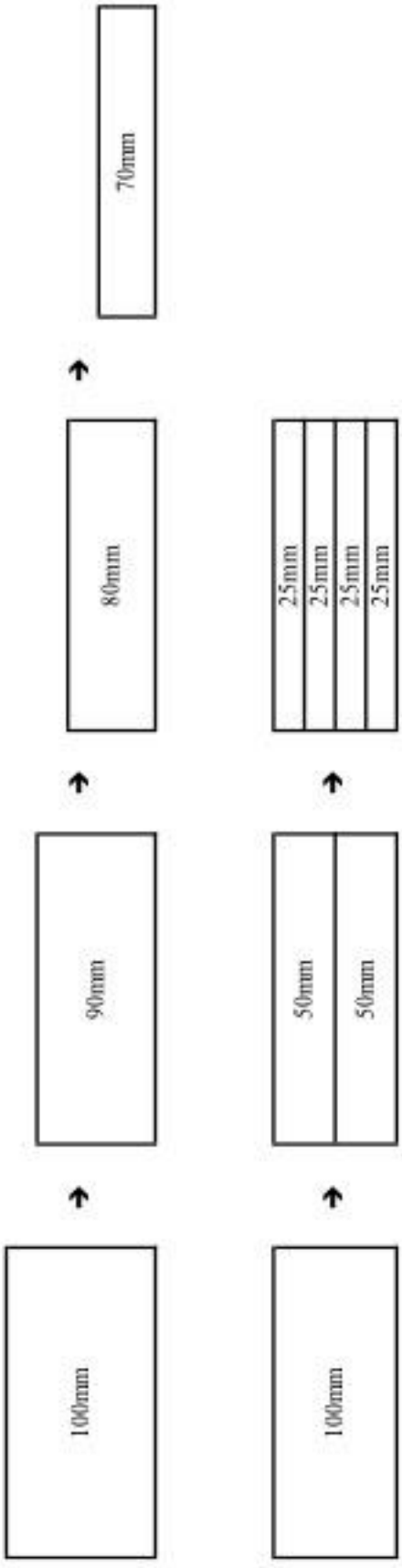

Figure 6- 4: samples width and sample configuration, samples were cut progressively narrow in step one (top picture) whereas the overall sample width is constant in step two (bottom picture)

6.3. A correlation of the vibration characteristics of transformer cores with the magnetostriction properties of the lamination steels

6.3.1. Magnetostriction measurement in rolling direction

In total 10 batches of 100*mm* by 500*mm*, laminations with 0.3*mm* thickness were received. All samples were cut using mechanical guillotine by Legnano Teknoelectric Company Ltd. Each batch contained 15 laminations cut in rolling direction for magnetostriction measurement.

Table 6-3 shows the grade of each of the batches and their coil and transformer number. Five random samples from each batch selected and their magnetostriction characteristic were measured. Each sample was tested three times.

Table 6- 3: Samples grade and their coil number

Grade	Origin coil number	Transformer coil	Number of sample	Total
CGO	S779922	A	15	105
	S779923	B		
	S77919	C		
	S77925	D		
	S77924	E		
	S77926	F		
	S77927	G		
HGO	51357GOLB	A		30
	513557GOLC	B		
Laser scribed	469242AD	A		15

6.3.2. 2-D magnetostriction measurement

The specific power loss and magnetostriction under 2D magnetisation were measured on the all three grades. Square samples with a diameter of 100 *mm* by 100 *mm* were cut from 100*mm* by 500*mm* laminations using mechanical guillotine. Then four holes for *b* coils with diameter of 0.50 *mm* were drilled by using high-

speed drill. After the holes were drilled the square samples were fixed between two steel plate and circular samples with diameter of 80*mm* were cut using wire cutting. The positions of the holes in respect to the round sample are shown in Figure 6-5.

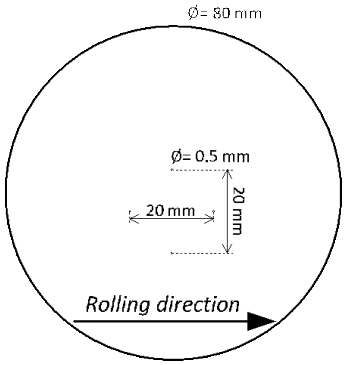

Figure 6- 5: Dimensions of specimens for the 2D magnetisation system, shows the position of the holes for *b* coil.

After the samples were cut, they were stress relief annealed, then a rosette strain gauge was attached at the centre and b_x and b_y coils was wound on each samples.

6.3.3. Core vibration measurement

In total, three transformer cores were tested for assessment of the core vibration. The specification of each core is given in Table 6-4. All the cores were assembled and bolted together at Legnano Teknoelectric Company Ltd (LTC). The selected cores consisted of three single-phase with step-lap, assembled one sheet per layer in five steps (6/3/0/-3/-6 *mm*). Also Five three-phase transformers were assembled with 1 sheet per layer in five steps, (6/3/0/-3/-6 *mm*) and one three-phase transformer with step-lap was assembled with three sheets per layer in two steps, (6/ -6 *mm*) the result from these core were not used for assessment of vibration. The core limbs were clamped by using a wooden clamp and non-magnetic bolts.

Table 6- 4: Specification of the single-phase cores

Core No	Set no.	Core weight	Material	Cross step type	Assembling	Phase	S [VA]	Cos j	Pc [W]	B [T]	W/kg
2	1	72	Laser scribed	17	0.2	1	248	0.297	73	1.7	1.03
3	1	72	HGO	17	0.2	1	217	0.378	81.9	1.7	1.14
4	0.5	72	CGO	17	0.2	1	531	0.178	94.6	1.7	1.31

The number of primary and secondary winding was calculated according to equation 6.1 and 6.2.

$$B = \mu_r H \tag{6.1}$$

$$H = \frac{NI}{l} \tag{6.2}$$

The primary winding consisted of 25 turns of 1.5mm wire and the secondary winding consisted of 25 turns of 1.5mm wire. The secondary winding was used for the magnetic flux density measurements. The windings were connected in the star configuration [6]. The single-phase transformer drawings are illustrated in Figure 6-6.

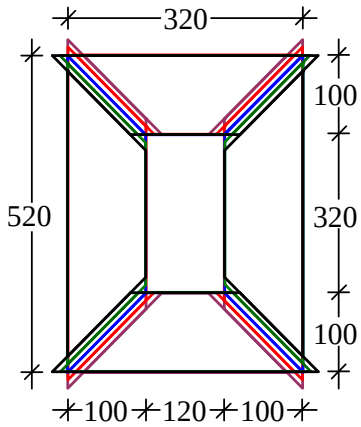

Figure 6- 6: Transformer cores dimensions of single-phase multi step lap, all dimensions are in mm

6.4. Round robin magnetostriction measurement

6.4.1. Introduction:

There is a growing international requirement from the manufacturers and the users of electrical steel for a universally agreed method of measurement and assessment of magnetostriction characteristics. Many different magnetostriction measurement methods and sample sizes are being used by laboratories around the world to measure the magnetostriction characteristics of electrical steel. These include the following sensing methods: piezoelectric accelerometer, piezoelectric pick-up, strain gauge, laser Doppler vibrometer, capacitive displacement sensors and linear variable differential transformer.

A round robin magnetostriction measurement [7] has been carried out in order to compare some of these different magnetostriction-measuring methods. A range of grain oriented electrical steel samples was circulated to participating laboratories to compare the measured magnetostriction characteristics The transfer of a single set of samples to all laboratories was ruled out due to the high stress sensitivity of magnetostriction, which might cause some error following repeated application of stress to the sample, damage to the edges etc. Therefore, samples were exchanged between the Wolfson Centre and each partner laboratory. Whilst we have high confidence in the Wolfson measurements, it was not the intention to establish this system as the reference measurement. However, the system has demonstrated very good repeatability and, as such, may be considered a reference for the purposes of this investigation.

6.4.2. Round robin structure:

A round robin test has been designed according to ASTM E691-13[7] inter-laboratory study which establishes the cooperation between multiple laboratories using similar test methods for measurements carried out on an exchanged sample[7].

6.4.3. Questionnaire:

As the first stage, a questionnaire was designed and sent out to all participating laboratories to determine the most common measurement parameters. A copy of the questionnaire is given in Figure 6-7. Five laboratories, excluding the Wolfson Centre, participated in the round robin experiment; each laboratory was assigned a number in order to keep the participating laboratories anonymous. Table 6-5 shows the laboratory declarations of the measurement parameters. All the participating laboratories had the facilities to measure the magnetostriction of the samples at a peak magnetic flux density of up to 1.7 T in the longitudinal direction and up to 1.5T in transverse direction. Moreover, it can be seen from the Table 6-5, that the most common sample size was 100 *mm* by 500 *mm* and 50 Hz was the most common magnetizing frequency.

Round Robin Questionnaire

Organization details:

Name:	Position:
Organization:	
Address:	
e-mail address:	
Telephone number:	

Please tick this box if you are willing for the information below to be disclosed	☐

System specification/detail:
Please fill the form below in order specify the capability of your measurement system

Measurement method:	Choose an item
Sample Size: Please specify if other:	other
Sample Thickness range:	From mm To mm
Applied Stress: Please specify if other:	Choose an item
Applied B range:	From T To T
Applied Frequency:	From Hz To Hz
Measured Parameters:	Peak-to-peak magnetostriction ☐ Zero-to-peak magnetostriction ☐ Velocity ☐ Acceleration ☐ Harmonics of magnetostriction ☐ If other please specify
Any other information:	

If you have publication/ literature on your system please attach.

CARDIFF UNIVERSITY
PRIFYSGOL CAERDYDD

Figure 6- 7: Magnetostriction round robin questionnaire

Table 6- 5: Measurement parameters

Measurement Laboratory		Sample size (mm)	Applied stress (MPa)	Peak to peak amplitude x 10-6						Method of measurement
				Fundamental	Harmonics		Fundamental	Harmonics		
				100 Hz	200 Hz	300 Hz	120 Hz	240 Hz	360 Hz	
Wolfson	a	100 x 500	- 10 to + 10	Y	Y	Y	Y	Y	Y	Piezoelectric accelerometers
	b	30 x 305								
Lab 1		100 x 610	0	Y	Y	Y	N	N	N	Laser Doppler
Lab 2		100 x 500	0	Y	Y	Y	Y	Y	Y	Piezoelectric accelerometers
Lab 3		180 x 40	- 10 to + 10	Y	Y	Y	Y	Y	Y	Piezoelectric strain sensor
Lab 4	a	100 x 500	0	Y	Y	Y	N	N	N	Laser Doppler
	b		0 to 20							Strain gauge
Lab 5		100 x 500	- 5 to 0	Y	Y	Y	Y	Y	Y	Laser Doppler

Samples were selected and prepared as explained in section 6.1. For 180*mm* × 40 *mm* samples and 30*mm* × 305*mm* samples comparisons were made between the neighbouring samples and the original samples (10*mm* × 500*mm*). The 100 *mm* x 610 *mm* size samples were not tested in Wolfson before shipping as the clamping process might have affected the sample due to application of compressive stress in the clamping area which could influence the results of that particular participating laboratory. Table 6-6 shows the test conditions for the samples with respect to the rolling and transverse directions. Each sample was tested three times.

Table 6- 6: Round robin test conditions with respect to the sample orientation

Direction	Flux density (Tesla)	Magnetising frequency (Hz)	Applied stress (MPa)
Rolling direction	1.0, 1.3, 1.4, 1.5, 1.7, 1.8	50, 60	From -10 to 10
Transverse direction	1.0, 1.3, 1.4, 1.5		

6.4.4. Magnetostriction variation

Figure 6-8 shows the magnetostriction variation on the Wolfson-A system, explained in Chapter5, between 15 samples (100 *mm* ×500 *mm*) in the rolling and transverse directions at 1.7 and 1.5 T respectively. Each sample was tested three times. The results show high consistency in the magnetostriction value in both directions, with a maximum standard division of 1.3 in the rolling direction and 0.78 in the transverse, which gives an indication of the uniformity of the properties of the sheet, such as coating stress and misorientation. These results show that the differences in magnetostriction values between neighbouring samples can be considered negligible for this comparison.

In order to confirm that the samples were not damaged during the round robin exercise, the magnetostriction values of the returned samples were re-measured and compared. The repeatability in magnetostriction between the original samples and returned samples are shown in Figure 6-9 and 6-10 for the rolling and transverse directions respectively.

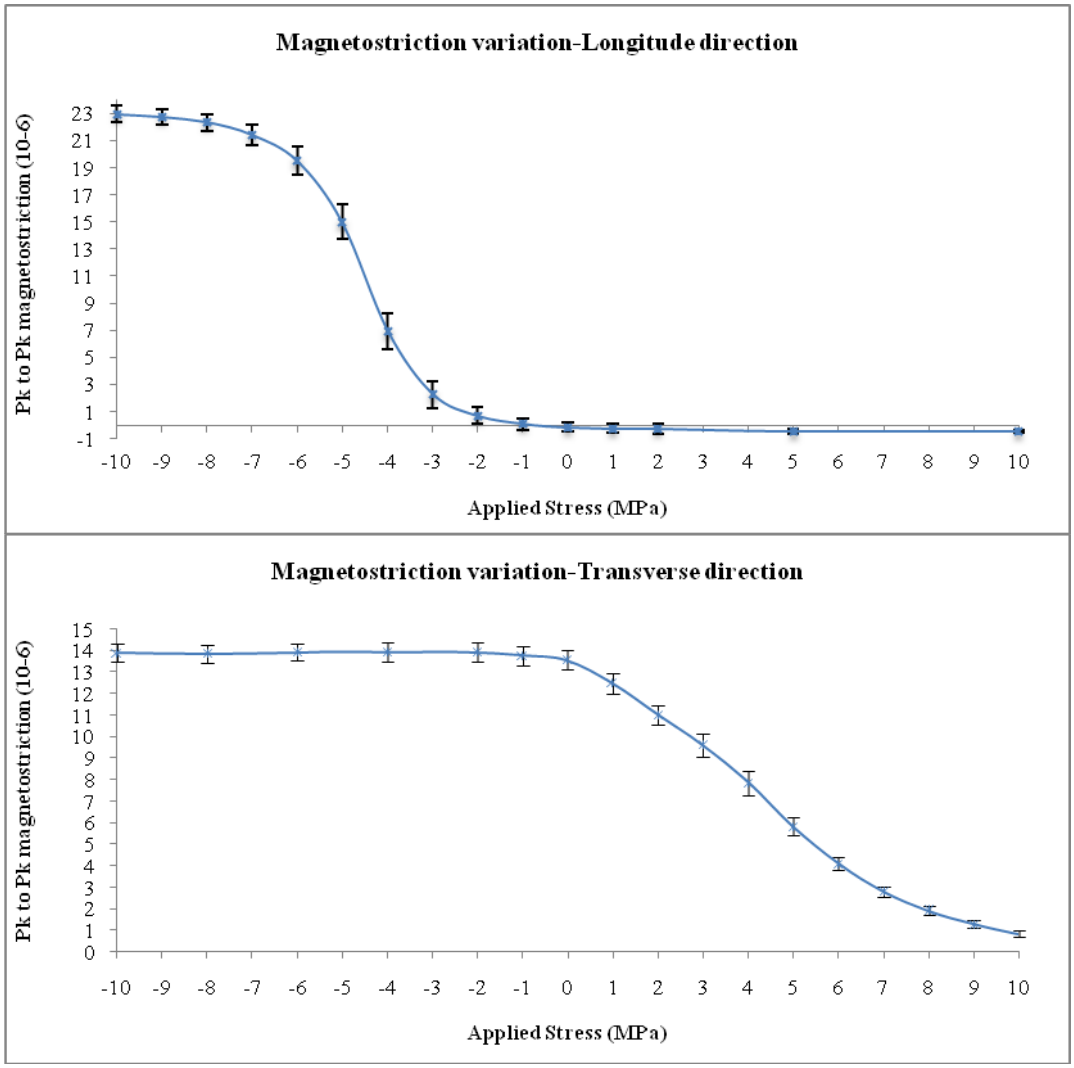

Figure 6- 8: Magnetostriction variation between 15 samples cut from the CGO core explained in chapter 6.1. Top) Rolling direction at 1.7T and 50Hz. Bottom) Transverse direction 1.5T 50Hz

The comparison between the samples before they were sent out and on their return show good agreement, with 4.3% and 3.6% difference in the magnetostriction saturation in the rolling and transverse directions respectively. This is within the magnetostriction measurement uncertainty of the system. Therefore, it may be concluded that the samples were packed properly and that they were not damaged during handling or testing in the laboratories and that the comparisons between the laboratories are valid.

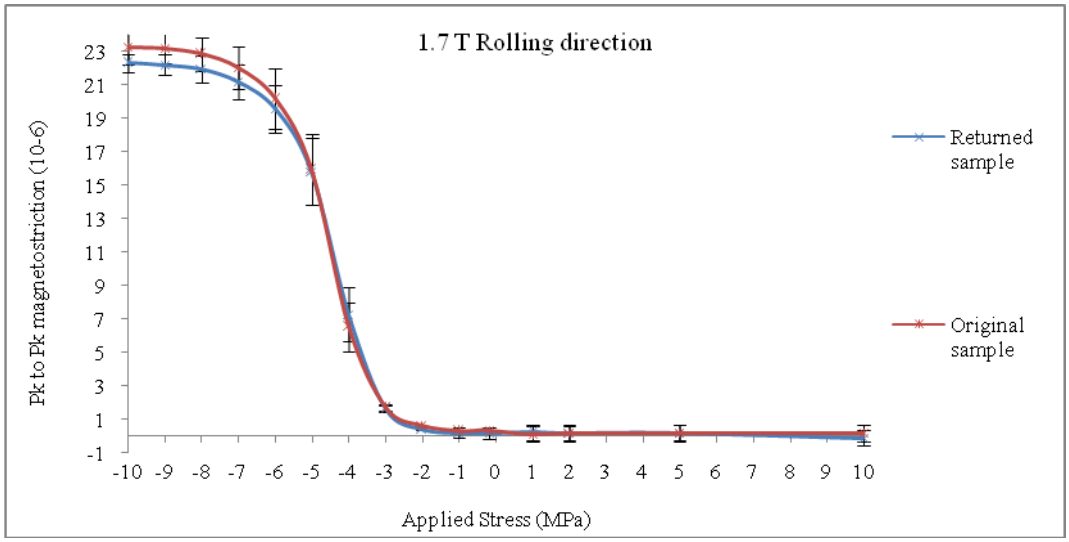

Figure 6- 9: Magnetostriction comparison between the original sample and the returned sample in rolling direction at 1.7 T and 50 Hz

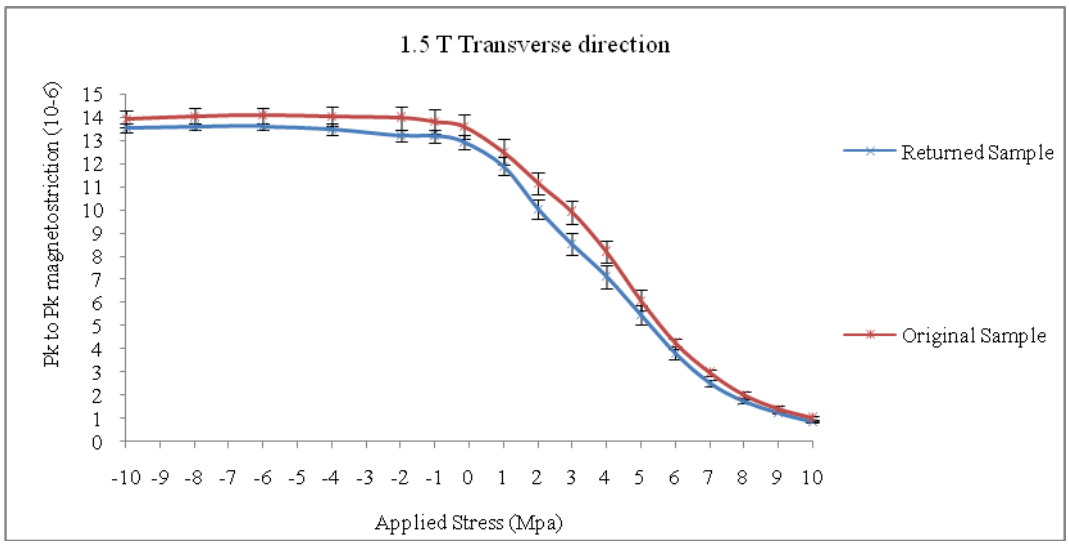

Figure 6- 10: Magnetostriction comparison between the original sample and the returned sample in rolling direction at 1.7 T and 50 Hz

6.4.5. Results:

Using the newly built Wolfson Centre-A system, explained in Chapter 5, all samples were tested and the comparison was made between Wolfson Centre-A (with sample size 100 *mm* by 500 *mm*) and the individual laboratories. Below, the systems of each of the participating laboratories are described briefly and the results of the comparison are shown. All the presented results are at 50Hz as it was the common magnetizing frequency between all the participating laboratories.

6.4.5.1. Wolfson Centre-B:

The Wolfson Centre-B measurement system was developed for the measurement of the magnetostriction of single Epstein strip-sized samples under controlled stress in the range ±10 MPa [8]. A schematic of the measurement system is shown in Figure 6-11. Flux closure is by means of a single wound grain oriented silicon steel C-yoke, placed in the horizontal configuration as shown in Figure 6-11.

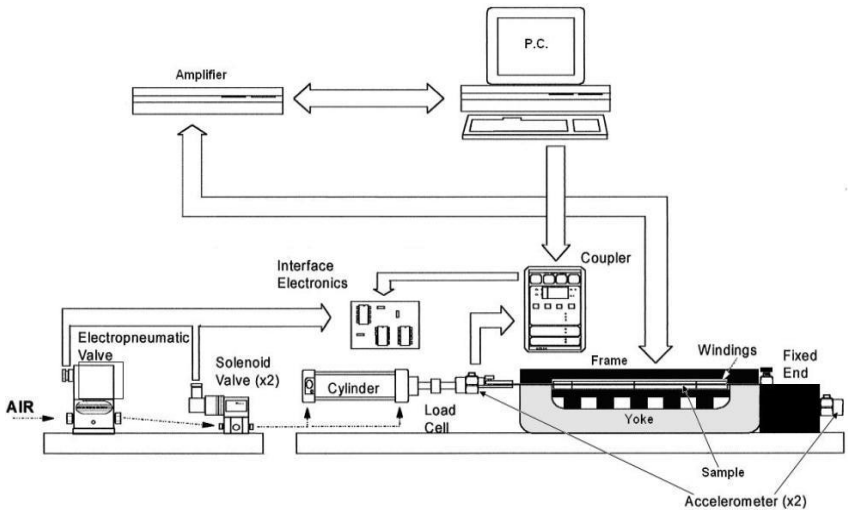

Figure 6- 11: Wolfson Centre-B measurement system schematic

Two accelerometers are used for the measurement of magnetostriction. The first accelerometer is mounted on the clamp at the fixed end of the strip thus providing a reference signal, whilst the second accelerometer is attached to the free end of the strip. The peak-to-peak magnetostriction is calculated from the double integration of the differential outputs of the piezoelectric accelerometers with an uncertainty of ± 0.5%, unstressed, and ± 5%, under an applied compressive stress of 10 MPa.

In total, six samples were compared, three in the rolling direction and three in the transverse direction. Figure 6-12 shows the comparison between the rolling direction samples at 1.0, 1.5 and 1.7 Tesla.

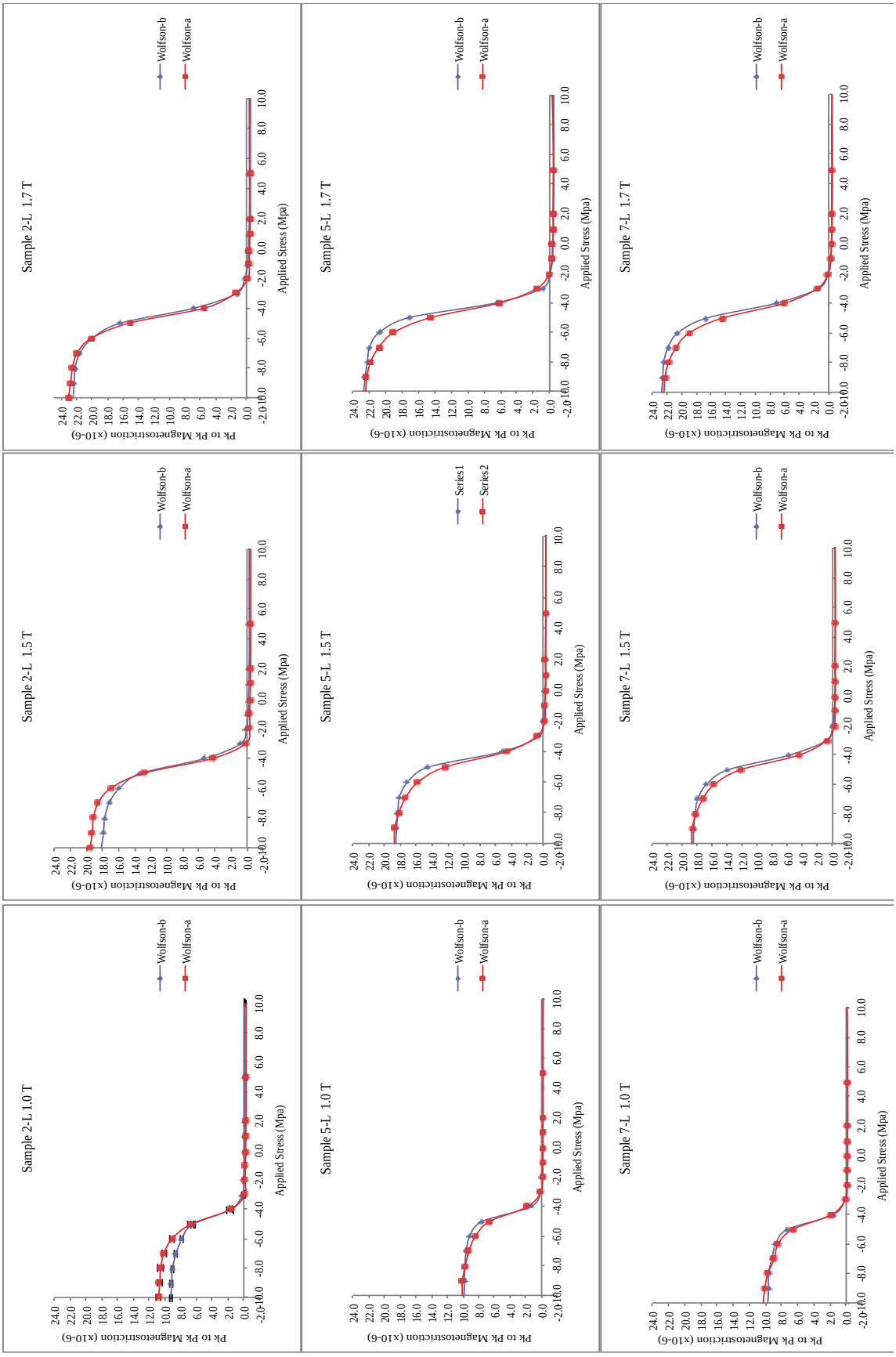

Figure 6- 12: Comparison results between Wolfson Centre A and B in the rolling direction at a frequency of 50 Hz

The results show good agreement between the two systems over the full stress range. The difference in magnetostriction measurements between the two systems is within the combined uncertainty of the two systems calculated according to UKAS M3003[9] despite the samples not being identical for the two measurements with a maximum 1.6% difference in saturation magnetostriction.

6.4.5.2. External Lab 1:

The Lab-1 measurement system uses a double yoke in the vertical configuration in order to provide the flux closure. The vertical configuration of the yokes is to avoid surface pressure being applied to the test specimen at the pole faces. The magnetostriction is measured using a laser Doppler vibrometer at a magnetizing frequency of 50Hz and at zero applied stress. The test specimen is clamped at one end and the laser beam is focused at the other end where it measures the sample movement.

The test specimen for this laboratory has a length of 610 *mm* and width of 100 *mm*. Therefore, samples were first tested in Lab 1 and then Wolfson Centre-A tested the samples. In total, five samples were tested in the rolling direction at a flux density of 1.0, 1.5 and 1.7 Tesla.

Figure 6-13 shows the comparison results between Lab 1 and Wolfson Centre-A. The results show good agreement between both laboratories. The maximum difference between the two laboratories was calculated to be around 0.2 micro-strain at 0MPa applied stress; that is, within the combined uncertainties.

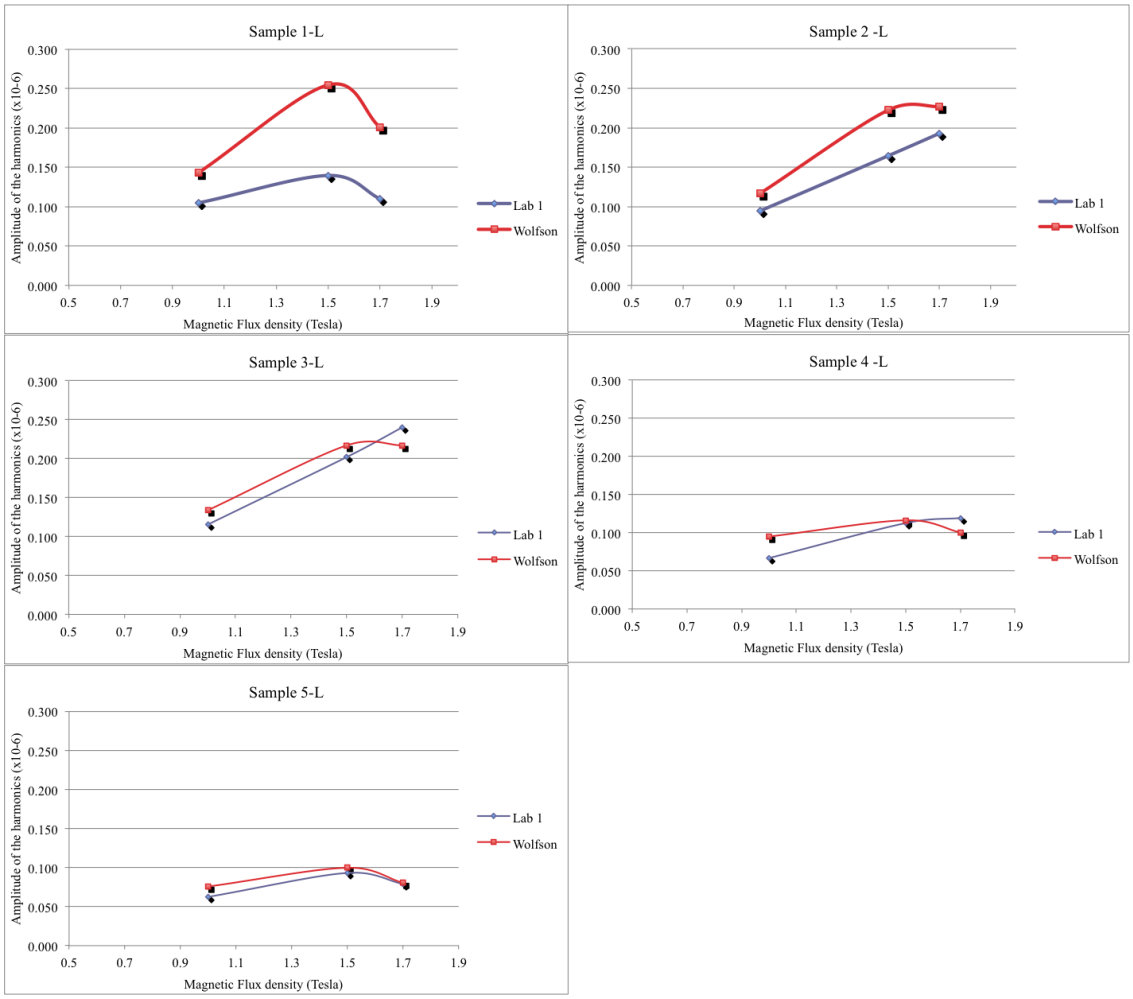

Figure 6- 13: Comparison results between Wolfson- Lab A and Lab 1 in the rolling direction and 50 Hz

6.4.5.3. External Lab 2:

The magnetostriction measurement system in Lab 2 is a single sheet tester with a single yoke. The test specimen is 500 *mm* long by 100 *mm* wide. Two accelerometers are used for the magnetostriction measurement. The test specimen is clamped at one end with a magnetized length of 0.4m. The system does not include a stress application system so all measurements were carried out at zero stress.

Figure 6-14 shows the comparison of results between the two laboratories. In total, six 100 *mm* by 500 *mm* samples were tested, three in the rolling direction and three in the transverse direction. In the transverse direction it can be seen that

there is a 3.5 micro-strain difference at 1.0 Tesla and a 5.2 micro-strain difference at 1.5 Tesla on average between the laboratories, which fall outside the combined uncertainties of two systems. This difference seems to be constant between the samples in the transverse direction. On the other hand, due to the small magnetostriction values (less than 1 micro strain) no trend can be seen in the rolling direction. The average difference in the rolling direction between two laboratories is 0.5 micro strain, which is larger than the combined uncertainties.

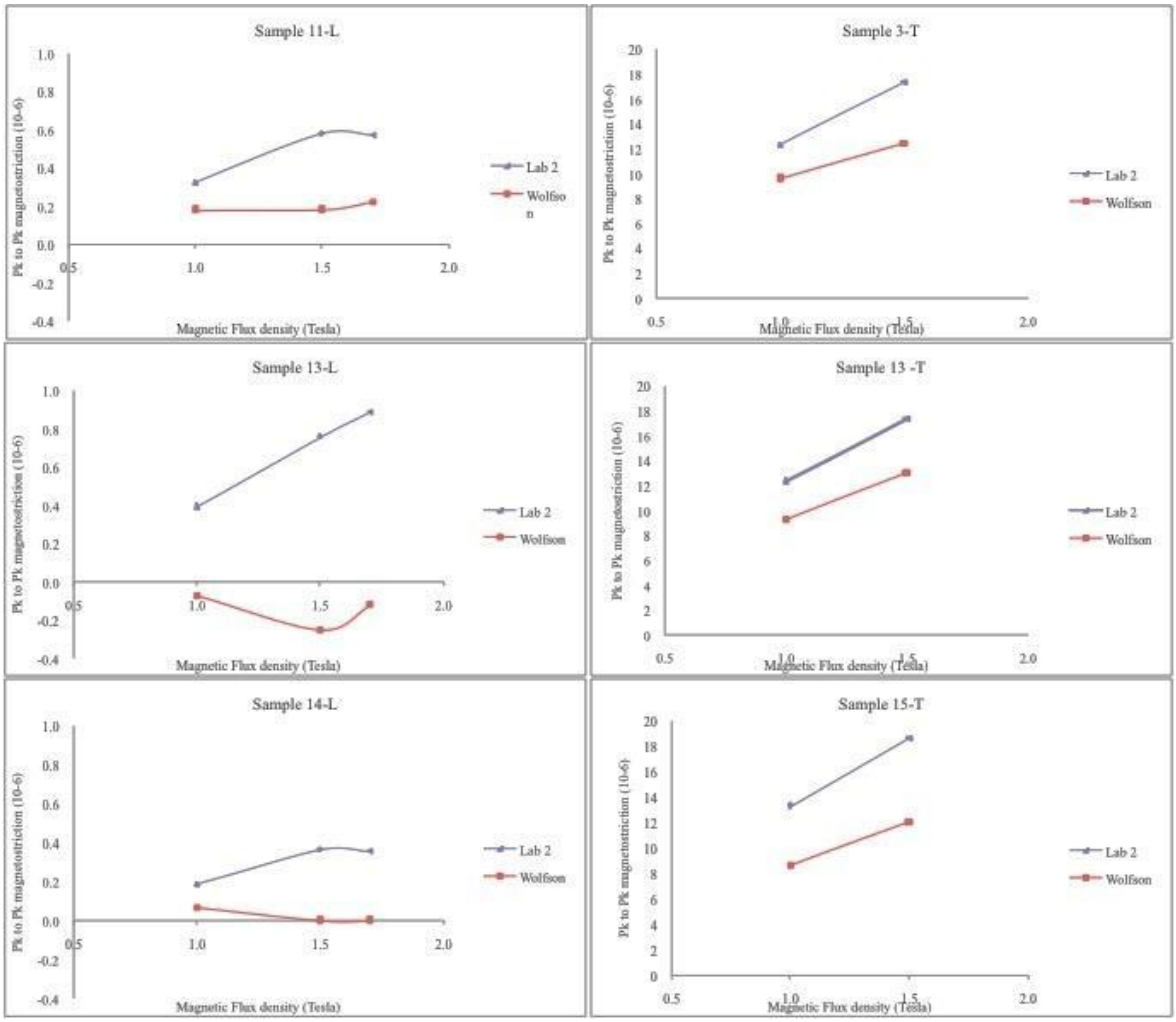

Figure 6- 14: Comparison of results between Wolfson-Centre A and Lab 2 in the longitudinal direction (marked with L) and transverse direction (marked with T) at 50 Hz

6.4.5.4. External Lab 3:

The magnetostriction is measured using two piezoelectric accelerometers. Each accelerometer is assembled from an aluminium plate, onto which a piezoelectric pick-up is mounted. Accelerometers are located on the top and bottom surfaces of the test specimen in order to reduce the influence of bending of the sample on the measurement.

The test specimen comprises a stack of ten 180 *mm* by 40 *mm* steel sheets and the measurement region is 40 *mm* by 40 *mm*. A single yoke provides the magnetic flux closure. Also a non-magnetic spacer is used in order to keep the gap between the yoke and the test specimen constant for a more uniform flux distribution.

The test specimen is subjected to mechanical stresses of -10, 0 and 10 MPa in the longitudinal direction by increasing the torsion on the threaded rod and spring system. The clamping force was controlled by the use of a torque wrench.

The standard measurement uncertainties for the peak-to-peak values of magnetostriction harmonics, measured at 1.7 T in Lab 3 are estimated at ±6% for the fundamental component.

In total, twenty 40 *mm* by 180 *mm* samples were given to Lab 3 (ten in each direction) and the results were compared by averaging the magnetostriction values from four of their neighbouring samples (100 *mm* by 500 *mm*), measured by Wolfson Centre-A. Figure 6-15 shows the comparison of the magnetostriction (the fundamental harmonic) versus applied stress in both the rolling and transverse directions.

The comparison results, shown in Figure 6-15 show an increase in the magnetostriction value with increasing applied stress in the rolling direction. The average difference between the two systems is higher than the combined uncertainty value of both systems, as the difference in magnetostriction saturation at 1.7T is larger than 5 micro strain and the combined uncertainty is less than 2 micro-strain. Whereas in the transverse direction there is a random difference at 1.5 Tesla, at 1.0 Tesla the differences between the two systems are negligible, 0.95 micro-strain on average, and fall within the uncertainty of the systems.

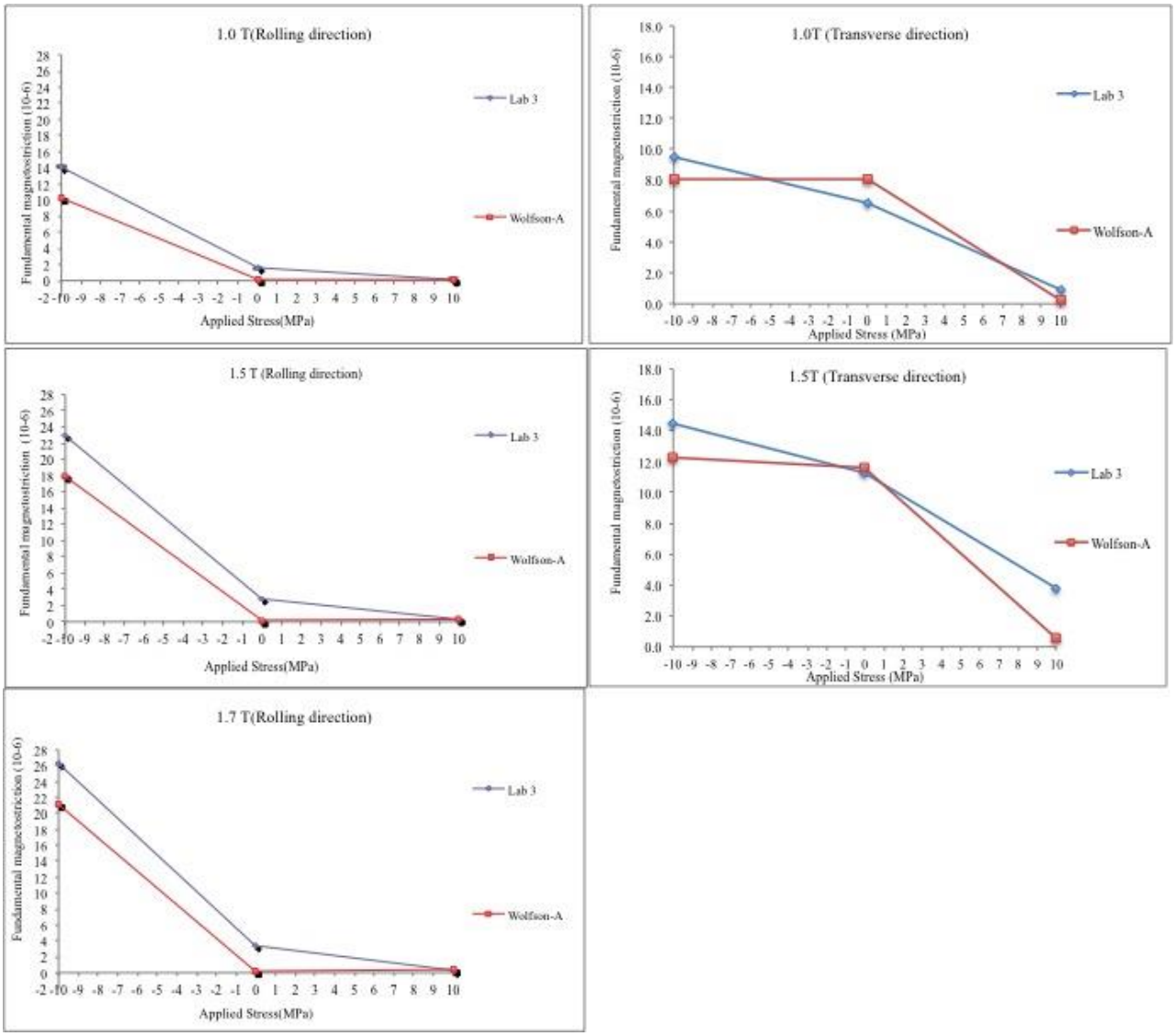

Figure 6- 15: Comparison result of Fundamental magnetostriction harmonic vs. Applies Stress at magnetizing frequency of 50Hz between the Wolfson Centre-A and Lab 3

6.4.5.5. External Lab 4:

Lab 4 uses two different measurement techniques, the first technique using a laser Doppler vibrometer (LDV) and the second system using a strain gauge. The test specimen for both systems has a length of 500mm and a width of 100mm.

The LDV system uses a horizontal double yoke for forming a closed magnetic circuit. Two optical targets (reflecting mirrors) are fixed on the test sample at a distance of 170mm apart. The system measures a single point, which is repeated for both targets alternatively. The difference in velocity between them is then calculated. The LDV system has a magnetostriction resolution of 3×10^{-9}. The LDV system does not apply any external stress to the sample.

The other system used in Lab 4 is a strain gauge magnetostriction measurement, which is a local measurement. As mentioned previously, this system uses the same sample size (100 *mm* ×500 *mm*). The strain gauge is adhered to the test sample surface. Two yokes are placed on either side of the sample to provide the magnetic closure. The magnetizing length for the system is 300 *mm*. The system is able to apply external stress of up to 20MPa tension by holes drilled in the specimen ends and clamping the stress jigs. The strain gauge size used for this experiment was 1mm long.

Figure 6-16 shows the comparison of results between Lab 4 LDV, STG and Wolfson Centre-A in the rolling direction at zero stress. The results show good agreement between the Wolfson Centre-A and the Lab4 LDV systems, with an average difference of around 0.25 micro strain, which is smaller than the combined uncertainty of the two systems. Whereas the Lab-4 STG does not agree with either of the systems (Lab4 LDV or Wolfson-A), at the higher magnetic flux density,

where the magnetostriction value increases, the difference becomes more noticeable.

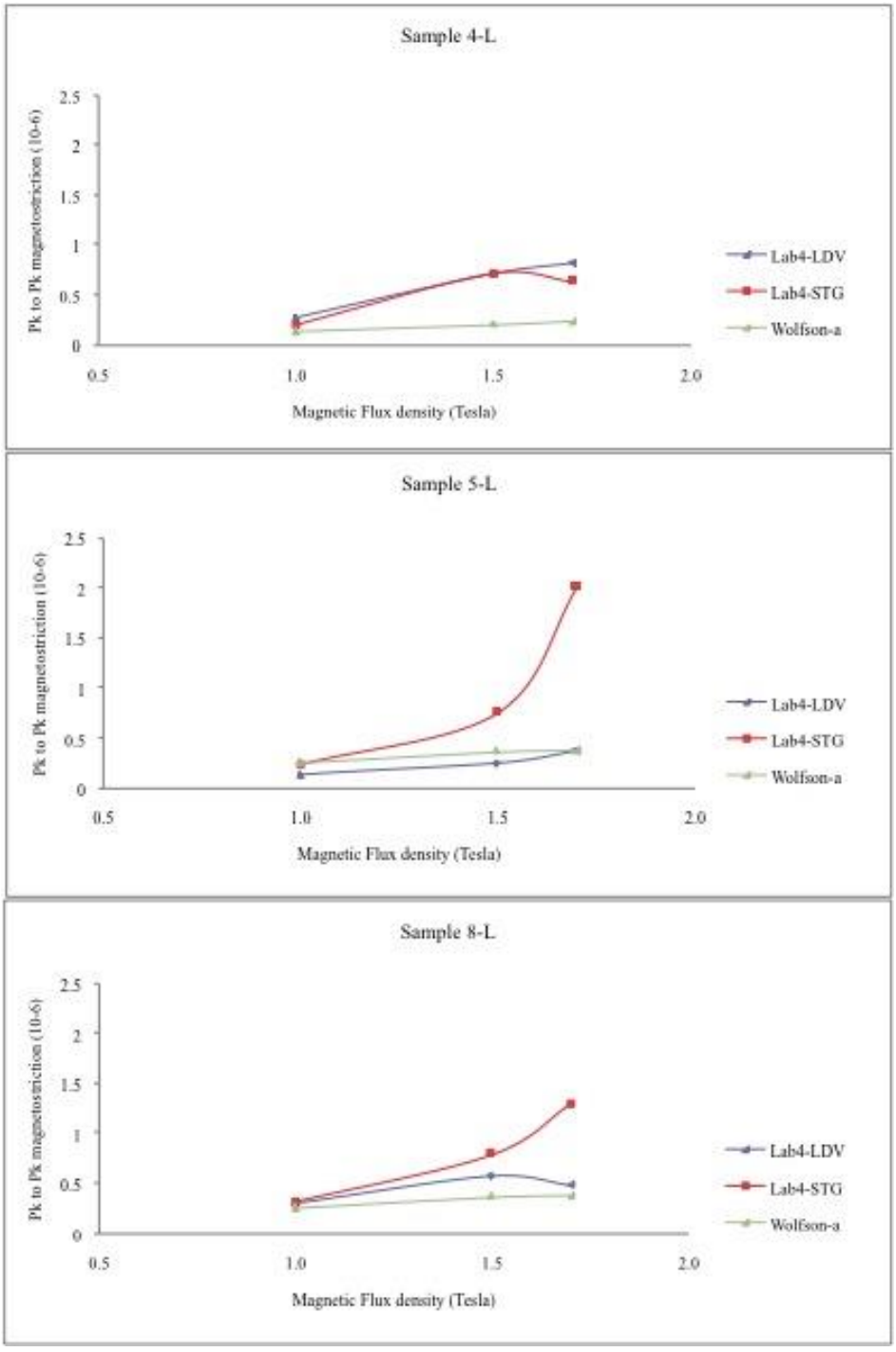

Figure 6- 16: Comparison results between Wolfson- Lab A and Lab 4 LDV and STG systems in the longitudinal direction (marked with L) at 50 Hz and zero stress

6.4.5.6. External Lab 5:

Lab 5 uses a Laser Doppler vibrometer for the measurement of magnetostriction. The test specimen for this system has dimensions of 100 *mm* by 500 *mm*. Magnetic closure is completed by using a horizontal single yoke. The sample is fixed to the base at one end and the other end is connected to the stressing device. The distance between the fixed clamp and the optical sensor is 270 *mm*. The sensor cancels the noise by detecting relative vibration between the optical sensor on the sample and the reflector fixed to the base.

The stress is applied to the test specimen by using an air cylinder and an electro-pneumatic valve. Figures 6-17 and 6-18 show the comparison of results between Lab 5 and Wolfson Centre-A in the rolling and transverse directions, under applied compressive stress at 50Hz.

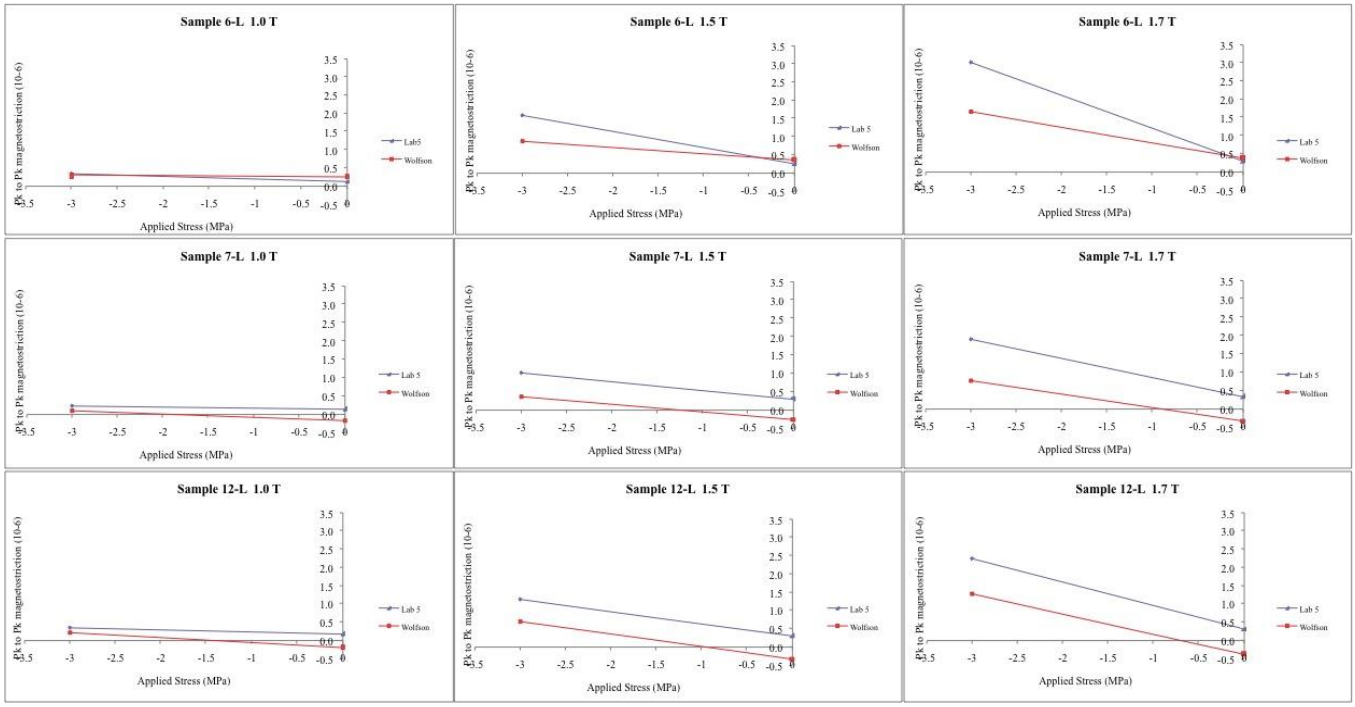

Figure 6- 17: Comparison of results between Wolfson Centre-A and Lab 5, in the rolling direction at 50 Hz

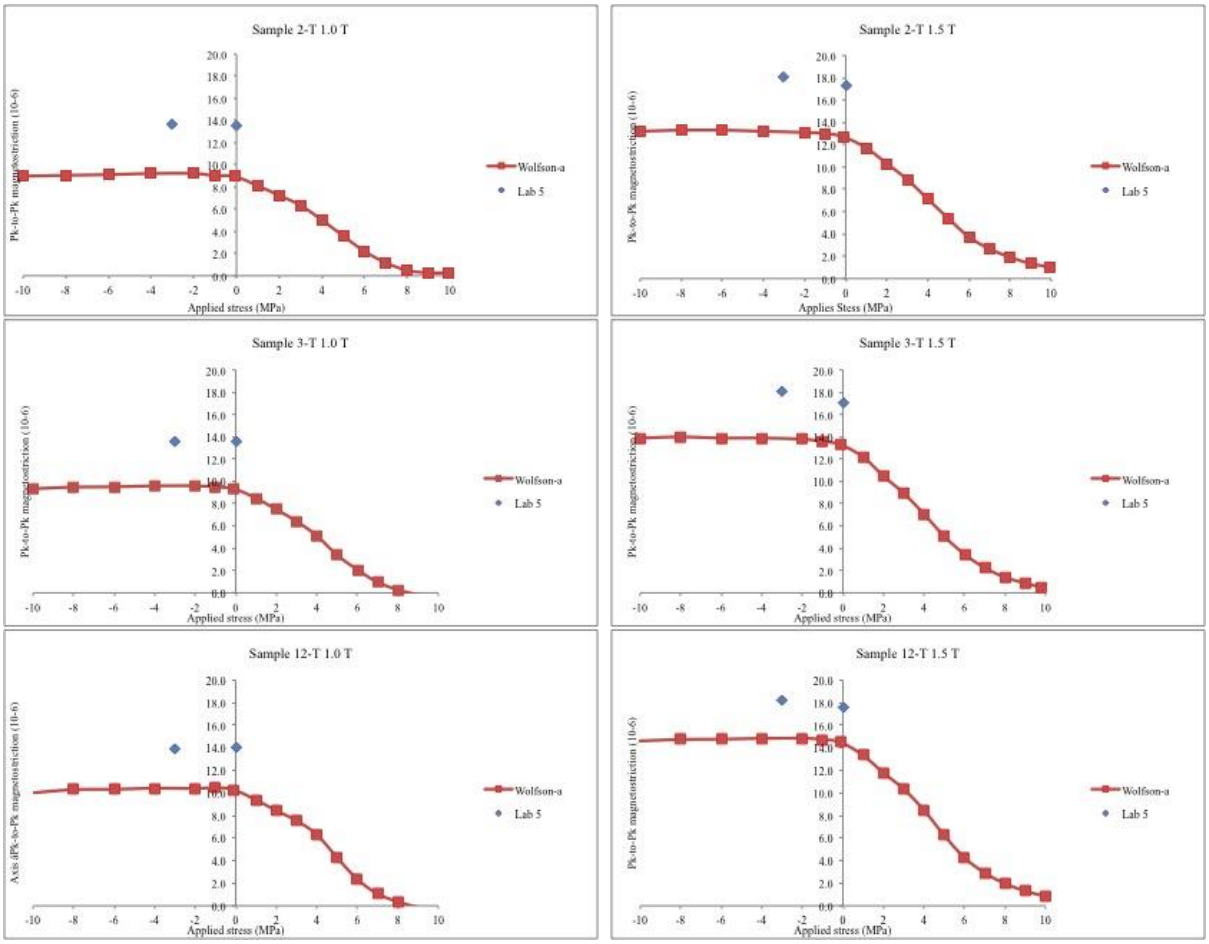

Figure 6- 18: Comparison of results between Wolfson Centre-A and Lab 5, in the rolling direction at 50 Hz

The results show a shift between the two laboratories' Pk-to-Pk magnetostriction values in both directions, which seem to be constant in most cases regardless of the peak magnetic flux density or applied stress.

6.4.6. Discussion and Conclusion:

To illustrate the difference between the laboratories, the magnetostriction value at a magnetizing frequency of 50 Hz has been selected. A range of different test methods and test configurations was used by these laboratories from localized measurement methods such as the strain gauge, piezoelectric accelerometer to non-contact methods such as the Laser Doppler vibrometer. Moreover, different

magnetizing systems were used, such as different yoke sizes, single or double yokes and horizontal or vertical configurations of the closure yokes.

The first magnetostriction round robin exercise shows a reasonable correlation between the different methods. In order to investigate the differences in more detail, further data and investigations would be required from each of the participating laboratories as at this time limited information were given. Some of the possible reasons for the differences between the measurement systems may be considered.

- Comparisons at zero stress, isolated measurement at zero stress, in the rolling direction could not be referenced as the magnetostriction value is so small and the differences are larger than the combined measurement uncertainty of the laboratories. As a result it is not valid.
- Due to the high stress sensitivity of magnetostriction, some non-uniformity in the applied stress could cause substantial differences in the measured magnetostriction, as the results show that the differences in the stressed measurements were mostly larger than the unstressed measurements.
- The various sample clamping arrangements of the test specimen by the individual participating laboratories could certainly influence the measured magnetostriction coefficient by significantly damping the magnetostriction coefficient.
- Through the use of a vibration reference point, the magnetostriction may be determined more accurately by subtracting the measurement system vibration from lamination vibration.

- It is recognized that the differing magnetizing lengths and magnetostriction measurement lengths and widths could significantly affect the measured magnetostriction coefficient as the measurements between laboratories may encompass differing active grains from localized measurements than in the longer test specimens. Also, it should be recognized that a measurement system that is very localized, and only includes a small number of grains, can show significant differences in magnetostriction from a larger sample system which includes the full range of grain misorientation which can be up to 7% for conventional grain oriented material[10] .
- There has been a wide variation in measured parameters between the participating laboratories which makes the full comparison impossible.
- This round robin exercise has represented the first international comparison of the measurement of the magnetostriction coefficient of grain oriented electrical steel. The project has encompassed a wide range of measurement techniques, each of which has been developed individually. The results have been very encouraging in that the magnetostriction characteristics are seen to be almost consistent between the various measurements. Nevertheless, special care should be taken for comparisons at zero stress in the rolling direction. Further comparisons of this nature would be very useful in order to develop recognized standardized methods of measurement of this parameter.

References for chapter 6

1. Homewood, J.A., D. Snell, and A.J. Moses, *Domain refinement techniques for improved magnetic properties of high permeability grain oriented electrical steel.* Ironmaking & Steelmaking, 1997. **24**(1): p. 84-89.
2. Fukawa, K. and T. Yamamoto, *Domain-Structures and Stress Distributions Due to Ball-Point Scratching in 3-Percent Si-Fe Single-Crystals with Orientation near (110) [001]*. Ieee Transactions on Magnetics, 1982. **18**(4): p. 963-969.
3. Snell, D. and P. Beckley, *Domain refinement of high-permeability grain-oriented electrical steel using low-friction ball units.* Journal of Magnetism and Magnetic Materials, 1994. **133**(1-3): p. 167-169.
4. Cole, R.W., *Effect of elastic bending on magnetic properties of oriented silicon iron.* Journal of Applied Physics, 1958. **29**(3): p. 370-371.
5. Neurath, P.W., *Magnetostriction and domain structure of materials for use in low-noise equipment.* Electrical Engineering, 1954. **73**(11): p. 991-994.
6. Lawhead. R, H.R.a.H.J., *Three Phase Transformer Winding Configurations and Differential Relay Compensation* in *60th Annual Georgia Tech* 2006.
7. ASTM, *ASTM E691-13 Standard Practice for Conducting an Interlaboratory Study to Determine the Precision of a Test Method*, in *Planning the interlaboratory study*2013.
8. Anderson, P., *A Novel Method of Measurement and Characterisation of Magnetostriction in Electrical Steels*, 2001 Cardiff of Wales
9. National Measurement Accreditation, S., *The expression of uncertainty and confidence in measurement for calibrations*. 1995: NAMAS.
10. Ushigami, Y., et al., *Recent development of low-loss grain-oriented silicon steel.* Journal of Magnetism and Magnetic Materials, 2003. **254-255**: p. 307-314.

Chapter 7: Experimental investigation of factors affecting magnetostriction

The influence of the following factors on the magnetostriction of 3% grain oriented silicon steel was investigated:

i. Domain refinement process
ii. Residual curvature (coil set)
iii. Geometry

7.1. Effect of domain refinement process on peak to peak magnetostriction of high-permeability 3% Si-Fe

Power loss is one of the most important magnetic properties for transformer core materials [1]. Domain refinement is known as one of the most effective methods for reduction of iron loss of high permeability grain oriented steel [2]. When the material is subjected to an external magnetic field, the width of the domains with flux paths primarily in the same direction as the external magnetic fields grow at the expense of other domains (explained in Chapter 2). Part of the input energy is converted into heat due to domain wall movement [2]. The width of the 180^{o} domains defines the distance that the domains walls need to move and therefore is strongly related to power loss, so if the domain width could be reduced then the energy loss would be reduced due to the reduction of anomalous eddy current losses [2, 3].

The magnetostriction measurement system has been used to gather magnetostriction data in this study of the effect of scribing on magnetostriction.

Static magnetic domain structures in samples were observed before and after domain refining using the Bitter technique [4, 5].

The Bitter technique uses a current carrying coil in order to generate a magnetic field of approximately 2.2 kAm^{-1} perpendicular to the surface of the steel sample. As a result any deviations of the (110) plane from the sample surface will cause the formation of free poles, and by using the small ferromagnetic particles of the Bitter fluid agglomerate, the domain structure can be revealed. A Schematic drawing of the technique is shown in Figure 7-1 [6].

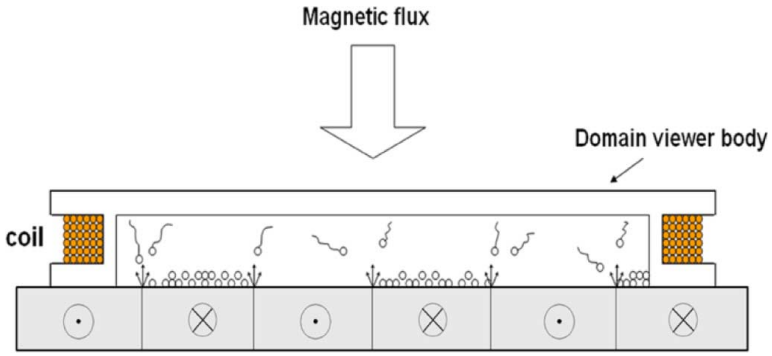

Figure 7- 1: Drawing of the magnetic domain viewer using Bitter technique[6].

7.1.1. Domain refinement techniques

7.1.1.1. Mechanical scribing:

In this method, an array of steel balls is pressed onto the steel surface along spaced line 90^{o} to the rolling direction. The applied pressure causes the region to be deformed depending on the elastic modulus of the ball and the steel strip [7]. The applied compressive stress changes the domain structure of the scribed area (explained in Chapter 3) and acts as an artificial grain boundaries [8]. The stress is applied after the final thermal flattening process as the heat treatment would stress relieve the steel and remove the effect [3]. The resultant stress pattern is shown in

Figure 7-2 [9]. The stress distribution resultant from mechanical scribing is expressed in stresses parallel to the surface with compressive stresses in the top and bottom surface, shown as C_1 and C_2 in the Figure 7-2, of the sample and tensile stresses in the remaining area shown as T in the Figure 7-1 [9, 10].

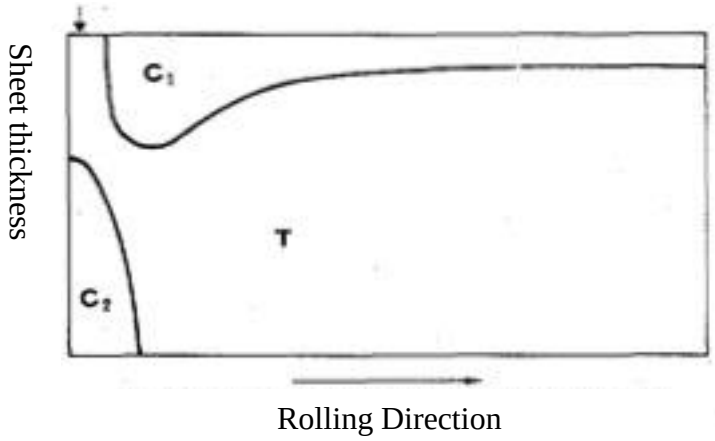

Figure 7- 2: schematic distribution of stress due to scribing, the regions with tensile perpendicular to the scribe line is indicated with (T), and (C) compressive [9].

The load applied by springs and variable load can be achieved by adjusting the number of spacers in the assembly [3]. The performance of this method is highly dependent upon the applied load level, diameter of the ball and distance between the lines [11].

- **Effect of mechanical scribing on domain structure and power loss:**

Fukawa.K and Yamamoto.T [9]suggested that domain structure due to ball-point scribing perpendicular to the rolling direction must have magnetization parallel to the scribe line and magnetization inclined ± 45^o to the sample surface by observing the domain structure in single crystal, scribed perpendicular to the rolling direction using scanning electron microscopy. The existence of these domains will reduce the magneto-static energy due to formation of flux closure path (explained in Chapter 2.3.2). Moreover, The stress distribution shown in

Figure 7-2 results in making the lancet closure domains unstable and refines the 180^{o} main domain wall spacing (explained in Chapter 2.3.4). Domain structures of a scribed sample perpendicular to the rolling direction are shown in Figure 7-3.

The stress pattern on the bottom surface under a scribe line and a saw tooth domain (triangle) domains which can be seen over a wide range near the scribed line, shown in Figure 7.3, on the top surface in the vicinity of a scribe line will both disappear under a tension parallel to rolling direction, These domains are believed to be surface domains providing flux closure for underlying domains perpendicular to longitudinal direction, As the [001] axis is inclined to the surface plane these domains form as sub domains to minimize the magneto-static energy. These 90^{o} closure domains form during the magnetization process [11]. Since the domain pattern on the top and bottom surfaces are quite different it can be concluded that the transverse domains are not continued through the whole cross section of the sample [9]. Figure 7-4 illustrates the schematic design of these domains.

Fukawa.K and Yamamoto.T [9] suggested that since these domains almost disappear under applied tension parallel to the rolling it can be inferred that there is a compressive stress perpendicular to the scribe line. [9, 10].

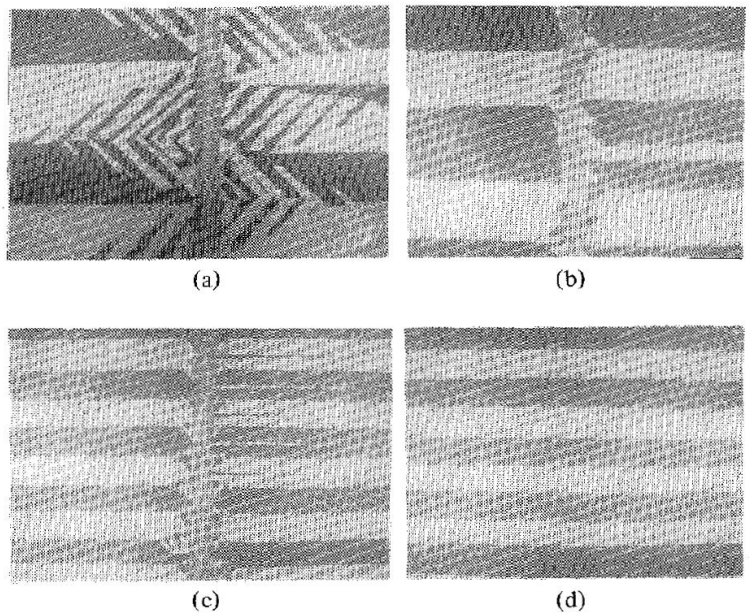

Figure 7- 3: Domain structure in single crystal with β= $0^{0,}$ scribed perpendicular to the rolling direction. A) Top surface after scribing. B) Bottom surface after scribing. C) Top surface, Tensile stressed. D) Bottom surface, Tensile stressed [9].

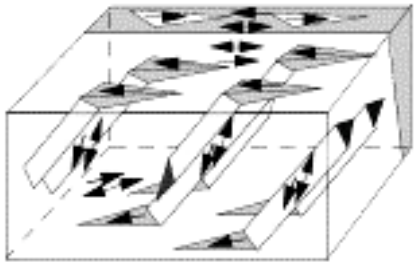

Figure 7- 4: Schematic design of the surface closure formed as a result of mechanical scribing [12]

Also from the Figure 7-2 can be predicted that the top surface has lower permeability than the bottom surface, which would affect flux distribution in the stressed area.

The degree of domain refinement is dependent on the line spacing, the ball diameter and the applied load. Moreover, the overall loss reduction is dependent on other variables such as grain size, grain orientation stress coating [3].

7.1.1.2. Laser scribing:

Laser scribing is a non-contact method for domain refinement, which uses laser irradiation. The energy of the laser irradiation (equation 7.1) is absorbed by the surface producing a temperature shock wave to travel through the material generating a large temperature gradient that produces an inhomogeneous expansion in the vicinity of the laser line [11], in the subsequent time the heat is liberated and the temperature decreases to its initial value. This causes regions of plastic deformation near laser lines and as a consequence creates compressive stress perpendicular to them and tensile stress between the lines [13] . Moreover, Iuchi, T [14] has showed that a high dislocation density is introduced by the laser irradiation, which generates local stress field .These results show that the domain refining by laser scribing is due to residual stress as in the case of mechanical scribing.

Figure 7-5, shows the relationship between U (J/cm^2) and core loss reduction, where U is the energy irradiated on the unit area of the specimen and can be calculated as follows:

$$U = {}^{E}/_{D \times l} \tag{7.1}$$

Where

E = Energy per pulse (J)

D = spot spacing along the direction perpendicular to the longitude direction (cm)

l = line spacing (cm)

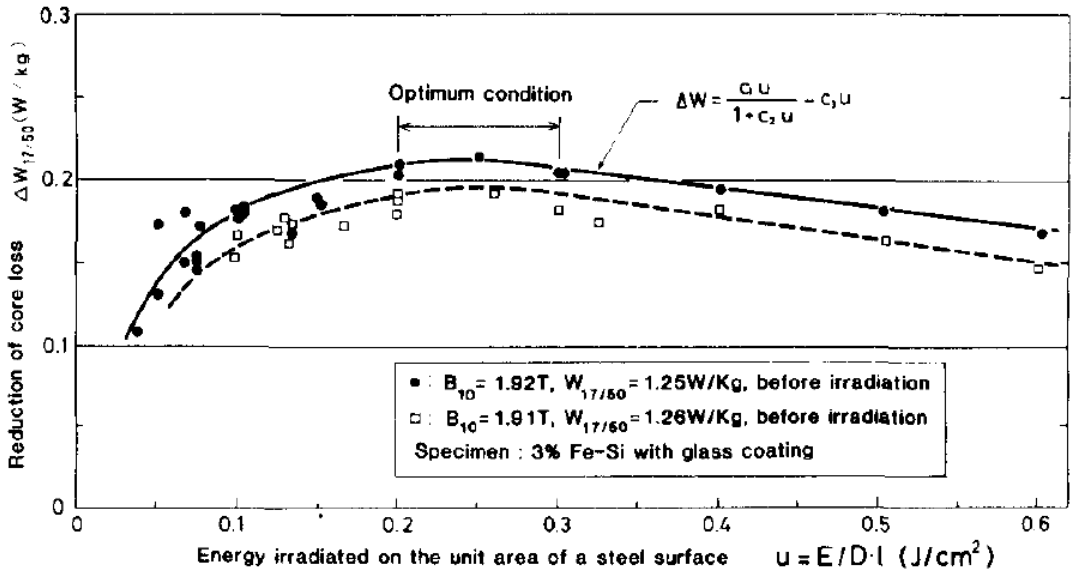

Figure 7- 5: relation between U and core loss reduction after laser scribing 3% Fe-Si with glass coating at 1.7T and 50 Hz [15]

It has been known that domain-refining effects by laser-irradiation are due to residual stress. Suzuki, H., et al [16] confirmed that magnetic domain refinement by laser-irradiation is due to induced tensile residual stress by assessing the distribution of stress using an X-ray measurement system as in the case of mechanical scribing and will be removed by stress-relief annealing [11].

On the other hand plastic deformation at the surface of the material due to laser irradiation, acts in the reverse way in terms of the iron loss due to an increase in the hysteresis component of loss[17-19]. The total power loss is determined by the balance of these effects [15].

- Effect of laser scribing on domain structure and power loss:

The Domain structure induced by laser irradiation indicates a compressive stress parallel to the roiling direction, and formation of 180^0 closure surface

domains along the scribed line, and the internal domain structure is aligned to the [100] and [010] direction in the sheet [15].

Since the laser scribing method is based on the same principle as mechanical ball scribing, the same sub-domains form near the trace of laser irradiation with transverse magnetization. Surface closure domains that have 90^o domains and transverse magnetization beneath and striped pattern with the same contrast as 180^o domains [10].

The domain arrangement due to laser scribing confirms the existence of compressive stress along the scribing lines and tensile stress perpendicular to them [10, 15]. Tensile stress between the laser scribe lines refines the domain-wall spacing thus inhibit the wall movement and reducing core loss [14].

7.1.2. Results and discussion:

As it was explained earlier, two method of domain scribing were used, laser scribing and ball pen scribing, the ball pen scribed samples were made in the Wolfson centre and the laser scribed samples were tested as received. Figure 7-6 shows the variation of the normalized power loss with stress of a lamination of the laser-scribed materials before and after annealing.

The corresponding peak-to-peak magnetostriction value is shown in Figure 7-7; values are normalized with respect to the Laser scribed samples before annealing. In order to have a better understanding of this effect, the domain structures of the samples were studied using the Bitter technique[4, 5]. Figure 7-8 shows the domain pattern of the sample before and after scribing.

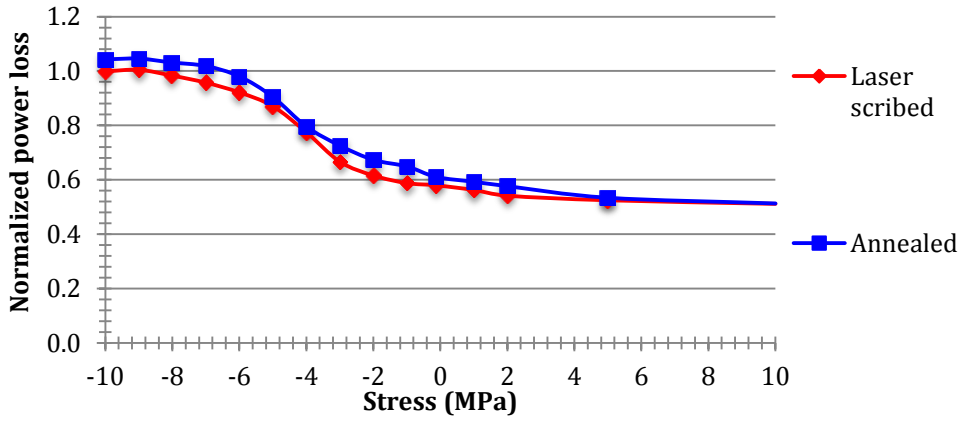

Figure 7- 6: Normalized power loss vs. applied stress, for Laser scribed sample before and after annealing.1.7t and 50 Hz. (each sample were measured tree times).

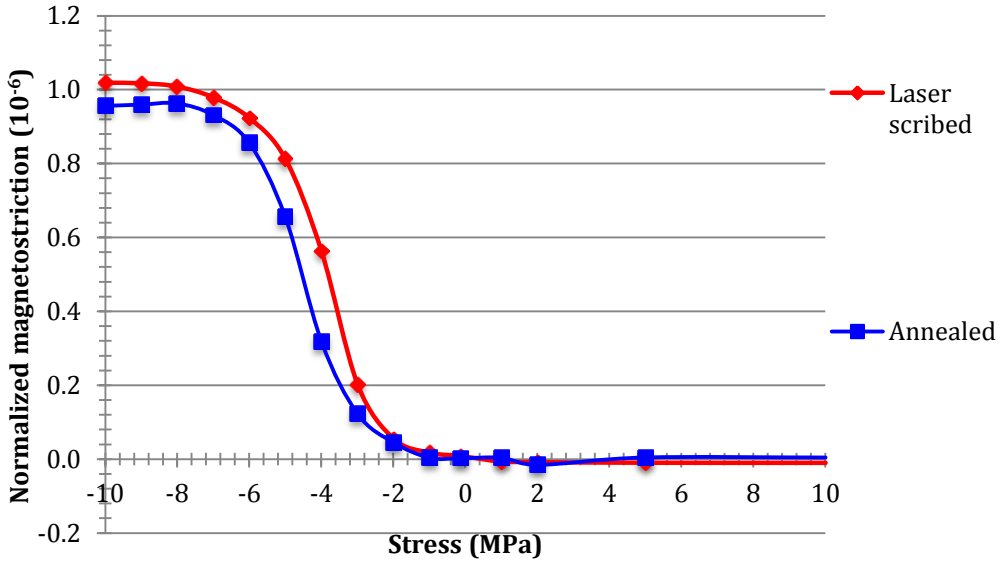

Figure 7- 7: Average Normalized Pk-to-Pk magnetostriction vs. applied stress, Laser scribed sample at 1.7 T and 50Hz of 5 samples (each sample were measured tree times)

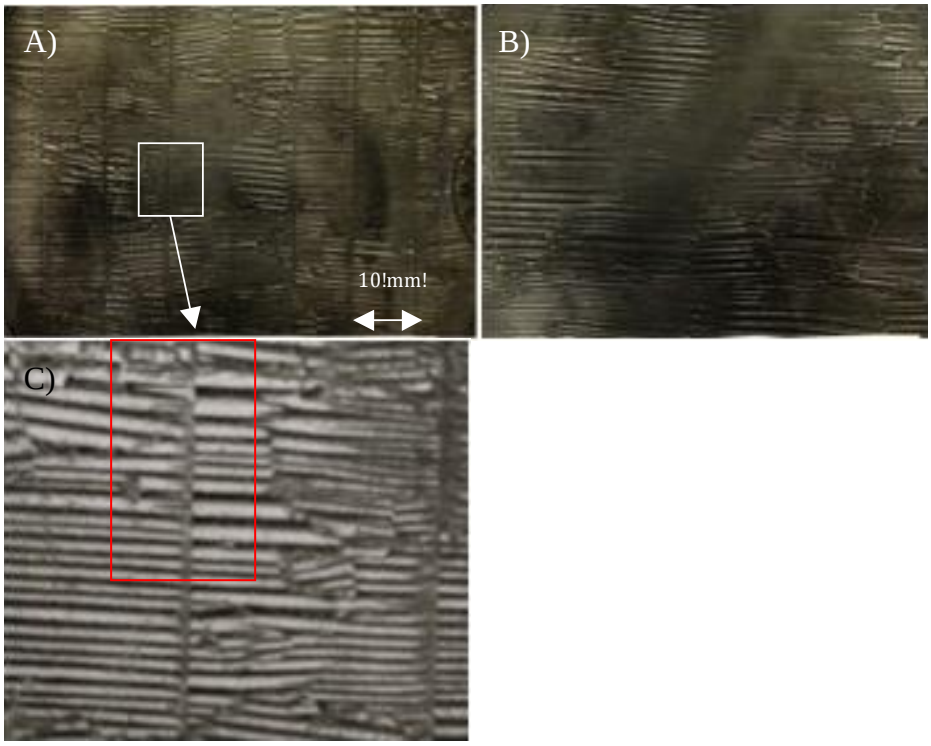

Figure 7- 8: A) domain pattern of the 10mm laser scribed sample, B) domain structure after stress relief annealing at 8109C for 1 Hr. C) newly formed saw-tooth domain near the scribed line

Figure 7-8 shows that the large domain wall spacing has been significantly reduced and the losses have been reduced by 10% on average. Due to the formation of new domain structure around the scribed line that is shown in Figure 7-8, there is more than a 10% increase in the magnetostriction value.

The newly formed saw-tooth domains (triangle shape domains) near the scribed line shown in the red box in Figure 7-8 are surface domains providing flux closure for underlying domains that are magnetized at a 90 degrees to the rolling direction, shown in Figure 7-4. The formation of these domains indicates the existence of compressive stress perpendicular to the scribe line [3]. Formation of the underlying transverse domains causes the changes in magnetostriction characteristics that can be predicted using a proposed model by Simmons and Thompson [20].

Since Laser scribing and mechanical scribing are both due to the same mechanism of induced residual stress, the effect of scribing on magnetostriction can be further investigated by applying the mechanical scribing method. Figure 7-9 and 7-10 show the repeatability of magnetostriction and power loss in five samples for each stage.

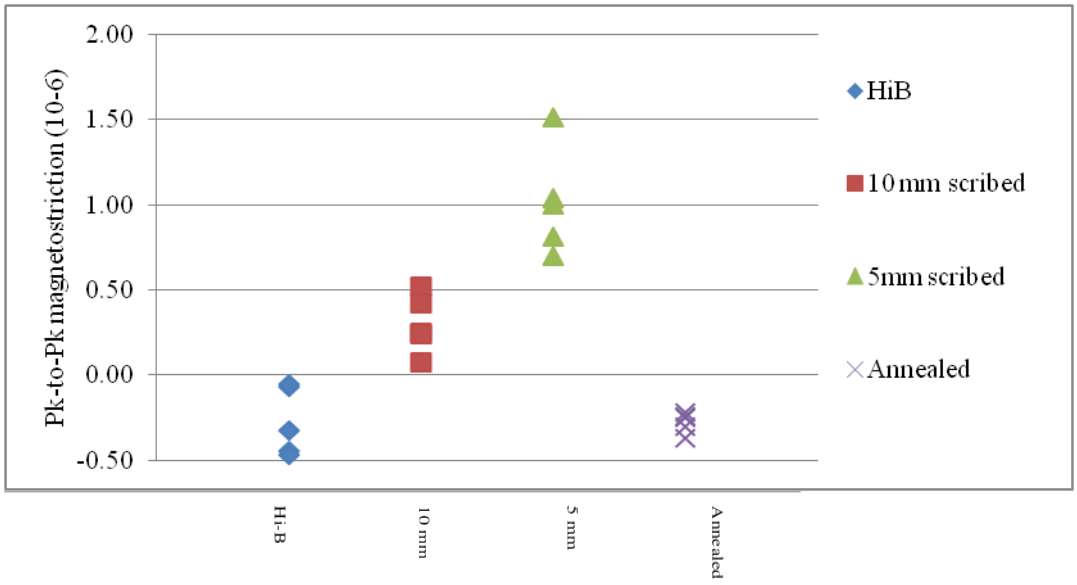

Figure 7- 9: Magnetostriction (Pk-to-Pk 10^{-6}) for five samples in each stage with no stress at 1.7T and 50 Hz. Each sample was tested three times and averaged.

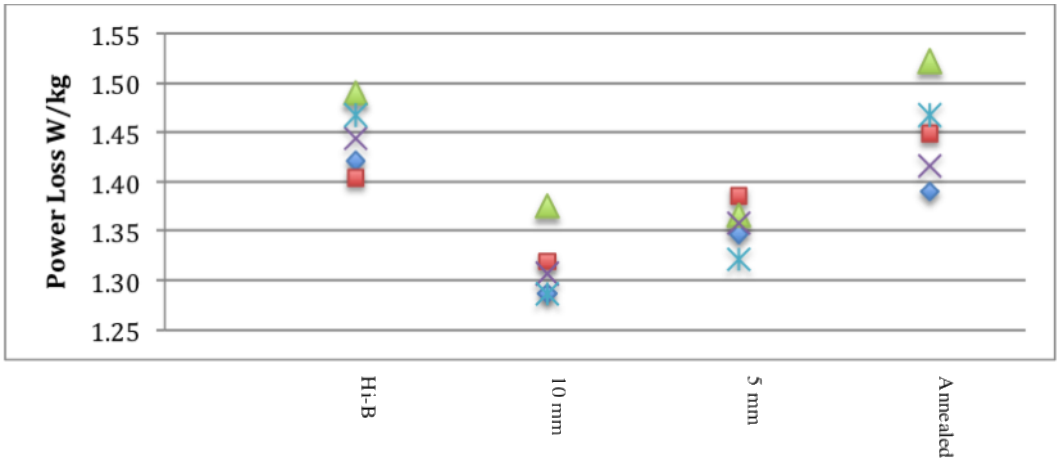

Figure 7- 10: Power loss (W/kg) for five samples in each stage with no stress at 1.7T and 50 Hz. Each sample was tested three times.

From Figure 7-9 it can be seen that the peak-to-peak magnetostriction value of the samples does not have significant changes for samples scribed with 10 mm spacing, Figure 7-10 shows power loss of the specimens scribed at 10 mm intervals transverse to the rolling direction of the strips, power loss shows 10% reduction on average.

By decreasing the scribing distance from 10 mm to 5 mm, there was a significant increase in the peak-to-peak magnetostriction value whereas the power loss has only a slight increase compared to the previous stage (around 9% power loss reduction comparing to the Hi-B sample).

Figure 7-11 shows the domain structure changes of the sample after each stage, by comparing picture B and C, it can be seen the increase of the saw-tooth domains and stress patterns formed along the scribed line. The formation of these domain structures indicates that there is a high compressive stress along the scribe line. The compressed area is two times higher as the one for 10 mm interval scribed samples.

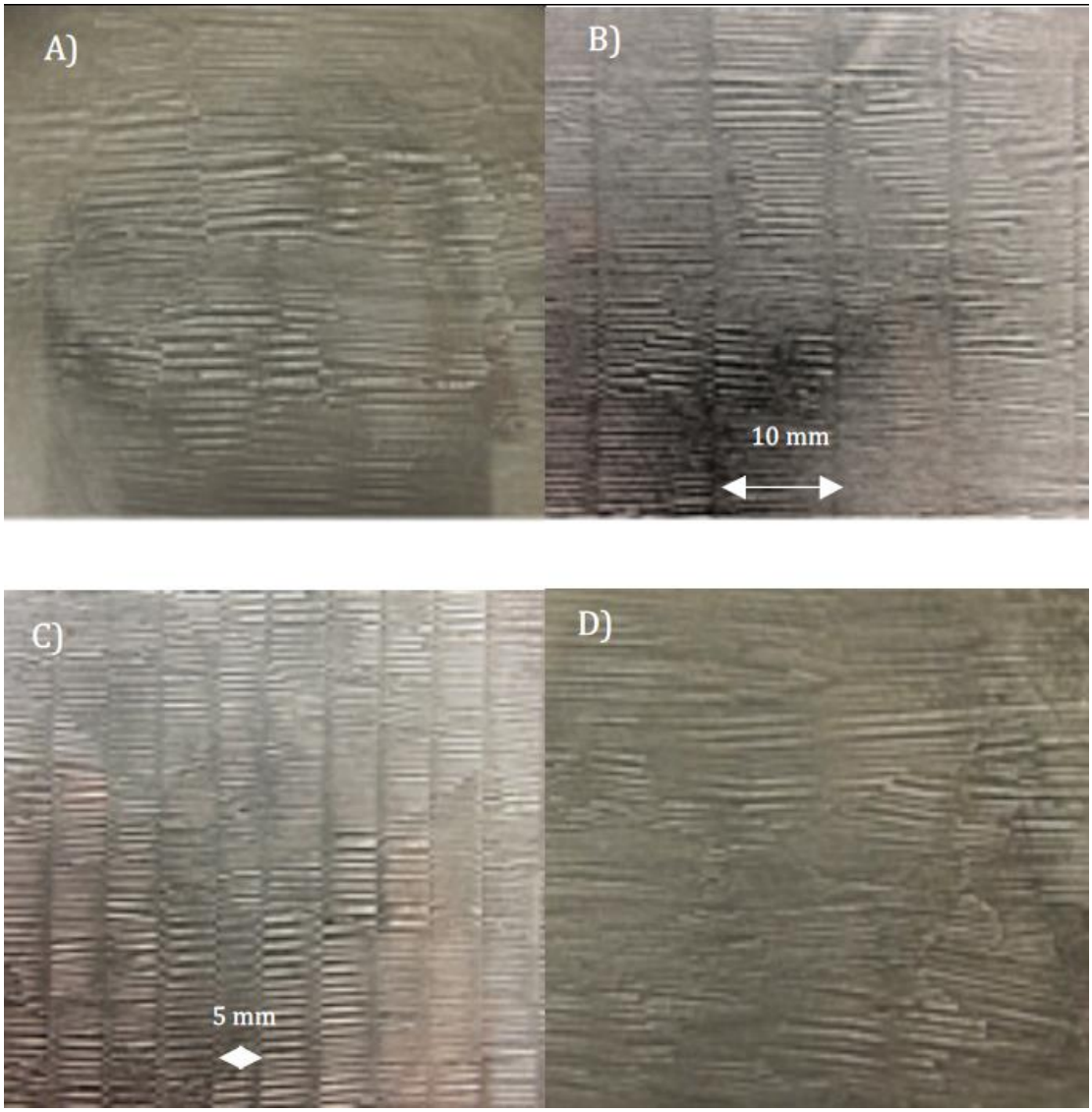

Figure 7- 11: A) annealed Hi-B samples, B) 10mm scribed space 616gram load, C) 5mm scribed, 616gram load, D) Annealed scribed sample

Due to the decrease in the scribe line spacing, the fraction of the compressed area shown in Figure 7-2 gets larger, therefore, there is an increase in [010] and [100] domains due to the stress domain patterns in this area shown in Figure 7-11 C), that is causing the increase in the peak-to-peak magnetostriction value, the increase in stressed area is calculated using the proposed model in section 7.1.3.

The increase of the compressed area and a resultant domain structure also exceeds the benefits in loss given by refined [001] domains. By comparing the power loss and magnetostriction value of the sample after annealing and before scribing no significant changes can be seen. Also by comparing the domain structures it can be seen that the domain structure due to the scribing has been removed fully and the domain width gets back to the starting width which indicate that the applied pressure was not too high to damage the coating and strip (causing plastic deformation) while it was high enough to achieve a degree of domain refinement.

Figures 7-12 and 7-14 show the effect of applied force on peak-to-peak magnetostriction for the sample scribed at 10 *mm* and 5 *mm*, respectively. Figures 7-13 and 7-15 show the corresponding normalized power loss. Values are normalized with respect to the Hi-B sample. The highest power loss reduction was achieved by scribing the sample with a 6.0 N applied load. The magnetostriction value shows a reduction compared to the lower applied load. This results agrees well with the results obtained from the commercial laser scribed samples and results presented by Snell, D. and Beckley, P. [3]of the industrial ball unit domain refinement system .

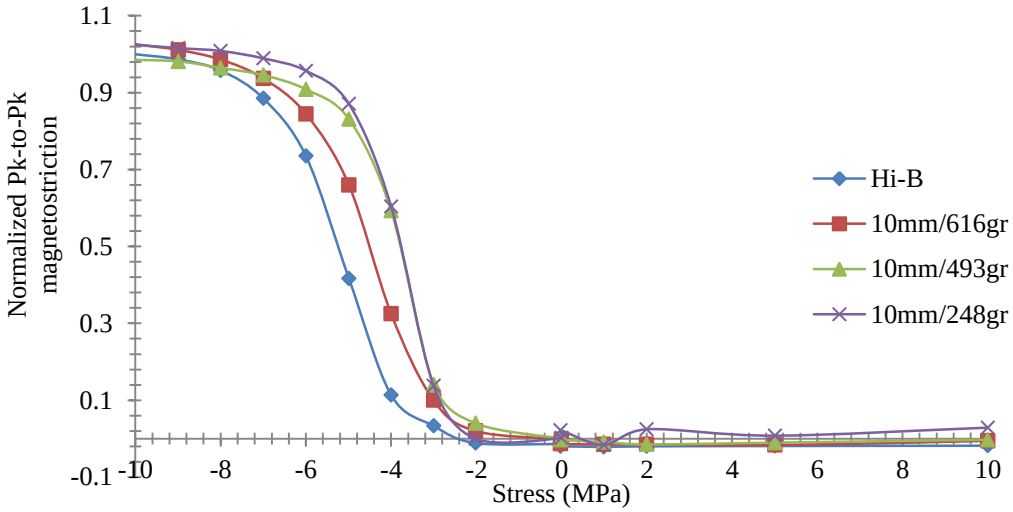

Figure 7- 12: Normalized Pk-to-Pk magnetostriction vs. applied stress, mechanical scribed samples at 1.7 T and 50Hz, scribed at 10mm intervals transverse to the RD of the strips.

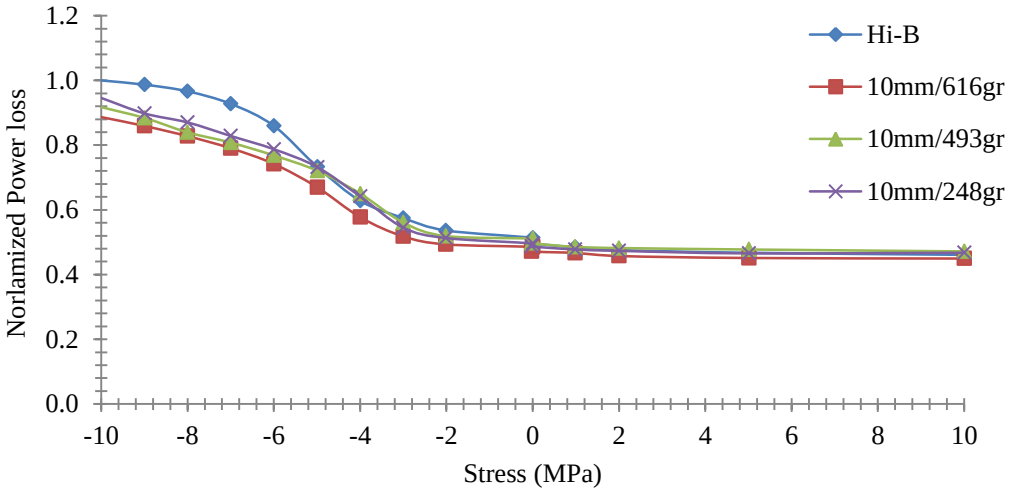

Figure 7- 13: Normalized power loss vs. applied stress, for Laser scribed sample before and after annealing.1.7t and 50 Hz. Scribed at 10mm intervals transverse to the RD of the strip

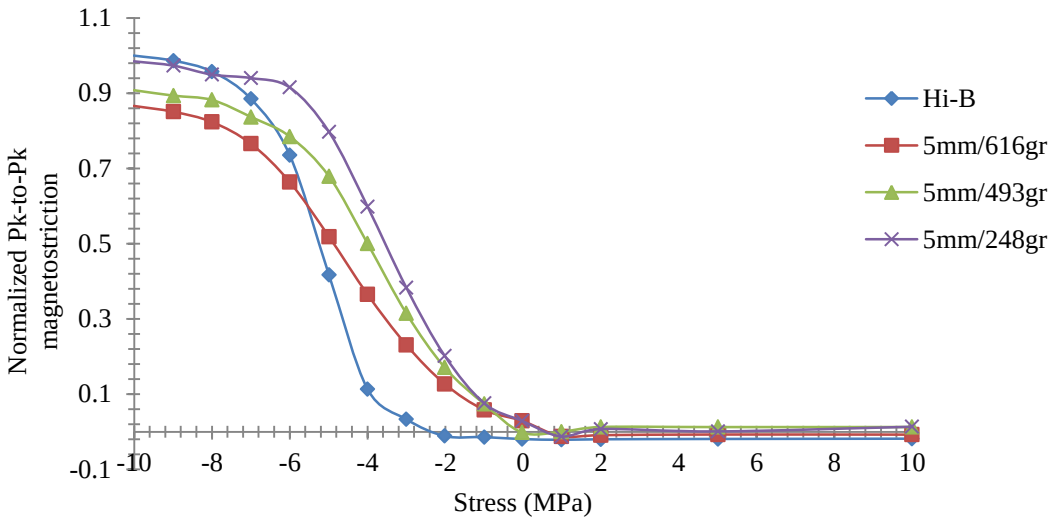

Figure 7- 14: Normalized Pk-to-Pk magnetostriction vs. applied stress, mechanical scribed samples at 1.7 T and 50Hz. Scribed at 5mm intervals transverse to the RD of the strip

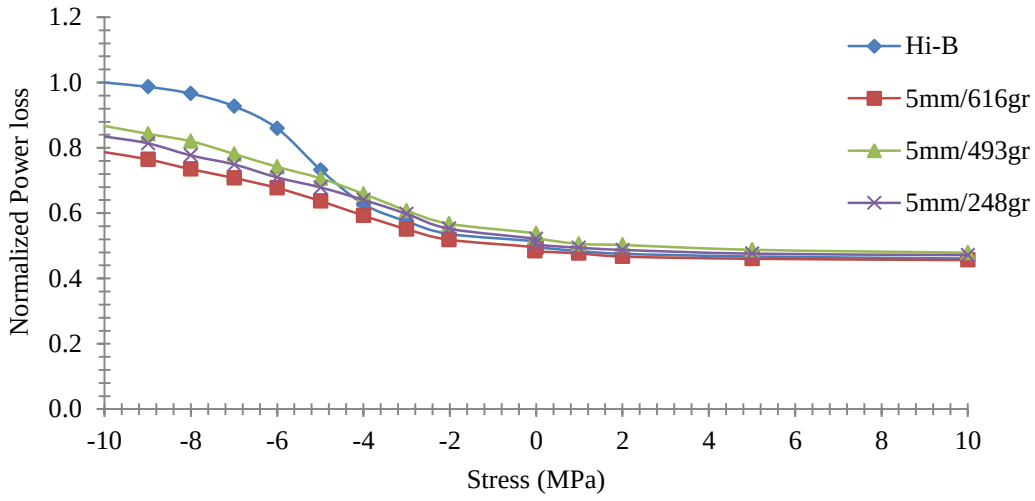

Figure 7- 15: Normalized power loss vs. applied stress, for Laser scribed sample before and after annealing.1.7t and 50 Hz. Scribed at 5mm intervals transverse to the RD of the strip

In order to have a better understanding of the effect of scribing on magnetostriction, the domain structure of the samples with 10 mm and 5 mm scribing line spacing is shown in Figures 7-16 and 7-17, respectively. The sample with 6.0 N of load shows a finer domain width after scribing, and a larger area of saw-tooth domains formed along the scribe line. The balance of the finer domain width and formation of new surface domains determines the total power loss. Eventually as the load increases the compressed area (Figure 7-2) becomes wider

and deeper and consequently the loss contribution from the resultant complex domain structure exceeds the benefits given by refinement of 180^{o} domains, as a result loss increases.

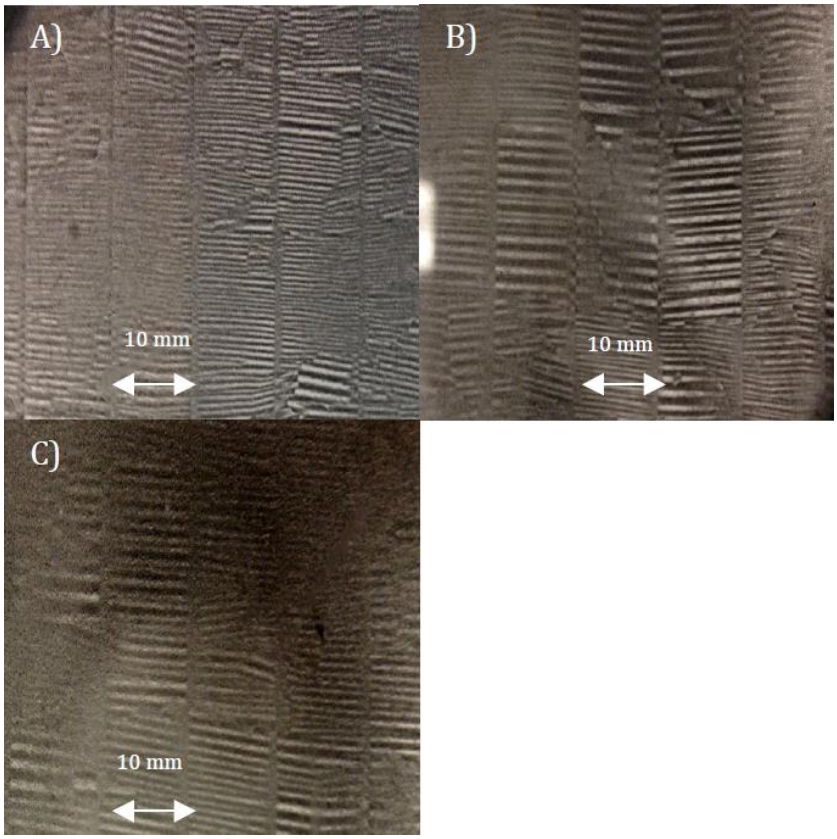

Figure 7- 16: domain pattern of the 10mm mechanical scribed sample, A) 616 grams, B) 493 grams and C) 248 grams

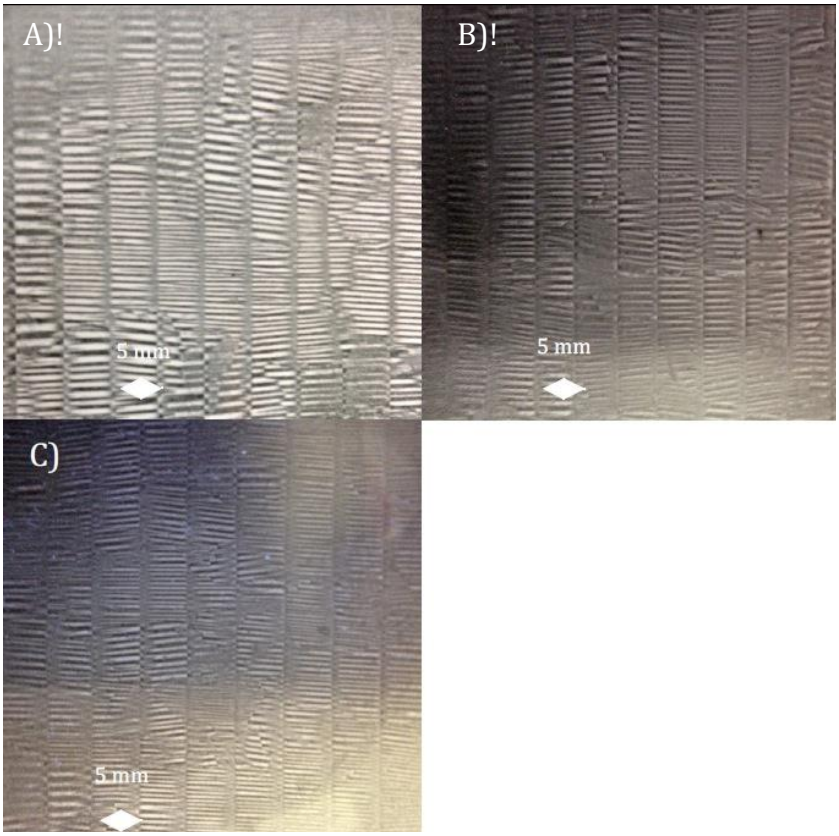

Figure 7- 17: domain pattern of the 5mm mechanical scribed sample, A) 616 grams, B) 493 grams and C) 248 grams

The induced residual stress due to scribing causes an increase in compressive stress in the top surface and tensile shear in the bulk and bottom surface of the sample, as a result scribed samples bend after the scribing process in order to reduce the induced stress gradient and lower the free energy. When testing for magnetostriction, the sample needs to be flattened which is causing a stress gradient in the sample to get back to its initial state (after scribing).

Also it is known that magnetostriction is more sensitive to compressive stresses than tensile stress (Chapter 3, Magnetoelastic energy) and as a result the benefit of the tensile stress in the bulk of sample is overcome by the increase of magnetostriction in compressed regions. Additionally, the newly formed [010] and [001] domains along the scribe line are increasing the magnetostriction value. The

balance of bending stress affects and newly formed domains determines the total magnetostriction value.

In order to eliminate the effect of bending, five HiB samples were chosen and scribed alternating on both sides with 10 mm intervals lines and 6.0 N applied pressure. Figure 7-18 compares the power loss of the sample before and after scribing, this shows an 11% reduction in power loss due to scribing which is similar to the power loss reduction achieved by scribing on one side.

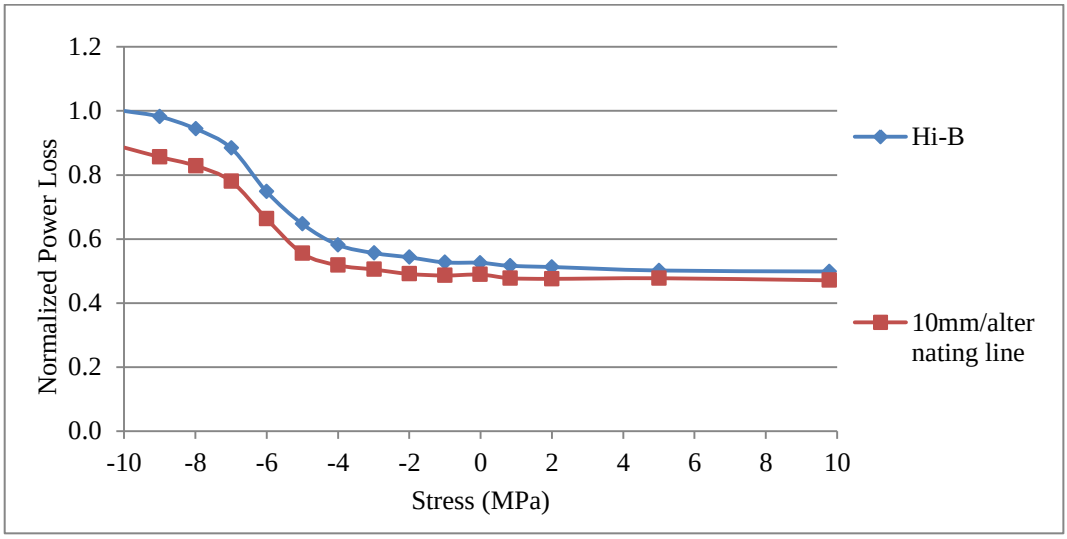

Figure 7- 18: Normalized power loss vs. applied stress, for Laser scribed sample before and after annealing.1.7t and 50 Hz. Scribed at 10mm intervals alternating transverse to the RD of the strip

The corresponding peak-to-peak magnetostriction value is shown in Figure 7-19 values are normalized with respect to the Hi-B samples. The result shows a small increase in magnetostriction after scribing, mainly in the tensile part of the graph. Figure 7-20 compares the normalized magnetostriction values of five samples scribed on single side verses both sides, each sample was tested three times. Results shows less increase in magnetostriction of the samples scribed on both sides than the samples scribed on one side.

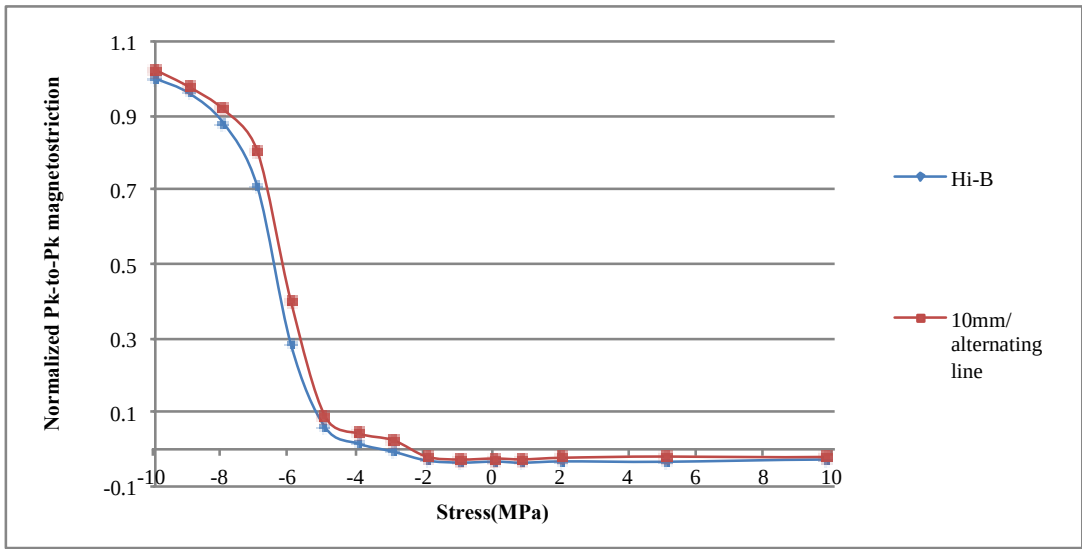

Figure 7- 19: Normalized Pk-to-Pk magnetostriction vs. applied stress, mechanical scribed samples at 1.7 T and 50Hz. Scribed at 10mm intervals transverse to the RD of the strip, alternating line on both side

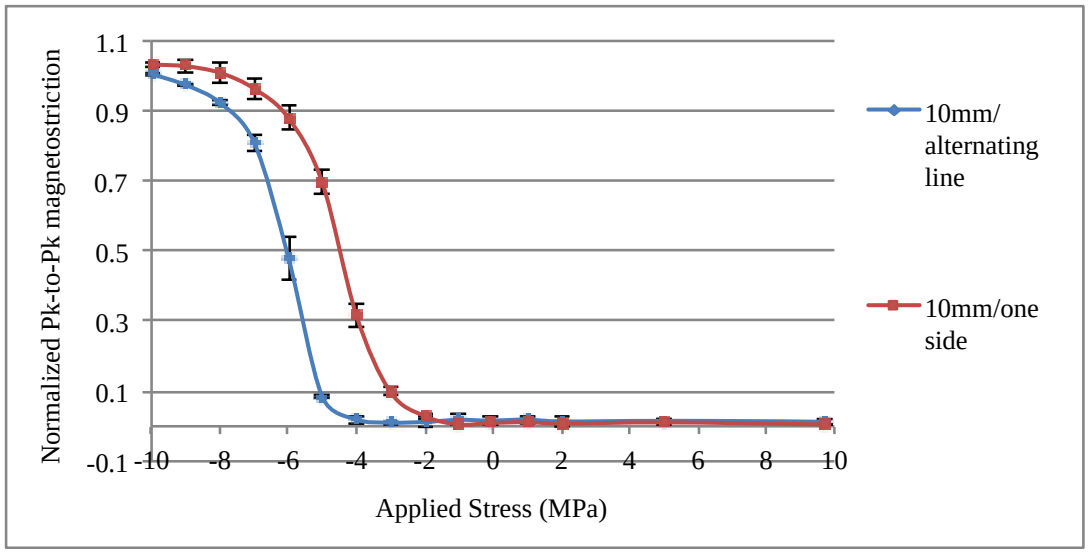

Figure 7- 20: Normalized Pk-to-Pk magnetostriction vs. applied stress, mechanical scribed samples at 1.7 T and 50Hz. Scribed at 10mm intervals transverse to the RD of the strip, alternating line on both side vs. on one side

In order to have better understanding of the effect of scribing on magnetostriction, the domain structure of the samples with 10mm scribing line spacing on one side and both sides (alternating scribing) are shown in Figures 7-21 A) and B) respectively.

Figure 7-21 A and B shows that, after scribing, the magnetic domain patterns, between the lines were satisfactory refined in both cases. The width of the magnetic domains was around 0.7-1.0 *mm* before applying magnetic domain refining processes, the width of these 180^{o} magnetic domains were refined to be approximately 0.28 *mm* in the both side scribed sample and around 0.31 *mm* in single side scribed sample. The domain widths were measured using National Instruments Vision Assistant.

Figure 7-21 B) shows that the sample that was scribed alternating shows finer bar domains compared with the sample scribed on one side, which indicates higher tensile stress. Comparing the domain structure, the sample scribed on both side shows fewer closure domains along the scribed line and hence less transverse domains compared to the sample scribed on one side. This may explain the smaller increase in magnetostriction value in the samples scribed on both side. The formation of these [010] and [110] domains would cause an increase in magnetostriction due to the 90^{o} domain wall movement. Also the formation of these domains indicate the existence of compressive stress which by comparing the result between the samples it shows that samples scribed on both sides have more uniform compressive stress distribution which is shown in Figure 7-22.

From the observed domain structures (shown in Figure 7-21) the stress profile of the domain-refined sample could be estimated and is shown in Figure 7-22. When the material is scribed on one side, the induced residual stress is causing an increase in compressive stress in the top surface and tensile in the bottom, as a result scribed samples will bend after the scribing process, when the sheet is flattened in a core, this would cause further increase in compressive stress on the top surface which is explained in more detail in the section 7-2.

On the other hand, samples scribed on both sides, show a more uniform distribution of residual stress on both sides of the sample as a result the sample does not bend after the scribing process.

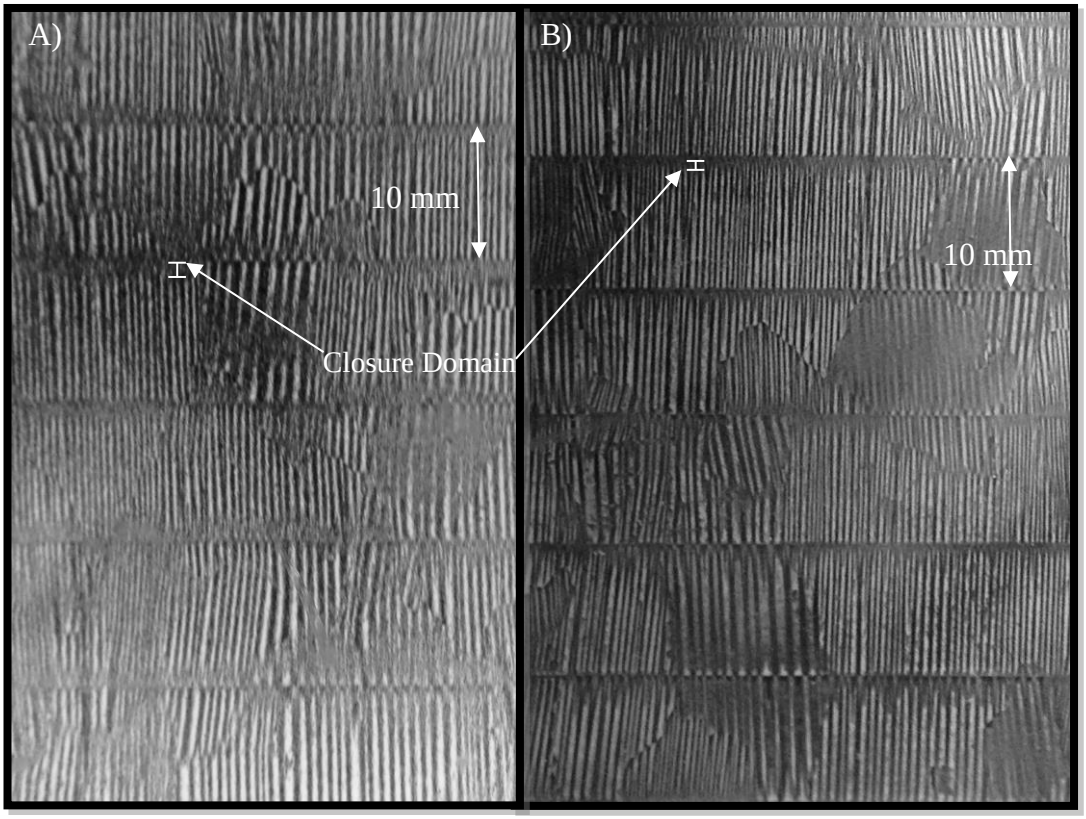

Figure 7- 21: domain structure of the sample after scribing a) scribed on one side 10mm interval 6.0 N applied load b) scribed 10mm alternating with 6.0N applied load

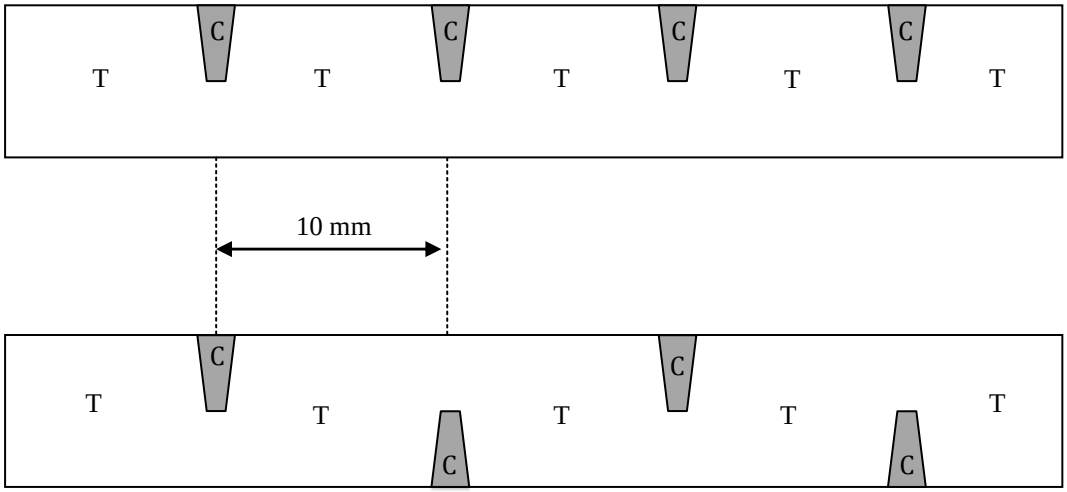

Figure 7- 22: stress profile of scribed sample Top) scribed on one side Bottom) scribed on both sides

7.1.3. Magnetostriction Model of scribed sample

The theoretical changes in magnetostriction due to scribing was calculated based on the proposed model by Simmons and Thompson [20] which is explained in Chapter 3.

In order to use this model it is necessary to calculate the volume fraction of each domain type and each region. Figure 7-23 shows the suggested domain structure of the scribed sample

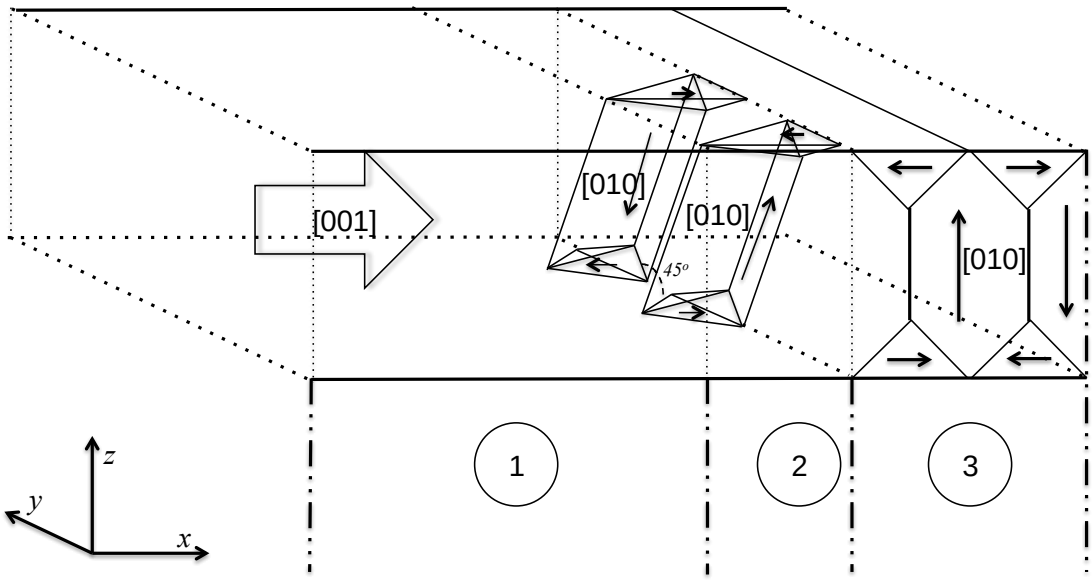

Figure 7- 23: Schematic design of a proposed domain structure of scribed sample

Where region 1 is the bulk of the sample and consists of [001] domains with misorientation angle, ϕ, region 2 is in the vicinity of a scribed line and has closure surface domains on the surface, and the internal domain structure is aligned to the [100] and [010] direction in the sheet. Region 3 is just below the scribed line is Stressed Pattern I, which consists of [100] domains and small triangular [001] closure domains on the surface.

The volume fraction of each region has been measured as follows:

- **Region 1**: The volume fraction of the region one, *V"f1*, was calculated by subtracting region 2 and 3's fraction from 1.
- **Region 2**: The volume fraction of the region two, *V"f2*, is measured by using Lab View Vision Assistant to calculate the percentage area of the surface closure domains in the vicinity of scribed lines. Shown in Figure 7-27.
- **Region 3**: Volume fraction of the region 3, *V"f3*. The area below the scribed line where the material is subjected to direct stress, shown in Figure 7-24, has been considered as region 3 and has been measured using optical microscopy to measure the width of the scribed line.

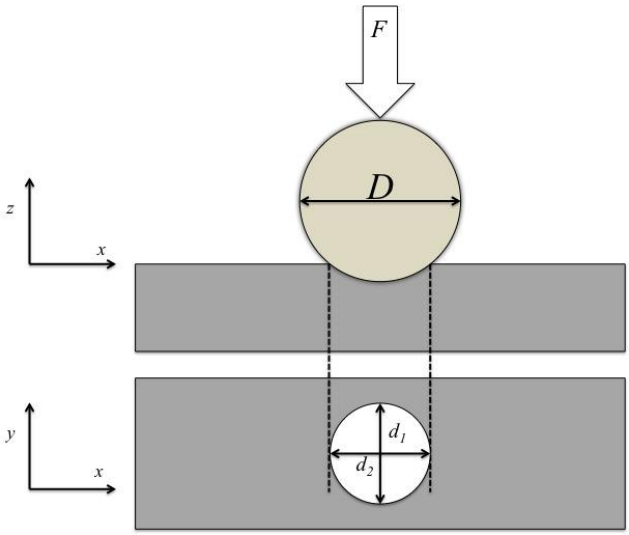

Figure 7- 24: Schematic drawing of compressed area, which is considered as region 3

7.1.3.1. Theoretical Magnetostriction measurement of each region:

Magnetostriction of region 1: Magnetostriction for main bulk domains along [100] direction is assumed to be zero since under 180^{o} domain wall movement magnetostriction does not occur because the magnetic moments under external field stay in the same direction as the spontaneous magnetization.

Magnetostriction of region 2: It is assumed that Region 2 consistent of two different domain structures surface closure domain [001] and the internal

domain structure is aligned to the [100] and [010] direction. A longitudinal section through the grain is shown in Fig 7-25, the material has *t* thickness, and the triangular surface closure domains have a width *'D'*. The closure domain walls make an angle of 'γ' and 'φ'with the surface. The volume fraction of [001] closure domain is given by:

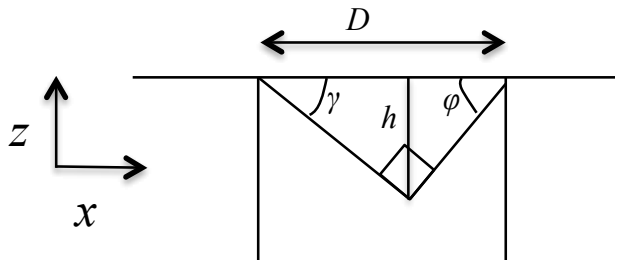

Figure 7- 25: Longitudinal section of domain structure through a grain is region 2

$$V_f = 2\left(\frac{D^2}{4}\sin(2\gamma)\right)\frac{1}{D \times t}$$

$$= \frac{D\sin(2\gamma)}{2t} \tag{7.2}$$

Magnetostriction for the closure domains along the [001] direction is measured for, $\alpha_1=0,\ \alpha_2=0,\ \alpha_3=1$, and $\beta_3 = \cos \emptyset$ is given by,

$$\lambda_{001} = \frac{3}{2}\lambda_{100}\left(cos^2\emptyset - \frac{1}{3}\right) \tag{7.3}$$

Magnetostriction for main bulk domains along [100] direction is measured for, $\alpha_1=1,\ \alpha_2=0,\ \alpha_3=0$, and $\beta_3=\sin \emptyset$ is given by,

$$\lambda_{010} = \frac{3}{2}\lambda_{100}\left(sin^2\emptyset - \frac{1}{3}\right) \tag{7.4}$$

The initial magnetostriction for the region 2 can be calculated by adding the volume contributions from each type of domain

$$\lambda_{initial} = \frac{3}{2}\lambda_{100}\left(cos^2\emptyset - \frac{1}{3}\right) \times V_f + \frac{3}{2}\lambda_{100}\left(sin^2\emptyset - \frac{1}{3}\right) \times (1 - V_f) \tag{7.5}$$

It is expected that at magnetic saturation the grain comprises of only [001] domains aligned along the magnetization direction, then, at a magnetic flux density B the volume fraction of [001] domains can be calculated from

$$V_f' = \frac{B}{B_s}\cos\emptyset \tag{7.6}$$

The final magnetostrictive strain is then given by

$$\lambda_{final} = \frac{3}{2}\lambda_{100}\left(cos^2\emptyset - \frac{1}{3}\right) \times V_f' + \frac{3}{2}\lambda_{100}\left(sin^2\emptyset - \frac{1}{3}\right) \times (1 - V_f') \tag{7.7}$$

The magnetostriction under applied field can be calculated from

$$\lambda_{Region\,2} = \lambda_{final} - \lambda_{initial} \tag{7.8}$$

Magnetostriction of region 3: Figure 7-26 shows the longitudinal section of domain structure in region 3. Region 3 has similar domain structure as the one in region two. The domain walls adjacent to the angle 'θ' are in the (111) plane. The volume fraction, V_f, of closure domains aligned in the [001] direction is given by:

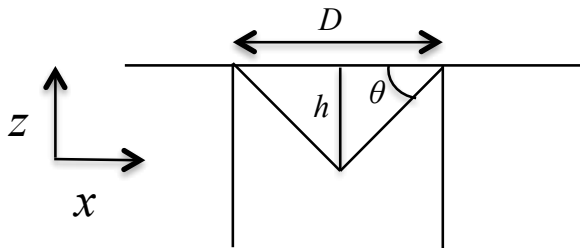

Figure 7- 26: Longitudinal section of domain structure through a grain in region 3 that is exhibiting Stress Pattern I

$$\tan\frac{\theta}{2} = \frac{D/2}{h}$$

$$V_f = 2(\frac{D}{2} \times \frac{D}{2}\tan(\theta/2))\frac{1}{D \times t}$$

$$= \frac{D}{2t}\tan\theta \tag{7.9}$$

The initial magnetostriction for the region 3 can be calculated by adding the volume contributions from each type of domain

$$\lambda_{initial}$$

$$= \frac{3}{2}\lambda_{100}\left(cos^2\emptyset - \frac{1}{3}\right) \times V_f + \frac{3}{2}\lambda_{100}\left(sin^2\emptyset - \frac{1}{3}\right) \times (1 - V_f)$$

$$= \frac{3D}{4t}\lambda_{100}(\tan\theta\cos 2\emptyset) + \frac{3}{2}\lambda_{100}(sin^2\emptyset - \frac{1}{3}) \tag{7.10}$$

The final magnetostrictive strain is then given by

$$\lambda_{final} = \frac{3}{2}\lambda_{100}\left(cos^2\emptyset - \frac{1}{3}\right) \times V_f' + \frac{3}{2}\lambda_{100}\left(sin^2\emptyset - \frac{1}{3}\right) \times (1 - V_f') \tag{7.11}$$

The magnetostriction under applied field can be calculated from

$$\lambda_{Region\,3} = \lambda_{final} - \lambda_{initial}$$

$$\lambda_{Region\,3} = \frac{3}{2}\lambda_{100}\cos 2\emptyset\,(\frac{B}{B_s}\cos\emptyset - \frac{D}{2t}\tan\theta) \tag{7.12}$$

Then

$$\lambda_{Total} = \lambda_{Region\,2}V_{f2}^{"} \times \lambda_{Region\,3}V_{f3}^{"} \tag{7.13}$$

The theoretical magnetostriction of the scribed sample based on the misorientation, stress pattern, and magnetic flux density can be calculated using equation (7.13). However D for region two and three, and also their volume fractions (V_{f2}'' and V_{f2}'') must be taken from domain observations. Table 7-1 shows average obtained data from domain images of five scribed sample at 10 *mm* and 5 *mm* interval lines. These images were taken by a digital camera and then analysed by Lab View Vision software as shown in Fig 7-27. The values of the Θ, φ, Y and were taken from [20-24]

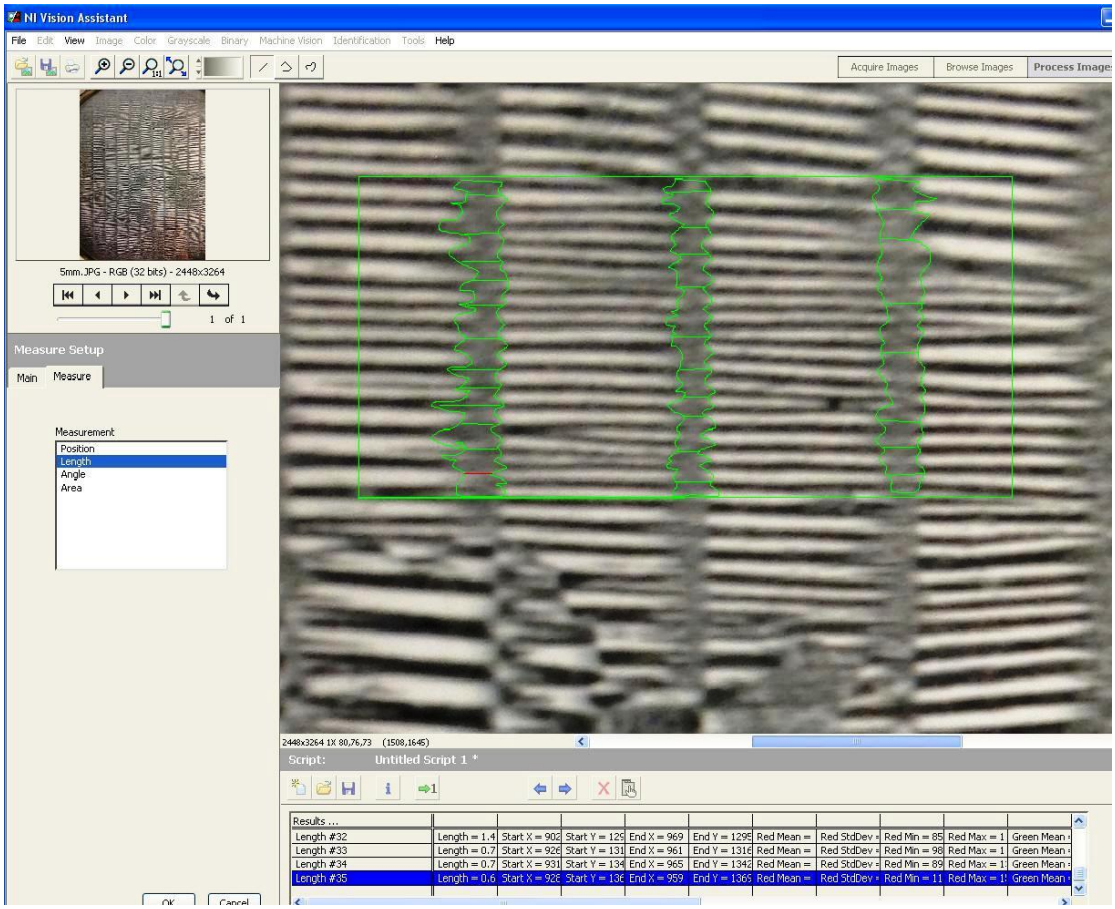

Figure 7- 27: Example of domain image analyse by Lab View vision to measure area of region 2 and 3

Table 7- 1: Average obtained data from domain image analysed by Lab view vision from five scribed sample at 10mm and 5mm interval lines.

	Region 2			Region 3		
	D *mm*	θ *(angle)*	V fraction %	D *mm*	γ *(angle)*	V fraction %
5mm	0.07	45	0.27	0.31	35	8.195
10mm	0.07	45	0.135	0.26	35	2.44

Figure 7-28 shows a comparison between measured (1.7 T, 50Hz) and calculated based on data from Table 7-1. A good agreement between measured and calculated Pk-to-Pk magnetostriction is achieved.

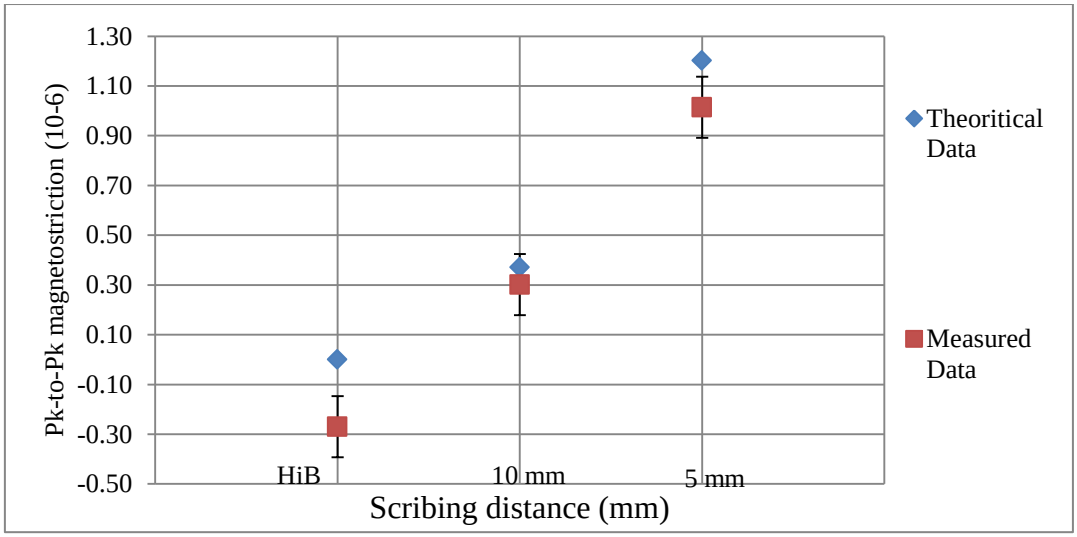

Figure 7- 28: Comparison of the measured and calculated magnetostriction versus scribing distance

The theoretical results confirm that the newly formed [010] and [001] domains along the scribing line are causing the increase in magnetostriction of scribed samples.

7.2. Influence of residual curvature (coil set)

It has been known for a long time that there is a strong correlation of the magnetic properties, especially magnetostriction on its state of stress [25]. Grain oriented silicon steel is more sensitive to compressive stress as was explained Chapter 3, the increase in compressive stress would result in an increase in magnetostriction as well as power loss due to changes in the domain structure as a result of an increase in magneto-elastic energy [11]. Possible causes of stress in the transformer cores are as follows:

i. Clamping stress

ii. Non-flat laminations

iii. Temperature gradient

The existence of residual curvature can set up a stress in laminations, which had been largely reduced by a careful heat-treatment in production line. Bending stress can be produced in handling, or storing loosely wound coils without being detectable as shown in Figure 7-29.Also uncoiled straps would have different curvature due to difference in coil diameter.

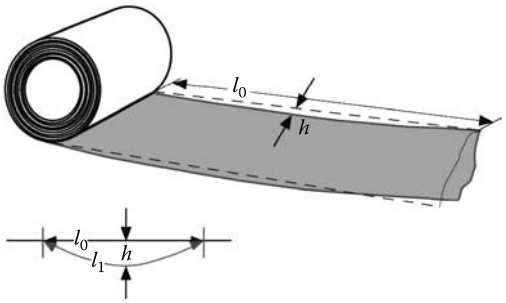

Figure 7- 29: Bending stress due to storing loosely wound coil [26]

Large stress can be introduced when the sheet is flattened in a core, either by their own weight or clamping [25]. The effects of elastic strain due to the bending in assembled core can cause an increase of 10% of the core loss [27].

Cole, R.W. [27] suggested that when a grain oriented sheet is elastically bent, the magnetization is in the [001] direction in at least half of the volume, in the remaining volume the magnetization is in transverse direction easy directions if the compressive stress applied has a magnitude greater than :

$$\frac{HI_s}{h_1} \tag{7.14}$$

Where H is the magnetic intensity

I_s is the saturation magnetization

And h_1 is magnetostriction constant (4×10^{-5})

Therefore the magnetic induction in the sheet could be calculated from equation 7.15:

$$B = \frac{1}{2}B_s[1 + \frac{HB_s}{4\pi h_1 \sigma_m}] \quad (7.15)$$

Where B_s is the saturation induction

σ_m is the maximum stress

Elastic bending would reduce the permeability, increase the AC core loss and also makes the hysteresis loop less rectangular [27].

The effect of bending stress on magnetic properties of grain oriented silicon steel has been studied before [11]. In this exercise, the effect of coil set been studied on longitudinal magnetostriction of a 3% CGO laminations. A jig was designed and machined for applying different curvatures to the sample. Two curvatures were choose with respect to an industry standard for coil set, with a 500 *mm* square, one with height of 10 *mm* and one with 5 *mm*. 5 samples were choose for each curvature samples were prepared according to section 6.2.2. The diagram 7-30 illustrates how the radius of the curvature was calculated.

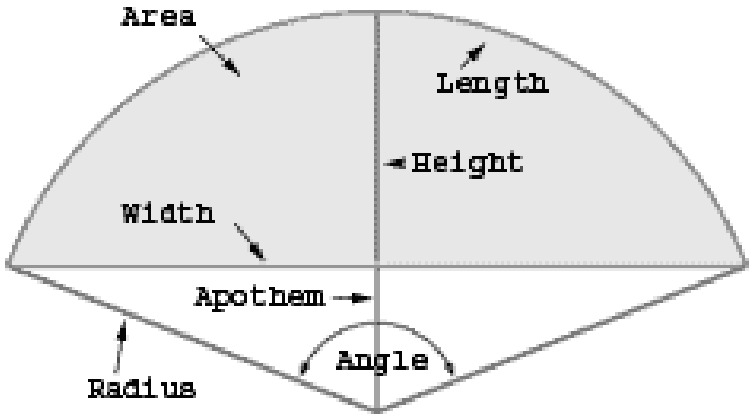

Figure 7- 30: Schematic drawing of the applied curvature on laminations

From the graph 7-28:

$$Arc = R \times 2\pi \times \frac{\theta}{360} \tag{7.16}$$

$$\cos\left(\frac{\theta}{2}\right) = \frac{(P-k)}{R} \tag{7.17}$$

$$\therefore \cos\left(Arc \times \frac{360}{4\pi R}\right) = \frac{(R-k)}{R} \tag{7.18}$$

Where

'R' is the radius

'θ' is the angle

'P' is the apothem

'*k'* is the height

The introduce stress by the curvature can be calculated form equation 7.19:

$$\sigma = {(E \times \frac{t}{2})}\Big/{(R + \frac{t}{2})} \tag{7.19}$$

Where

'E' is the Young's modulus

't' is the sample thickness

According to the above the stress on the laminations were calculated and is presented in Table 7-2. Bending results in compression on one side and tension on the other side

Table 7- 2: Induced stress due to bending as a function of arc of the curve.

Arc	Height	Radius	Stress (MPa)
500 mm	10 mm	2246 mm	7.35
500 mm	5 mm	2256 mm	7.31

7.2.1. Result and discussion

Figure 7-31 shows the repeatability of the magnetostriction at 1.7 Tesla and 50 Hz for a sample with a curvature of 5mm height, with 5.0% repeatability in samples with 2246 *mm* radius and 6.3% repeatability for samples with 2256 *mm* radius (the presented repeatability is the worst case repeatability in the results).

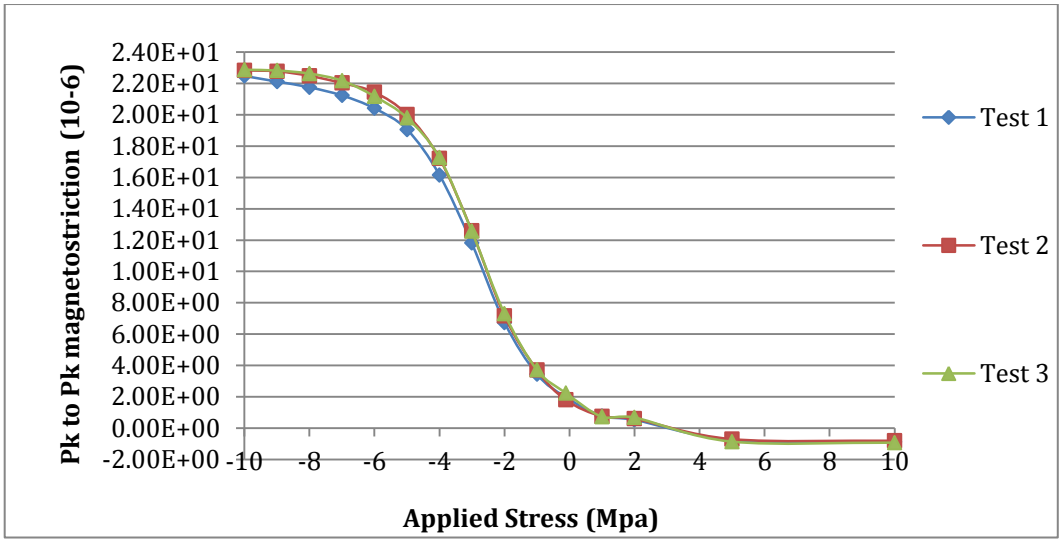

Figure 7- 31: Repeatability in magnetostriction after applying curvature, 2246 mm radius, 1.7 T and 50Hz

7.2.2. Effect of curvature on domain structure

In order to have a better understanding of the effect of curvature on magnetostriction, the domain structure was studied before and after annealing samples under curvature, on both sides of the sample. When the magnetostriction of samples is measured, they are flattened in the measurement rig. This applies compressive stress on the samples top surface and tensile stress on the samples bottom surface as shown in Figure 7-32 in the bent state about one half of the sheet volume must be under compressive stress.

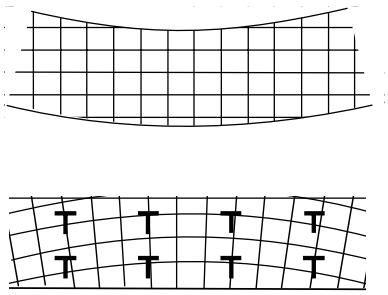

Figure 7- 32: stress distribution inside the sample due to flattening curvature samples.

The domain pattern was observed by using Bitter technique [5]. Figure 7-33 shows domain pattern of a CGO sample after stress relief annealing at 810^{o}C for 1 hour.

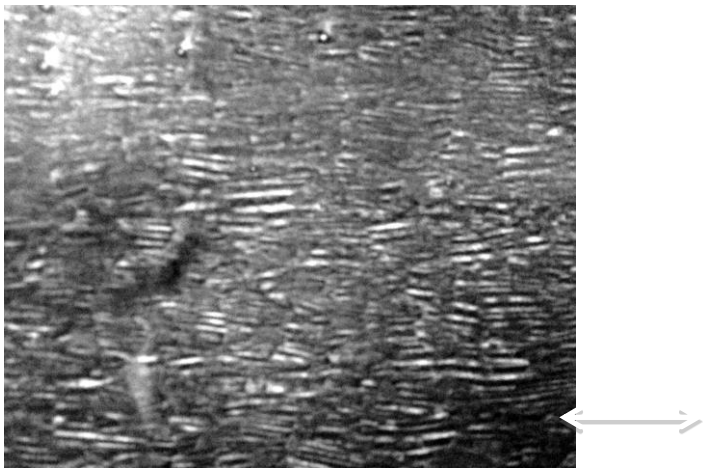

Figure 7- 33: domain structure of a CGO sample after stress relief annealing at 810^{o}C for 1 hour.

Figure 7-34 (A) shows the domain pattern on the concave side of the sample with a radius of 2246 *mm*. As shown in Figure 7-32 the concave side is subjected to tensile stress, the effect of tensile stress on domain structure is explained in section 3.1.1. As a result of the applied tensile stress, the Magnetoelastic energy is reduced; also the width of the domains reduces in order to compensate the increase of the Magnetostatic energy. As a result in the concave side the [001] direction is energetically favourable. By comparing the domain structure of the stress free

sample presented in Figure 7-33 by domain structure of the concave side of the sample, the concave sides domain structure shows a decrease in the width of the domains.

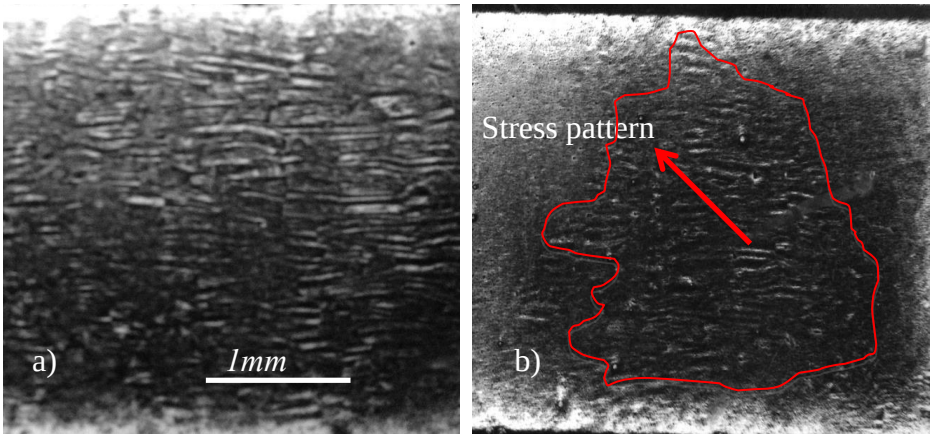

Figure 7- 34: a) Domain structure of the concave side due to tensile stress, b) domain structure of the convex side due to compressive stress

Figure 7-34 b) shows the domain pattern of the convex side of the sample, the effect of compressive stress on domain structure is explained in section 3.1.2. The application of compressive stress would result in an increase of Magnetostatic energy and [010] and [100] directions become energetically favourable. Consequently the domain pattern rearranges to decrease the total energy by increasing the volume of supplementary domains. Stress patterns can be observed in Figure 7-34 b) which confirms the existence of compressive stress. Percentage of the stress pattern on the convex side was measured to be ≈ 58% using National Instruments vision assistant.

The domain structure from both sides of the samples shows some differences from the domain structure of a sample under in plane-applied stress, which indicates that the domain structure of both sides influence the other one.

Also there is a rotation in domain direction from [010] and [100] in the convex side to [001] direction in concave side.

7.2.3. Effect of curvature on magnetostriction:

The graph 7-35 shows the effect of curvature on magnetostriction, results are normalized with respect to the saturation magnetostriction of the flat sample at 1.7T and 50 Hz.

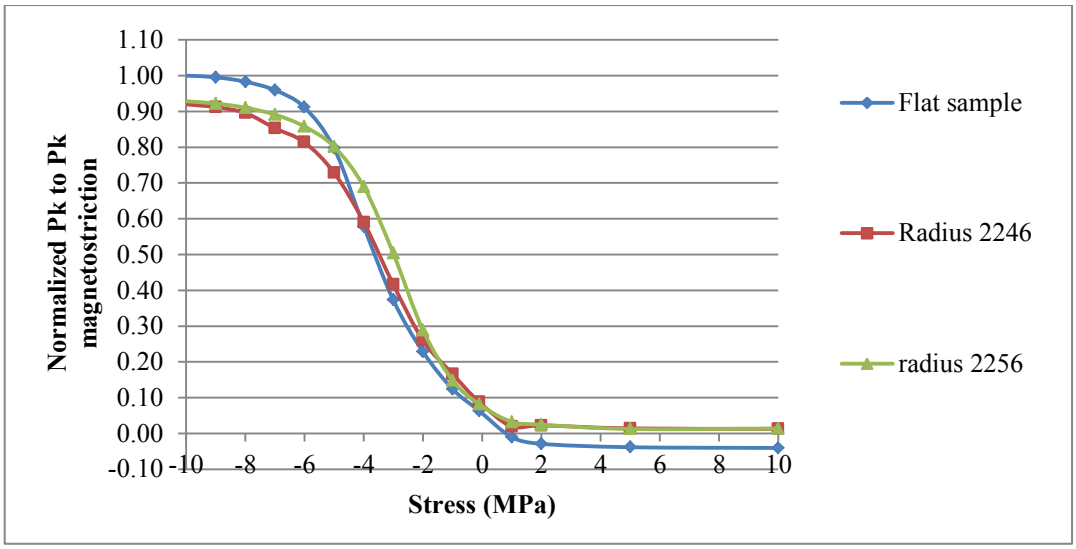

Figure 7- 35: Effect of curvature on magnetostriction value at 1.7 T and 50 Hz

The magnetostriction of the curved samples increases compared to the stress free sample under tensile stress. The change of magnetostriction characteristics is due to the domain structure change in the concave side of the sample, which is under compressive stress of around 7MPa (Table 7-1).

As can be seen from Figure 7-35 the stress-free sample shows a negative magnetostriction at zero stress, which is due to the reorganization from longitudinal domains to transverse supplementary domains during the magnetisation process. Whereas in the curved samples due to the existence of the

compressive stress in about one half the volume, and the removal of the [100] domains in the stressed stage to [001] domains, magnetostriction becomes positive.

The difference in magnetostriction between the stress-free sample and curved sample in higher applied stress is due to a delay of rotation of the magnetization vector in the concave side of the bent sample, which due to the existence of tensile stress in this side is delaying the formation of stress patterns under compressive stress.

The theoretical magnetostriction under applied stress was estimated using two different methods. In the first method, the magnetostriction value is calculated based on the fraction of coverage area by stress patterns using the formula below [21] :

$$\lambda = (\frac{\lambda_s \times C_s}{100\%})/2 \tag{7.20}$$

In the second method, the resultant stress due to the bending was calculated first. Then the resultant magnetostriction due to the same in plane stress was measured, as discussed previously when bent about one half of the sheet volume must be under compressive stress and the other half under tensile stress. Finally the magnetostriction of each side is multiplied by its fraction to give the total magnetostriction, as it is explained in the equation below:

$$\lambda = \lambda_{compresive} \times 1/2 + \lambda_{tensile} \times 1/2 \tag{7.21}$$

The calculated magnetostriction from both methods at1.7T and zero applied stress is shown in the Table 7-3 as well as the measured magnetostriction value of a bent sample. As can be seen from the Table 7-3, none of the methods gives close estimation of the magnetostriction value, which is because in both methods it was assumed that half of the volume is under compressive stress and the other half is under tensile stress. However in reality the stress is gradually changing from compressive to tensile and as a result the domain direction changes slowly through the thickness from [100] and [010] directions on the convex side to [001] direction in concave side. These changes would affect the resultant magnetostriction and causes less increase in magnetostriction.

Table 7- 3: Calculated Magnetostriction based on method 1 and 2 vs. measured magnetostriction at 1.7 T, 0 MPa.

$\lambda_{Measured}$ (10^{-6})	$\lambda_{Method\ 1}$ (10^{-6})	$\lambda_{Method\ 2}$ (10^{-6})
≈ 2.60	5.45	11.20

7.3. Influence of strip width on magnetostriction of grain oriented silicon steel

As shown in Chapter 3, application of compressive stress causes a rapid increase in magnetostriction. This increase in magnetostriction is due to rearrangement of domains so as to minimize the total free energy. When the sheet is magnetised along its rolling direction, [001], high magnetostriction happens due to the rotation of the main transverse domains, [010] and [100], into [001] directions. Therefore the value of magnetostriction depends on the volume fraction of domains oriented in these principle axes. The saturation magnetostriction can be

calculated based on a model proposed by Simmons and Thompson [20] which is explained in Chapter 3.3.2.

For measured CGO samples the λ_{100} =24×10^{-6}, B_S=2.03 Tesla, the average misorientation from the rolling direction is 7^o and t was 0.30 *mm*. The objective of this exercise is to study the effect of strip width on magnetostriction and see if the changes the strip width affects the width of stress pattern, which can be calculated from equation 7.21:

$$d = \frac{2t}{\tan \emptyset}\left(\frac{B}{B_s}\cos \emptyset - \frac{2\lambda_{measured}}{3\lambda_{100}\cos 2\emptyset}\right) \tag{7.21}$$

Samples were selected and prepared as explained in Chapter 6.2.3. The magnetostriction of each of the strips in each stage was measured three times over the flux density of 1.0T to 1.7 T at stress up to ± 10 MPa.

Figure 7-36 shows the average values of peak-to-peak magnetostriction vs. applied stress in the rolling direction at 1.7 T, 50 Hz. Each data point is the average magnetostriction in each of the three strips in each batch measured three times. The highest difference in magnetostriction value is 8.6% at which occurs at 10MPa applied pressure, this difference is significant and much higher than the system's uncertainty (1.1%) measured for 100 *mm* width sample presented in Chapter 5.4.

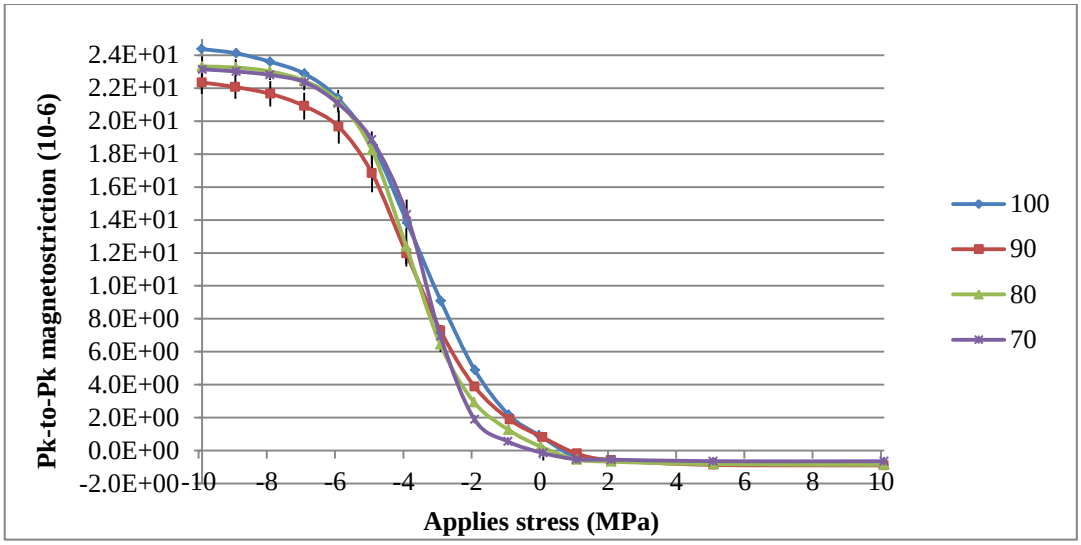

Figure 7- 36: variation of magnetostriction under applied stress due to strip width, measured in rolling direction under 1.7T at 50 Hz.

The difference in the magnetostriction value is mainly due to damping effect. The ratio of the clamp weight and friction to sample width rises by decreasing the strip width.

In the second stage 100 *mm* wide samples were cut into two 50 *mm* width strips and three 33 *mm* strips, the cut strips were stress relief annealed and then put back together, Figures 7-37 and 7-38 show the average values of peak-to-peak magnetostriction as stress sensitivity curves magnetised at 1.7 T, 50 Hz in the rolling direction for 50 *mm* strips and 33 *mm* strips respectively. Each data point is the average magnetostriction in each of the three strips in each batch measured three times.

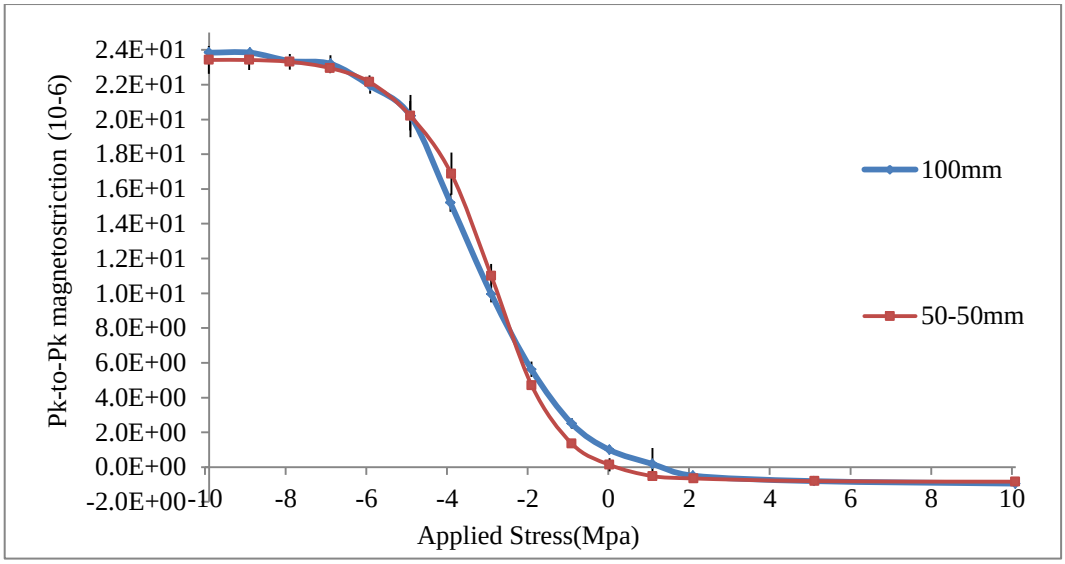

Figure 7- 37: variation of magnetostriction under applied stress due to strip width, measured in rolling direction under 1.7T at 50 Hz. 100mm width sample were cut into two 50mm strips.

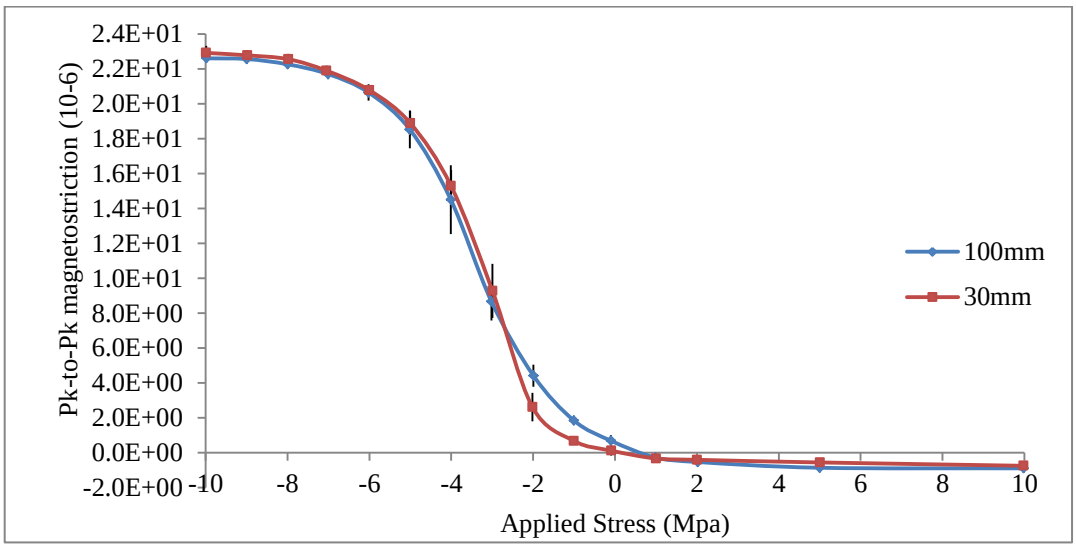

Figure 7- 38: variation of magnetostriction under applied stress due to strip width, measured in rolling direction under 1.7T at 50 Hz. 100mm width strip were cut into three 33mm strips.

The difference in magnetostriction saturation between 100 *mm* width strips before and after cut is negligible and in the range of the uncertainty of the system.

On the other hand, the difference in peak-to-peak magnetostriction value around zero stress is larger than the uncertainty in this range that is 2.6%, which is mainly due to the damage to the edges that causes new domain to be formed and increases the magnetostriction.

So it can be concluded that cutting the sample into narrower strips does not have any effect on the width of surface closure domains.

7.4. Conclusion

The scribing process was satisfactory for power loss reduction, but resulted in a deterioration of the magnetostriction. Applying 6.0 N and a 10 *mm* space between the lines achieved the ultimate power loss reduction and lowest increase of magnetostriction and a good correlation was obtained with the previews research. The power loss reduction percentage of the laboratory ball scribed samples was similar to those presented in [3].

The study shows that both laser scribing and mechanical scribing have similar effect on sample's domain structure and magnetostriction, as they both are based on the effect of induced residual stress and will increase the magnetostriction value.

The surface subjected to the domain refinement treatment proves to be concave. On the other hand, samples scribed on both side, shows more uniform distribution of residual stress and as a result lower magnetostriction.

A proposed domain model was used successfully to estimate the effect of scribing on magnetostriction. The theoretical results confirm that the newly formed [010] and [001] domains along the scribing line are causing the increase in magnetostriction of scribed samples.

The effect of bending stress on domain pattern is different from the effect of in plane compressive/tensile stress. As the domain structure of both side influences each other in the bent sample.

The changes of magnetic domain structure were confirmed by comparison of magnetostriction before and after curvature. The increase in magnetostriction is due to the domain changes in the compressive side of the sample

The width of surface closure domains was found to be constant and independent of width in all the strips investigated.

References for Chapter 7

1. Ueno, K., N. Takahashi, and T. Nozawa, *The Latest Advance in Very Low Core Loss Grain Oriented Silicon Steels.* Journal of Materials Engineering, 1990. **12**(1): p. 11-20.
2. Homewood, J.A., D. Snell, and A.J. Moses, *Domain refinement techniques for improved magnetic properties of high permeability grain oriented electrical steel.* Ironmaking & Steelmaking, 1997. **24**(1): p. 84-89.
3. Snell, D. and P. Beckley, *Domain refinement of high-permeability grain-oriented electrical steel using low-friction ball units.* Journal of Magnetism and Magnetic Materials, 1994. **133**(1-3): p. 167-169.
4. Taylor, R.J., *A Large Area Domain Viewer*, in *SMM*1990.
5. Bitter, F., *Experiments on the nature of ferromagnetism.* Physical Review, 1932. **41**(4): p. 507-515.
6. Xu, X.T., et al., *A comparison of magnetic domain images using a modified bitter pattern technique and the Kerr method on grain-oriented electrical steel.* IEEE Transactions on Magnetics, 2011. **47**(10): p. 3531-3534.
7. Wang, H., et al., *Effect of ball scribing on iron loss of CGO and HGO electrical steel.* Journal of Harbin Institute of Technology (New Series), 2013. **20**(3): p. 81-85.
8. Nozawa, T., et al., *Magnetic properties and domain structures in domain refined grain-oriented silicon steel (invited).* Journal of Applied Physics, 1988. **63**(8): p. 2966-2970.
9. Fukawa, K. and T. Yamamoto, *Domain-Structures and Stress Distributions Due to Ball-Point Scratching in 3-Percent Si-Fe Single-Crystals with Orientation near (110) [001]*. Ieee Transactions on Magnetics, 1982. **18**(4): p. 963-969.
10. Nozawa, T., Yabumoto, M. and Matsuo, Y., *studies of domain refining of grain oriented silicon steel*, in *Soft Magnetic Materilas* 1985, Wolfson center of Magnetic Tecchn: Blackpool. p. 131-136.
11. Cole,R, W.,*Effects of elastic bending on magnetic properties of oriented silicon iron*,Journal of Applied Physics,1958,**29**(3):P370-371.
12. Yabumoto, M., et al., *Recent development in grain-oriented electrical steel with low magnetostriction.* Journal of Materials Engineering and Performance, 1997. **6**(6): p. 713-721.
13. Dragoshanskii, Y.N., et al., *Development of stresses in grain-Oriented electrical steel during laser treatment.* Physics of Metals and Metallography, 2011. **112**(2): p. 133-137.
14. Iuchi, T., et al., *Laser processing for reducing core loss of grain oriented silicon steel.* Journal of Applied Physics, 1982. **53**(3): p. 2410-2412.
15. Krause, R.F., et al., *EFFECT OF LASER SCRIBING ON THE MAGNETIC PROPERTIES AND DOMAIN STRUCTURE OF HIGH-PERMEABILITY 3% Si-Fe.* Journal of Applied Physics, 1983. **55**(6 pt 2B): p. 2121-2123.
16. Suzuki, H., et al., *Mechanism of magnetic domain refinement on grain-oriented silicon steel by laser irradiation.* Materials Science Research International, 2002. **8**(4): p. 207-212.

17. Honma, H., Y. Ushigami, and Y. Suga, *Magnetic properties of (110)[001] grain oriented 6.5% silicon steel.* Journal of Applied Physics, 1991. **70**(10): p. 6259-6261.
18. Moses, A.J., *Energy efficient electrical steels: Magnetic performance prediction and optimization.* Scripta Materialia, 2012. **67**(6): p. 560-565.
19. Imafuku, M., et al., *Effects of laser irradiation on iron loss reduction for Fe-3%Si grain-oriented silicon steel.* Acta Materialia, 2005. **53**(4): p. 939-945.
20. Simmons, G.H. and J.E. Thompson, *Magnetic properties of grain- oriented silicon iron- 5.* Proceedings of the Institution of Electrical Engineers, 1971. **118**(9): p. 1302-1306.
21. Klimczyk, P., *Novel Techniques for Characterisation and Control of Magnetostriction in G.O.S.S*, in *Wolfson Centre for Magnetics*2012, Cardiff University. p. 215.
22. Ozdemir, O., X. Song, and D.J. Dunlop, *Closure domains in magnetite.* Journal of Geophysical Research, 1995. **100**(B2): p. 2193-2209.
23. Hubert, A. and R. Schäfer, *Magnetic domains : the analysis of magnetic microstructures*. 1998, Berlin ; New York: Springer. xxiii, 696 p.
24. Anderson, P.I., A.J. Moses, and H.J. Stanbury, *Assessment of the stress sensitivity of magnetostriction in grain-oriented silicon steel.* Ieee Transactions on Magnetics, 2007. **43**(8): p. 3467-3476.
25. Moses, A.J., *Effects of stresses on magnetic properties of silicon-iron laminations.* Journal of Materials Science, 1974. **9**(2): p. 217-222.
26. Ginzburg, V.B., *Flat-rolled steel processes : advanced technologies*. 2009, Boca Raton, Fla.: CRC ; London : Taylor & Francis [distributor].
27. Cole, R.W., *Effect of elastic bending on magnetic properties of oriented silicon iron.* Journal of Applied Physics, 1958. **29**(3): p. 370-371.

Chapter 8: Magnetostriction characteristic of different grades of grain oriented silicon steel

8.1. Magnetostriction measurement in rolling direction

8.1.1. Magnetostriction repeatability:

Samples were selected and prepared as explained in Chapter 6.3.1. Magnetostriction of samples was measured using the new magnetostriction system in Wolfson as described in Chapter 5. Figures 8-1, 8-2 and 8-3 shows the repeatability of magnetostriction at 1.7T and 50 Hz for each grade for CGO, HiB and laser domain refined strips respectively. Each strip was measured three times.

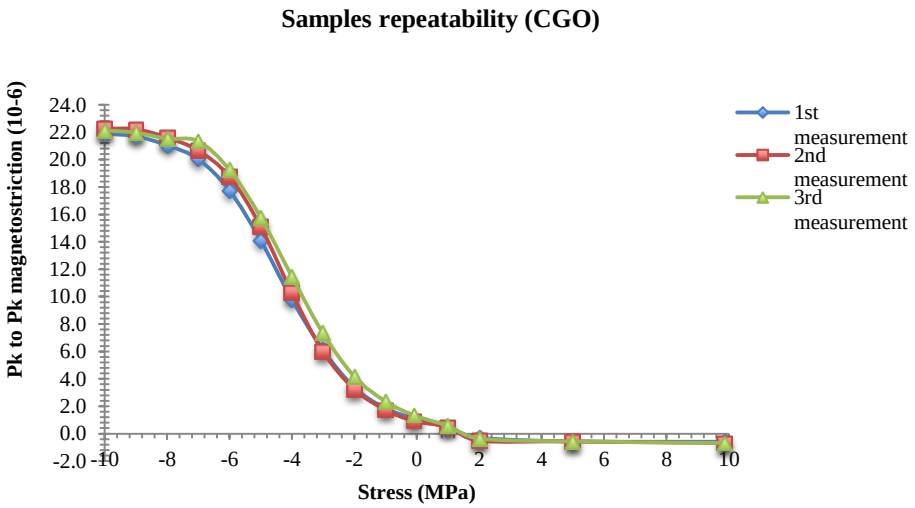

Figure 8- 1: Typical CGO sample repeatability at 1.7T and 50 Hz

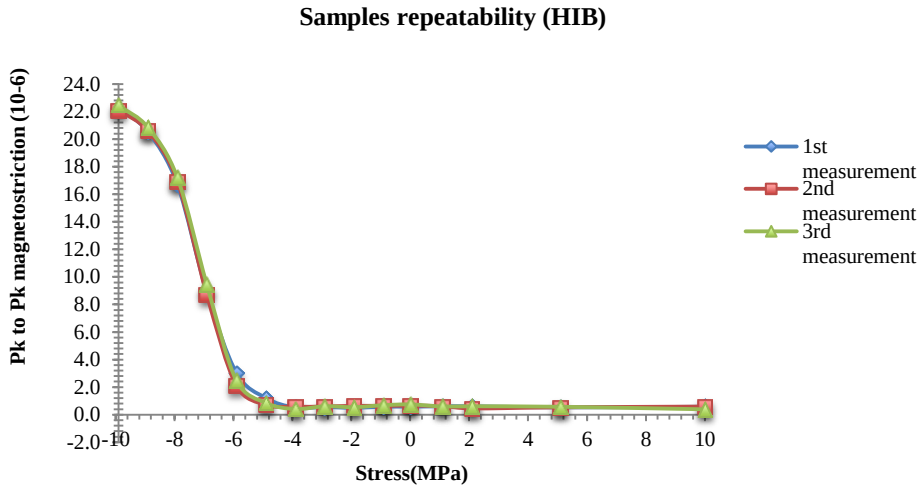

Figure 8- 2: Typical HIB sample repeatability at 1.7T and 50 Hz

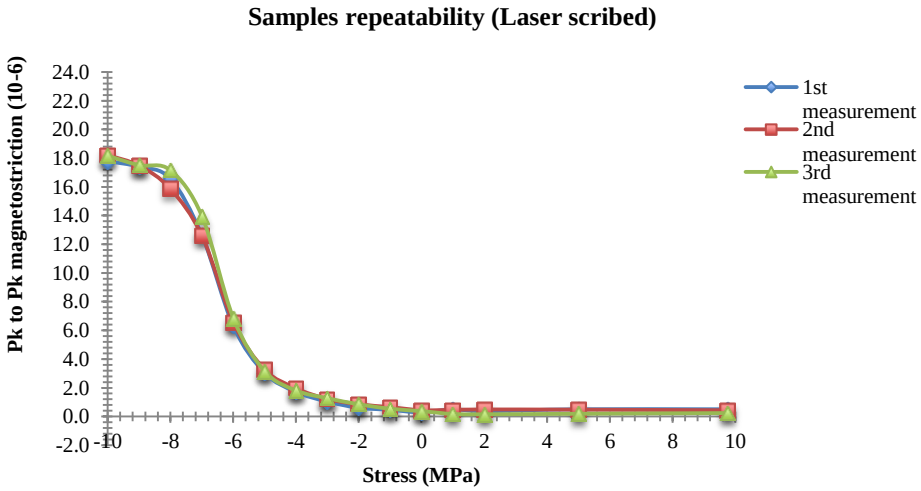

Figure 8- 3: Typical Laser scribed sample repeatability at 1.7T and 50 Hz

High repeatability was obtained in strips, which indicate that the system has good repeatability when samples are in a good condition i.e. no burrs, low cutting stress, no waviness or bent sample[1] .

Figure 8-4 shows a typical variability between the peak-to-peak magnetostriction of five strips. Each data point is the average magnetostriction in each strip measured three times, each time the samples were unclamped and

removed from the rig. The results show a good repeatability (3.6% repeatability), which shows the consistency in magnetic and mechanical properties of the samples.

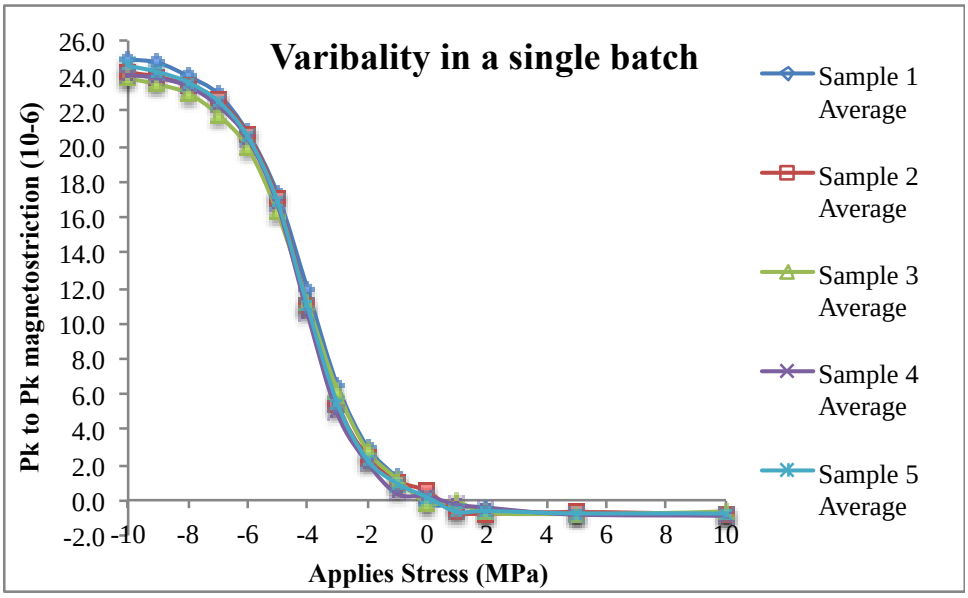

Figure 8- 4: Variability of magnetostriction in a single batch of samples. CGO sample at 1.7 T and 50 Hz

Overall results illustrate high repeatability within the measurement with maximum standard deviation of 0.64. That shows, a good consistency in Pk to Pk magnetostriction measured value under applied stress among samples in a batch was achieved, that shows uniform properties among the samples and also indicates that the cutting damage was either negligible or repeatable between the samples.

Figures 8-5 and 8-6 illustrate the variation of magnetostriction between seven different batches of CGO and two batches of HiB samples respectively. Each data point is the average Pk-to-Pk magnetostriction in each of the five strips in each batch measured three times. Results show 10% difference in magnetostriction saturation for CGO material and 3% difference for HiB strips.

The difference could be due to difference in coating thickness or cutting stress between different batches or possibly as a result of the misorientation

between the batches, it is shown in section 8.1.2 that CGO materials have a misorientation of around 7% compared to an average of 3% misorientation among HiB samples (10 samples in total) that causes a variation of the Magnetoelastic energy from grain to grain. This would cause the Stress Patterns to appear at different stress values in all of the grains is giving the smooth shape to the characteristic. In addition higher misorientation would create more closure structures at the grain boundaries.

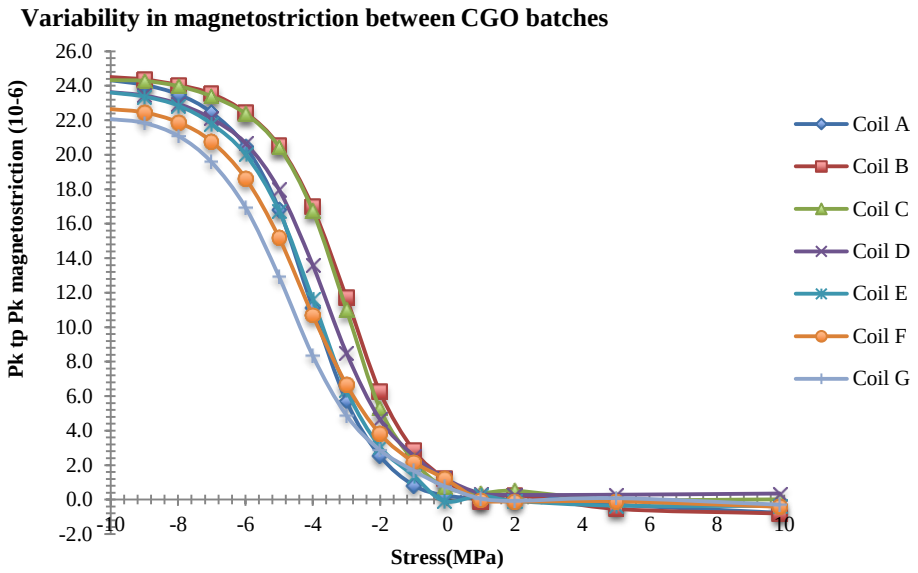

Figure 8- 5: magnetostriction variability between seven batches of CGO samples at 1.7 T and 50 Hz

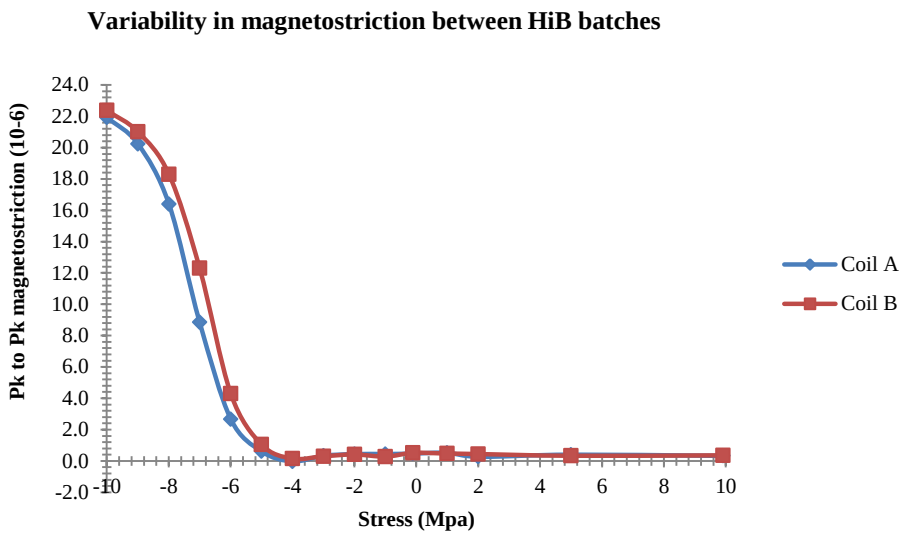

Figure 8- 6: magnetostriction variability between two batches of HIB samples at 1.7 T and 50 Hz

8.1.2. Domain Structure

The domain patterns were observed by using the Bitter technique [2] as described in section 7.1. The angle of misorientation from the rolling direction was calculated for each grade by averaging the misorientation of ten domains measured by National Instruments Vision Assistant. The domain structure of CGO, HiB and the domain-refined strips is shown in Figure 8-10.

CGO has the highest misorientation as expected with average approximate of 7.4^{o}, whereas HiB have low misorientation with 3.2^{o} and laser scribed (Domain refined) have average misorientation of 3.6^{o}. These measured misorientations will be used to estimate the magnetostriction characteristics.

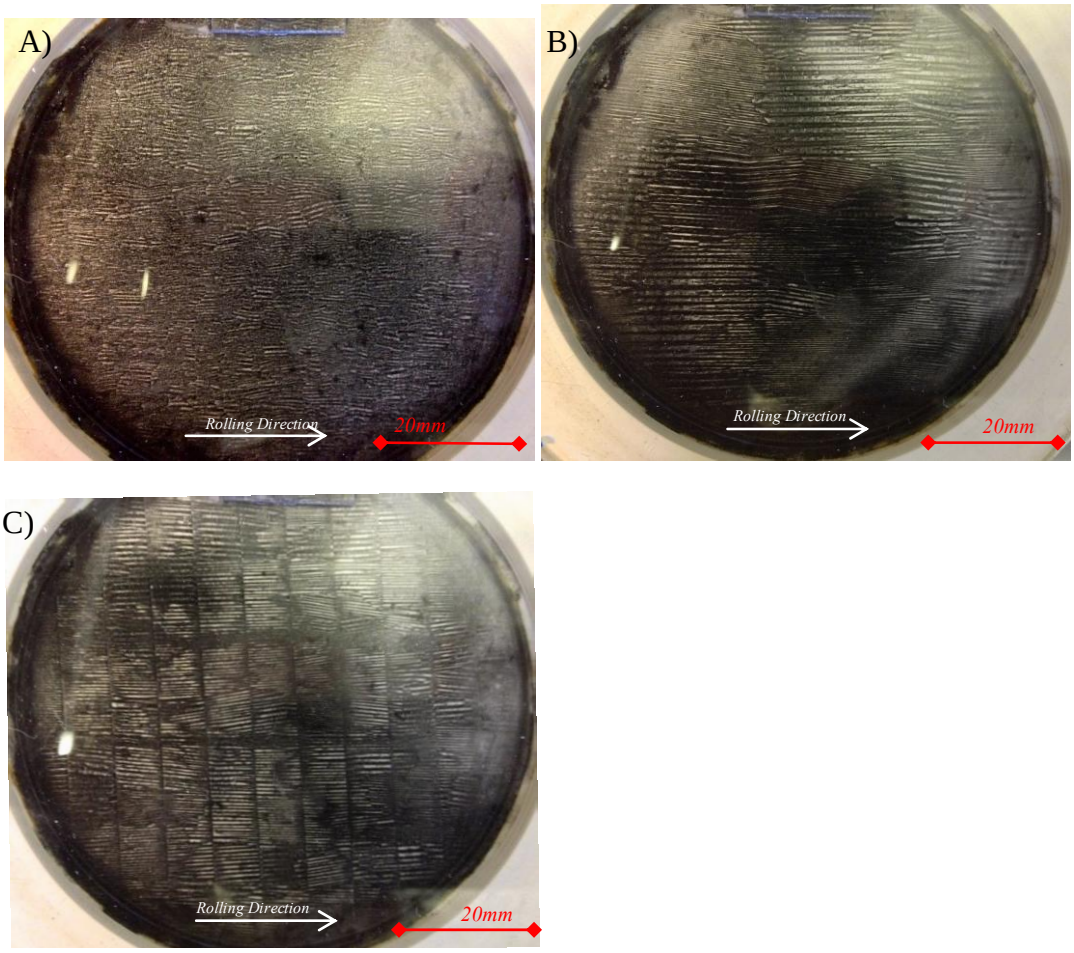

Figure 8- 7: Domain structure of A) CGO B) HIB and C) Laser scribed 0.3mm strips, observed with a Bitter domain viewer

8.1.3. Magnetostriction characteristics:

In order to compare the magnetostriction characteristic of different grades, the Magnetostriction - stress curves are identified using three parameters from fitting the data to a Boltzmann function [3, 4] as presented in equation (8.1).

$$y = \frac{C}{1 + e^{\frac{(x_\sigma - A)}{B}}} - y_0 \tag{8.1}$$

Where,

y is Magnetostriction (μ strain)

x_σ is applied stress (MPa)

y_0 Magnetostriction offset (μ strain)

C (Parameter 1): magnetostriction saturation (μ strain)

B (Parameter 2): the slope of the curve.

A (Parameter 3): The stress shift for zero magnetostriction.

These parameters are illustrated in the graph 8-8 below [5]. Parameter A is correlated to the external applied stress such as coating to the sample that causes a horizontal stress shift of the magnetostriction sensitivity curve.

The slope of the curve (parameter 2) can be measured directly from the curve by fitting the trend line manually to the measured curve, which is *-4.664* in this case.

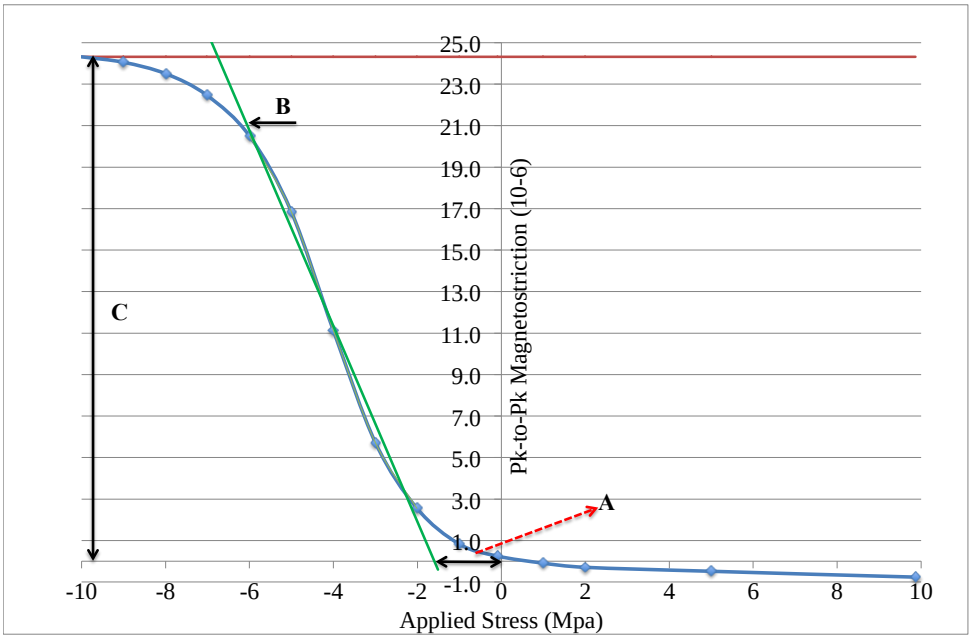

Figure 8- 8: illustration of three parameters for identifying magnetostriction characteristics under stress (CGO at 1.7 T and 50 Hz)

Figure 8-9 shows the average magnetostriction vs. stress curve for each grade. The three parameters for each batch of materials at 1.7 T and 1.5 T determined from magnetostriction versus stress graphs is shown in Table 8-1.

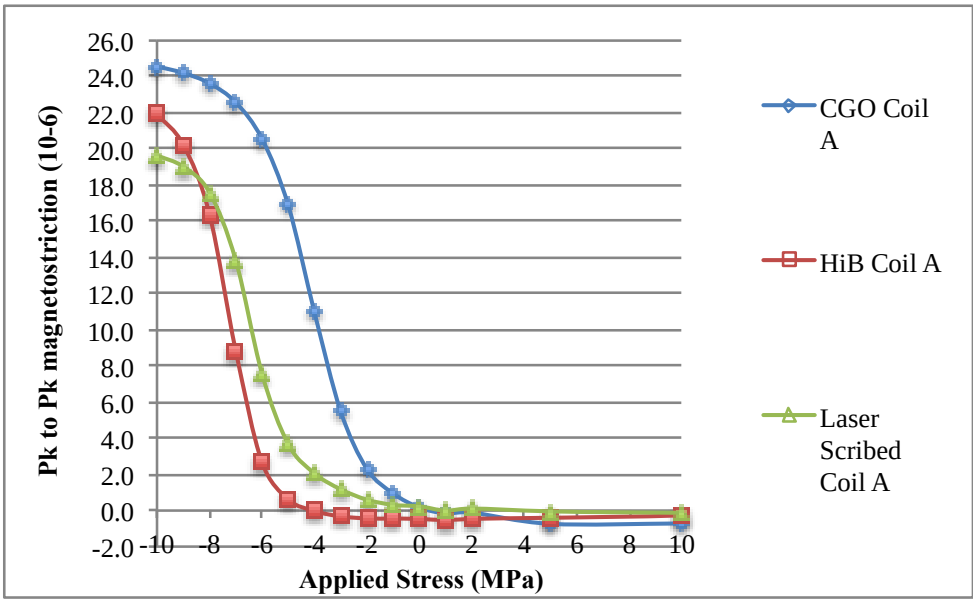

Figure 8- 9: Average magnetostriction Vs. Stress curve at 1.7 T and 50 Hz for CGO, HIB and laser scribed materials

Table 8-1 shows that the CGO samples have the highest magnetostriction saturation at 1.7T and 50 Hz with 24.5 ($\times 10^{-6}$) and the lowest was obtained by Laser scribed sample. The magnetostriction saturation under compressive stress (λ_{100}) is affected by the strip thickness as well as the chemical composition.

As discussed previously in this chapter, parameter one presents the magnetostriction saturation. All grades have same thickness of 0.3 *mm* and similar chemical composition, 3% silicon, that indicated they all should have the same magnetostriction saturation, nevertheless, as it can be seen from the Figure 8-9 the laser scribed material and the Hi-B materials are not yet saturated at 10MPa compressive stress due to the shift in their magnetostriction stress graph applied by coating tension.

Table 8- 1: three parameters for all batches at 1.7 T and 1.5 and 50 Hz

1.7 T										
Grade	**Laser Scribed**	**HIB**		**CGO**						
Coil No	Coil A	Coil A	Coil B	Coil A	Coil B	Coil C	Coil D	Coil E	Coil F	Coil G
Parameter 1/C (Max Pk-to-Pk Magnetostriction)	19.5	21.9	22.4	24.3	24.5	24.3	23.6	23.6	22.6	22.1
Parameter 2/B (slope of the magnetostriction stress curve)	-4.1	-5.3	-5.4	-4.7	-4.7	-4.8	-4.2	-4.4	-3.8	-3.6
Parameter 3/A (Zero magnetostriction shift)	-3.8	-5.2	-4.9	-1.6	-0.4	-0.7	-0.9	-1.4	-1.1	-1.5

1.5 T										
Grade	**Laser Scribed**	**HIB**		**CGO**						
Coil No	Coil A	Coil A	Coil B	Coil A	Coil B	Coil C	Coil D	Coil E	Coil F	Coil G
Parameter 1/C (Max Pk-to-Pk Magnetostriction)	15.7	18.1	19.6	20.9	21.2	20.8	20.0	20.4	19.4	19.8
Parameter 2/B (slope of the magnetostriction stress curve)	-4.1	-4.9	-5.1	-4.2	-4.2	-4.3	-4.1	-4.2	-3.7	-3.8
Parameter 3/A (Zero magnetostriction shift)	-19.2	-22.8	-25.6	-7.8	-3.2	-3.5	-5.6	-7.5	-7.4	-6.8

Using colour marks the highest and lowest values in table 8-1 are shown; yellow is used for the highest and blue for the lowest value. Same trend can be spotted from Table 8-1 at 1.5 and 1.7 Tesla which accomplish the precision of the model, and so that this can be used at different flux densities.

Parameter two shows the slope of the line, this parameter indicates the misorientation, and the shallower the slope is, the higher misorientation is. Since magnetostriction is due to 90^{o} domain wall and moment rotation movement and lower misorientation means more domains wall are aligned in the [100] direction

which consequently results in more grains switches to Stress Pattern at similar stress values resulting in a steeper slope.

By comparing parameter two, it can be seen that Hi-B samples have the lowest average misorientation. Also a variation can be seen by comparing parameter two (slope of the curve) between different batches of CGO which is due to the large misorientation in CGO and the fact that each of these batches were selected from different parts of the reference coil and could have different misorientation to the others. Moreover, Laser scribed materials shows a shallower slope than HiB due to the existence of closure domains along the scribe lines as explained and proven by a model in Chapter 7.

As explained previously the transverse domain volume fraction is the major parameter for controlling magnetostriction, the volume fraction of transverse domains under the lancet domains decreases and disappears below 1 degree, consequently lancet domains will cause a sharper slope in magnetostriction stress curve as more grains will switch to Stress Pattern at similar stress values resulting in a steeper slope [6],

Sablik, M.K and Jiles, D.C. showed [7] that the hysteresis in magnetostriction is coupled to hysteresis in the magnetization due to the dependence of magnetostriction on the magnetization. Also it was proposed that the slope of the hysteresis curve depends on domain density, temperature and saturation magnetization. The hysteresis loop can be explained by the effect of magnetic field on domain structure explained in Chapter 3. The magnetostriction hysteresis loop can be divided into three parts, and explained regarding the domain structure under external magnetic field shown in Figure 8-10.

i. Increasing the field from zero initiates 180^{o} domain wall movement and as a result $\Delta\lambda$ is (ideally) zero.

ii. In the second stage, by increasing the magnetic field magnetostriction increases until all domains are aligned in the easy direction and magnetostriction is saturated. 90° domain wall motion is the main mechanism. Figure 8-10 illustrates how domain structures of a grain oriented silicon steel change under external field.

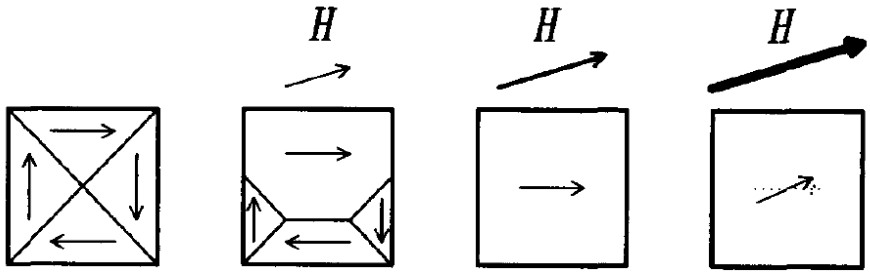

Figure 8- 10: Domain reorientation by external magnetic field

iii. In the last part of the graph, the magnetostriction in the rolling direction drops by an increase of flux density due to the rotation mechanism. All domains rotate from the easy direction to the magnetizing direction. Figure 8-11 illustrates a schematic drawing of moment rotation, which is causing a drop in magnetostriction value, Θ is the angle between domains easy direction [001] and flux direction, as it demonstrates in the Figure 8-11 magnetostriction would drop by "*r (1-sin Θ)*".

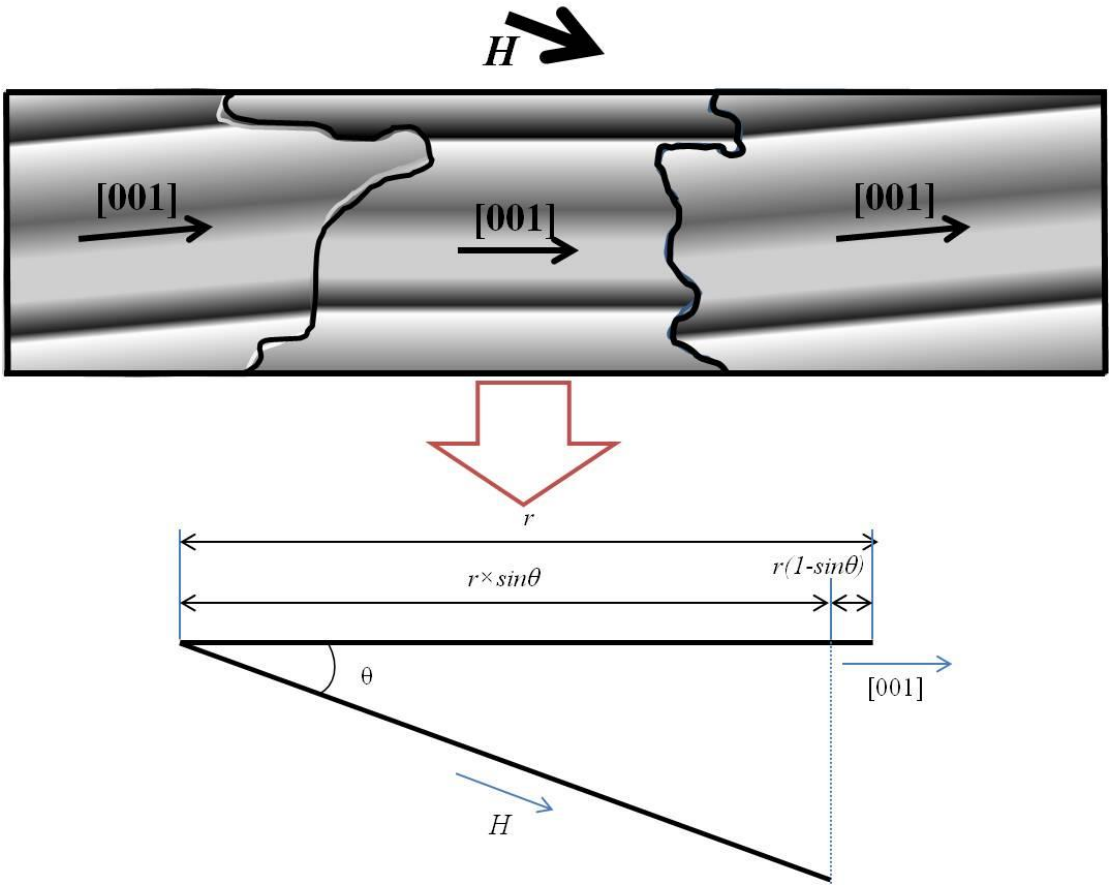

Figure 8- 11: schematic drawing of motion mechanism

By plotting the magnetostriction against induction for a period of magnetization, the butterfly loop has been determined. The peak-to-peak magnetostriction is determined as the amplitude of the magnetostriction in a period of magnetization [8].

The Butterfly loop for the three grades is shown in Figure 8-12 and 8-13 for 5 and 10 MPa compressive respectively magnetised at 1.7 T, 50 Hz in the rolling direction. Each data point is the average magnetostriction in each of the five strips in each batch measured three times. Figure 8-12 confirms that CGO has the highest misorientation; HiB shows the lowest magnetostriction and is less sensitive to magnetising field. Whereas Domain refined strips have higher magnetostriction due to the existence of residual stress that has been applied during scribing and

formation of transverse domains along the scribed lines, explained in more detail in Chapter 7.1.

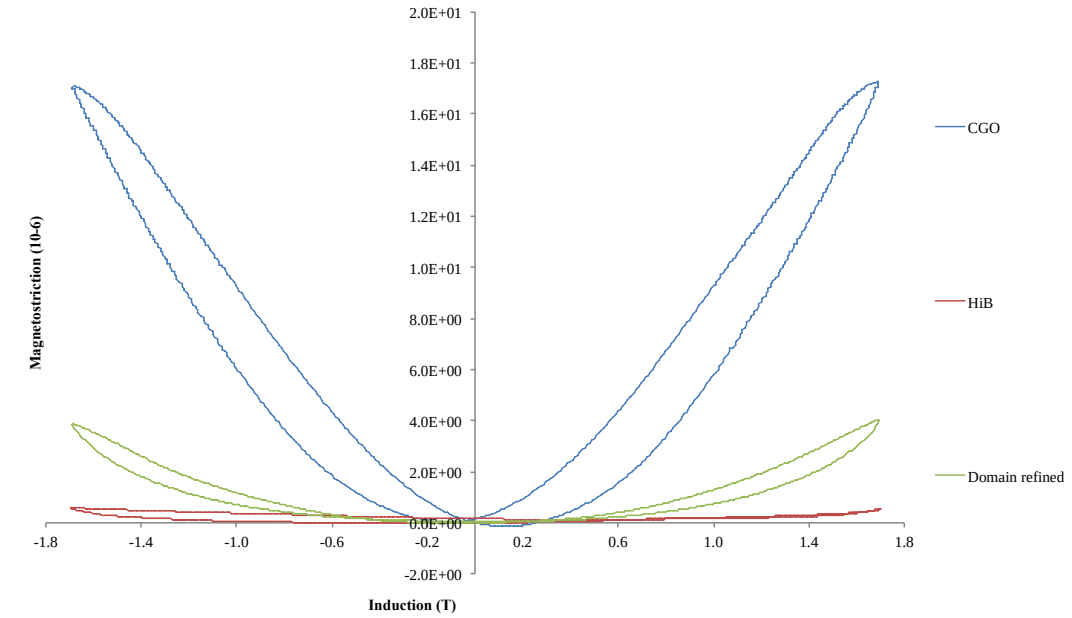

Figure 8- 12: Magnetostriction hysteresis loop at 5MPa magnetised at 1.7T, 50Hz for CGO, HIB and laser scribed materials

Figure 8-13 displays the magnetostriction butterfly loop at 10MPa compressive; CGO has still the highest Pk-to Pk magnetostriction. HiB and Laser scribed strips show the same trend as expected as both materials have similar misorientation and under high compressive stress both grades will exhibit Stress Pattern, the main domain is still in the same [100] direction but the domain walls change from 90^0 to the [010] direction as explained in Chapter 3. As a result the surface of the applied stress, strips surface would be covered by closure domain structure in order to reduce the overall energy.

Moreover, as explained in Chapter 7, the tensile stress distribution between the scribed lines due to domain refinement process causes the lancet closure domains to be unstable according to the Magnetoelastic energy and this refines the

180^{o} main domain wall spacing, the application of compressive stress would overcome the benefit of domain refinement due to the tensile stress Therefore the domain pattern reorganizes in order to reduce the overall energy and lancet domains and Stress Patterns appears again consequently the effect of scribing disappears.

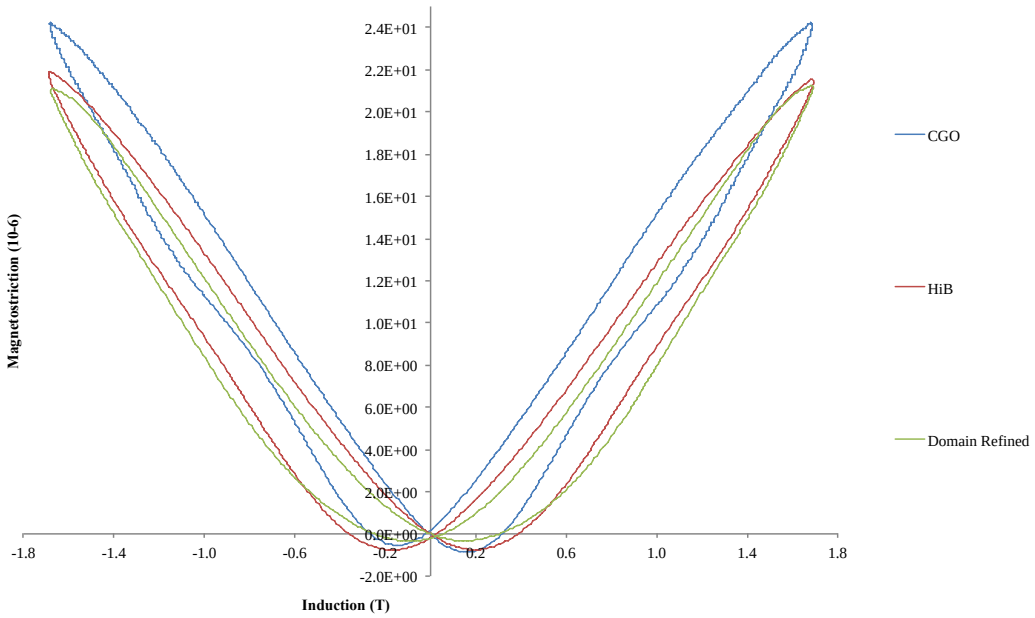

Figure 8- 13: Magnetostriction hysteresis loop for at 10MPa magnetised at 1.7T, 50Hz for CGO, HIB and laser scribed materials

Parameter three indicates the amount of the external stress applied to the laminations. The shift of the magnetostriction stress curve is related to the release of a tensile stress in the sample in the rolling direction and a release of compressive in transverse direction [9]. The difference in the shift could be due to the difference of the coating thickness or even to the conditions of the sample such as cutting stress. In domain refined material as it was explained in chapter 7.1 the induced residual stress by laser scribing created 90^{o} domains near scribed lines. These domains were partially suppressed in the strips by coating tension, when the strip is subjected to a compressive stress these domains grow and magnetostriction

increases. But, in HiB there is less increase in magnetostriction by compressive stress, which is due to lower volume fraction of lancet domains due to better orientation and lower residual stress.

8.2. Modelling of Butterfly loops

The hysteresis in ferromagnetic material is related to the existing of lattice imperfections acting as pinning sites impending the domain wall motion[10, 11].As a result it can be expected that in the absence of imperfections, the material would be hysteresis free and the magnetic induction would be single value functions of the magnetic field[11, 12].

So In order to be able to define the magnetostriction value of a sample as a function of flux (*B*) it can be assumed that the behaviour of magnetostriction with respect to *B* is anhysteretic. Moreover *B* and *M* are assumed to be equivalent due to their high relative permeability as a result at low magnetisation the approximation in equation (8.2) can be made:

$$\lambda = bM_{an}{}^{2} \tag{8.2}$$

Where M_{an} is the anhysteretic magnetisation and b is the magnetostriction coefficient and can be obtained from the experimental by fitting a parabolic function. The anhysteretic magnetisation can be described as a function of applied stress based on a proposed model by Jiles [12, 13]using a modified Langevin equation

$$\frac{M_{an}}{M_s} = \coth\left(\frac{H_{effective}}{a}\right) - \left(\frac{a}{H_{effective}}\right) \tag{8.3}$$

Where

M_s *is* saturation magnetisation,

$H_{effective}$ is the effective applied field

a is a material parameter given by:

$$a = \frac{TK_B}{m\mu_0} \tag{8.4}$$

Where

T is temperature,

K_B is the Boltzmann constant,

m is the atomic magnetic moment

μ_0 is permeability of free space.

'$H_{effective}$*'* can be determined based on a proposed theory by Sablik et.al.[14] The equation for the anhysteretic magnetization under stress can be written as:

$$H_{effective} = H + \alpha M + H_\sigma \tag{8.5}$$

Where 'H' is the applied field,

αM is the mean field

H_σ is the stress equivalent that is given by:

$$H_\sigma = \frac{3}{2}\frac{\sigma}{\mu_0}\left(\frac{\delta\lambda}{\delta M}\right) \tag{9.6}$$

This can be further simplified by determining the derivative ($\delta\lambda/\delta M$) from equation (8.2) the anhysteretic magnetisation for stressed sample can be also simplified and defined by:

$$M_{an} = M_s[\coth\left(\frac{H + M\left(a + \frac{3\sigma b}{\mu_0}\right)}{a}\right) - \frac{a}{H + M\left(a + \frac{3\sigma b}{\mu_0}\right)}] \quad (8.7)$$

$\coth x \approx 1/x + x/3 + \ldots$ [15](8.8)

$\therefore$

$$\approx \frac{M_s}{3a - \left(a + \frac{3b\sigma}{\mu_0}\right) M_s} \quad (8.9)$$

By substituting the equation 8.9 into equation 8.2 magnetostriction can be predicted at low magnetisation by:

$$\lambda = \frac{bM_s^2}{(3a - \left(a + \frac{3b\sigma}{\mu_0}\right) M_s)^2} \quad (8.10)$$

But as discussed previously equation 8.10 is only valid at low magnetisation where magnetostriction is a square function of magnetization. In order to be able to calculate the relative volumes of domain structures and harmonics it is necessary to model the butterfly loop over the full range of magnetization. Mathematical software origin 8.1 was used to find the best fitting Lorentz equations as presented in equation 8.11 showed the closest fit:

$$y = y_0 + \frac{2A}{\pi} \times \frac{w}{4(x - x_c)^2 + w^2} \quad (8.11)$$

These parameters are illustrated in the graph 8-14:

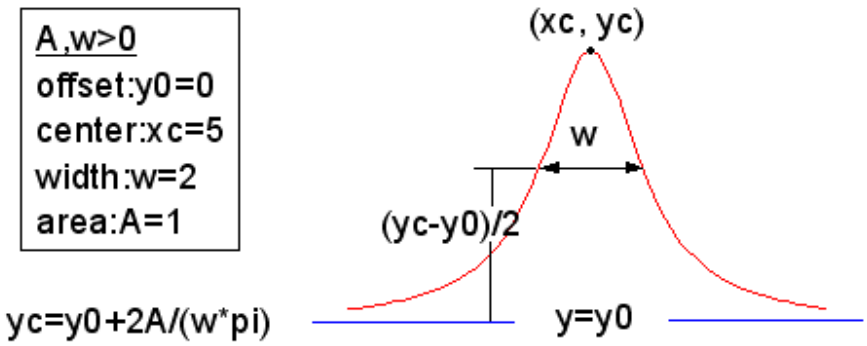

Figure 8- 14: Typical Lorentz curve, showing parameter presented in the equation 9.12

Where 'A' is a constant 'y_c' and 'x_c' defined the centre of the curve and 'w' is the width on the curve at half of its saturated value. Figure 8-15 shows the measured butterfly loop for CGO material at flux density of 1.7T under 5 and 10 MPa applied pressure as well as the Lorentz fit.

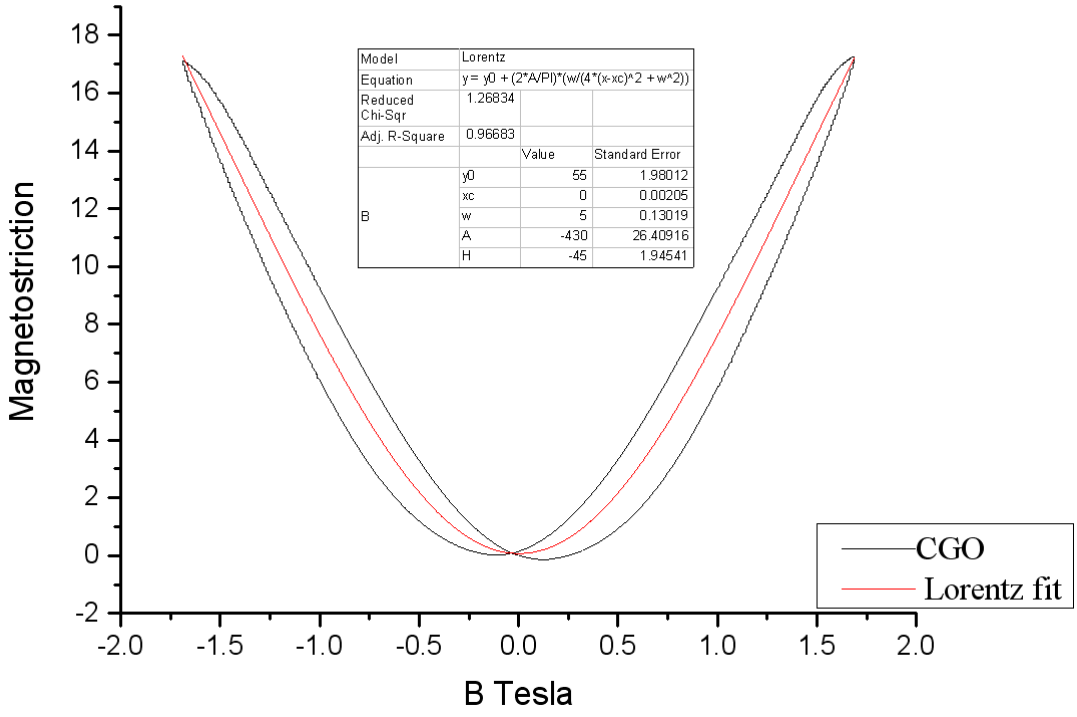

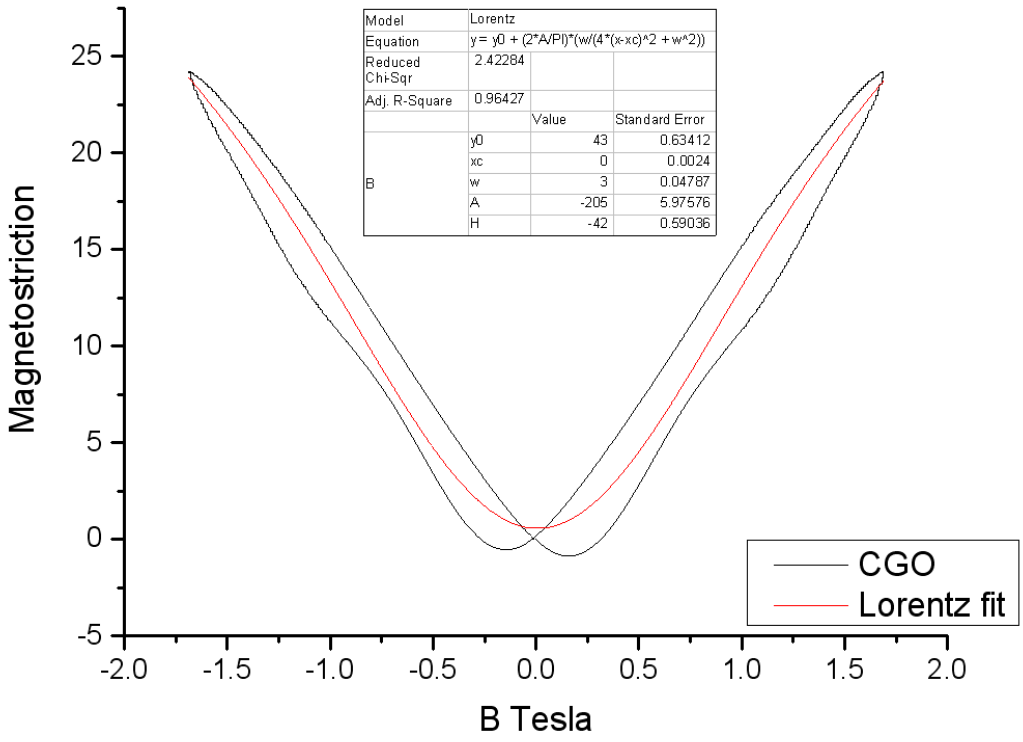

Figure 8- 15: Magnetostriction hysteresis loop of a CGO material at 1.7T Top) under applied pressure of 5MPa Bottom) under applied pressure of 10 MPa, the red line shows the Lorentz fit

As shown in equation 8.12, flux density (B) is a square function of magnetostriction (λ), which would result in having magnetostriction frequency twice the magnetizing frequency as shown in equation 8.13 that agrees with the theory. Figure 8-16 shows a simulated magnetostriction frequency over one cycle as well as flux density based on the proposed model.

$$\lambda \propto \frac{1}{B^2} \tag{8.12}$$

$$B = \hat{B}\cos(\omega t)$$

$$\omega = 2\pi f$$

$$\therefore B^2 = \frac{\bar{B}^2}{2}\cos(2 \times 2\pi f \times t)$$

$$=\widehat{B^2}sin(2 \times 2\pi f \times t \times) \quad (8.13)$$

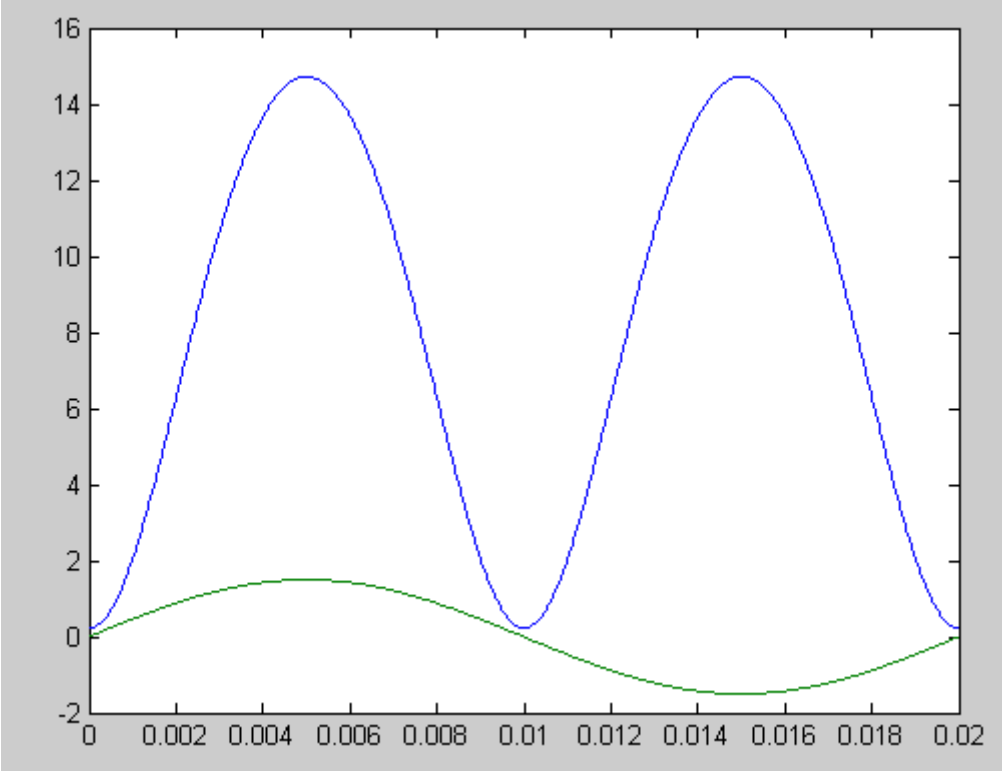

Figure 8- 16: simulated magnetostriction frequency based on the Lorenz fitting equation for sinusoidal magnetising frequency of 50 Hz. Blue line represent magnetostriction λ, Green line is Flux density.

Table 8-2 shows the Lorentz fitting variable for CGO, HiB and Domain Refined material under applied stresses of -2, -5 and -8 MPa at 1.7T. As it is shown in the Figure 8-14 Lorentz fitting variable *'A'* can be calculated form equation 8.14:

$$A = \pi W \times \frac{(Y_c Y_0)}{2} \quad (8.14)$$

Similarly the variable '*w*' is defined as the width of the curve at (Y_c-Y_0/2). Also as it can be seen from the Table 8-2, '*w*' is inversely proportional function of 'Y_c'. Also from the Table it can be concluded that 'Y_c' which defined the maximum/peak value of the curve is directly proportional to the applied stress, σ.

Table 8- 2:Lorentz fitting variables for CGO, HiB and Domain Refined material under -2, -5 and -8 MPa applied stress, under 1.7 T and 50 Hz

	CGO			HiB			Domain Refined		
σ (MPa)	-2	-5	-8	-2	-5	-8	-2	-5	-8
Y_c	24	53.7	42.2	1.07	3.4	47	14.47	28.6	60.24
w	9.7	5.2	3.1	9.8	7.2	4.7	11.2	8.5	5.2
A	-373.8	-439.5	-216.3	15.5	-36.4	-347.9	-256.3	-383.2	-496.6

Then in the next stage a Fast Fourier Transform (FFT) program was used to analyse the ac magnetostriction harmonics of a model signal. Table 8-3 shows a comparison between the measured harmonic and model harmonic for all CGO, HiB and domain refined material at applied stress of -5 MPa. The average standard deviation of calculated value is 0.32. The results show a good agreement with the measured data for HiB and Domain Refined materials, whereas for the CGO material there is approximately 20% difference between the measured and calculated data that is due to the fact that the measured butterfly loop has hysteresis, which in the model is, has not been taken into the account.

Table 8- 3: Calculated magnetostriction harmonics based on the Lorentz equation vs. measured harmonics at applied stress of -5MPa, 1.7T, all values are in order of (10^{-6})

Frequency	CGO		HiB		DR	
	Measured	Calculated	Measured	Calculated	Measured	Calculated
1st harmonic	16.800	11.800	0.619	1.110	3.040	5.270
2nd harmonic	1.960	7.540	0.145	0.145	0.370	0.294
3rd harmonic	0.099	0.280	0.071	0.000	0.050	0.016
4th harmonic	0.057	1.04E-02	0.028	6.14E-07	0.026	9.12E-04
5th harmonic	0.115	3.84E-04	0.011	1.26E-09	0.007	5.08E-05
6th harmonic	0.042	1.43E-05	0.007	2.60E-12	0.011	2.83E-06
7th harmonic	0.011	5.29E-07	0.004	5.13E-15	0.004	1.58E-07
8th harmonic	0.007	1.96E-08	0.002	9.93E-16	0.002	8.79E-09
9th harmonic	0.004	7.28E-10	0.001	2.56E-16	0.002	4.90E-10
10th harmonic	0.003	2.70E-11	0.001	5.74E-16	0.001	2.73E-11

8.3. Magnetostriction Harmonics and a-weighted magnetostriction velocity:

Application of stress changes the domain structure in grain-oriented steel as explained in Chapter 3. Applying compressive stresses in the rolling direction results in increasing Magnetoelastic energy in [001] direction and as result [010] and [100] directions becomes energetically favourable. The changes in domain structure leads to distortion of the B-H loop. In a real transformer any distortion would generate an additional third-harmonic of the magnetic flux density waveforms in transformer limbs that leads to increased harmonic content in the magnetostriction waveform[16].

The first 10 harmonics of magnetostriction were recorded, although the frequency range of the accelerometer (explained in Chapter 5) is sufficient for analysing frequencies up to 3 kHz however these higher harmonics leads to larger accelerations as the acceleration has a frequency squared relation to the amplitude of the vibration. As a result the acceleration becomes out of sensitivity range of the

accelerometers for harmonics above the ninth harmonic. Figures 8-17, 18 and 19 show magnetostriction harmonics for the first five harmonics for CGO, HiB and Laser scribed. Harmonics with a frequency higher than five times the fundamental frequency are smaller than the sensitivity of the accelerometer and therefore must be neglected. Each data point is the average value of five strips, each measured three times. All grades show similar harmonic trends under applied stress. The difference in harmonics at zero stress and under tension is negligible compared to compressive zone.

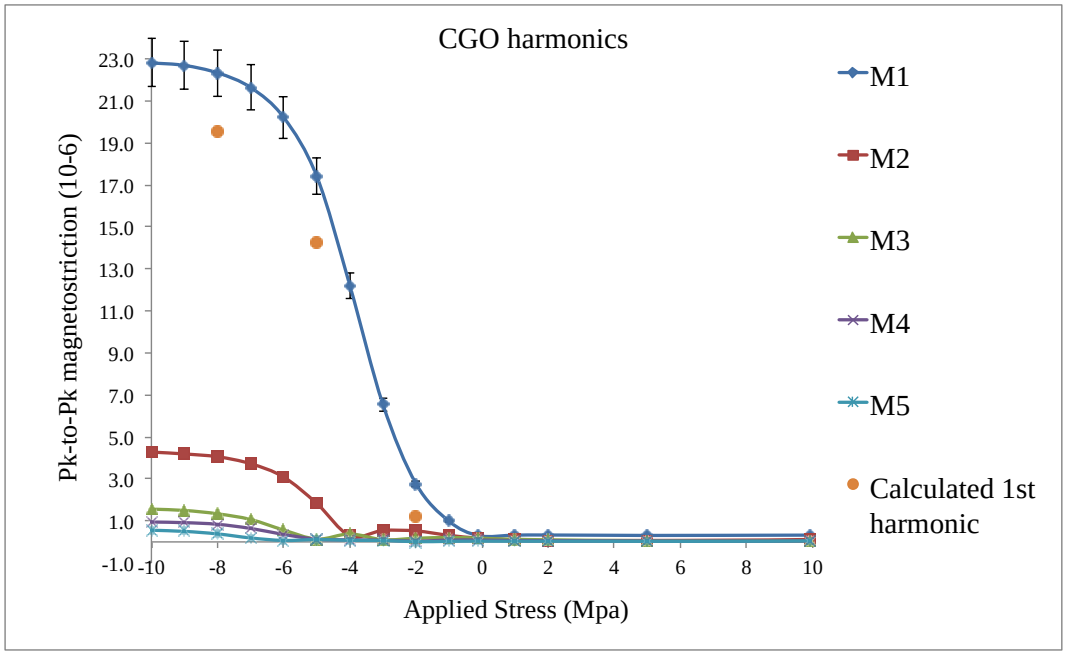

Figure 8- 17: First five magnetostriction harmonics of CGO sample at 1.7 T and 50 Hz, M1: first harmonic (100Hz), M2: 2nd harmonic (200Hz)…M5: 5th harmonic (500 Hz)

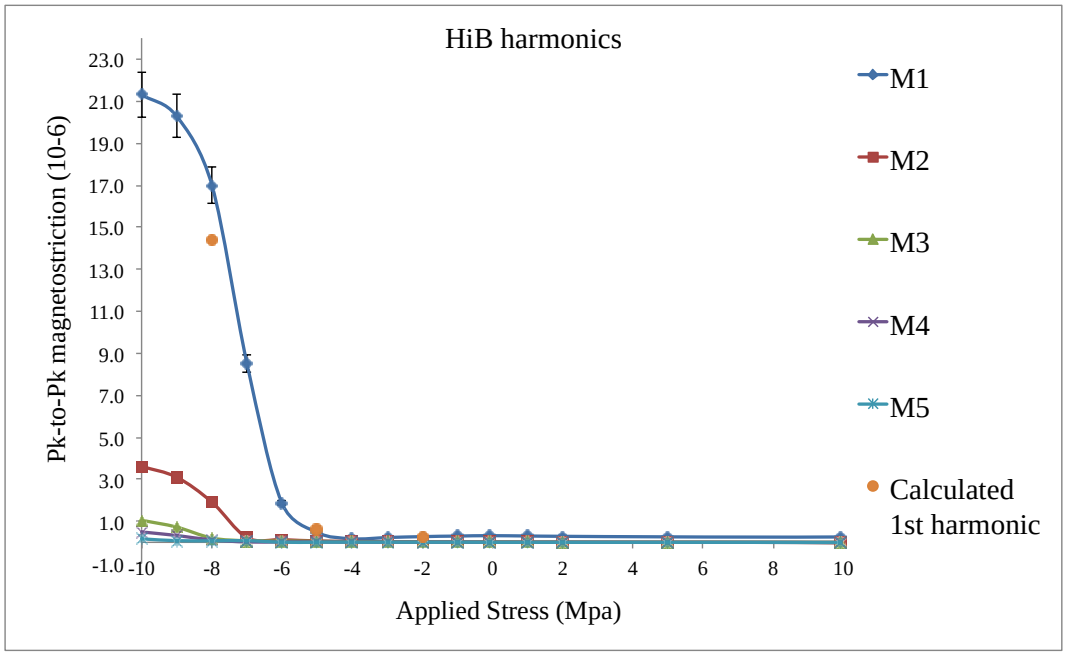

Figure 8- 18: First five magnetostriction harmonics of Laser scribed sample at 1.7 T and 50 H, M1: first harmonic (100Hz), M2: 2nd harmonic (200Hz)…M5: 5th harmonic (500 Hz)

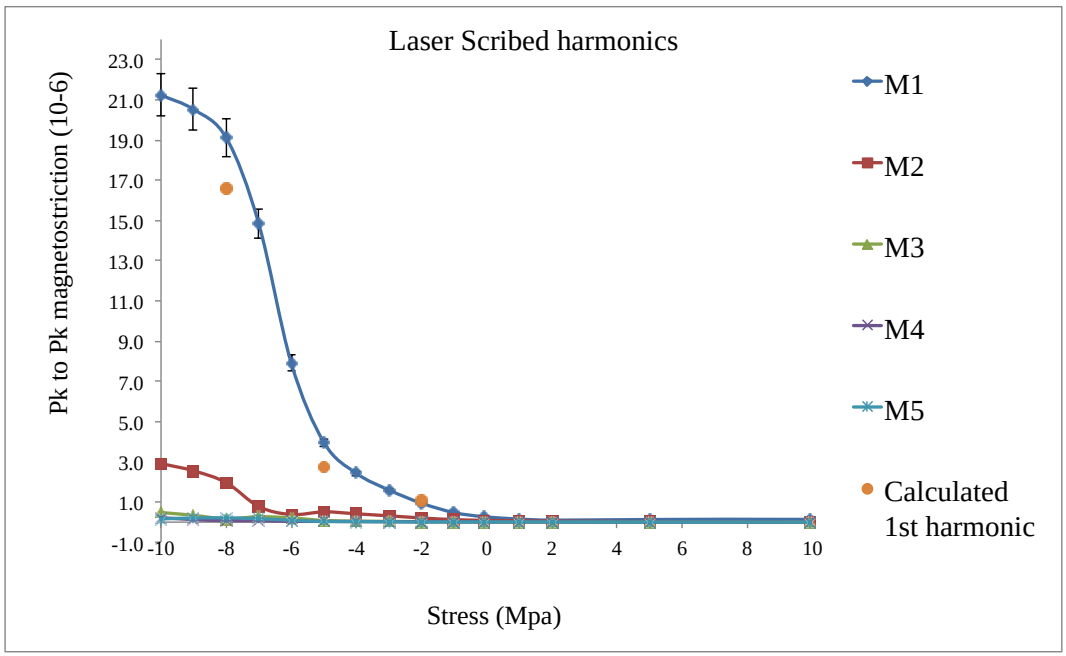

Figure 8- 19: First five magnetostriction harmonics of Laser scribed sample at 1.7 T and 50 Hz, M1: first harmonic (100Hz), M2: 2nd harmonic (200Hz)…M5: 5th harmonic (500 Hz)

The Fast Fourier Transform (FFT) analysis of the secondary voltage signal measured by the system showed less than 0.05% third harmonic. Also, significant harmonics were presented in the magnetostriction waveform. These findings agree well with those of Mapps and White [17].

From the graphs above, 8-17, 18 and 19 show a significant fundamental component at 100 Hz with a second harmonic of around one fifth of the magnitude and a third harmonic with a further decrease in the magnitude. Above the third harmonic the magnetostriction magnitude typically becomes less than 0.1 microstrain at 10MPa compression stress at a magnetic flux density of 1.7 Tesla. Table 8-4 shows the first three harmonics of the above sample for better comparison. Reiplinger [18] was one of the first researchers to study the effect of magnetostriction harmonics. He found that the peak-to-peak magnetostriction alone is not enough to correlate magnetostriction to transformer noise.

Table 8- 4: First three harmonics of CGO, HIB and laser scribed samples at 1.7 T and 50 HZ, harmonics value are in order of 10^{-6}

B Pk [T]	Stress (MPa)	1st harmonic			2nd harmonic			3rd harmonic		
		CGO	HiB	Laser	CGO	HiB	Laser	CGO	HiB	Laser
1.7	10	0.687	0.227	0.158	0.086	0.004	0.014	0.028	0.006	0.008
	5	0.671	0.261	0.131	0.069	0.006	0.032	0.058	0.008	0.01
	2	0.478	0.286	0.101	0.063	0.01	0.052	0.1	0.011	0.013
	1	0.326	0.302	0.152	0.09	0.013	0.066	0.124	0.013	0.013
	0	0.3	0.317	0.274	0.18	0.017	0.09	0.179	0.016	0.016
	-1	0.988	0.3	0.477	0.311	0.021	0.129	0.211	0.017	0.019
	-2	2.774	0.273	0.94	0.523	0.026	0.21	0.175	0.02	0.028
	-3	6.548	0.228	1.598	0.542	0.033	0.316	0.105	0.024	0.038
	-4	12.198	0.173	2.424	0.293	0.044	0.413	0.38	0.029	0.056
	-5	17.385	0.472	3.952	1.824	0.067	0.512	0.136	0.046	0.084
	-6	20.215	1.868	7.921	3.091	0.13	0.38	0.569	0.064	0.214
	-7	21.631	8.524	14.846	3.722	0.227	0.778	1.067	0.076	0.268
	-8	22.324	16.987	19.108	4.053	1.912	1.963	1.339	0.202	0.165
	-9	22.684	20.292	20.527	4.188	3.105	2.555	1.498	0.728	0.343
	-10	22.802	21.304	21.233	4.278	3.613	2.911	1.559	1.049	0.48

It has been known that the sound pressure in the fluid surrounding a vibrating object is relative to the velocity rather than to the displacement of the

object [19] and correlation between A-weighted magnetostriction velocity and the A-weighted sound pressure level has been proposed [18, 20-22].

In order to assess noise pollution, comparison between different grade's harmonics and the '*A*' weighted scale is applied that takes into account the frequency response of the human ear as explained earlier. The A-weighted magnetostriction velocity relates a sound pressure level to the magnetostriction of a unit length of material under sinusoidal magnetic polarization and is defined by [21].

$$L_{vA} = 20\log_{10}\frac{\rho c\sqrt{\sum_i[(2\pi f_i)\times(\lambda_i/\sqrt{2})\times\alpha_i]^2}}{P_{e0}} \tag{9.14}$$

Where:

L_{vA} is the A-weighted magnetostriction velocity (dB (A))

ρ is the density of the atmosphere (kilogram per Cubic Square)

c is the sound velocity (meter per second)

π is the circular constant (3.141592…)

f_i is the frequency of the i-th harmonic components

f_0 is the frequency of the magnetic polarization

λ_i is the magnitude of the i-th harmonic component of magnetostriction

α_i is the A-weighting coefficient at the frequency f_i

P_{e0} is the minimum audible sound pressure (2×10^{-5} Pascal)

Figure 8-20 shows the A-weighted magnetostriction velocity of three different steel grades. The third and second harmonics are amplified significantly but the fundamental frequency, 100Hz, is still the primary noise generator. Figure 8-20 shows that CGO has the highest sound pressure level and depending on the stress range HiB and laser-scribed material could have same or different sound pressure level. The main reason for a high A-weighted magnetostriction in CGO material is that in calculating the A-weighted magnetostriction, frequencies sensitive to human ear are emphasized while the very high and very low frequencies where the human ear is insensitive to them are attenuated. Also it should be pointed out that the fundamental magnetostriction frequency (100 Hz for 50 Hz magnetization) is relatively less important to the acoustic noise level than higher harmonics. It can be seen from Table 8-4 that the CGO material has relatively wide magnetostriction harmonics distribution compare to HiB and Domain refined in harmonics than the other two grades, this result also can be predicted by using the proposed butterfly loop model which is shown in Figure 8-20. The calculated values agree well with the measured A-weighted magnetostriction with average standard deviation of 4.35.

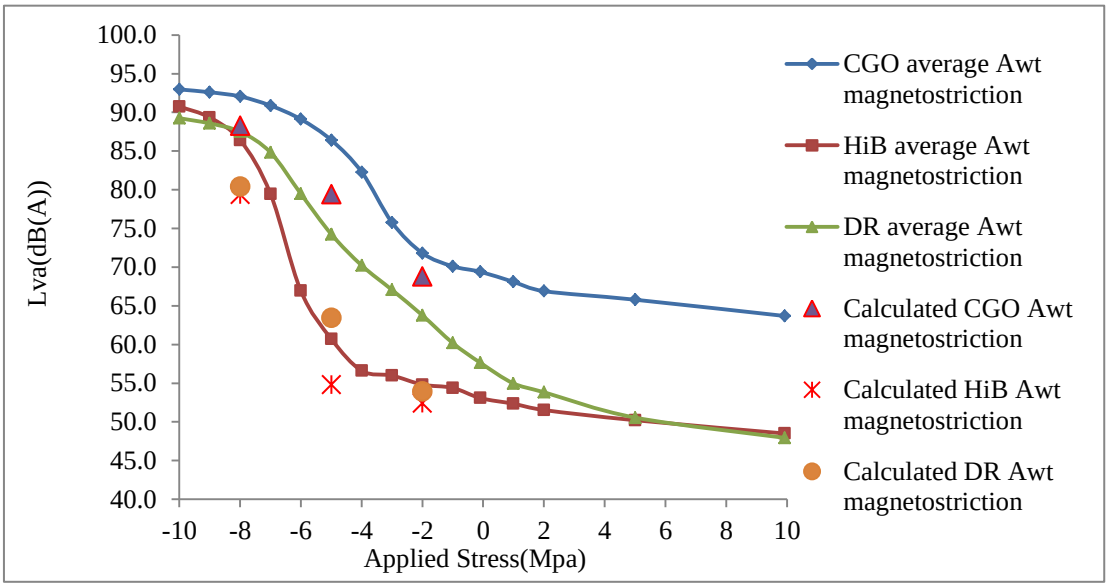

Figure 8- 20: A-weighted magnetostriction velocity of CGO, HIB and laser scribed samples at 1.7 T and 50 Hz

8.4. Conclusion:

The domain patterns of all three grades (CGO, HiB and Domain refined) of grain oriented silicon steel were observed by using Bitter technique and it was confirmed that CGO has the highest misorientation.

The magnetostriction stress sensitivity curves were identified using three parameters as follows:

Parameter 1: Magnetostriction saturation, which depends on strip thickness and chemical composition (the chemical composition is not considered as all tested material has same chemical composition)

Parameter 2: The slope of the curve, relates to misorientation angle

Parameter 3: The stress shift for zero magnetostriction, identify external stresses applied to strips due to coating, cutting etc.

It was illustrated that the better orientation (either by coating or manufacturing process) is the most fundamental solution without changing the chemistry of a material, to reduce the magnetostriction in lower applied stresses, due to reduction of the number of 90^{o} domain wall movement in the material. However eventually material reaches its saturation under high compressive stress and magnetic field and the only solution would be to apply a coating, which could apply higher tensile stress.

CGO has the highest A-weighted magnetostriction velocity and hence expected to have the highest sound pressure level (this is followed up in Chapter10); depending on the stress range HiB and laser-scribed material could have same or different sound pressure level. Below the -8MPa applied stress HiB is expected to have lower sound pressure level whereas higher the -8MPa it should have higher sound pressure level.

References for Chapter 8

1. Klimczyk, P., et al., *Challenges in magnetostriction measurements under stress.* Przeglad Elektrotechniczny, 2009. **85**(1): p. 100-102.
2. Bitter, F., *Experiments on the nature of ferromagnetism.* Physical Review, 1932. **41**(4): p. 507-515.
3. Bender, C.M. and S.A. Orszag, *Advanced mathematical methods for scientists and engineers*. International series in pure and applied mathematics. 1978, New York ; London: McGraw-Hill. xiv, 593 p.
4. Klimczyk, P., *Novel Techniques for Characterisation and Control of Magnetostriction in G.O.S.S*, in *Wolfson Centre for Magnetics*2012, Cardiff University. p. 215.
5. Anderson, P., *A Novel Method of Measurement and Characterisation of Magnetostriction in Electrical Steels*, 2001 Cardiff of Wales
6. Arai, S., M. Mizokami, and M. Yabumoto, *Magnetostriction of grain oriented Si-Fe and its domain model.* Przeglad Elektrotechniczny, 2011. **87**(9B): p. 20-23.
7. Sablik, M.J. and D.C. Jiles, *Coupled Magnetoelastic Theory of Magnetic and Magnetostrictive Hysteresis.* Ieee Transactions on Magnetics, 1993. **29**(4): p. 2113-2123.
8. Commission, I.E., *Electrical steel - Methods of measurement of the magnetostriction characteristics by means of single sheet and Epstein test specimens*, 2010, IEC: Geneva.
9. Anderson, P.I., A.J. Moses, and H.J. Stanbury, *Assessment of the stress sensitivity of magnetostriction in grain-oriented silicon steel.* IEEE Transactions on Magnetics, 2007. **43**(8): p. 3467-3476.
10. Desimone, A., *Hysteresis and imperfection sensitivity in small ferromagnetic particles.* Meccanica, 1995. **30**(5): p. 591-603.
11. Jiles, D.C. and D.L. Atherton, *Theory of ferromagnetic hysteresis.* Journal of Magnetism and Magnetic Materials, 1986. **61**(1-2): p. 48-60.
12. Jiles, D.C. and D.L. Atherton, *Theory of the magnetisation process in ferromagnets and its application to the magnetomechanical effect.* Journal of Physics D: Applied Physics, 1984. **17**(6): p. 1265-1281.
13. Jiles, D.C. and J.B. Thoelke, *Theory of ferromagnetic hysteresis: Determination of model parameters from experimental hysteresis loops.* IEEE Transactions on Magnetics, 1989. **25**(5): p. 3928-3930.
14. Sablik, M.J. and D.C. Jiles, *A model for hysteresis in magnetostriction.* Journal of Applied Physics, 1988. **64**(10): p. 5402-5404.
15. Kreyszig, E., *Advanced engineering mathematics*. 1962, New York,: Wiley. 856 p.
16. Mapps, D.J. and C.E. White, *Phase-Shifted Flux Harmonics and Magnetostriction in (110) [001] Silicon-Iron.* Ieee Transactions on Magnetics, 1982. **18**(6): p. 1505-1507.
17. Mapps, D.J. and C.E. White, *Magnetostriction harmonics measurement using a double piezoelectric transducer technique.* Journal of Physics E: Scientific Instruments, 1984. **17**(6): p. 472-476.

18. Reiplinger, E., *Assessment of Grain-Oriented Transformer Sheets with Respect to Transformer Noise.* Journal of Magnetism and Magnetic Materials, 1980. **21**(3): p. 257-261.
19. Ver, I.L. and L.L. Beranek, *Noise and Vibration Control Engineering Principles and Applications Second Edition Preface.* Noise and Vibration Control Engineering: Principles and Applications, 2nd Edition, 2006: p. Vii-+.
20. M. Mizokami, M.Y., H. Mogi and T. Kubota, *agnetostriction of grain-oriented electrical steel and noise of transformers*, in *Properties and Applications of Magnetic Materials*2005.
21. Ishida, M., S. Okabe, and K. Sato, *Analysis of noise emitted from three-phase stacked transformer model core.* Kawasaki Steel Technical Report, 1998(39): p. 29-35.
22. Commission, I.E., *Electroacoustics - Sound level meters - Part 1: Specifications*, in *IEC 61672-1 ed1.0*2002, IEC.

Chapter 9: A correlation of the vibration characteristics of transformer cores with the magnetostriction properties of the lamination steels

9.1. Introduction

Acoustic noise produced by a transformer core results from several contributions and can be categorized into two main elements. The first element of transformer noise is caused by core magnetization and is referred to as no-load noise. The second element of noise mostly emanates from the windings on the transformer core and is termed “winding noise”. This is caused by the electromagnetic forces created by the magnetic field of the current flowing in the windings [1].

It is believed [1-9]that the transformer core noise (no-load noise) is mainly related to the magnetostrictive vibration of the laminations, and the Maxwell forces due to the effect of attractive and repulsive forces between laminations, which occurs in loose laminations. These take place mainly at the transformer joint[10, 11]. The separation of the influence of these two factors and their relative effects is particularly challenging, especially in the corner areas where these two factors are mostly interlinked [2].The main objective of this experiment was to determine the importance of magnetostriction in the core vibration by comparing the core vibration of different grades of grain oriented electrical steel with differing magnetostriction characteristics. Moreover, the effects of clamping pressure, magnetic flux density and core design have been studied.

9.1.1. Flux distribution in transformer core

In order to have better understanding of the effect of magnetostriction and Maxwell forces in cores, it is first essential to investigate flux distribution in transformer cores. Where, apart from flux in the rolling direction (RD), there are components in the transverse direction (TD) and normal direction (*z*-component) [12].

In the joint regions overlap arrangements are required to bridge the air gaps, which is essential for the mechanical stability of the core. As shown in Figure 9-1[13]cutting stresses will cause a deterioration of the local magnetic characteristics and, as a result, the flux will partly pass around the air gap region, which could saturate the bridging sheet area.

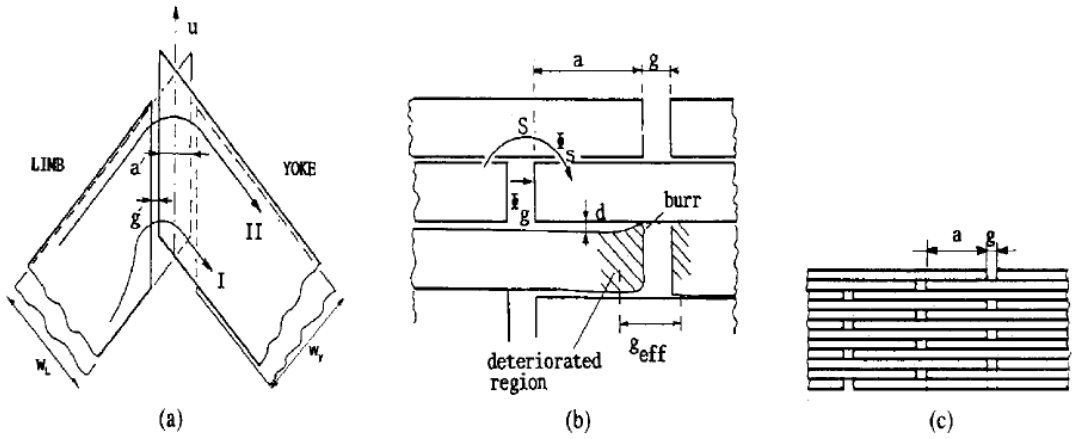

Figure 9- 1: Schematic design of overlap region. (a) Elevation, '*a*' overlap length, '*g*' gap length. (b) Side view of the SSL joint. (c) Side view of the MSL case [13]

The critical induction B_c at which air-gap bridging sheet regions are saturated, saturates the region S in the Figure 9-1 and the finite gap flux Φ_g which arises, can be calculated from the equation below:

$$B_c = \frac{2N}{(N+1)} \qquad \text{[14](9.1)}$$

Where N is the number of overlaps.

With increasing the number of overlaps, N, the bridge is saturates at a higher flux density due to the higher tendency of flux to flow normal to the direction of the bridging region.

In the joint region, below the critical flux density (B_c), the flux tends to flow normal to the direction of the bridging region and leaves in the rolling or transverse direction. Figure 9-2 shows a schematic illustration of flux in the overlapping region; also coils A and B shown in the Figure 9-2 were used to measure flux density normal to the laminations. Also the inter-package flux Φ_z is very low in this case [15].

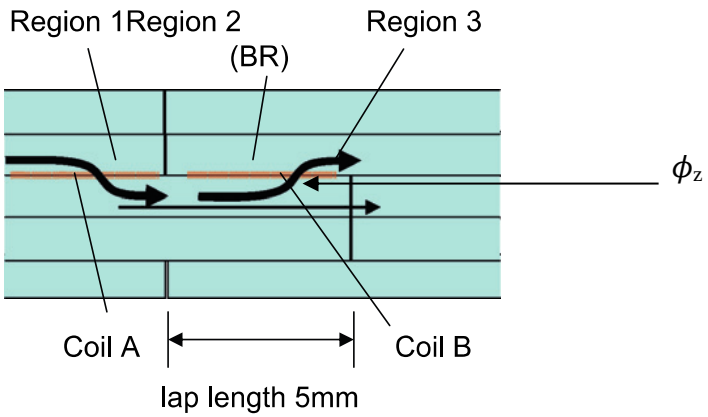

Figure 9- 2: schematic design of flux distribution in an overlap region [12]

In the case of $B > B_c$ (critical flux) the overlap region is saturated, since roughly half of the flux exceeding the critical values has to go through the air gap which has an extremely high reluctance[16]. Moreover, an increased portion of flux is transferred into normal flux corresponding to higher planar eddy current loses.

Due to imperfections in the assembly of transformer cores, the air gaps may get as large as a few *mm*, where the resulting variations cause inhomogeneous flux distribution related to the *z*-components [14]. This can also change the flux distribution in the corner joints, where the flux decreases towards the peripheral edge due to increasing magnetic path length in the case of zero air-gap (as shown in Figure 9-3). However, by increasing the air gap to 2 mm the flux shows constant distribution along the corner joint region with increasing flux in the *z*-direction [13, 17] Loffler, F., et al [14] showed that the MSL (multi step lap) benefit is not reflected in perfectly assembled cores. This research also shows that MSL cores are not so sensitive to air gaps as SSL (single step laps) cores due to having higher B_c.

Also Weiser, B., et al. [2] showed that MSL has lower in plane flux and an increased amplitude of Φ_z but less distortion in overall flux compared to SSL.

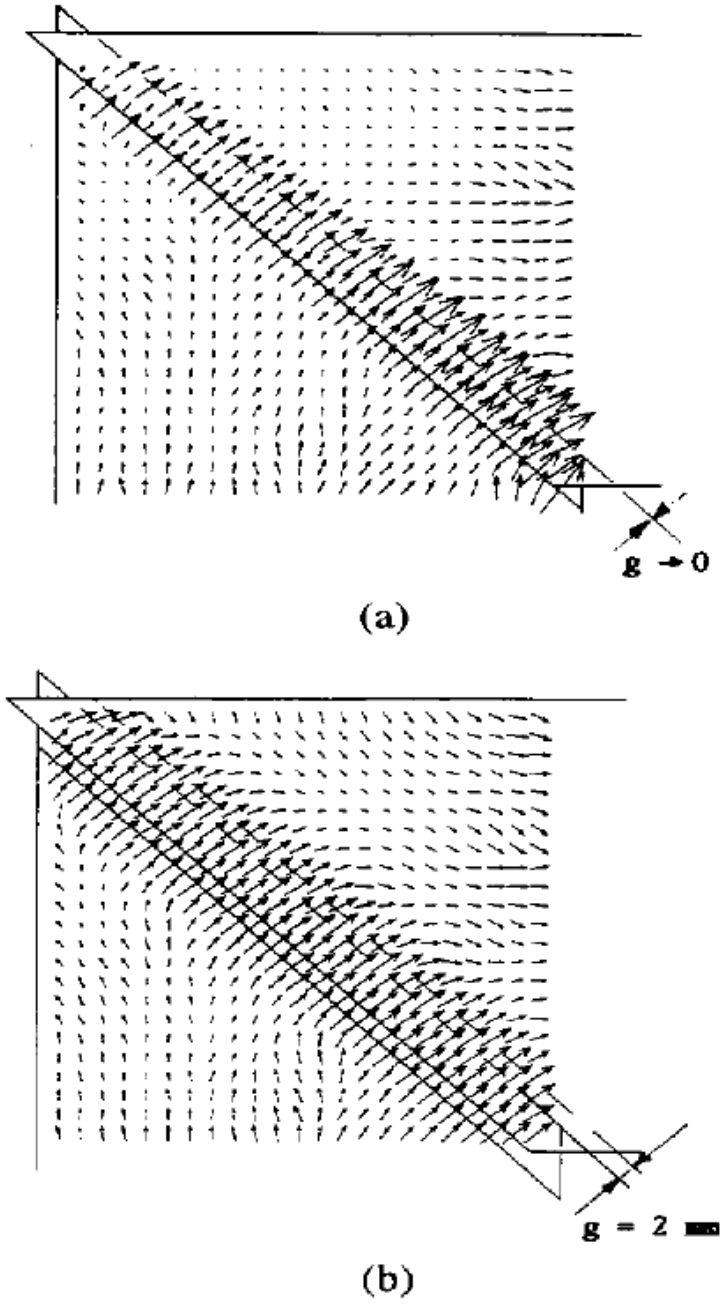

Figure 9- 3: Field distribution in corner of a single step lap transformer (a) air gap =0 (b) air gap =2mm [14]

9.1.2. Magnetostriction and Maxwell's forces

- **Maxwell force:**

Magnetic bodies separated by an air gap carrying a flux density experience a tensile stress in the direction of the flux and a force on each member which is called Maxwell force [18] and can be calculated as

$$\sigma = \frac{B^2}{2\mu_0} \tag{9.2}$$

For a sinusoidal flux density

$$B = \hat{B}\cos(\omega t) \tag{9.3}$$ [18]

Where ω is equal to $2\pi f$ so:

$$\cos^2 x = \frac{1}{2[1+\cos(2x)]} \tag{9.4}$$ [19]

$$B^2 = \frac{\hat{B}^2}{2} \times \cos(2 \times 2\pi f \times t) \tag{9.5}$$

Equation 9.5 shows that the Maxwell force would create a vibration at twice the magnetizing frequency. The Maxwell force may also be expressed as equation 9.6 in terms of vectors in order to describe the types of interactions caused by Maxwell force[2].

$$p = (B_a n)H_a - 0.5 \times (B_a H_a)n \tag{9.6}$$

Where n is the normal vector

H_a is the field vector

B_a is the induction vector

According to equation 9.6 two types of interaction may happen in a transformer

i. *Attractive forces:* which take place in overlap regions and act between the laminations due to in plane flux in the air gap and interlaminar due to the normal flux [1, 2, 20] as shown in Figure 9-4.
ii. *Repulsive forces:* these exist between neighbouring layers of a homogenously magnetized section of limbs and yokes shown in Figure

9-4 [1, 2, 20]. In such a region the field H_a equals the field H of the material that is directed in the x-direction. The second part of equation 9.6 would result in an interlaminar repulsive stress ($-0.5\mu_0 H^2$). Even for a global induction of 1.7 T, the Φ_z would be extremely small and the repulsive force is in the order of mPa and can be neglected [1, 20].

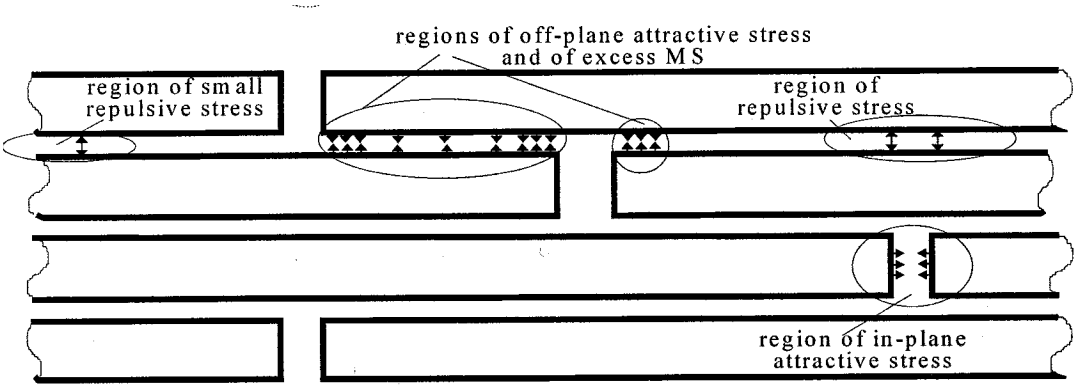

Figure 9- 4: schematic drawing of possible vibration mechanism [1]

- **Magnetostriction:**

To this point magnetostriction behaviour has been studied under sinusoidal excitation. However, in practice, the localized voltage waveform in the joints or corner is not purely sinusoidal [21] and there are always some higher harmonics that are produced from non-linear voltage current characteristics[22, 23]. Mapps [24] explained how the increased third harmonic content of the magnetic flux density waveforms in transformer limbs could lead to increased harmonic content in the magnetostriction waveform and this can be demonstrated by introducing the third harmonic into the voltage waveform of the model presented in Chapter 8 . Table 9-1 shows a comparison between ten magnetostriction harmonics (100, 200…1000Hz) under sinusoidal excitation versus a sinusoidal signal with third harmonic for a CGO material at 1.7 Tesla with 0.5 Tesla induced 3rd harmonic.

The results show that the induced third harmonic content of the magnetic flux density waveform causes a significant increase in harmonic content of the magnetostriction waveform, which consequently leads to an increase in A-weighted magnetostriction (explained in Chapter 8) .The signal, is simulated using the proposed model for the magnetostriction butterfly loop in Chapter 8.

Table 9- 1: Effect of 3rd harmonic of flux on magnetostriction harmonics

No of harmonic	Magnetostriction under Sinusoidal current	Magnetostriction under Sinusoidal with 0.5T 3rd harmonic	Change percentage
1st harmonic	1.84E-15	1.97E-15	7%
2nd harmonic	1.17E+01	5.72E+00	-51%
3rd harmonic	3.65E-16	2.40E-15	559%
4th harmonic	2.39E+00	6.82E+00	185%
5th harmonic	6.65E-16	3.99E-16	-40%
6th harmonic	4.86E-01	2.19E+00	350%
7th harmonic	5.04E-16	5.93E-16	18%
8th harmonic	9.90E-02	1.08E+00	994%
9th harmonic	5.65E-16	5.60E-16	-1%
10th harmonic	2.02E-02	4.66E-01	2210%

Another factor affecting magnetostriction is mechanical stress applied due to clamping and flattening of the laminations, which would change the magnetostriction characteristics of the laminations [11, 25]. The effect of stress on magnetostriction has been explained in detail in Chapter3.

Finally, as explained previously in section 9.1.1 joint regions show high levels of local flux in the normal direction, which would cause increased magnetostriction in the normal direction. Unfortunately, experimental data to support this is not available. However, an approximation can be made based on the

similarity with magnetostriction in the transverse direction due to conservation of volume [1].

9.1.3. Resonance in electrical steels:

Resonance happens as a function of magnetising frequency and magnetostrictively induced velocity. Vibrations normal to the surfaces of the core resulting from magnetostriction and Maxwell force can be very significant. These vibrations can pair with core resonant vibrations resulting in amplification of the static vibrations. Phway [26] proposed that the magnetising frequency at resonance, $f_{m,}$ can be calculated from equation 9.7:

$$f_m = \frac{n}{4l}\sqrt{\frac{E}{\delta}} \tag{9.7}$$

Where E is the modulus of elasticity

l is the length

δ is the density

And n is the nth harmonic order.

So a lamination of grain oriented silicon steel cut along the rolling direction with approximate length of 0.5 m would resonate at under 1kHz magnetization. It is more complex to evaluate the natural frequency for the complete transformer, as it would require a model incorporating mass, shape, volume etc.

9.2. Results:

9.2.1. Effect of flux density on single phase transformer vibration

All the cores, explained in Chapter 6.3.3, were magnetized at 1.0, 1.5 and 1.7 Tesla. Figure 9-5 shows the effect of magnetic flux density on the harmonics of the core vibration on the top surface at 4 Nm clamping torque. Also Figure 9-6 shows the effect of flux density on the whole core vibration for CGO material at 4Nm clamping pressure. Increasing the flux density leads to an increase in the core vibration for all three grades of material. The picture is obtained from the laser vibrometer system presented in chapter 5

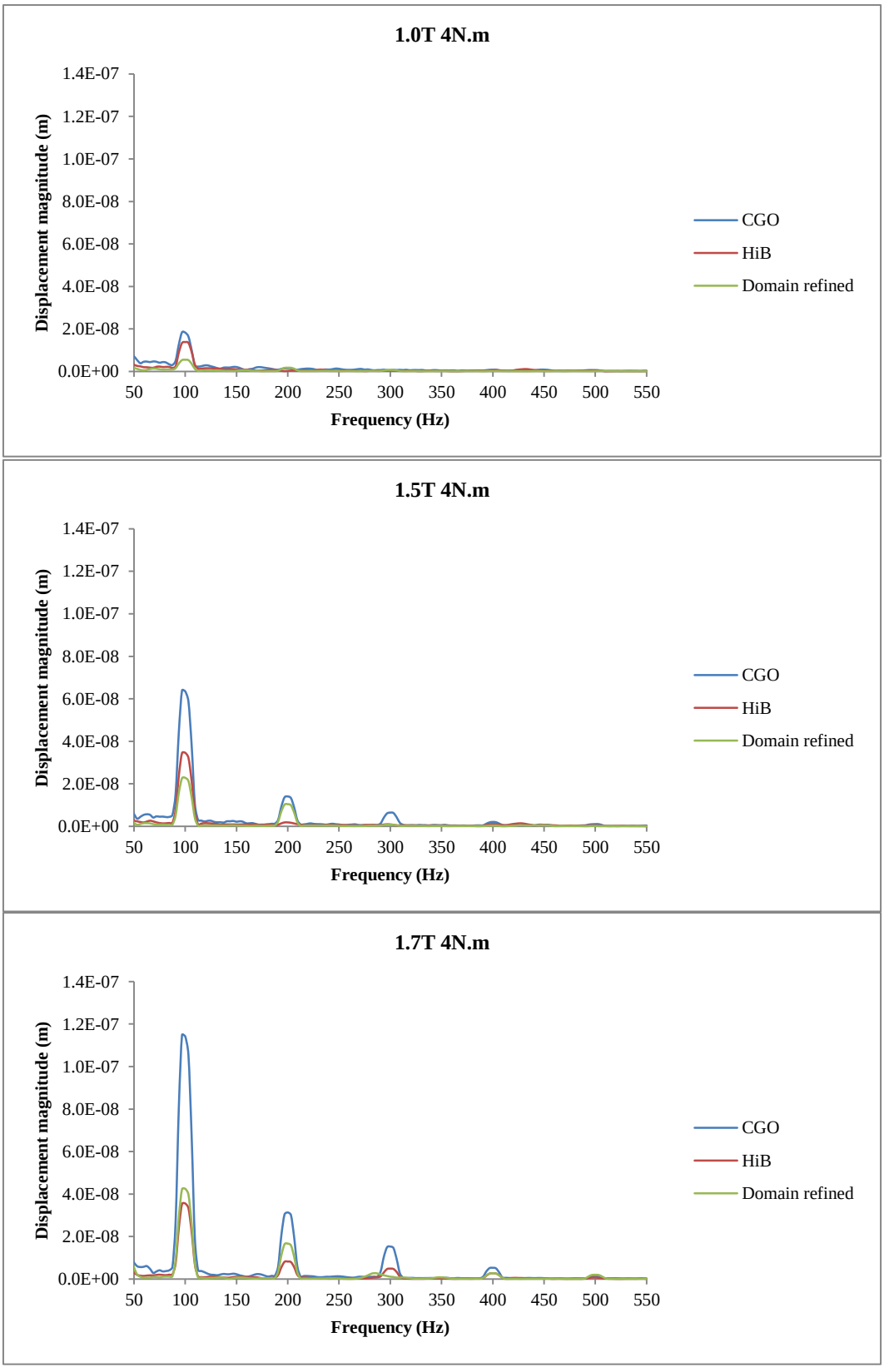

Figure 9- 5: Fast Fourier Transformation (FFT) of different core vibrations of different flux densities on the Top-surface. Figure shows the Displacement magnitude (m) vs. Frequency (Hz) of a top surface, single-phase transformer, magnetized at 50 Hz

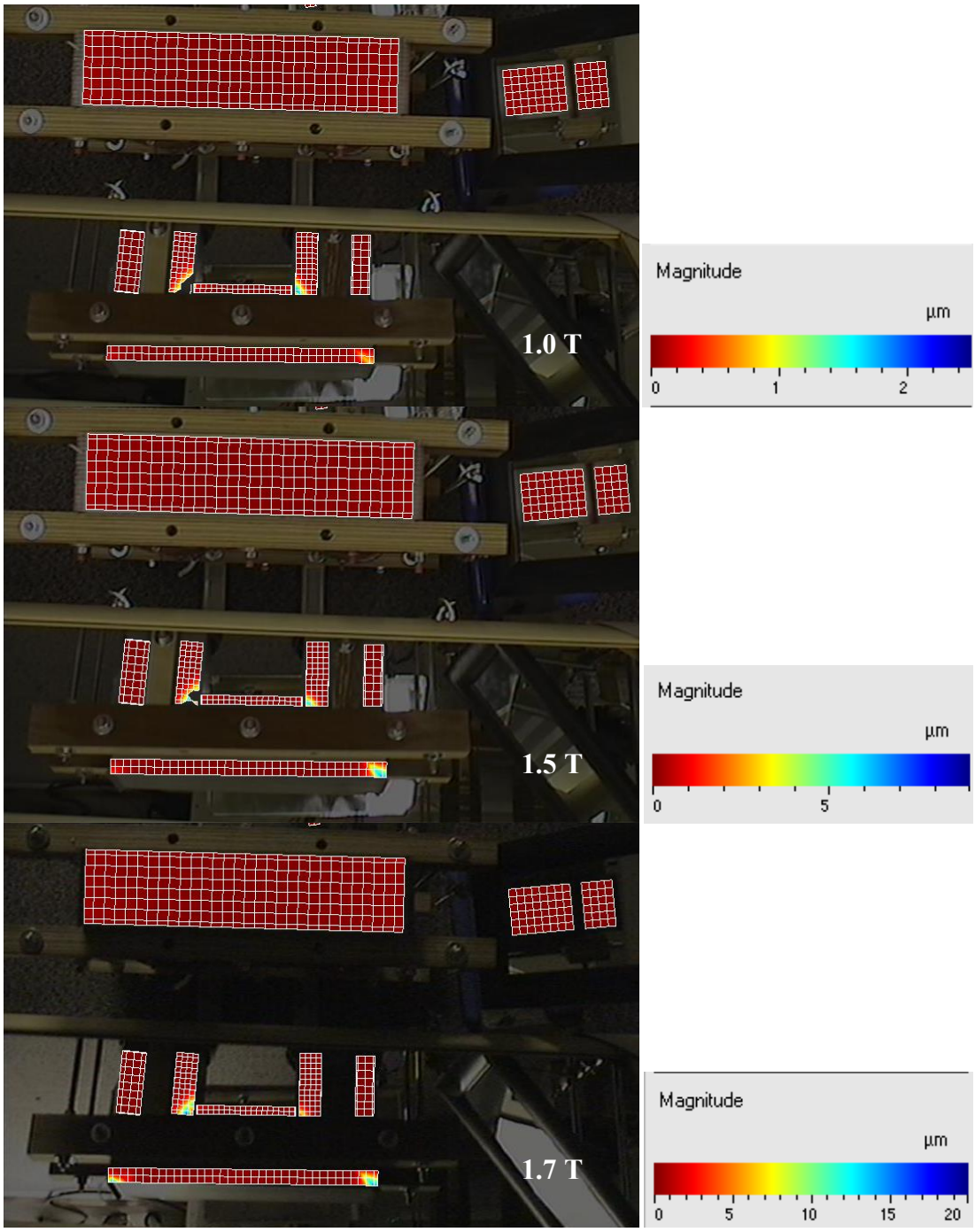

Figure 9- 6: Effect of increase of magnetic flux density on side, corner and top area of CGO single phase transformer vibration, magnetized at 50 Hz and 4Nm clamping torque.

9.2.2. Effect of clamping pressure on the vibration of the single-phase transformer

Three different clamping pressures were applied at each flux density and the effect of clamping pressure on the core's vibration was examined. Figures 9-7

and 9-8 show the effect of clamping pressure on the top surface and joint area of the transformers at 1.7T.

Figure 9-7 shows the displacement in the transverse direction, as the laser vibrometer is only able to measure the vibration in the direction where the beam is irradiated. There is a significant increase in vibration among all three grades by increasing the clamping torque from 2 Nm to 4 Nm, and by increasing the clamping torque from 4 Nm to 6 Nm there is a minor increase in the displacement value.

On the other hand, Figure 9-8 shows the displacement normal to the surface in the joint area of the core and it can be seen that the displacement is at its minimum value at the clamping torque of 4 Nm for CGO and HiB laminations. It then increases again by increasing the clamping torque to 6 Nm, whereas no clear trend can be determined for domain-refined laminations.

The average core vibration of the CGO and HiB was lowest at 4 Nm clamping torque, whereas, the vibration of the domain refined core was lowest at 2 Nm clamping torque.

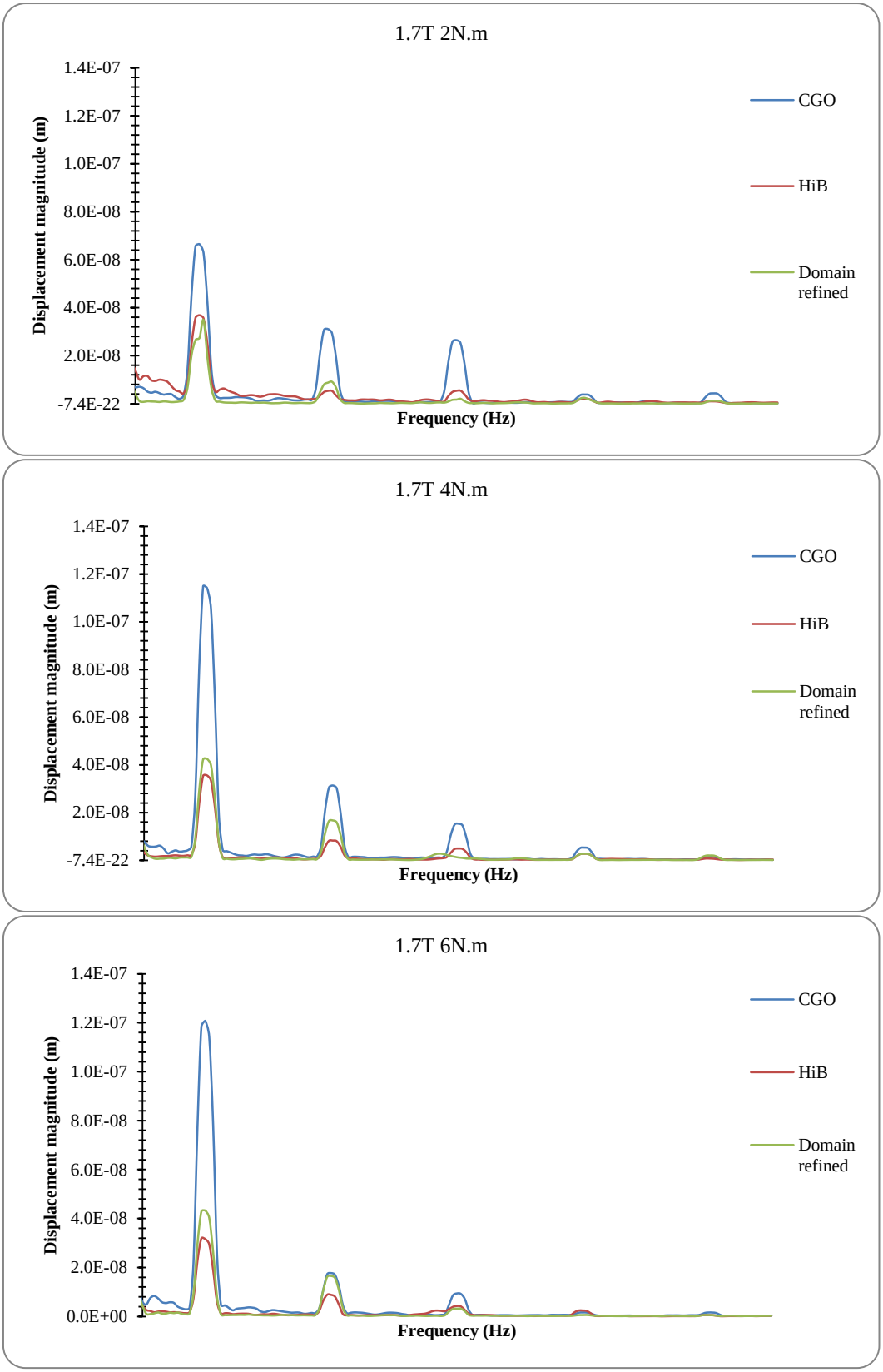

Figure 9- 7: Fast Fourier Transformation (FFT) of different core vibrations of different clamping torques on the Top-surface at 1.7 Tesla vs. frequency (Hz)

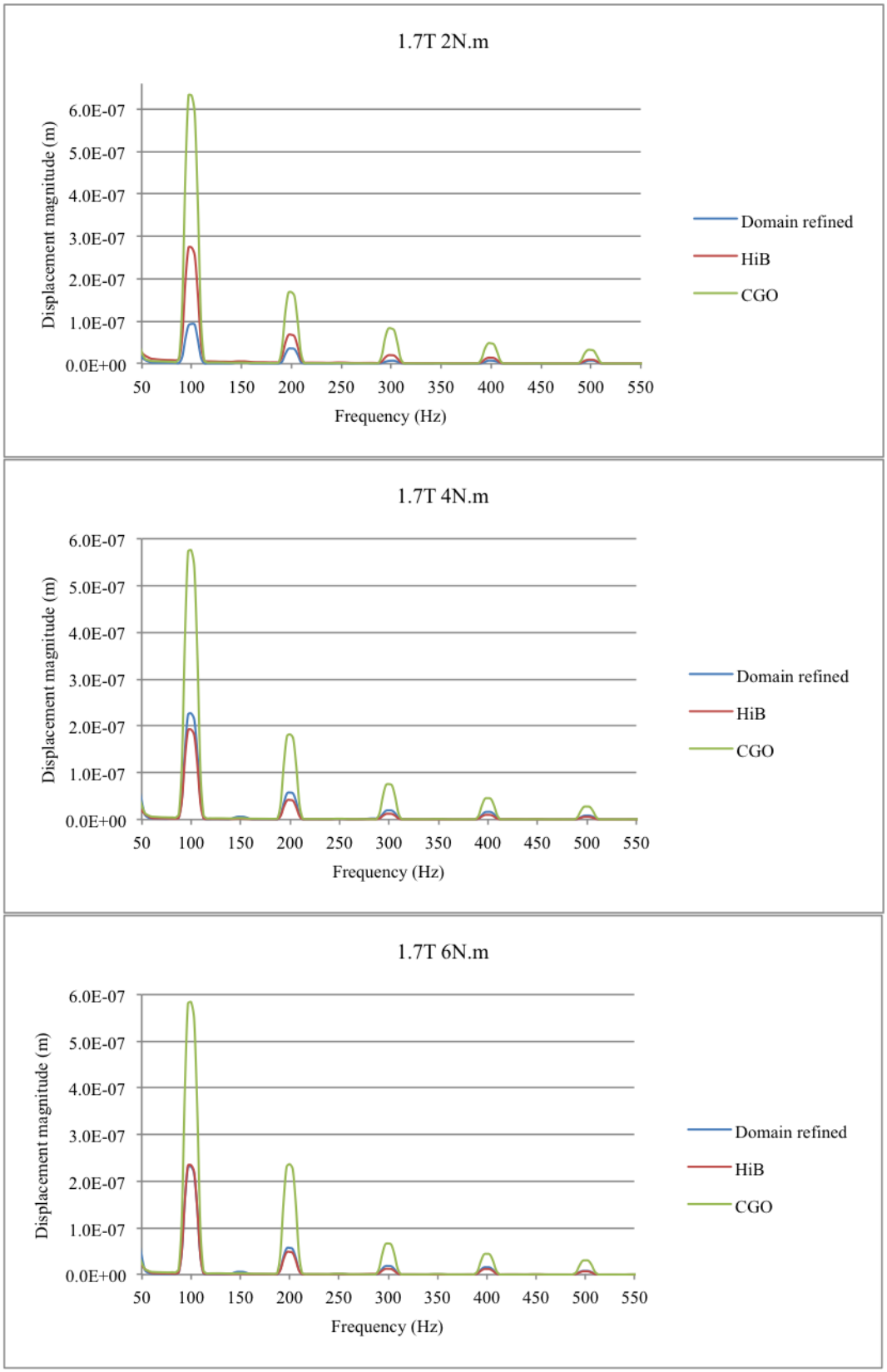

Figure 9- 8: Fast Fourier Transformation (FFT) of different core vibrations of different flux densities on the Joint area at 1.7T vs. frequency (Hz)

9.2.3. Vibration of different areas of a single-phase transformer

As noted previously, the vibration of single-phase transformers was analysed in 4 areas: the top surface, side surface, corner and joint. In this section the vibration results of these areas are compared for different materials at 1.7 T and 4 Nm. The vibration maps of the cores are shown in Figures 9-9, 9-10 and 9-11 for CGO, HiB and domain refined material respectively. These pictures were all obtained from the laser vibrometer system.

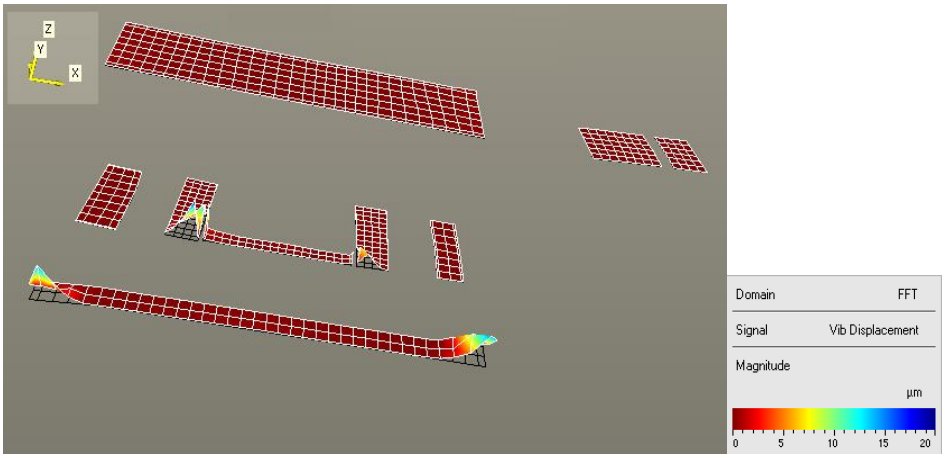

Figure 9- 9: Fast Fourier Transformation (FFT) map of core vibrations of the CGO, single phase core at 1.7 Tesla, 4N.m, the corners and the joints area are showing the highest vibration of more than 20 μ m displacement

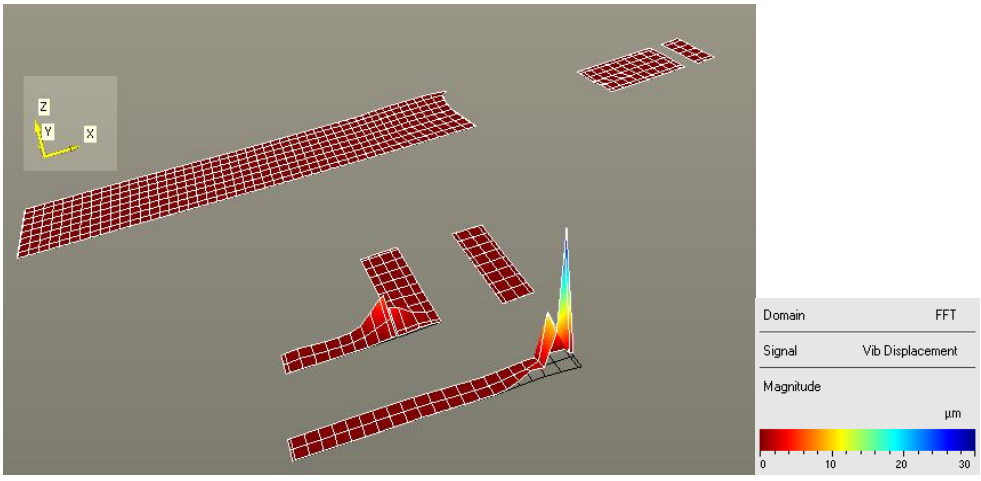

Figure 9- 10: Fast Fourier Transformation (FFT) map of core vibrations of the HiB, single phase core at 1.7 Tesla, 4N.m, corner area shows the highest vibration by approximately 30 μ m displacement.

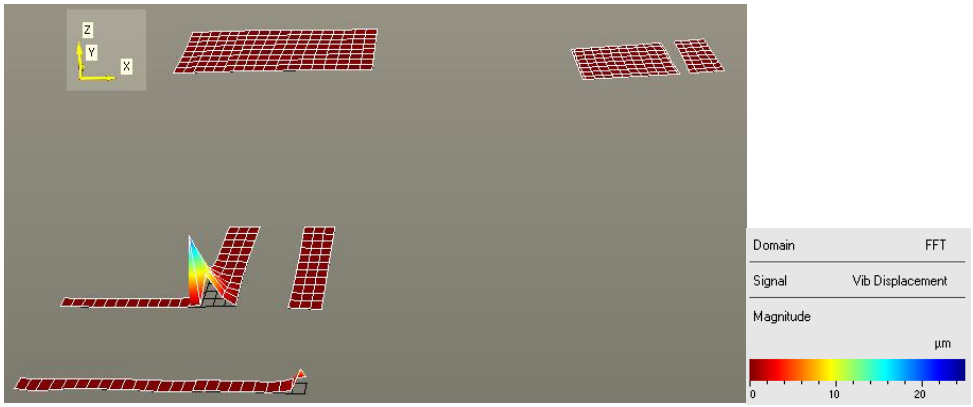

Figure 9- 11: Fast Fourier Transformation (FFT) map of core vibrations of the domain refined material, single phase core at 1.7 Tesla, 4N.m, the joint area shows the highest vibration by approximately 25 μ m displacements.

It can be seen from the above Figures that the highest vibration is taking place in the corner and joint areas for all the cores.

9.3. Discussion

9.3.1. Harmonic characteristics of different steel grades and correlations with their magnetostriction characteristics

The fundamental frequency of all the waveforms is 100 Hz; double that of the exciting frequency. Figure 9-12 shows the normalized peak-to-peak magnetostriction harmonics (the fundamental, 2nd, 3rd, 4th and 5^{th} harmonics) versus frequency at three different applied stresses (-10, -5 and 0 MPa) at 1.7 Tesla, the distribution of the magnetostriction harmonics changes by increasing the applied pressure. For instance, CGO has a wide distribution band at zero stress, which becomes narrower by increasing the applied pressure. The changes in the harmonics distribution are mainly due to the existence of the stress pattern and average domain misorientation angle.

Also, the results show a large fundamental characteristic at 100Hz for all grades and the 2^{nd} to5^{th} harmonics displaying a reduction in amplitude. The same

trend can be seen from the displacement frequency distribution of transformers shown in Figure 9-13. So it can be suggested that the vibration within the sheet planes on the top (transverse displacement or y-direction) and side surfaces (longitude displacements or x-direction) are mainly due to magnetostriction. Whereas in the corner area the normal displacements are due to the z-flux arising at overlap regions, as explained earlier, which would cause an increase in the Maxwell forces as well as magnetostriction.

Figure 9-13 also illustrates that the transformer cores primarily vibrates at 100 Hz. Furthermore, it points out that the second harmonic of transformation vibration of Domain refined is larger than HiB in all measured regions, this can be explained due to the existence of the induced domain structure as a result of scribing (explained in Chapter 7) which would cause wider butterfly loop and consequently larger harmonics.

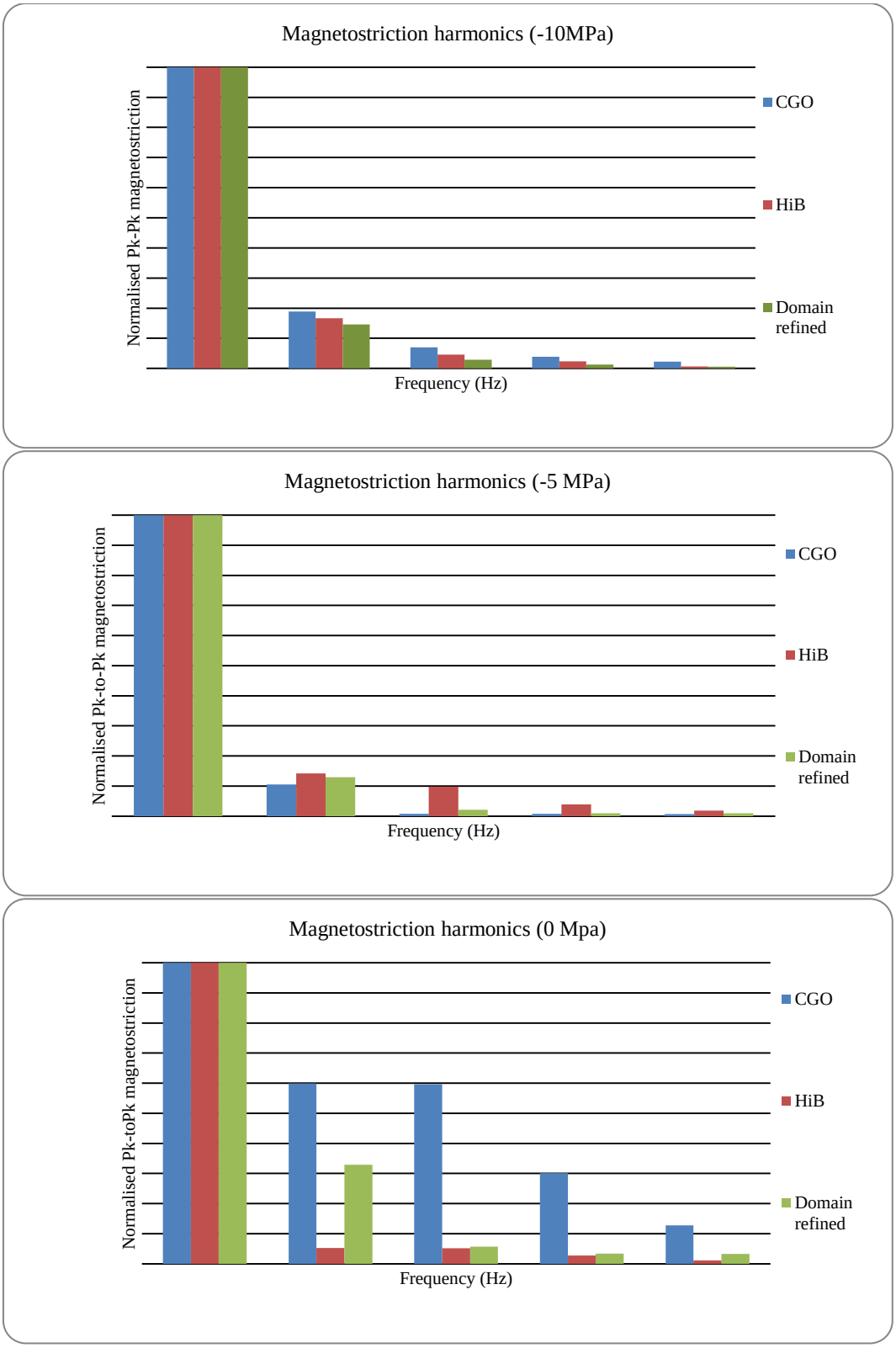

Figure 9- 12: Normalized Pk-to-Pk magnetostriction harmonics of CGO, HiB and Domain refined materials at 1.7T under three applied stresses of 0, -5 and -10 MPa

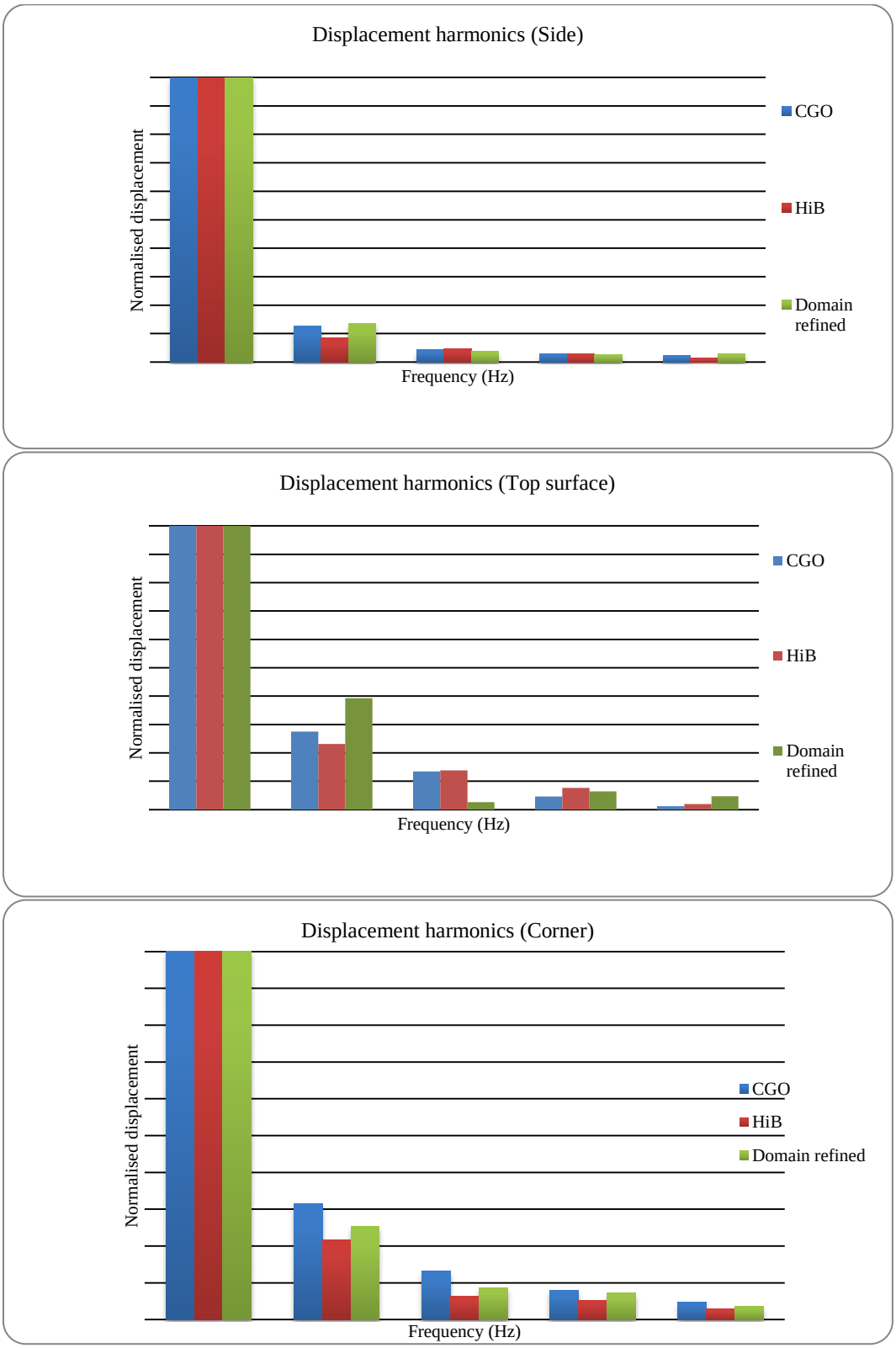

Figure 9- 13: Normalized displacement magnitude harmonics of CGO, HiB and domain refined single phase transformer at Corner, Side and top surfaces under applied flux density of 1.7T and 4Nm clamping torque

9.3.2. Effect of flux density on vibration

Figures 9-5 and 9-6 show an increase in core vibration due to the increase in magnetic flux density. Both the magnetostrictive force and magnetic forces are dependent on the flux distribution through the core. The effect of flux density on these forces is considered, as follows.

As it was explained earlier in section 9.1.2 the magnetic force can be divided into two main mechanisms. As explained in section 9.1.1, at flux densities below the critical flux density (B_c) the flux tends to flow in the normal direction to the bridging region and leaves in the rolling or transverse direction, which would cause attractive forces between the laminations. This force could be neglected due to small values of normal flux in the joint regions (about 0.1 T) [1, 18].

By increasing the flux to 1.7 T, which is higher than the critical flux B_c for the measured transformers ($B_c \approx$1.65T), the overlap region is saturated and the excess portion of flux goes through the air gap, which, consequently, causes high attractive Maxwell forces in-plane directions, which could be estimated using equation 9.2, (B is assumed to be 0.5 T) to be approximately 0.1MPA.

The magnetostriction magnitude also increases with the increase in magnetic flux density. Figure 9-14 shows the effect of flux density on magnetostriction of the three grades of steel under applied stress. It can be observed from Figure 9-14 that that the magnetostriction of HiB material, which was higher than domain refined material below 1.5 Tesla, increased more rapidly and became higher by increasing the applied stress. The same trend can be spotted in all three flux densities occurring around 8MPa-applied stress. The shift in the magnetostriction value due to the increase in applied stress can be explained using

the basic theory of energy in ferromagnetism. By increasing the applied compressive stress the Magnetostatic energy reduces, consequently the domain pattern reorganizes so as to decrease the overall energy by increasing the volume of supplementary domain structure. In the case of domain refined material the compressive stress along the rolling direction has no effect on the transverse domains in the vicinity of scribed lines (explained in a proposed model presented in Chapter 7) And only the bulk domains rotate from [100] direction to [010] and [100] directions, whereas in the case of Hi-B due to the higher portion of [100] domains, more domains rotate and consequently Hi-B material will have higher magnetostriction under high-applied stress.

By comparing the measured Pk-to-Pk magnetostriction presented in Figure 9-14 with the peak vibration harmonic of transformers it may be surmised that approximately 8.0 MPa compressive stress were applied within the laminations in the measured area at 4 Nm clamping torque, the predicted stress value agrees with the reported stress by Moses[11].

Figure 9-15 illustrates the effect of flux density on magnetostriction at constant applied stress. It can be seen from Figure 9-15 that the magnetostriction of domain refined material, which was lower than HiB at 1.5 T at -8MPa applied stress, increased more rapidly and became higher when magnetized at 1.7 T. Figure 9-16 shows the effect of magnetising field on the fundamental vibration harmonic of different transformers at 4Nm clamping torque.

This effect can be explained by using a proposed domain model presented in Chapter 7. At low flux density (below 1.5 T) when domain refined samples are magnetised in the rolling direction, this would cause the domains in the direction

of the field to rotate to the direction of the applied field and grow so the main mechanism of magnetostriction is due to the rotation of the 90^{o} domain wall movement of miss-oriented domains.

By increasing the applied magnetic field above 1.5 T, the transverse domains start to rotate from the [010] direction into the magnetizing direction [001] to minimize the energy condition. This rotation occurs at high magnetic field due to the high energy needed for the transverse domains to rotate.

In the transformer, the higher the applied field the larger the flux density in the lamination would be. Therefore more regions reach this critical flux level and, as a result, more domains reorient to the [001] direction resulting in an increase in the peak magnetostriction and vibration of the transformer.

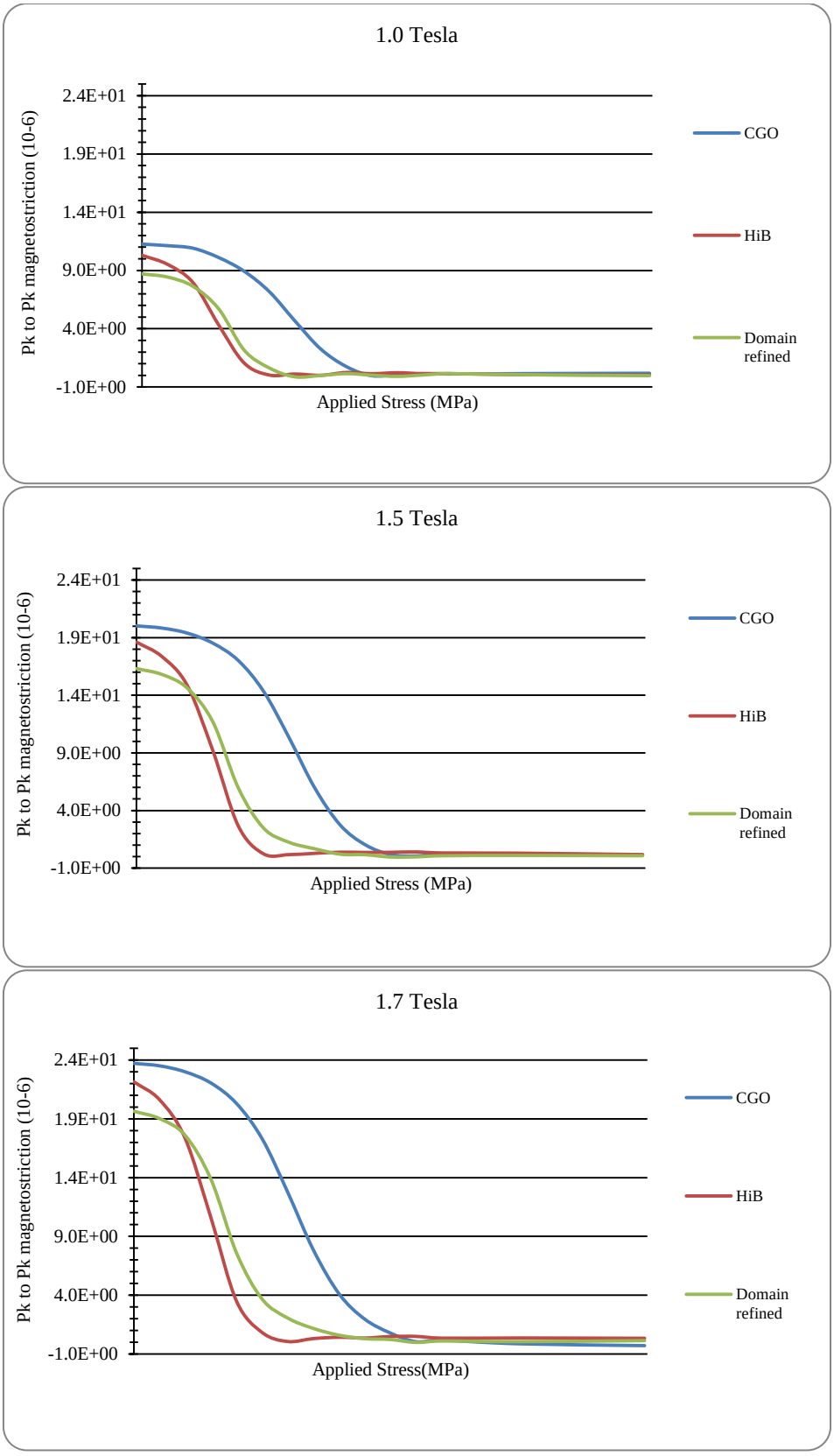

Figure 9- 14: Pk-to-Pk magnetostriction vs. applied stress for CGO, HiB and domain refined materials at flux densities of 1.0, 1.5 and 1.7 Tesla under applied stress of -10 to 10 MPa

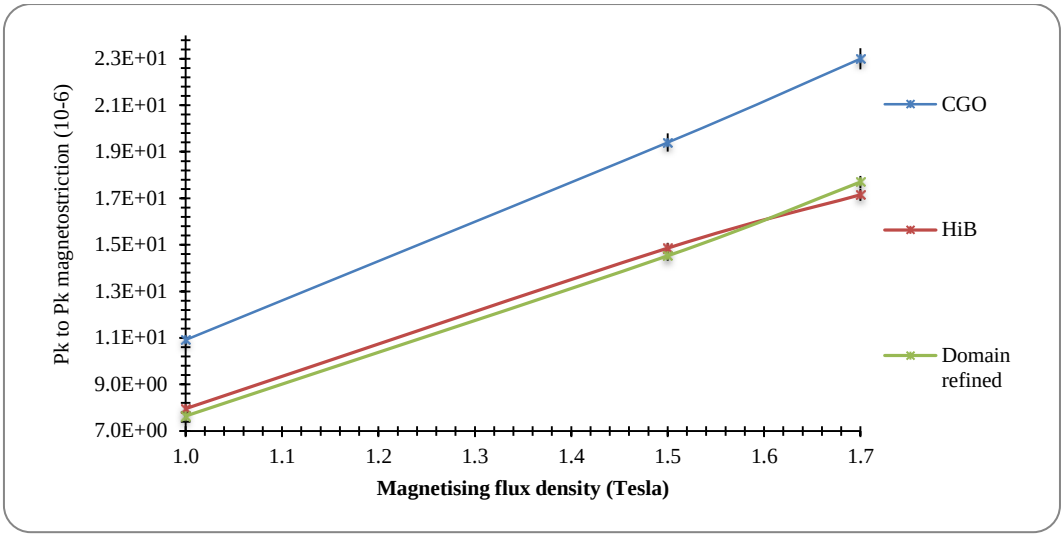

Figure 9- 15: Pk-to-Pk magnetostriction vs. magnetising flux density for CGO, HiB and domain refined materials at applied stress of -8MPa

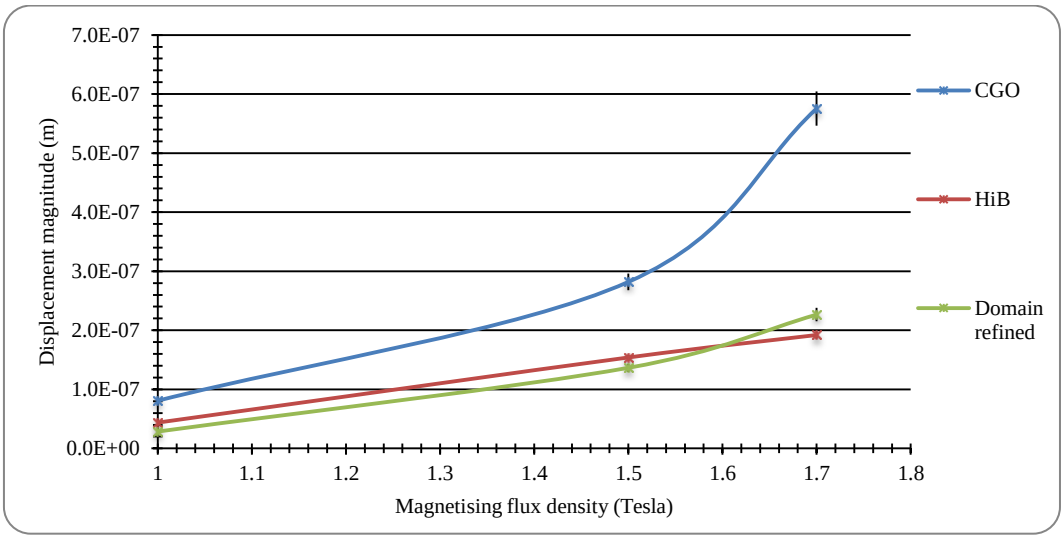

Figure 9- 16: Effect of flux density on fundamental vibration harmonic of side area of CGO, HiB and Domain refined single-phase transformer at 4 Nm clamping torque

9.3.3. Effect of clamping pressure on vibration

The FFT analysis of the vibration displacement of the top surface area and joint area is shown in Figures 9-7 and 9-8. It is shown that by increasing the clamping torque from 2 Nm to 4 Nm the core vibration in the joint and corner areas is reduced as well as the overall core vibration, but the vibration normal to the top surface has been increased. The following possible reasons are considered.

Figure 9-17 shows the effect of clamping torque on the fundamental vibration value (100 Hz) on the top surface at 1.7 Tesla.

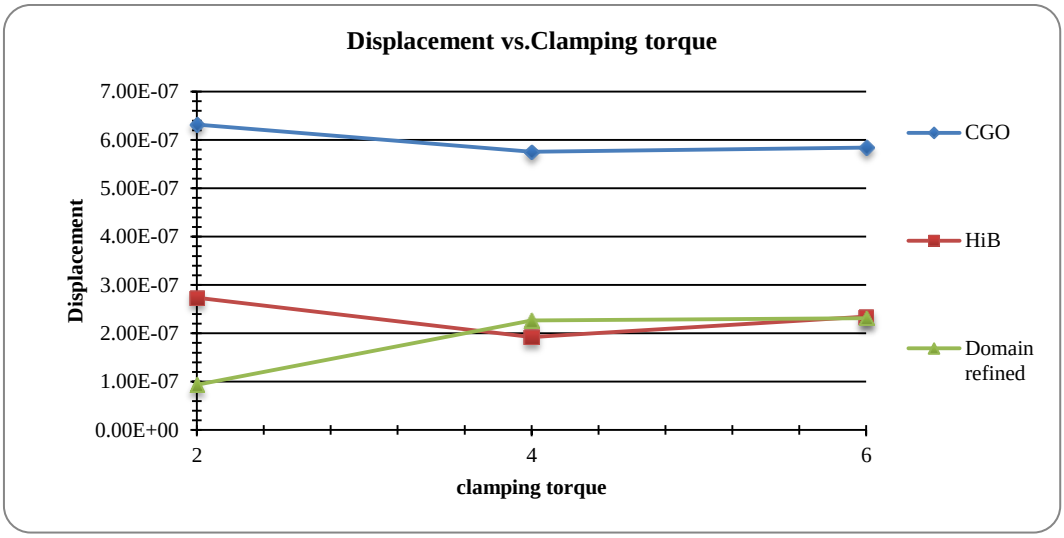

Figure 9- 17: Fundamental vibration frequency of CGO, HiB and Domain refined single-phase transformer vs. clamping torque at flux density of 1.7 Tesla

As previously explained, there are mainly two Maxwell forces in the joint regions: the first one is the attractive force between the lamination due to the normal flux and the second is in-plane attractive force due to the flux in the air gap[27]. Increasing the clamping torque from 2 Nm to 4 Nm applies a normal force, which can be calculated from the equation (9.8); the increased force reduces the vibration of laminations which were caused in the normal direction due to the Maxwell force, calculated to be approximately 0.1MPa based on the equation 9.2 at 1.7 T.

$$F_i = \frac{T}{Kd} \tag{9.8}$$

$$\sigma = \frac{F_i}{A}$$

Where T is the applied torque,

K is the material constant that is 0.7 for the fibre reinforced plastic bolt

d is the diameter of the bolt

A is the clamping area.

Table 9-5 shows the calculated applied stress for three applied bolt torques based on equation 9.8.

Table 9- 5: calculated applied clamping force and average applied stress due bolt torque

Bolt torque (Nm)	Clamping force (N)	Applied stress to the laminations (MPa)
2	350	0.16
4	700	0.33
6	1050	0.49

The friction force has a direction opposing the applied force and can be calculated from the equation 9.9:

$$F_f = 2kPA_n \qquad [18](9.9)$$

Where P is the clamping pressure,

k is the coefficient of static friction,

A_n is the clamping area.

Through increasing the clamping pressure (P) the frictional forces (F_f) between the laminations are increased, which restricts the vibration of the core. Moreover, in the corner regions, an increase in clamping stress reduces the freedom of the laminations to vibrate freely in the normal direction according to equation 9.9.

On the other hand, it is known that the magnetostriction of electrical steel is very sensitive to stress[25]. Also, it is known that laminations are not perfectly flat (explained in Chapter 7), and in this case they can have 10 mm curvature along 500 mm long lamination (average measurement of 30 samples, 10 from each grade). By increasing the clamping pressure the curved laminations flattened and a shearing stress of up to around 7.3 MPa could be raised in the laminations (calculated based on the equation 7.19 presented in the Chapter 7.2). The induced bending stress would affect and change the domain structure of the laminations. On the concave side the [001] direction is energetically favourable, whereas on the convex side the [010] and [100] directions become energetically favourable (explained in Chapter 7.2), and the domain direction changes slowly through the thickness from [100] and [010] directions on the convex side to the [001] direction on the concave side. The change of the domain structure due to bending effects on the magnetostriction value is explained in Chapter 7.2.

By increasing the clamping torque from 4 Nm to 6 Nm it can be seen that the core vibration again increases as shown in Figure 9-7, 8 and 17. It is assumed that there is no change in the air gap between the laminations and, as a result, there would be no change in the Maxwell force effect. But, on the other hand, the increase in the clamping pressure would result in an increase in the inter-laminar pressure in both directions and also increase the shear stress due to a reduction of the curvature of the laminations. This would cause an increase in magnetostriction value in both the rolling and transverse directions. The overall effect is that this would increase the vibration of the core. (The effect of curvature on magnetostriction has been explained in more detail in Chapter 7.2)

9.3.4. Vibration analysis of different areas of a single-phase transformer

Figures 9-9, 9-10 and 9-11 show a 3D map of the displacement vibration for CGO, HiB and domain refined materials respectively at 1.7 Tesla and 4Nm clamping torque. The highest displacement is taking place in the joint and corner area of the transformers and can be described by two mechanisms that have been discussed previously.

The first mechanism is the Maxwell force that is generated by the presence of magnetic flux across the air gap and can be expressed as equation (9.2). This mechanism arises mainly in the joint and corner areas due to in-plane flux in the air gap and in overlap regions and act between the laminations due to in plane flux in the air gap.

The other mechanism corresponding to the displacement in the joint and corner areas is due to out of plane magnetization where the flux flows through [010] easy direction that results in high magnetostriction and can be predicted by measuring the magnetostriction in the transverse direction. This would result in an increase in the vibration in the joint and corner areas [25, 28].

The magnetizing fields in the rolling direction and transverse direction were controlled to generate an AC magnetisation vector at an angle Θ to the rolling direction using the 2D magnetisation system for three peak flux densities of 1, 1.3 and 1.5 Tesla and the Pk-to-Pk magnetostriction was recorded using a strain gauge, as explained in Chapter 5, for all grades. The measurements were repeated five times and the average taken. Peak to peak magnetostriction measured in the disc samples at 1.5 Tesla is shown in Figure 10-18. As can be seen from the Figures 9-18 the magnetostriction in the transverse direction, λ_T, is almost half of that in the

longitude direction, λ_R, which agrees well with theory [29, 30].This means that if a sheet expands in the rolling direction, it contracts in the transverse and normal directions and the result suggests that the magnetostriction in the transverse direction can be predicted by measurement in the rolling direction.

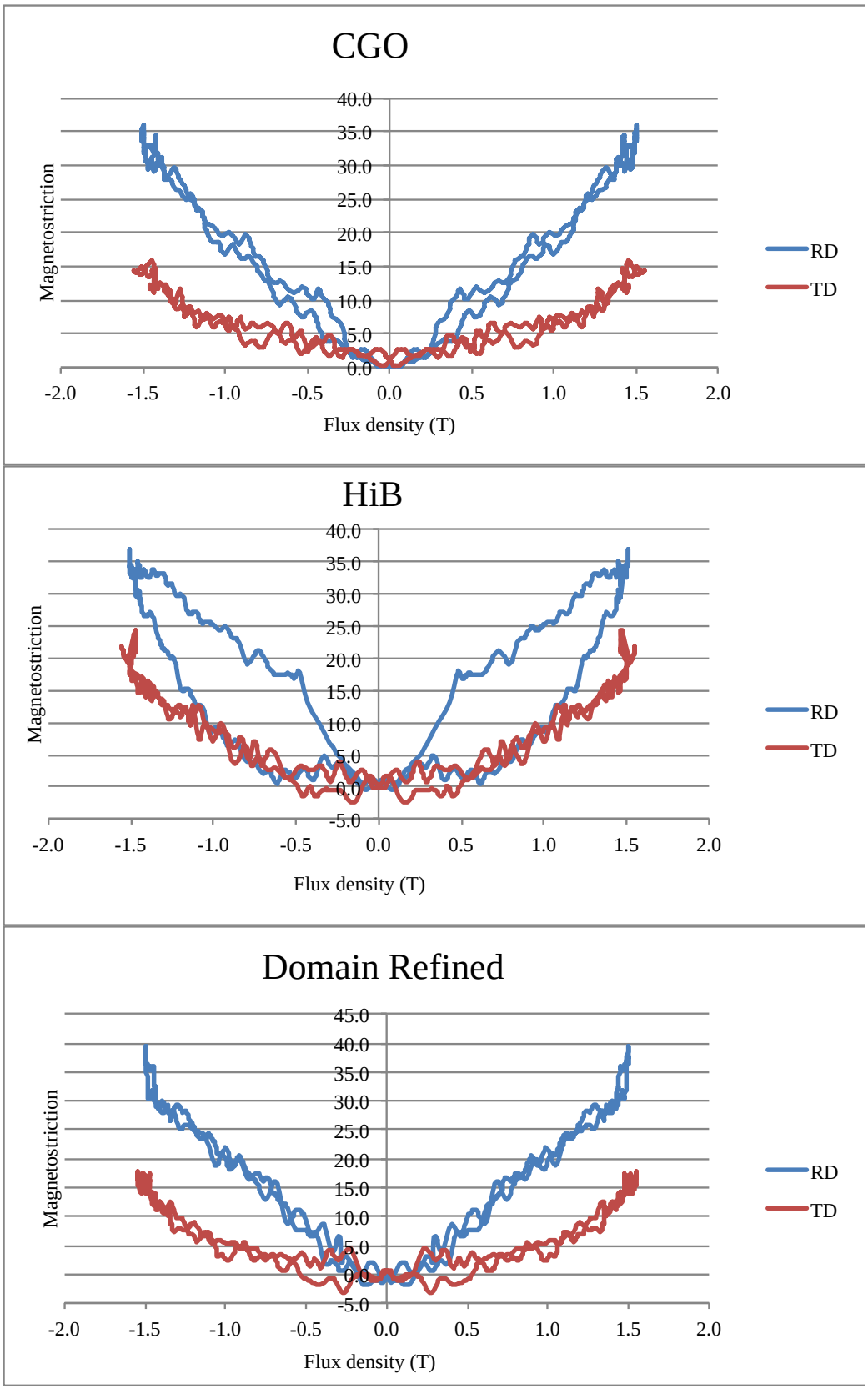

Figure 9- 18: Peak to peak magnetostriction measured in the disc samples under rotational 1.5 Tesla, 50 Hz, it shows that the λ RD ≈ 2λTD

9.3.5. The influence of steel grades on the core vibration and correlations with their magnetostriction characteristics:

In order to study the effect of the magnetostriction characteristics of different grades of electrical steel on the transformer core vibration, the fundamental displacement harmonics of each of the cores were compared at 1.5 and 1.7 Tesla and 4 Nm clamping torque and is shown in Figure 9-19.

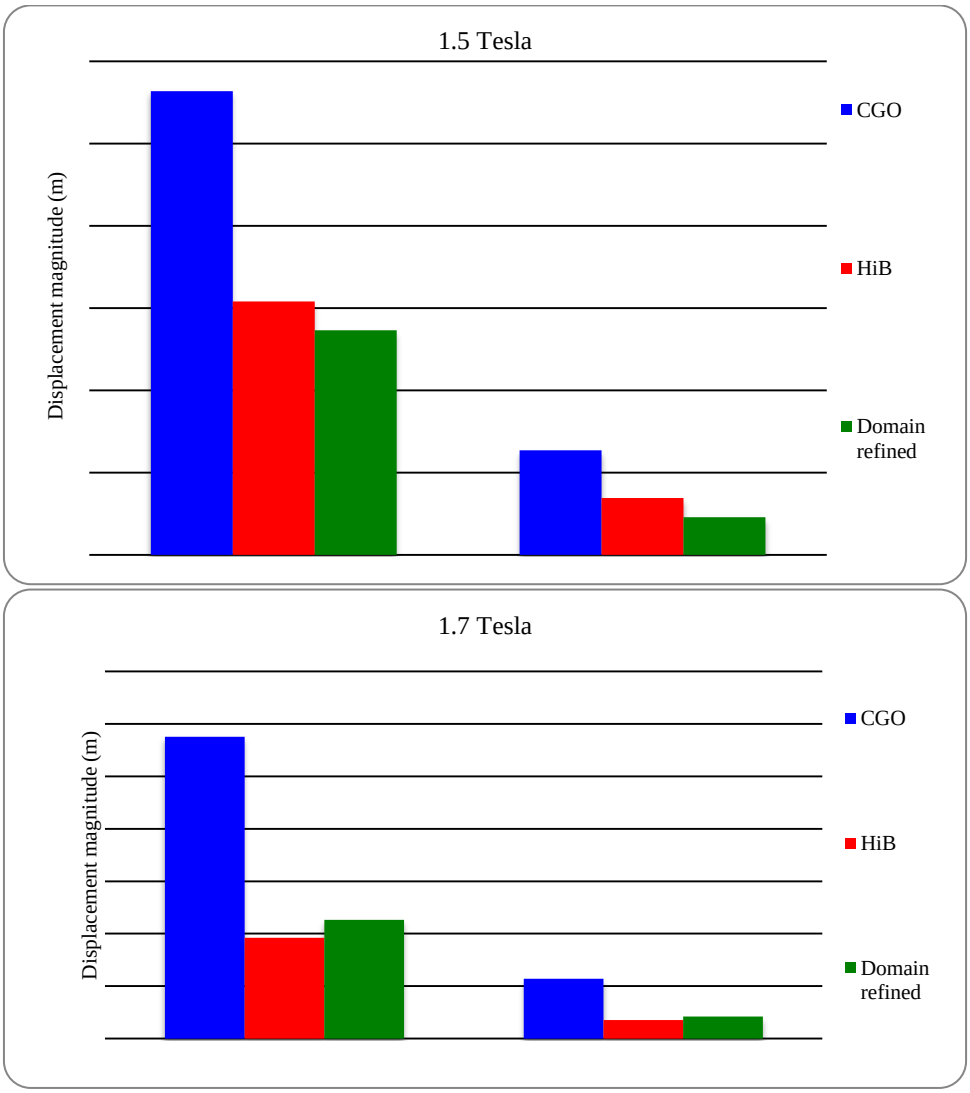

Figure 9- 19: Fundamental displacement magnitude harmonic of CGO, HiB and Domain refined single-phase transformer at A) 1.5 Tesla and B) 1.7 Tesla at 4Nm clamping torque

As mentioned before, the Maxwell force is only dependent upon the magnetic flux density across the air gap. If it were assumed that all three cores

have the same air gap between the laminations, the relative effect of the Maxwell force would be eliminated.

Also, the resonant frequency would be almost the same between different cores, as the resonant frequency would be affected by length, weight and clamping pressure which is assumed to be the same across all the measured transformers.

Consequently, it is assumed that the difference in the vibration would be due to the difference in magnetostriction characteristics between the different grades. Figure 9-19 shows the magnetostriction characteristics for CGO, HiB and domain refined material at 1.5 and 1.7 Tesla in the rolling direction under -8.5MPa applied stress.

By comparing the graphs of Figures 9-19 and Figure 9-20 it can be noted that the displacement vibration in the transformer has same trend (order) as magnetostriction e.g. at 1.5 T , CGO has the highest vibration and domain refined the lowest which same order can be spotted in the core vibration presented in Figure 9-20 .

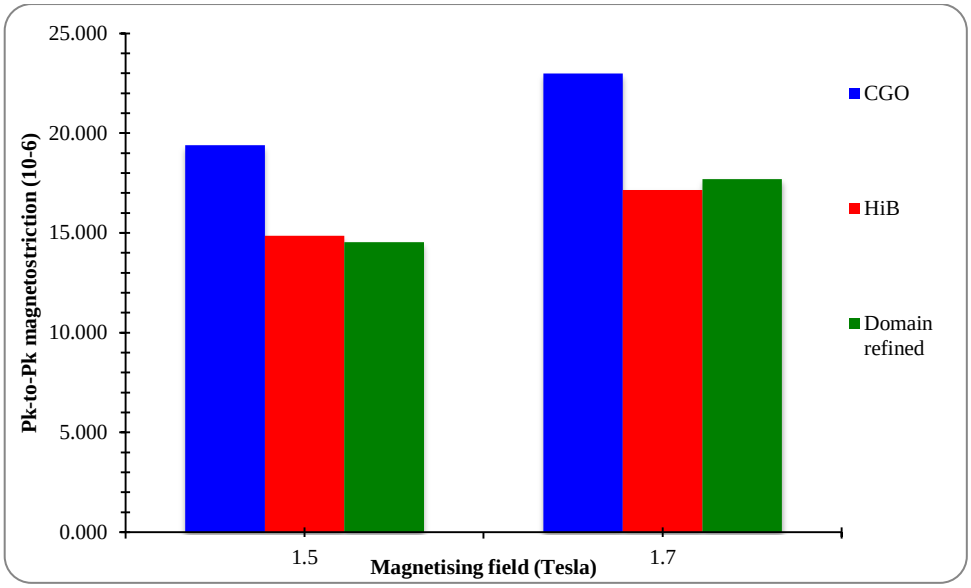

Figure 9- 20: Pk-to-Pk magnetostriction vs. applied stress for CGO, HiB and domain refined materials at 1.5 and 1.7 Tesla

Figure 9-21 shows A-weighted magnetostriction velocity in the range of -7MPa to -10MPa (expected stress in the transformer cores based on the conclusion of section 9.1.2) for three grades of steel.

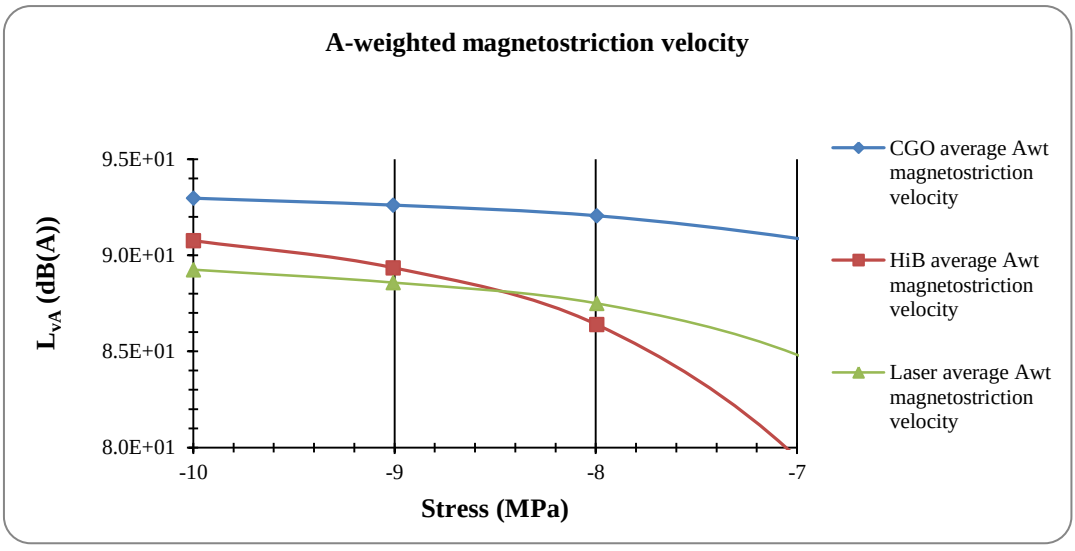

Figure 9- 21: A-weighted magnetostriction velocity of CGO, HIB and domain samples at 1.7 T and 50 Hz,

Figure 9-22 shows A-weighted vibration of transformers for all three grades at 1.7T and 4Nm-clamping torque. As expected CGO shows the highest average value among the other grades. In addition, HiB shows the lowest A-

weighted value. A similar result can be spotted from A-weighted magnetostriction presented in Figures 9-21 by approximating the applied stress to the laminations, as it was estimated earlier in this chapter, an applied stress of -8MPa is expected in the transformer. From the Figure 9-21 it can be seen that at -8MPa applied stress HiB has the lowest A-weighted magnetostriction, which matches the results from the transformer.

The result suggests that A-weighted magnetostriction may be used to predict the expected vibration level of a transformer if the approximate stress applied to the laminations is known.

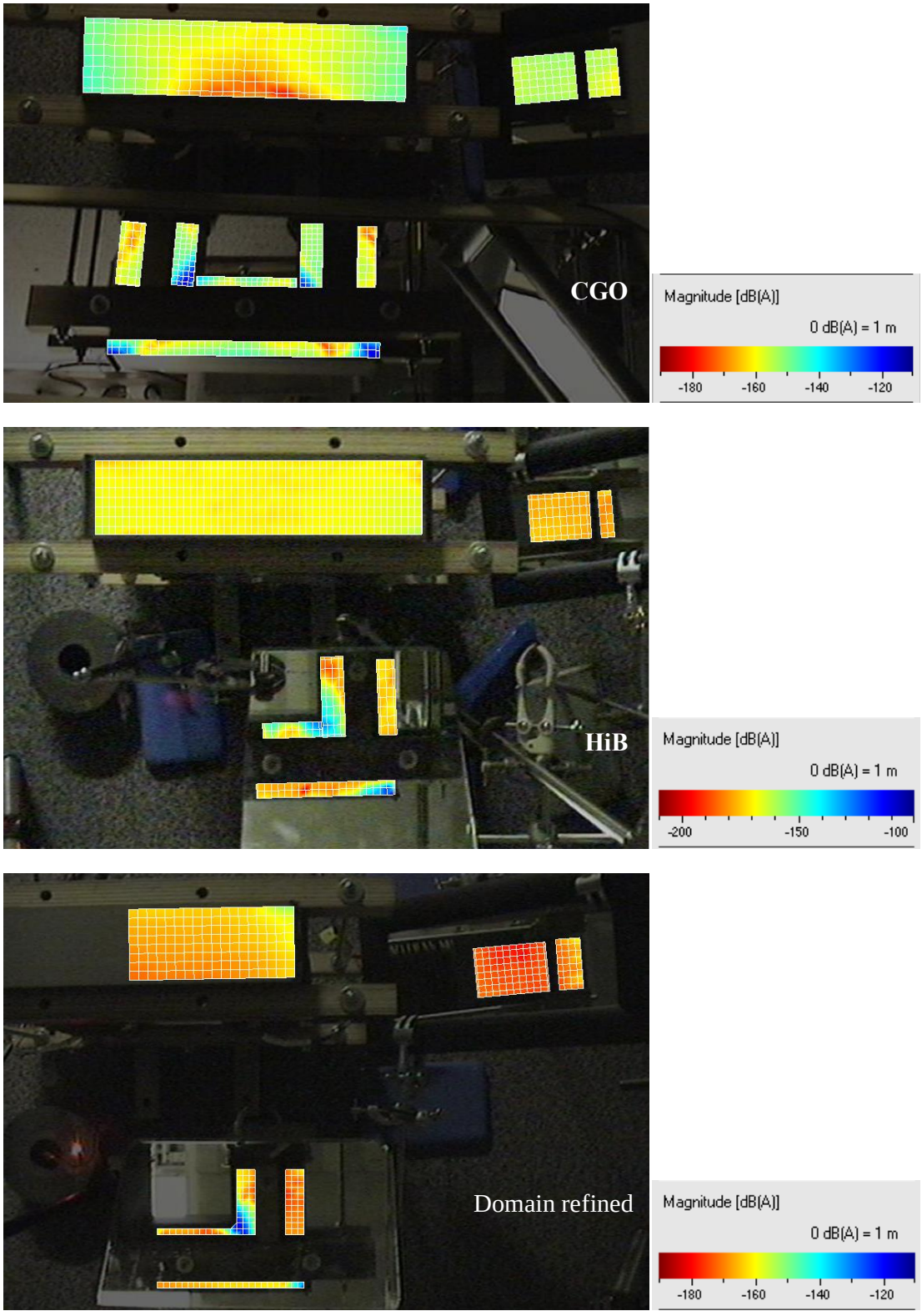

Figure 9- 22: Measured A-weighted displacement of CGO, HiB and domain refined single phase magnetized at 1.7 T, 50 Hz. Clamping torque 4N.m

9.4. Conclusion:

The following conclusions may be drawn:

- It has been shown that increasing the magnetic flux density causes an increase in vibration of the core due to the increase in both magnetostriction and Maxwell force.
- In MSL transformers at $B < B_c$ the effect of Maxwell forces may be neglected in the joint regions due to small value of normal flux, whereas in the case of $B > B_c$ this effect would be significant in the joint regions.
- Increasing the clamping pressure to 4Nm can decrease the out of plane vibration in the joint regions due to the increase of friction and reduction of air gap which reduces the air gap flux and consequently the Maxwell forces.
- Increasing clamping pressure from 4Nm to 6Nm continues the flattening stresses by applying high pressure would increases magnetostriction and thus increases the core vibration.
- The highest vibration levels in single-phase transformer were determined in the joint and corner areas for all three cores.
- The main reason for high vibration levels in the joint area is due to:
    - Out of rolling direction magnetization that results in high rolling direction magnetostriction
    - The significant effect of Maxwell's forces due to the presence of the air gaps for $B > B_c$.
- It has been shown that the leading source for the differences between the vibration of the cores under the same magnetic excitation and clamping

pressure in the measured cores is due to the differences in the magnetostriction characteristics of the grades of electrical steels.

- Correlations between the magnetostriction harmonics and the vibration of the cores have been determined.
- It has been shown that A-weighted magnetostriction could be used for indicating transformers vibration.

References for Chapter 9

1. Weiser, B., H. Pfützner, and J. Anger, *Relevance of magnetostriction and forces for the generation of audible noise of transformer cores.* IEEE Transactions on Magnetics, 2000. **36**(5 II): p. 3759-3777.
2. Weiser, B., et al., *Mechanisms of noise generation of model transformer cores.* Journal of Magnetism and Magnetic Materials, 1996. **160**: p. 207-209.
3. Moses, A.J., *MEASUREMENT OF MAGNETOSTRICTION AND VIBRATION WITH REGARD TO TRANSFORMER NOISE.* IEEE Transactions on Magnetics, 1974. **MAG-10**(2): p. 154-156.
4. Neurath, P.W., *Magnetostriction and domain structure of materials for use in low-noise equipment.* Electrical Engineering, 1954. **73**(11): p. 991-994.
5. Peng, W., et al., *Study on an audible noise reduction measure for the filter capacitors in the HVDC converter station based on the MPP absorber.* IEEE Transactions on Power Delivery, 2009. **24**(4): p. 1756-1762.
6. Ruan, X.Y., Z.Y. Li, and H.Z. Wei. *The noise prediction and control for UHVDC converter stations*. 2011.
7. Saha, P., *POWER TRANSFORMER NOISE - GENERATION, PROOPAGATION AND CONTROL - A REVIEW.* American Society of Mechanical Engineers (Paper), 1981.
8. Valkovic, Z., *Effect of electrical steel grade on transformer core audible noise.* Journal of Magnetism and Magnetic Materials, 1994. **133**(1-3): p. 607-609.
9. Yang, Y. and X. Zhang, *Study on noise reduce for equipment at UHVDC converter station.* Gaodianya Jishu/High Voltage Engineering, 2006. **32**(9): p. 149-152.
10. Becker, R. and W. Döring, *Ferromagnetismus*. 1939, Berlin: J. Springer. vii, 440 p.
11. Moses, A.J., Pegler, S.M. , *The effects of flexible bonding of laminations in a transformer core.* Journal of Sound and Vibration, 1973. **29**: p. 103-112
12. Yamaguchi, H., H. Pfützner, and E. Mulasalihovic, *3D-measurements of magnetic flux on joint regions of SiFe steel model core.* Journal of Magnetism and Magnetic Materials, 2008. **320**(20): p. e935-e938.
13. Pfutzner, H., et al., *Three-dimensional flux distributions in transformer cores as a function of package design.* IEEE Transactions on Magnetics, 1994. **30**(5 pt 1): p. 2713-2727.
14. Loffler, F., et al., *Relevance of step-lap joints for magnetic characteristics of transformer cores.* IEE Proceedings: Electric Power Applications, 1995. **142**(6): p. 371-378.
15. Loffler, F., et al., *Influence of Air Gaps in Stacked Transformer Cores Consisting of Several Packages.* Ieee Transactions on Magnetics, 1994. **30**(2): p. 913-915.

16. Schönhuber, P. and H. Pfützner, *Flux distribution analysis in a mitred transformer core corner.* Journal of Magnetism and Magnetic Materials, 1991. **101**(1-3): p. 86-88.
17. Pfützner, H., *Performance of new materials in transformer cores.* Journal of Magnetism and Magnetic Materials, 1992. **112**(1-3): p. 399-405.
18. Loizos, G. and A.G. Kladas, *Core vibration analysis in Si-Fe distributed gap wound cores.* IEEE Transactions on Magnetics, 2012. **48**(4): p. 1617-1620.
19. Kreyszig, E., *Advanced engineering mathematics*. 1962, New York,: Wiley. 856 p.
20. Mizokami, M., M. Yabumoto, and Y. Okazaki, *Vibration analysis of a 3-phase model transformer core.* Electrical Engineering in Japan, 1997. **119**(1): p. 1-8.
21. Moghadam, A.T. and A.J. Moses, *Comparison of flux distribution in three-phase transformer cores assembled from amorphous material and grain oriented silicon iron.* IEEE Transactions on Magnetics, 1989. **25**(5): p. 3964-3966.
22. Anderson, P., *Measurement of the stress sensitivity of magnetostriction in electrical steels under distorted waveform conditions.* Journal of Magnetism and Magnetic Materials, 2008. **320**(20): p. E583-E588.
23. Ghalamestani, S.G., et al., *Magnetostriction and the Influence of Higher Harmonics in the Magnetic Field.* Ieee Transactions on Magnetics, 2012. **48**(11): p. 3981-3984.
24. Mapps, D.J. and C.E. White, *Longitudinal and Transverse Magnetostriction Harmonics in (110) [001] Silicon-Iron.* Ieee Transactions on Magnetics, 1984. **20**(5): p. 1566-1568.
25. Anderson, P.I., A.J. Moses, and H.J. Stanbury, *Assessment of the stress sensitivity of magnetostriction in grain-oriented silicon steel.* IEEE Transactions on Magnetics, 2007. **43**(8): p. 3467-3476.
26. Phway, T.P.P. and A.J. Moses, *Magnetisation-induced mechanical resonance in electrical steels.* Journal of Magnetism and Magnetic Materials, 2007. **316**(2): p. 468-471.
27. Penin, R., et al. *Estimation of relative magnetostriction and Maxwell's forces in stacked Grain Oriented steel structures*. 2012.
28. Arai, S., M. Mizokami, and M. Yabumoto, *Magnetostriction of grain oriented Si-Fe and its domain model.* Przeglad Elektrotechniczny, 2011. **87**(9B): p. 20-23.
29. Shilling, J.W. and G.L. Houze Jr, *MAGNETIC PROPERTIES AND DOMAIN STRUCTURE IN GRAIN-ORIENTED 3% Si-Fe.* IEEE Transactions on Magnetics, 1974. **MAG-10**(2): p. 195-223.
30. Jiles, D., *Introduction to magnetism and magnetic materials*. 2nd ed. 1998, London: Chapman & Hall. xxvii, 536 p.

Chapter 10: final conclusion and further work:

10.1. Main conclusions of the thesis

The main conclusions of this work are categorized as followed:

- The World's first magnetostriction round robin exercise shows a reasonable correlation between the different methods. Some of the possible reasons for the differences between the measurement systems were pointed out. Most importantly it should be highlighted that Comparisons at zero stress in the rolling direction could not be referenced as the magnetostriction value is so small and the differences are larger than the combined measurement uncertainty of the laboratories.
- It was shown that both laser scribing and mechanical scribing have a similar effect on a sample's domain structure and magnetostriction. A proposed domain model was used successfully to estimate the effect of scribing on magnetostriction. The theoretical results confirm that the newly formed [010] and [001] domains along the scribing line are causing the increase in magnetostriction of scribed samples.
- The changes of magnetic domain structure were confirmed by comparison of magnetostriction before and after curvature. The increase in magnetostriction is due to the domain changes in the compressive side of the sample
- Lorentz fitting was used to model the magnetostriction butterfly loop. Calculated harmonics, and A-weighted, from the Lorentz fitting equation show a good agreement with the measured data. The difference between the measured data and calculated is due to the fact that the measured butterfly loop has hysteresis, which in the model has not been taken into the account.

- The highest vibration levels in single-phase transformer were determined in the joint and corner areas for all three cores.
- It was proposed that an average stress of approximately -8MPa is applied to the laminations in the cores by using 4Nm-clamping torque.
- It has been shown that the leading source for the differences between the vibration of the cores under the same magnetic excitation and clamping pressure in the measured cores is due to the differences in the magnetostriction characteristics of the grades of electrical steels.

10.2. Future work:

- Further comparisons of magnetostriction measurement systems would be very useful in order to develop recognized standardized methods of measurement of this parameter.
- Further investigation on magnetostriction characteristics under 2D magnetisation is needed in order to study vibration of three-phase transformer.
- Additional study on transformer cores is needed to look into the exact effect of Maxwell force and magnetostriction by carefully studying flux distribution, stress distribution in the transformer core.
- A magneto-mechanically coupled FEM model is required to simulate the magnetostriction behaviour material and with the ability to take into account the inhomogeneous properties

Appendix:

Contribution of magnetostriction to transformer noise. Presented at 2010 *45th International Universities' Power Engineering Conference*, UPEC 2010; Cardiff; United Kingdom; 31 August 2010 through 3 September 2010

Round-robin assessment of the measurement of magnetostriction of Grain Oriented 3% silicon steel. Presented at: *Soft Magnetic Materials Conference (SMM21)*, Budapest, Hungary, 1-4 September 2013.Submitted to IEC.

Effect of domain refinement process on peak-to-peak magnetostriction of high-permeability 3% Si-Fe. Writing up stage, to be submitted to IEEE

Correlation of the vibration characteristics of single-phase transformer cores with the magnetostriction properties of Grain Oriented 3% silicon steel. Writing up stage, to be submitted to IEEE